4-6-2018 10:00 AM

Imaging Biomarkers of Pulmonary Structure and Function

Dante Capaldi
The University of Western Ontario

Supervisor
Dr. Grace Parraga
The University of Western Ontario

Graduate Program in Medical Biophysics
A thesis submitted in partial fulfillment of the requirements for the degree in Doctor of Philosophy

Abstract

Asthma and chronic obstructive pulmonary disease (COPD) are characterized by airflow limitations resulting from airway obstruction and/or tissue destruction. The diagnosis and monitoring of these pulmonary diseases is primarily performed using spirometry, specifically the forced expiratory volume in one second (FEV_1), which measures global airflow obstruction and provides no regional information of the different underlying disease pathologies. The limitations of spirometry and current therapies for lung disease patients have motivated the development of pulmonary imaging approaches, such as computed tomography (CT) and magnetic resonance imaging (MRI). Inhaled hyperpolarized noble gas MRI, specifically using helium-3 (^{3}He) and xenon-129 (^{129}Xe) gases, provides a way to quantify pulmonary ventilation by visualizing lung regions accessed by gas during a breath-hold, and alternatively, regions that are not accessed - coined "ventilation defects." Despite the strong foundation and many advantages hyperpolarized ^{3}He MRI has to offer research and patient care, clinical translation has been inhibited in part due to the cost and need for specialized equipment, including multinuclear-MR hardware and polarizers, and personnel. Accordingly, our objective was to develop and evaluate imaging biomarkers of pulmonary structure and function using MRI and CT without the use of exogenous contrast agents or specialized equipment. First, we developed and compared CT parametric response maps (PRM) with ^{3}He MR ventilation images in measuring gas-trapping and emphysema in ex-smokers with and without COPD. We observed that in mild-moderate COPD, ^{3}He MR ventilation abnormalities were related to PRM gas-trapping whereas in severe COPD, ventilation abnormalities correlated with both PRM gas-trapping and PRM emphysema. We then developed and compared pulmonary ventilation abnormalities derived from Fourier decomposition of free-breathing proton (^{1}H) MRI (FDMRI) with ^{3}He MRI in subjects with COPD and bronchiectasis. This work demonstrated that FDMRI and ^{3}He MRI ventilation defects were strongly related in COPD, but not in bronchiectasis subjects. In COPD only, FDMRI ventilation defects were spatially related with ^{3}He MRI ventilation defects and emphysema. Based on the FDMRI biomarkers developed in patients with COPD and bronchiectasis, we then evaluated ventilation heterogeneity in patients with severe asthma, both pre- and post-salbutamol as well as post-methacholine challenge, using FDMRI and ^{3}He MRI. FDMRI free-breathing ventilation abnormalities were correlated

with but under-estimated ^{3}He MRI static ventilation defects. Finally, based on the previously developed free-breathing MRI approach, we developed a whole-lung free-breathing pulmonary ^{1}H MRI technique to measure regional specific-ventilation and evaluated both asthmatics and healthy volunteers. These measurements not only provided similar information as specific-ventilation measured using plethysmography, but also information about regional ventilation defects that were correlated with ^{3}He MRI ventilation abnormalities. These results demonstrated that whole-lung free-breathing ^{1}H MRI biomarker of specific-ventilation may reflect ventilation heterogeneity and/or gas-trapping in asthma. These important findings indicate that imaging biomarkers of pulmonary structure and function using MRI and CT have the potential to regionally reveal the different pathologies in COPD and asthma without the use of exogenous contrast agents. The development and validation of these clinically meaningful imaging biomarkers are critically required to accelerate pulmonary imaging translation from the research workbench to being a part of the clinical workflow, with the overall goal to improve patient outcomes.

Keywords

X-ray Computed Tomography, Magnetic Resonance Imaging, Hyperpolarized Noble Gas MRI, Fourier Decomposition MRI, CT Parametric Response Mapping, Four-dimensional MRI, Specific Ventilation, Pulmonary Imaging, Imaging Biomarkers, Asthma, Bronchiectasis, Chronic Obstructive Pulmonary Disease

Co-Authorship Statement

The following thesis contains four manuscripts. Three manuscripts have been published in scientific journals and one manuscript is *in-press* for publication. As first author for all these manuscript, I significantly contributed to the manuscript preparation and submission including all aspects of the studies performed. The specific tasks I performed include: contributing to the study design and subject recruitment, organization and management of study visits, the development of the CT and MRI acquisition and reconstruction protocols, and acquisition of pulmonary function test and subject data. The tasks that were included following data acquisition were: image analysis, database organization, statistical analysis and interpretation, clinical/physiological interpretation of the data, drafting and final approval of the manuscripts. Dr. Grace Parraga provided ongoing guidance and was responsible for study conception and experimental design, data analysis and interpretation, drafting and final revisions and approval of the manuscripts, as the Principal Investigator and Supervisor. She is also the guarantor of integrity of the data as well as responsible for Good Clinical Practice (GCP). Study visits and acquisition of pulmonary function data was performed under the supervision of Sandra Blamires and Lyndsey Reid-Jones. Polarization of the ^{3}He gas was performed by Andrew Wheatley, Heather Young, Eric Lessard, and myself. MRI acquisition was performed by Trevor Szekeres and David Reese. Listed below are the specific contributions for all other co-authors for each manuscript contained in this thesis.

Chapter 2 is an original research article entitled "*Pulmonary Imaging Biomarkers of Gas-trapping and Emphysema in COPD: ^{3}He MR Imaging and CT Parametric Response Maps*" and was published in the journal *Radiology* in 2016. This manuscript was co-authored by Dante PI Capaldi, Nanxi Zha, Fumin Guo, Damien Pike, David G McCormack, Miranda Kirby, and Grace Parraga. Nanxi Zha and Fumin Guo assisted with the algorithm design and image analysis tools as well as interpretation of the data. Damien Pike and Miranda Kirby assisted with the recruitment of study participants, acquisition of data, statistical analysis, and interpretation. David G McCormack and Miranda Kirby were responsible for clinical/physiological interpretation of the data.

Chapter 3 is an original research article entitled "*Free-breathing Pulmonary ^{1}H and Hyperpolarized ^{3}He MRI: Comparison in COPD and Bronchiectasis*" and was published in

the journal *Academic Radiology* in 2015. This manuscript was co-authored by Dante PI Capaldi, Khadija Sheikh, Fumin Guo, Sarah Svenningsen, Roya Etemad-Rezai, Harvey O Coxson, Jonathon A Leipsic, David G McCormack, and Grace Parraga. Khadija Sheikh and Fumin Guo assisted with the algorithm design and image analysis tools as well as interpretation of the data. Sarah Svenningsen was responsible for the recruitment of study participants, and assisted with acquisition and interpretation of data. Roya Etemad-Rezai provided clinical expertise and aided in interpretation of the CT images. Harvey O Coxson assisted with the interpretation of MRI and CT data. Jonathon A Leipsic assisted with the interpretation of the CT data. David G McCormack was responsible for clinical/physiological interpretation of the data.

Chapter 4 is an original research article entitled "*Free-breathing Functional Pulmonary MRI: Response to Bronchodilator and Bronchoprovocation in Severe Asthma*" and was published in the journal *Academic Radiology* in 2017. This manuscript was co-authored by Dante PI Capaldi, Khadija Sheikh, Rachel L Eddy, Fumin Guo, Sarah Svenningsen, Parameswaran Nair, David G McCormack, and Grace Parraga. Khadija Sheikh and Fumin Guo assisted with the algorithm design and image analysis tools as well as statistical analysis and interpretation of the data. Rachel L Eddy and Sarah Svenningsen were responsible for the recruitment of study participants, and assisted with acquisition and interpretation of data. Parameswaran Nair and David G McCormack were responsible for clinical/physiological interpretation of the data.

Chapter 5 is an original research article entitled "*Free-breathing Pulmonary MR Imaging to Quantify Regional Ventilation*" and has been accepted to the journal *Radiology* and is currently *in-press*. This manuscript was co-authored by Dante PI Capaldi, Rachel L Eddy, Sarah Svenningsen, Fumin Guo, John SH Baxter, A Jonathan McLeod, Parameswaran Nair, David G McCormack, and Grace Parraga. Fumin Guo, John SH Baxter, and A Jonathan McLeod assisted with the algorithm design and image analysis tools as well as interpretation of the data. Rachel L Eddy and Sarah Svenningsen were responsible for the recruitment of study participants, and assisted with acquisition and interpretation of data. Parameswaran Nair and David G McCormack were responsible for clinical/physiological interpretation of the data.

To my Family and Friends: Past, Present, and Future…

"My mother made me a scientist without ever intending to. Every other Jewish mother in Brooklyn would ask her child after school, 'So? Did you learn anything today?' But not my mother. 'Izzy,' she would say, 'did you ask a good question today?' That difference - asking good questions - made me become a scientist."

- Isidor Isaac Rabi
Nobel Prize in Physics in 1944
for his discovery of
Nuclear Magnetic Resonance

Acknowledgments

First and foremost, I would like to thank my supervisor Dr. Grace Parraga for taking a leap of faith in me and giving me countless opportunities throughout my journey over the past four years. Your endless support, ever-continuing patience, dedication, and guidance have been invaluable to me throughout my graduate career. I am truly grateful for the opportunities you have given me and pushing me beyond my boundaries to areas that I really believed were outside my reach. I sincerely appreciate all of the life lessons and many discussions with you, which have broadened my understanding of research not only as a pure science, but as an art.

To my advisory committee, Dr. Ian Cunningham, Dr. Robert Bartha, and Dr. David Palma: thank you for your guidance and support with not only my research, but my career trajectory. To Dr. Cunningham, I am truly thankful for your guidance and mentorship -especially during your course where you not only taught me the fundamental principles of imaging, but also to never lose the excitement of learning something new. To Dr. Bartha, thank you for your guidance, support with my research, and teaching me the physics behind MRI. To Dr. Palma, thank you for providing me with clinical insight behind my research and the opportunity to shadow you in clinic. I am grateful to Dr. David McCormack and Dr. Aaron Fenster for the opportunity to discuss results and receive insightful comments about research that have been very helpful.

To the Department of Medical Biophysics: thank you for providing me with the resources and support while as a graduate student and your continual nurturing to grow professionally as a medical physicist. To Wendy Hough and Kathleen Petts: thank you for always being available to answer any of my questions and having a few laughs along the way. To Dr. Jerry Battista and Dr. Rob Stodilka: thank you for the guidance you provided me during my journey in graduate school and the wonderful music (J2B).

To the Parraga lab members: It has been wonderful working with all of you and thank you for making my time in London so memorable. I am especially grateful for the incredible friendships and support over the past few years. To Lyndsey Reid-Jones: thank you for teaching me about patient care -I have never met a more caring and compassionate individual who has taught me so much, both professionally and personally. To Andrew Wheatley: thank you for training me and giving me the confidence to perform the technical tasks required for

the lab. To David Reese and Trevor Szekeres: thank you for being MR rock stars and always helping us acquiring superb quality data. To Dr. Alexei Ouriadov: thank you for your guidance and teaching me the fundamentals of inhaled gas MRI. To Dr. Khadija Sheikh: thank you for always being there for me, from the late nights at Robarts to the fun festivities like murder mystery nights or Chaucer's on Thursday nights (just to name a few); I couldn't have asked for a better friend and mentor. Thank you for always being able to put a smile on my face. To Dr. Fumin Guo: thank you for being the computer guru when it came to image processing and for all of the laughs; you will forever be my official roommate no matter what conference I go to. To Tamas Lindenmaier and Gregory Paulin: we started graduate school together, we struggled together, and most importantly, we kept each other company, if it was either at work, or at the school's gym or just out on the town; I couldn't have asked for better lab mates and friends. To Eric Lessard, Rachel Eddy, and Megan Fennema: although in my eyes all of you will be the official lab newbies, you all have taught me so much; I can't wait to see all of you excel in your future endeavors. To Heather Young: your dedication while in the lab was truly inspiring; thank you for always making me believe that team work makes the dream become reality. To Andrew Westcott: thank you for all the laughs in my last year of graduate school and being a rock star when running the polarizers. To Dr. Sarah Svenningsen and Dr. Damien Pike: thank you for all the fun adventures. Thank you to all the other members of the lab who have helped make our research possible: Dr. Nanxi Zha, Robert DiCesare, Dr. Anurag Bhalla, Dr. Colin Adams, Michal Stankiewicz, Emma Bluemke, Matthew Schweers, Andrea Kassay, and Janhavi Patel.

Most importantly, I would like to thank my family and friends. To my parents: thank you for all your love, patience, and never wavering support in my dreams to better myself. Mom, thank you for always telling me to "find what you love doing and be the very best at it." Dad, thank you for always forcing me to think outside the box, making me ask the right questions, and providing me with guidance and support. André, thank you for helping me see the impact of my work. To Tomi Nano, I can honestly say that if it wasn't for your friendship and endless support, I would not have succeeded; thank you for being such an amazing friend, especially during my most difficult times. You are one of the most brilliant and driven individuals I know. To Derek Gillies, you are a constant reminder that there are absolutely amazing people in this world; thank you for always believing in me. Your impenetrable logic and wisdom is

second to none. To Terenz Escartin, thank you for all the thought provoking discussions and really making me think outside the box. Your creativity and ingenuity is something to admire. Tomi, Derek, and Terenz: I can't wait to see what the future has in-store for all of you. To Emmanuel Rufo, Claire Vannelli, Dilraj Sanghera, Dr. Aneesh Dhar, Quinn Camlis, Anmol Dhar, Dr. Kurtis Dekker, Jordynne Ropat, Kyle Burgers, Lisa Hur, Golafsoun Ameri, Adam Paish, Allie Blokker, Jessica Rodgers, Justin Michael, Dr. Ian Connell, Olivia Stanley, Dickson Wong, Amy Schranz, Yonathan Araya, Dr. Patrick Lim, Nivin Nyström, and Nolan Broeke, thank you for your friendships and support; you truly made my time over the past few years memorable.

Finally, I would like to express my gratitude to the various sources of funding that I have received over the past four years. I acknowledge funding support from the Natural Sciences and Engineering Research Council of Canada (NSERC), the Ontario Graduate Scholarship (OGS), and the Schulich School of Medicine and Dentistry Doctoral Excellence Research Award (DERA), as well as the Western Graduate Research Stipend (WGRS).

Table of Contents

List of Tables

List of Figures

List of Appendices

List of Abbreviations

AATD	Alpha-1 Antitrypsin Deficiency
ACQ	Asthma Control Questionnaire
ADC	Apparent Diffusion Coefficient
ANOVA	Analysis of Variance
Anti-IgE	Anti-immunoglobulin E
AQLQ	Asthma Quality-of-Life Questionnaire
ATS	American Thoracic Society
BMI	Body Mass Index
bSSFP	Balanced Steady-State Free Precession
BW	Bandwidth
CI	Confidence Interval
COPD	Chronic Obstructive Pulmonary Disease
CT	Computed Tomography
$CTDI_{vol}$	Volumetric CT Dose Index
DL_{CO}	Diffusing Capacity of the Lung for Carbon Monoxide
DPM	Dynamic Proton Map
DSC	Dice Similarity Coefficient
ERS	European Respiratory Society
FDMRI	Fourier Decomposition Magnetic Resonance Imaging
FEV_1	Forced Expiratory Volume in 1 second
FFT	Fast Fourier Transform
FGRE	Fast Gradient Recalled Echo
FOV	Field of View
FRC	Functional Residual Capacity
f_{size}	Size-Dependent Conversion Factor
FVC	Forced Vital Capacity
G	Gradient amplitude
GCP	Good Clinical Practice
GINA	Global Imitative for Asthma
GOLD	Global Initiative for Chronic Obstructive Lung Disease
GUI	Graphical User Interface
HIPAA	Health Insurance Portability and Accountability Act
HU	Hounsfield Unit
IC	Inspiratory Capacity
ICS	Inhaled Corticosteroid
IRB	Institutional Review Board
LA	Lumen Area
LABA	Long Acting Beta-agonist
LAMA	Long-Acting Anticholinergic
LCI	Lung Clearance Index
LTRA	Leukotriene Receptor Antagonist
MBNW	Multiple Breath Nitrogen Washout
MCh	Methacholine Challenge
MIND	Modality Independent Neighbourhood Descriptor
mMRC	modified Medical Research Council
MRI	Magnetic Resonance Imaging

NEX	Number of Excitations
NS	Number of Slices
NSCLC	Non-small-cell Lung Cancer
OCS	Oral Corticosteroid
PC_{20}	Provocative Concentration that lowered FEV_1 by 20%
PET	Positron Emission Tomography
PIP™	Pulmonary Imaging Platform
PRM	Parametric Response Map
RA_{856}	Relative Area under -856 HU
RA_{950}	Relative Area under -950 HU
R_{AW}	Airways Resistance
RF	Radiofrequency
RV	Residual Volume
SABA	Short Acting Beta-agonist
SAMA	Short-Acting Anticholinergic
SD	Standard Deviation
SI	Signal Intensity
SOC	Spatial Overlap Coefficient
SPECT	Single Positron Emission Computed Tomography
SpO_2	Oxygen Saturation
SSDE	Size-Specific Dose Estimate
ST	Slice Thickness
SV	Specific Ventilation
T_1	Spin-Lattice Relaxation Time (a.k.a. longitudinal relaxation time)
T_2	Spin-Spin Relaxation Time (a.k.a. transverse relaxation time)
TCV	Thoracic Cavity Volume
TLC	Total Lung Capacity
TE	Echo Time
TR	Repetition Time
TV	Tidal Volume
UTE	Ultra-short Echo Time
VC	Vital Capacity
VDP	Ventilation Defect Percent
VDV	Ventilation Defect Volume
VIF	Variance Inflation Factor
VP	Ventilation Percent
WA%	Wall Area Percent
WHO	World Health Organization

CHAPTER 1

1 INTRODUCTION

Lung diseases, including but not exclusive to asthma and chronic obstructive pulmonary disease (COPD), are characterized by airflow limitation resulting from airway obstruction and/or tissue destruction. In this thesis, the nature of airflow limitation is studied using non-contrast enhanced imaging biomarkers of pulmonary structure and function and compared with inhaled contrast magnetic resonance imaging (MRI) to develop a better understanding of the role of ventilation heterogeneity in the etiology and progression of lung disease.

1.1 Motivation and Overview

Pulmonary diseases, such as chronic obstructive pulmonary disease (COPD) and asthma, affect hundreds of millions of people throughout the world and account for millions of deaths each year. According to the World Health Organization (WHO), respiratory disease is the 4th leading cause of death worldwide,[1] as shown in **Figure 1-1**. Globally, COPD and asthma affect over 500 million people[2] and were, in 2015, the leading causes of death among all other chronic respiratory diseases (**Figure 1-1**).[2]

In Canada, asthma and COPD were reported to affect over 3 million people in 2014,[3] where COPD accounted for the highest rate of hospitalization, followed by angina and asthma,[4] as shown in **Figure 1-2**. These hospitalizations contribute significantly to the economic burden, where on average the cost for a COPD patient's hospital stay is approximately $10,000 per patient and the total cost was approximately $1.5 billion per year in 2008.[5] In Ontario, the total economic burden (including both direct and indirect costs) of asthma and COPD in 2011 were $1.8 billion and $3.9 billion, respectively.[6]

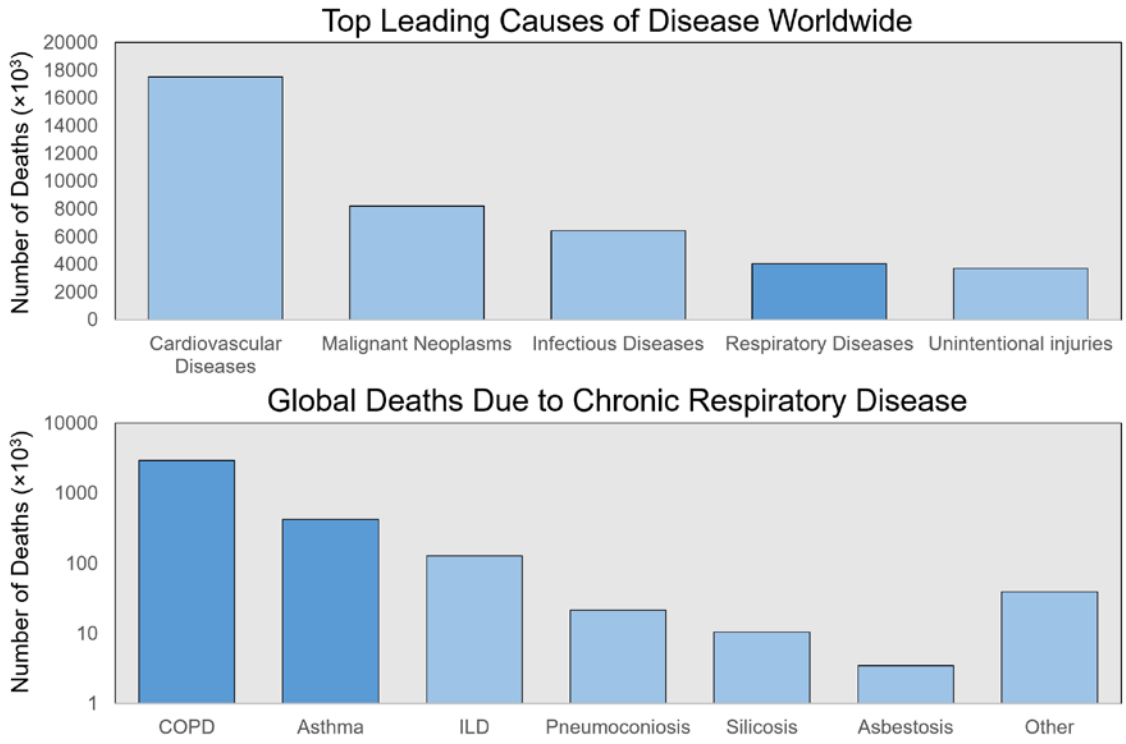

Figure 1-1 Global Deaths Worldwide and Due To Chronic Respiratory Diseases
Above: Top five leading causes of death. Below: Deaths globally from chronic lung disease in 2015 using a logarithmic scale.

These alarming statistics, as well as the overwhelming health care and economic burden of lung disease patients, provides evidence of the gap that still remains in the management and treatment of these patients. Currently, volumes derived from pulmonary function tests are used as objective measures for diagnosis, management, and treatment effectiveness. Although pulmonary function tests are easy to obtain and the generated measurements are reproducible,[7] they do not provide any regional information about the different underlying pathophysiology in lung disease patients and only provide a global measurement of lung function. This major limitation of pulmonary function tests has motivated the development of pulmonary imaging approaches, such as computed tomography (CT) and magnetic resonance imaging (MRI), to identify and provide regional measurements of lung structure and function for longitudinal monitoring and image-guided treatments.

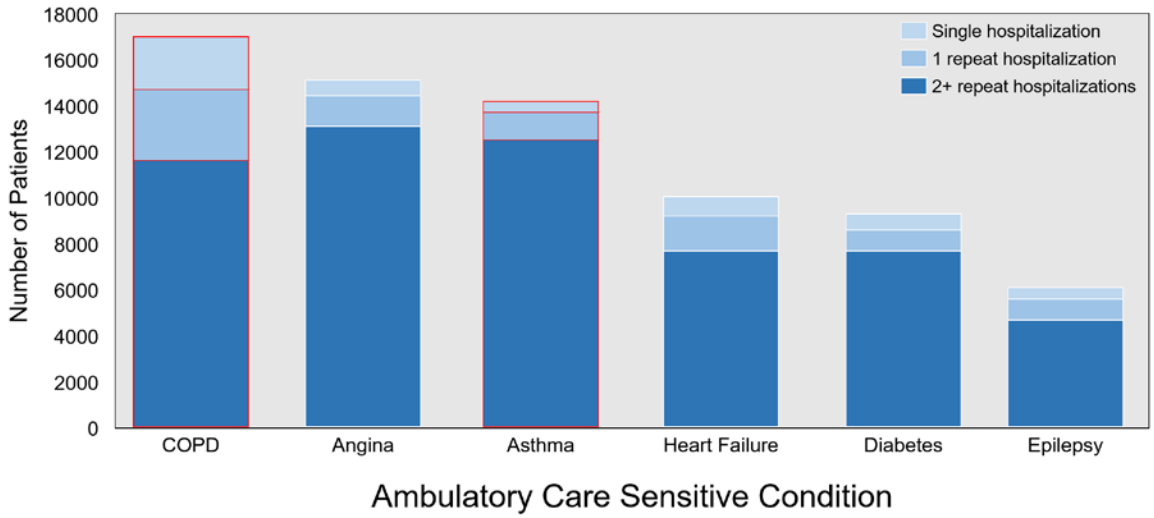

Figure 1-2 Repeated Hospitalizations by Condition at First Admission
Number of patients (in Canada excluding Quebec) with a single, one repeat, and two or more repeat hospitalizations at first admission. This was adapted from the Canadian Institute for Health Information (2008).[4]

Emerging methods based on pulmonary MRI are being developed to quantify lung structure and function regionally with the use of inhaled contrast agents. However, despite the numerous studies demonstrating the undeniable opportunities for clinically relevant pulmonary biomarkers, translation of these imaging approaches has been hampered due to a number of key limitations including the relatively high cost associated with inhaled gas contrast and requirement of multinuclear MR hardware and analysis software, restricting these techniques to a few specialized research centres. This thesis focuses on the development and application of imaging biomarkers of pulmonary structure and function using MRI and CT without the use of exogenous contrast agents or specialized equipment. These methods were used to evaluate pulmonary structure-function regionally in subjects with COPD and asthma and validated using hyperpolarized noble gas MRI. The development and validation of these clinically meaningful non-contrast enhanced imaging biomarkers are critically required to accelerate translation of pulmonary imaging from the research workbench to the clinical workflow with the overall goal to improved patient outcomes.

In this Chapter, the background knowledge relevant to this thesis is provided in order to motivate the original research presented in **Chapters 2 to 5**. A general overview of

structure and function in the respiratory system will be presented **(1.2)**, followed by the underlying disease mechanisms of asthma and COPD **(1.3)**. The current clinical standard to measure and evaluate lung function will be presented next **(1.4)** followed by a discussion on current and developing pulmonary imaging techniques used both in clinic and in the research setting **(1.5)**. Lastly, the hypotheses and objectives of this thesis will be introduced **(1.6)**.

1.2 The Respiratory System: Structure and Function

The chief responsibility of the respiratory system is to deliver air from the external environment to the blood for gas exchange between oxygen and carbon dioxide. To perform this task, the respiratory system is composed of nasal and oral cavities, the lungs, the chest wall, and the diaphragm. Specifically, the lungs are composed of bronchi, bronchioles, alveolar ducts, and alveolar sacs. All of these components function together to deliver air from outside of the body to the alveoli in order to perform gas exchange. In this section, the processes involved with the movement of air from the external environment through the body to the alveoli are discussed.

1.2.1 The Airways: Respiratory and Conducting Zones

The airways can be separated into the respiratory and conducting zones within the lungs. As shown in **Figure 1-3**, the conducting zone consist of the first 17 airway generations (0-16), while the remaining seven generations in the airway tree make up the respiratory zone.[8] The conducting airways are responsible for guiding air from outside the body to the locations in the lungs where gas exchange occurs. Following inspiration, air enters the nasal and oral cavities where it travels through the pharynx, larynx, and then into the trachea, where it enters the conducting zone. The trachea, generation 0 in the branching structure illustration in **Figure 1-3**, is a hollow pipe ribbed with cartilage rings that branches into the primary bronchi, where each bronchus feeds air into the left and right lung. Asymmetrical branching of the airway tree continues while the bronchi decrease in diameter, but growing geometrically in number. The branching bronchi, similar to the trachea, are also supported by cartilage to hold open the airway tree. This bronchi branching then leads into bronchioles that are no longer supported by cartilage and are

collapsible. It should be noted that the conducting zone does not participate in gas exchange directly and that this region of the airway tree is considered the "dead-space" (approximately 150mL).

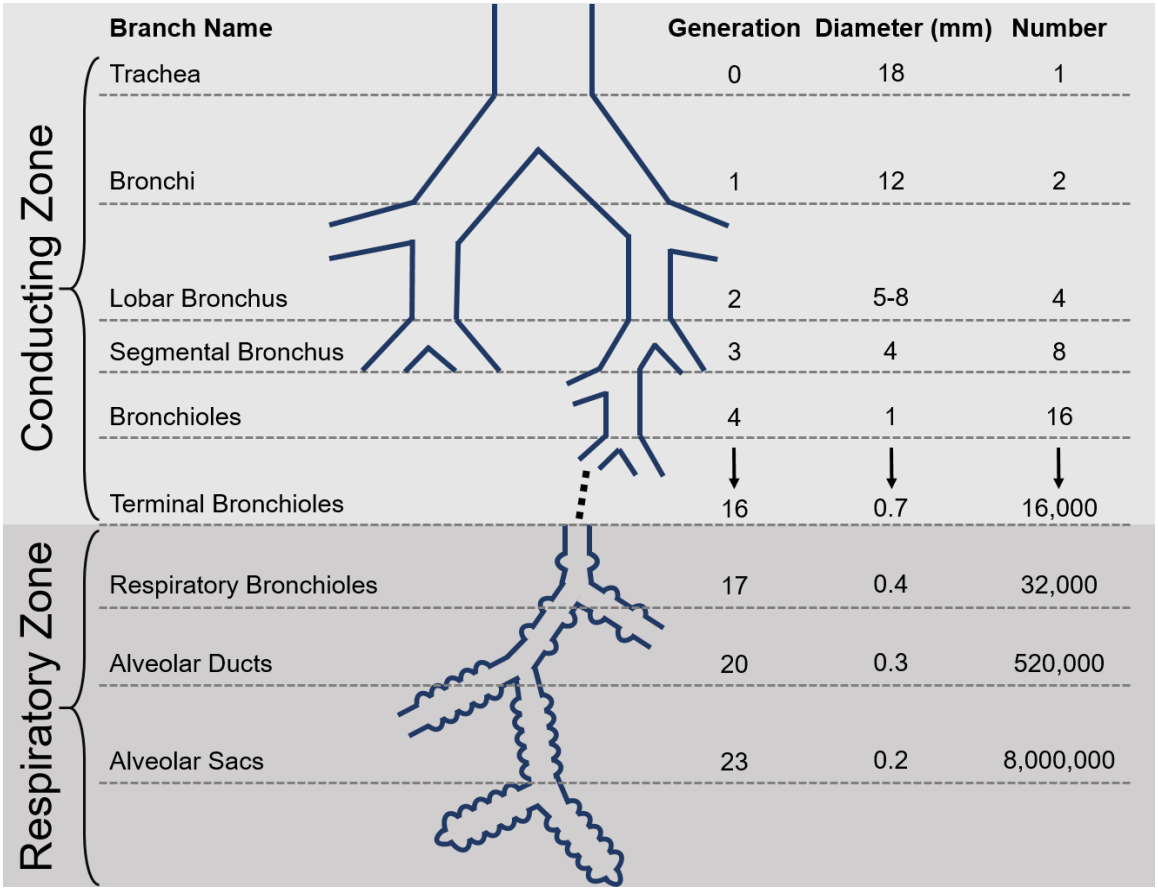

Figure 1-3 A Schematic of the Human Airway Tree
The conducting airways consist of generations 0-16, and the last 7 generations make up the respiratory zone. The conducting zone is responsible for guiding air to the alveoli, while the respiratory zone is lined with alveoli and is where gas exchange occurs. This was adapted from West, JB, Respiratory Physiology: The Essentials, Ninth Edition.[8]

Following the airway tree to the respiratory zone, starting at generation 17 shown in **Figure 1-3**, this is the region of the lung where gas exchange occurs. The airways at this point in the airway tree start to be lined with alveoli in the respiratory bronchioles. As the airways further divide, they start to form alveolar ducts where the number of alveoli dramatically increase in number. The alveolar ducts are then followed by the alveolar sacs of the terminal airways, which are completely surrounded by alveoli to provide the maximum amount of surface area for gas exchange to occur. As a result of the dramatic number of

airways in the respiratory zone, the overall cross sectional area is very large, where these airways account for most of the volume in the lung (approximately 2.5-3L).[8,9]

1.2.2 The Alveoli: Site of Gas Exchange

The alveoli, as mentioned above, are the functional units of the lungs where gas exchange occurs -specifically diffusion of oxygen and carbon dioxide. Approximately 480 million alveoli line the respiratory zone[10] each with an approximate diameter of 300μm.[8] The extremely thin walls of the alveoli (approximately 0.2μm thick) are composed of two types of cells (Type I and Type II) to maximize diffusion. The thinner Type I cells allow for gas exchange while the thicker Type II cells secrete surfactant.

1.2.3 Ventilation

Ventilation can be expressed as the volume of air that is exchanged between the body and the external environment as a function of time. Accordingly, the average adult inhales approximately 500mL of air with every breath. Of this 500mL, only 350mL reaches the alveoli because of the dead-space in the conducting zone. The generation of negative pressure within the lungs via diaphragmatic and intercostal muscle contractions results in air being drawn into the lungs.[9] The compliance of the lungs, which is a description of volume change related to pressure change, dictates the rate and force of inspiration and expiration. Assuming a rate of 15 breaths per minute, the total ventilation[8] and alveolar ventilation[8] would be 7500mL and 5250mL of air exchange per minute, respectively.

1.3 Pathophysiology of Lung Disease: Asthma and COPD

Lung diseases, specifically asthma and COPD, are characterized by airflow limitation, measured at the mouth using pulmonary function tests, which is persistent and caused by changes in the airway lumen, airway wall or peribronchial region. Airflow obstructions are not uniform in nature, but rather heterogeneously distributed throughout the lungs. Accordingly, ventilation abnormalities that result in ventilation heterogeneity are a hallmark finding in many respiratory disorders that involve the airways, such as asthma, or both the airways and pulmonary parenchyma, such as COPD. This section of the thesis will focus on the pathophysiology of lung disease, specifically in asthma and COPD.

1.3.1 Asthma

Asthma is a chronic and often debilitating airways disease, characterized by intermittent worsening of breathlessness, cough, chest-tightness and wheeze, which are typically reversible with the use of a bronchodilator.[11] Airflow limitations in asthma derive from the narrowing of the airway lumen, as illustrated in **Figure 1-4**, caused by increased hyper-responsiveness of the smooth muscle lining the airways, inflammation, and the presence of mucus due to hypersecretion.[12] These affects are observed throughout both the central and peripheral airways in an asthmatic[13] and involve both cellular (i.e. infiltration of eosinophils) and structural (i.e. airway remodeling) changes. Eosinophils in the walls of the airways promote constriction and bronchial smooth muscle shortening. The structural changes include increases in smooth muscle mass, bronchial wall edema, and mucous gland hypertrophy. These all lead to remodeling of the airways towards thickened walls that contribute to the overall airflow limitation and increased airways resistance. Furthermore, this airways resistance contributes to difficulty in emptying the lungs, resulting in hyperinflation (i.e. gas-trapping). The hyper-responsive nature of the airways in an asthmatic result in sudden and rapid airway narrowing in response to an environmental stimuli (i.e. allergens),[14] which is referred to as an "asthma attack."

1.3.2 Chronic Obstructive Pulmonary Disease

COPD is diagnosed and disease severity stratified based on not fully reversible airflow obstruction. Irreversible airflow obstruction develops over a COPD patient's lifetime as a result of primarily exposure to cigarette smoke,[15,16] but also can advance due to genetic conditions, such as alpha-1 antitrypsin deficiency (AATD), as well as via exposure to occupational chemicals and dust, air pollution. Airflow obstruction, symptoms, and exercise capacity measurements in COPD are related to both parenchyma destruction and airway remodeling, as shown in **Figure 1-4**.[7,17] Specifically, obstruction in COPD occurs in both the large (chronic bronchitis) and small airways (small airway disease), as well as the parenchyma (emphysema). Chronic bronchitis is characterized by excessive mucus production and airway inflammation of the large airways (greater than 4mm in diameter), specifically the epithelium of the central airways and extending to the mucous gland ducts.[18-20] The small airways, which are the bronchioles (less than 2mm in diameter) in

the airway tree illustrated in **Figure 1-3**, are the major site of airflow obstruction in COPD.[21] As mentioned in **Section 1.2.1**, although each airway has a small diameter, the number of airways increases rapidly, increasing the overall cross sectional area. Consequently, the small airways attribute very little to the overall measured airway resistance, where airway resistance is mainly dominated by the large airways. As a result, small airways disease may silently accumulate over many years without being detected.[22]

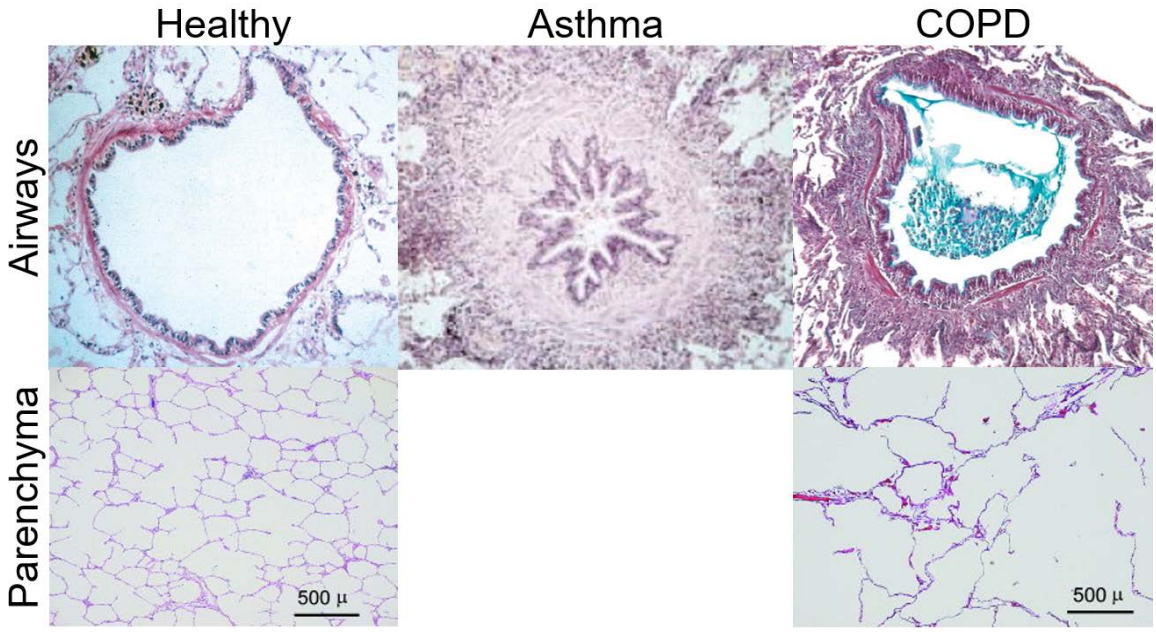

Figure 1-4 Parenchyma and Small Airways Pathologies in Asthma and COPD
Above: Healthy - normal small airways, asthmatic - muscle constriction/thickening of airway wall/increased smooth muscle mass resulting in luminal occlusion, and COPD - lumen partly filled with inflammatory exudate with airways inflamed and walls thickened. This was adapted from Hogg JC, Lancet (2004)[19] and Saetta M et al. Eur Respir J (2001).[12]
Below: Healthy - normal lung parenchyma, and COPD - parenchymal destruction. This was adapted from Woods et al. Magnetic Resonance in Medicine (2006).[23]

Emphysema is the destruction of parenchymal tissue, where airspaces in the lung are permanently enlarged, as illustrated in **Figure 1-4**.[24,25] This permanent enlargement results in the loss of alveolar walls and the number of small airways, as compared to a healthy subject, and consequently reduces the overall surface area. Emphysema can be divided into three major types: centrilobular, paraseptal, and panlobular emphysema.[26] Centrilobular emphysema, mostly associated with cigarette smoking, mainly affects the respiratory bronchioles while preserving the distal alveolar ducts and sacs. In contrast,

paraseptal emphysema affects the peripheral airspaces near the lung pleura and septa. Panlobular emphysema, more common in non-smoking patients with COPD (i.e. AATD), uniformly affects the entire distal bronchiole starting from respiratory bronchioles to the alveoli.

1.4 Established Clinical Measurements of Lung Function

Currently, the clinical standard for evaluating lung function is through the use of pulmonary function tests, which involve patients performing a variety of breathing maneuvers that provide global lung function and lung volume measurements. The measurements that are generated from pulmonary function testing are used to diagnose, monitor, and evaluate treatment effective and efficacy in patients with lung disease at in the clinic. These tests can be divided into spirometry, plethysmography, diffusing capacity of the lung for carbon monoxide, and multiple breath nitrogen washout. Furthermore, these measurements are often expressed as a percent predicted value ($\%_{pred}$) based on the patient's age, height, sex, and ethnicity.[27]

1.4.1 Spirometry

Measurements made using spirometry can be derived from breathing maneuvers made using a handheld device, such as the one shown in **Figure 1-5**. While sitting in the upright position, patients are instructed to make a tight seal with their lips around the mouthpiece while wearing nose plugs. As shown in the volume-time curve in **Figure 1-5**, patients are instructed to start with normal tidal breathing, for approximately 3-4 breaths, and then instructed to inhale using maximum effort, until they reach total lung capacity, followed by a maximally forced exhalation, until they cannot expel any more air.[28] The important measurements that are acquired through spirometry are the forced vital capacity (FVC), which is the amount of air that the patient can exhale after a full inspiration, and the forced expiratory volume in one second (FEV_1), which, as the name suggests, is the amount of air that the patient can exhale in one second.

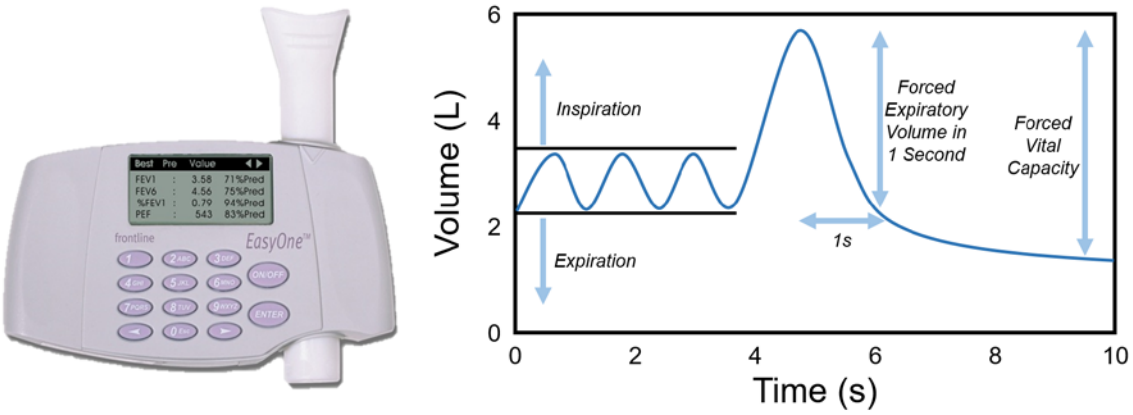

Figure 1-5 Pulmonary Function Test - Spirometry
Left: Handheld spirometer. Right: Volume-time curve that is measured by the spirometer to determine the forced expiratory volume in one second (FEV_1) and the forced vital capacity (FVC).

1.4.2 Plethysmography

A plethysmograph, shown in **Figure 1-6**, is an air-sealed chamber (or "body-box") where patients sit upright to perform breathing maneuvers to generate volume-time traces, as shown in **Figure 1-6**. The primary volume that is measured in plethysmography is functional residual capacity (FRC), from which residual volume (RV) and total lung capacity (TLC) can be quantified.[29] FRC is the volume of air that is within the lung after passive expiration, RV is the volume of air after forceful expiration, and TLC is the total volume of air within the lung after full inspiration. Other volumes that are obtained using plethysmography are the following: inspiratory capacity (IC), vital capacity (VC), and tidal volume (TV). IC is the volume of air that can be inhaled from the end of a normal exhalation during a tidal breathing maneuver, VC is the volume of air expelled from total lung capacity down to residual volume, and TV is the volume of air that is inhaled/exhaled during the respiratory cycle.[29] Furthermore, specific-ventilation (SV),[30] which is the movement of air into and out of the lungs during normal tidal breathing, is a dimensionless quantity that measures how efficiently the lungs are being ventilated, as shown below in **Equation 1-1**:

$$SV = \frac{TV}{FRC} \tag{1-1}$$

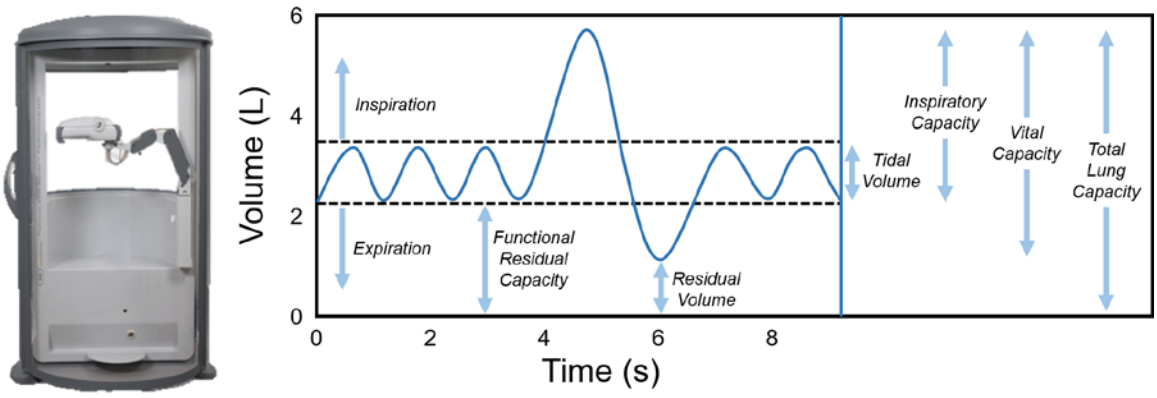

Figure 1-6 Pulmonary Function Test - Plethysmography
Left: Whole body plethysmograph. Right: Volume-time curve used to determine lung volumes measured by the plethysmograph.

1.4.3 Diffusion Capacity of the Lung

The diffusing capacity of the lung for carbon monoxide (DL_{CO}) can be measured through pulmonary function testing to evaluate patients with emphysema since this metric provides an indirect measure of gas diffusion across the alveolar membrane. When performing this test, patients are instructed to completely empty their lungs (to RV), and to forcefully inhale a gas mixture until they are completely filled (to TLC), where they are instructed to hold their breath for 10s before exhalation. The gas mixture that the patients inhale contains a very low concentration of carbon monoxide (0.3%). The breath-hold with the gas mixture allows the carbon monoxide to diffuse through the alveolar membrane into the blood, where the exhaled gas after the breath-hold is analyzed. It should be noted that the first approximately 150mL of exhaled gas is discarded because of the dead-space in the lungs. The analysis of the exhaled gas is performed by comparing the concentration of carbon monoxide exhaled versus the concentration that was inhaled to determine the amount of carbon monoxide diffusion.[31]

1.4.4 Multiple Breath Nitrogen Washout

Multiple breath nitrogen washout (MBNW) is a technique to measure lung volumes and ventilation heterogeneity.[32] This test is generally performed with participants sitting in the upright position and breathing 100% oxygen through a mouthpiece while wearing nose clips. While breathing in pure oxygen during normal tidal breathing, and knowing that air

contains mostly nitrogen gas, after each tidal breath, there is a decrease in the concentration of exhaled nitrogen. When the nitrogen gas concentration has decreased to 1/40th of the starting concentration by washing-out the lungs using pure oxygen, the test is complete. One measurement that is most commonly derived from MBNW tests is the lung clearance index (LCI).[33] LCI is calculated as the cumulative expired gas volume, based on the number of lung turnovers needed to clear the lungs of nitrogen gas, normalized to FRC, which is thought to be representative of whole lung ventilation heterogeneity.[34]

1.5 Pulmonary Imaging

Although pulmonary function tests are inexpensive and easily implemented, they only provide a global measurement of airflow obstruction with no regional information.[35,36] In COPD, they are weakly predictive of disease progression, as well as insensitive to early disease stages[37-39] where in asthma, they are relatively insensitive to changes in the small-airways,[40,41] which are thought to be the main sight of inflammation.[42] These limitations have motivated the development of pulmonary imaging approaches to provide direct and regional measurements of the underlying pathological features in both asthma and COPD patients. Pulmonary imaging provides regional structural (anatomical) and functional (physiological) information with high spatial and temporal resolution, and has been used for longitudinal monitoring and image-guided treatments with the overall goal of improving patient outcomes. The functional and structural imaging techniques discussed in this thesis include planar chest x-ray, x-ray computed tomography (CT), positron emission tomography (PET), single photon emission computed tomography (SPECT), and magnetic resonance imaging (MRI).

1.5.1 Structural Imaging

The anatomy of the lung can be identified and monitored non-invasively using high resolution structural imaging. Planar chest x-ray, x-ray CT, and MRI have previously been investigated to image the anatomy of the lung, including the airways and parenchyma.

1.5.1.1 Planar Chest X-ray

Since the advent of planar x-ray imaging, in 1895 by Wilhelm Röntgen where he notably captured an image of his wife's hand, it has now become the most common imaging method in lung disease. The broad dissemination of x-ray imaging was due in part to the low cost, low radiation dose, and short acquisition window, making it a commanding diagnostic tool. A typical dose associated with a chest x-ray is approximately 0.01mSv,[43] where in comparison, the average annual background radiation dose is 2-3mSv.[43] Chest x-ray images (or radiographs) are generated by having an x-ray source directed towards a patient's chest. The x-ray beam then travels from the source to the patient, where some of the x-rays are absorbed by the body. The absorption (or attenuation) of x-rays by the body depends on the path that the x-ray travels through. The x-rays that are not absorbed pass through the body to the detector, which is located on the other side of the patient. These x-rays are then measured by the detector to generate an x-ray image. The resulting image is thus a superposition of all anatomy in the path of the x-ray. The contrast of the image is related to the number of absorbed (or attenuated) x-rays along each path and is dependent on the mass attenuation coefficient of the tissue. The mass attenuation coefficient is dependent on the photon (x-ray) energy, atomic number, and mass density of the absorbing material. Highly attenuating (absorbs many x-rays) material, such as bone, appears white on an x-ray image, while low attenuating (absorbs fewer x-rays) structures, such as lung tissue, appears black, as shown in **Figure 1-7**.

Lung abnormalities can be visibly identified using chest radiographs in patients with asthma and COPD (**Figure 1-7**). In asthma, the most common abnormalities are associated with increased lung volumes (hyperinflation) and bronchial wall thickening.[44,45] In COPD, radiographs are used to detect hyperinflation in moderate-to-severe emphysema[46] and appear as elongated lung volumes, change in the cardiac silhouette, and flattened diaphragm.[47] The limiting factors of planar chest radiographs, including the poor contrast and loss of depth information, have motivated the development of three-dimensional imaging approaches, specifically x-ray CT imaging.

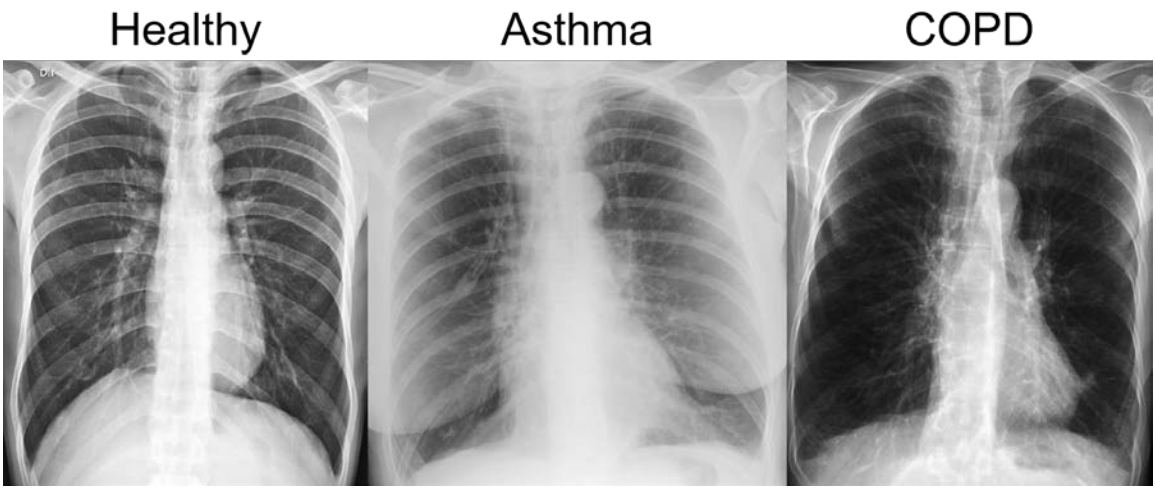

Figure 1-7 Chest Radiographs (Posterior-Anterior) of a Healthy, Asthmatic, and COPD Patient
Asthmatic: Lung appears hyperlucent and the diaphragm is flattened indicative of hyperinflation. COPD: Lung is hyperinflated, which is consistent with a flat diaphragm and secondary to emphysema. Healthy volunteer case courtesy of Dr Bruno Di Muzio, Radiopaedia.org, rID: 37906. Asthmatic case courtesy of Dr. Ian Bickle, Radiopaedia.org, rID: 33470. COPD patient case courtesy of A.Prof Frank Gaillard, Radiopaedia.org, rID: 8512.

1.5.1.2 X-ray Computed Tomography

Similar to planar x-ray imaging, x-ray CT leverages the attenuating properties of x-rays in material, but alternatively acquires many different x-ray projections at different angles around the patient to generate a three-dimensional volume of the anatomy. CT was first pioneered in the 1970s, and over the past few decades, has become the modality of choice for evaluating lung disease patients because it allows for the assessment of the airways and parenchymal density changes, while eliminating the structural superposition inherent to chest radiographs.[48-50]

X-ray CT images are acquired by having a patient lay supine on the scanner bed, where the bed is passed through the imaging components of the scanner. The x-ray source and an array of detector elements are positioned opposite to one another, where the source and detector rotate around the patient to acquire multiple x-ray projections. The projections can be reconstructed into a three-dimensional volumetric image using computational reconstruction techniques, such as filtered back projection and iterative reconstruction.[51] In the generated CT volumetric image, each voxel is represented as a relative measurement

of the tissue density to that of water using the Hounsfield Unit (HU),[52] as shown below in **Equation 1-2**:

$$Hounsfield\ Unit = \left(\frac{\mu_{tissue} - \mu_{water}}{\mu_{water}}\right) \times 1000\ [HU] \qquad (1\text{-}2)$$

where μ_{tissue} and μ_{water} are the linear attenuation coefficients of tissue and water, respectively. A typical dose associated with a chest CT is approximately 7-8mSv,[53] which is approximately 3-4 times the dose received annually from natural background radiation. More recent advancements in image reconstruction have resulted in the reduction of the typical CT dose to approximately 0.1mSv (ultra-low-dose CT),[54] although these techniques have not yet been implemented in the clinic.[55]

CT imaging of the chest has been used to evaluate both airways disease and parenchymal destruction in lung disease, such as asthma and COPD. In asthma, expiratory CT provides regional visualization of air-trapped regions,[56] while inspiratory CT has been used to evaluate airway remodelling.[57] Air-trapping can be quantified automatically based on thresholds of the expiratory CT density histogram. CT estimates of airways disease can be generated using measurements of airway wall area percent (WA%) and lumen area (LA) and quantified using software, such as Pulmonary Workstation V.2.0 (VIDA Diagnostics, Coralville, Iowa, USA), for the reconstruction of the large airways (to the fifth-sixth airway generation) from volumetric datasets. Relative to healthy subjects, CT bronchial wall thickness measurement in asthma are greater[58] and have been shown to be associated with airflow obstruction.[59,60] In regard to the small airways, the spatial resolution limitation of CT restricts the direct evaluation of these airways (diameter <2mm). As a result, an indirect measurement of small airways disease can be evaluated using a densitometry threshold on expiratory CT to measure air-trapping (relative area under <-856HU [RA_{856}]).[61] Similarly in COPD patients, inspiratory CT can be used to visualize and quantify airways disease[62,63] and emphysema.[64-66] Emphysema can be automatically quantified based on thresholds in inspiratory CT (relative area under <-950HU [RA_{950}]),[64,66,67] as shown in yellow in **Figure 1-8**.

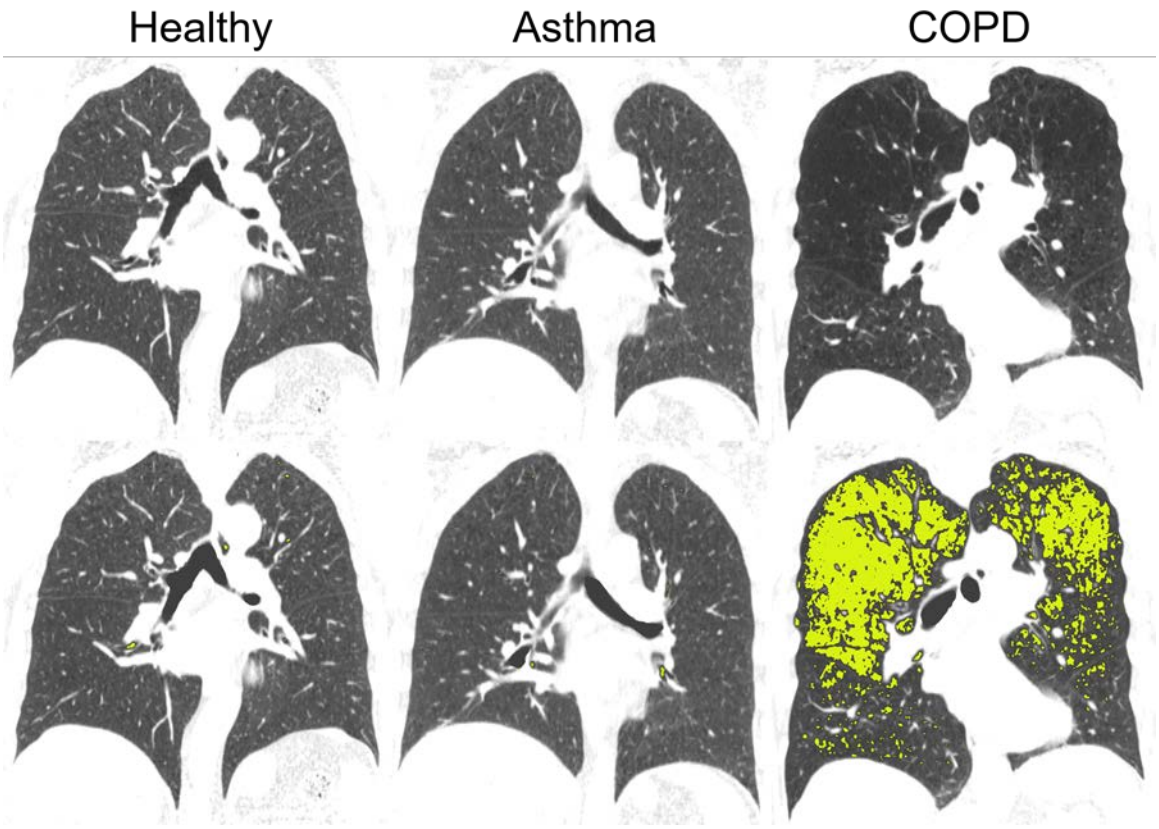

Figure 1-8 Coronal X-ray CT Images and Corresponding Lung Density Threshold Maps for a Healthy, Asthmatic, and COPD Subject
Shown in yellow are lung regions below -950HU.

Thoracic x-ray CT has been shown to provide a wealth of information about the anatomical structures within the lung, but it should be noted that the use of such x-ray based methods is limited, especially in serial studies of treatment response and longitudinal studies, particularly in children and younger adults with chronic lung disease. This is a result of the potential risks related to radiation doses stemming from ionizing x-ray radiation.[68]

1.5.1.3 Magnetic Resonance Imaging

Unlike x-ray imaging methods, magnetic resonance imaging (MRI) uses non-ionizing radiation radiofrequency (RF) waves to manipulate nuclear spins (mainly proton [^{1}H] atoms) to generate images that provide excellent soft tissue contrast of the anatomy with high spatial resolution. Conventional ^{1}H MRI of the lung, despite all the advantages, has been challenging to develop due to a number of limitations.

First, MRI signal is dependent on the number of ^{1}H, specifically in water molecules. Unfortunately in the lung, it is mostly air-filled and consists of only 800g of tissue across 4-6L,[69] and as a result, the signal-intensity of the lung is low. Furthermore, the countless air-tissue interfaces, as a result of the millions of alveoli within the lung, leads to local magnetic field inhomogeneities,[70,71] which are problematic for high spatial resolution MRI. The protons at these air-tissue interfaces spin at different rates since proton spin precession frequency is determined by the local magnetic field, which causes the transverse signal to decay very quickly (0.4-0.9ms).[72,73] As a result, this leads to increased dephasing of the magnetization and signal loss. Additionally, cardiac and respiratory motion during tidal breathing causes blurring artefacts in the image. The accumulative result of all these limitations result in the lungs appearing as black holes with no information that can be obtained about lung anatomy, as shown in **Figure 1-9**, making images acquired in a healthy volunteer indistinguishable from those of a lung disease subject.

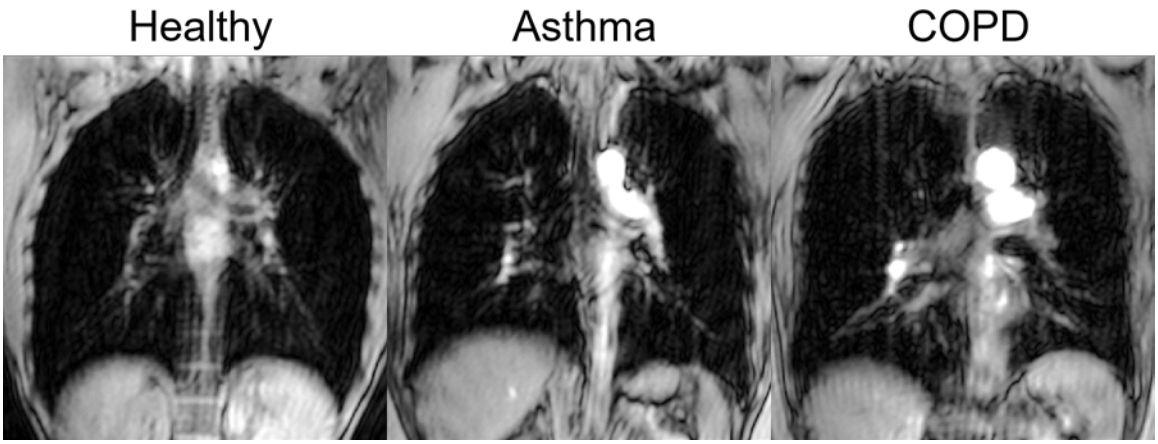

Figure 1-9 Representative Conventional ^{1}H MR Coronal Images for a Healthy, Asthmatic, and COPD Subject
Structural information with the lung is difficult to visually distinguish due to the inherent low tissue and ^{1}H density.

In order to overcome the increased dephasing of the transverse signal, ultra-short echo time (UTE) MRI acquisition protocols have been developed to reduce the time between the RF excitation pulse and data acquisition to acquire signal from the parenchymal tissue before it decays.[70] The enhancement in signal due to the reduced echo time (TE) has resulted in recent studies showing that UTE MRI provides comparable visualization of pulmonary anatomy as compared with CT.[74] As compared to **Figure 1-9**, there is an enhancement in

signal in the UTE MRI for a healthy, asthmatic, and COPD subject (**Figure 1-10**). In asthmatics, UTE MRI lung signal intensities were lower as compared with healthy volunteers, and correlated with lung function and CT radiodensity measurements.[75] Similarly in COPD, previous studies have shown correlations between CT emphysema measurements and lung function tests with UTE MRI lung signal-intensity measurements.[76]

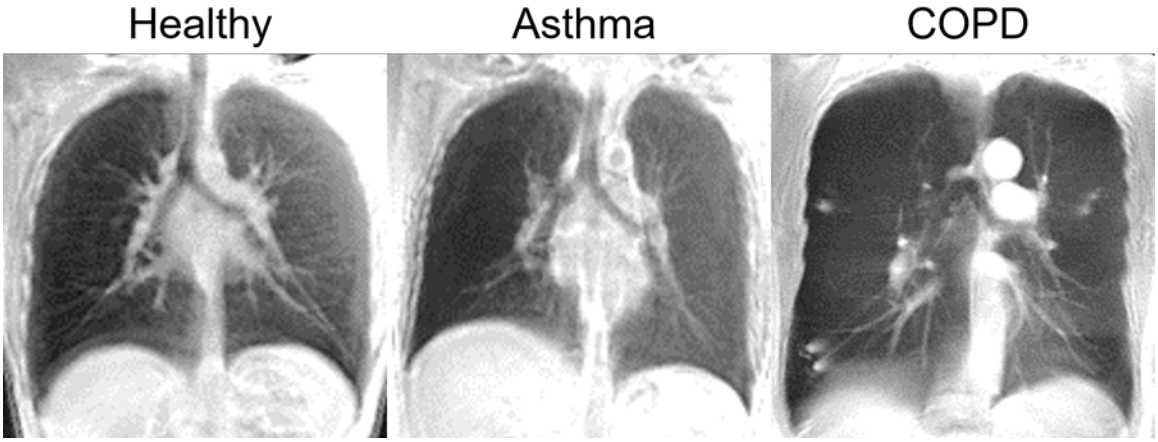

Figure 1-10 Representative UTE ^{1}H MR Coronal Images for a Healthy, Asthmatic, and COPD Subject
In contrast to the conventional ^{1}H MR images in **Figure 1-9**, regions of low signal-intensity are visually obvious in the UTE MR images for the obstructive lung disease subjects compared to the healthy volunteer.

1.5.2 Functional Imaging

The chief function of the lung is ventilation where oxygenated air is delivered to the alveoli within the lung and carbon dioxide is removed. With regard to medical imaging, there are several methods to generate functional maps to identify regions of the lung that are ventilating versus regions that are not. Ventilation imaging can be performed either with (contrast enhanced) or without (non-contrast enhanced) inhaled gases.

1.5.2.1 Contrast Enhanced Functional Imaging

Inhaled contrast agents can be used to directly image the distribution of the contrast within the lung to measure ventilation. Nuclear medicine, CT, and MRI all provide measurements of ventilation with the use of inhaled gases.

Nuclear Medicine

Nuclear medicine methods use radioactive tracers that emit radiation. These methods involve inhalation of the radioisotopes to the peripheral airspaces to generate functional images of ventilation. The two nuclear medicine imaging techniques that have been developed to generate ventilation images are single photon emission computed tomography (SPECT) and positron emission tomography (PET).

SPECT imaging involves patients inhaling radioisotopes that emit a single gamma-ray as they decay. Patients lay on a bed where three-dimensional tomographic images are generated by using a ring of gamma cameras or by rotating a single or multiple gamma cameras around the patient to acquire multiple projections at different angles. These projections can be reassembled to provide volumetric information about the radioisotope distribution within the lungs. Ventilation scans require gaseous radioisotopes, such as ^{81m}Kr, ^{133}Xe, aerosolized ^{99m}Tc-diethylenetriaminepentaacetate (DTPA) or an ultrafine dispersion of ^{99m}Tc-labeled carbon ("Technegas"), to generate regional ventilation images by measuring the distribution of the gas within the lungs as the radionuclide decays.

In a similar manner, PET imaging involves patients inhaling a radioisotope, but in this case, the radioisotope emits positrons as it decays through the process of beta decay. As the radioisotope decays, a positron is ejected from the nucleus of the unstable atom. Once ejected, the positron travels a short distance where it will encounter an electron and undergo a process known as annihilation. The annihilation of both of these particles will result in the generation of two photons, each with equal energy of 0.511MeV, that are emitted approximately 180° from one another. The simultaneous creation of these gamma-rays travelling antiparallel to each other can be detected at or very close to the same time, and are considered to be coincident. The spatial location of the source particle can therefore be determined from detection of the coincident gamma-rays detected by two detector elements geometrically. The location of the radioactive decay of the radioisotope is therefore restricted to that line, which can then be sorted out and reconstructed into a volumetric image of the distribution of the inhaled radionuclide in the lungs. Ventilation imaging using PET can be performed using inhaled ^{68}Ga-carbon nanoparticles ("Galligas")

or ^{13}N isotope (either by bolus injection or inhalation). For ^{13}N, it is not soluble in blood/tissue,[77] so following bolus injection of this radioisotope, it will travel to the lungs via the bloodstream and cross the alveolar membrane. Accordingly, gas-trapped regions of the lung retain the tracer while well ventilated regions of the lung quickly wash away the tracer. Alternatively, using the inhaled methods, the tracers do not reach the poorly ventilated regions of the lung.

SPECT imaging has been used to evaluate airway closure,[78] and changes following bronchoconstriction[79,80] and bronchodilation in asthma.[81] Similarly, poorly ventilated regions post bronchoconstriction have been identified using PET imaging.[82] In COPD subjects, the evaluation of airflow limitation severity[83,84] and intrabullous ventilation in emphysema patients[85] have been performed using SPECT imaging. The ventilation/perfusion ratio that can be generated using PET imaging has been identified as a measurement to separate the different phenotypes of COPD (i.e. emphysema "pink puffer" versus airways disease "blue bloater").[86] Although promising, limitations of SPECT and PET include the risk of cumulative radiation exposure for longitudinal monitoring, low spatial resolution, and specifically for PET, the need for a cyclotron for the production of isotopes.

X-ray Computed Tomography

CT imaging, specifically imaging at two energies (dual-energy CT), provides a way to regionally measure ventilation using inhaled xenon.[87] This method leverages the differing x-ray attenuation properties of xenon at two separate energies. Recent developments in CT technology, specifically dual-source CT scanners, has allowed the simultaneous acquisition of data at different tube voltages for material differentiation. This method involves the patient fitted with a positive pressure ventilation mask laying supine on the CT bed, where they are instructed to breathe in a mixture of xenon and oxygen for approximately 2-3 minutes. The images that are acquired at both the high and low energies are then used to perform three-material decomposition, by which xenon can be differentiated from other materials in the lung (air and soft tissue), to generate a xenon distribution map.

Dual-energy CT using inhaled xenon has been used to evaluate patients with asthma where ventilation defects that appeared in the xenon-enhanced images were related to airflow limitation and airway wall thickening,[88] and are sensitive to both bronchodilation[89] and bronchoconstriction.[90] Xenon-enhanced dual-energy CT has also been used to evaluate the regional distribution of structural and ventilation abnormalities simultaneously in patients with COPD.[91] Although this technique is promising, there are several limitations including radiation exposure, side effects of xenon (specifically respiratory depression), and cost.

Magnetic Resonance Imaging

There are several different inhaled contrast agents that have been developed for MRI. MR ventilation images can be generated with the use of O_2, ^{19}F, ^{3}He, and ^{129}Xe.

O_2-enhanced MRI was first developed in the 1990s to non-invasively assess regional ventilation in the human lung.[92] This method involves measuring the change that occurs in the longitudinal relaxation time (T_1) of protons in lung tissue with differing concentration of O_2. Molecular O_2 is weakly parametric magnetic and the presence of O_2 accelerates the longitudinal relaxation of protons. Ventilation images using O_2 are generated by comparing T_1-weighted ^{1}H images acquired whilst breathing room air (~21% [O_2]) and pure oxygen (100% [O_2]). Previous studies that have evaluated asthma patients using O_2-enhanced MRI showed that the measured O_2-enhancement ratio related with pulmonary function tests and disease severity.[93,94] In COPD patients, O_2-enhanced MRI was shown to be correlated with lung diffusion capacity,[95] pulmonary function tests,[96] and the presence of emphysema evaluated using CT.[96]

Inert ^{19}F gas MRI involves patients inhaling fluorinated gases, such as tetrafluoromethane (CF_4), sulfur hexafluoride (SF_6), hexafluoroethane (C_2F_6) and perfluoropropane (C_3F_8 or PFP) which are nontoxic and contain multiple ^{19}F nuclei. Despite the weak signal from thermal equilibrium polarization, the rapid longitudinal relaxation time of ^{19}F allows for extensive signal averaging.[97] Additionally, the presence of O_2 does not have a dramatic effect on the T_1 of fluorinated gases, thus fluorinated gases can be mixed with O_2 to improve patient safety. Current imaging protocols *in vivo* involve patients breathing 5-7 breaths of a fluorinated gas mixture (C_3F_8/O_2) to reach an approximate steady state gas

concentration in the lung and then performing a breath hold maneuver with inhalation of 1L of the same fluorinated gas mixture.[98,99] Recent studies have shown the application of ^{19}F MRI in both asthma and COPD patients where there was a visual increase in heterogeneity of the distribution of gas within the lung as compared to a never-smoker with normal lungs.[98]

Noble gas MRI, using either hyperpolarized ^{3}He or ^{129}Xe gases which are stable isotopes, since its first description[100,101] has provided non-invasive measurements of lung ventilation. ^{3}He and ^{129}Xe nuclei, although MR visible, have a low spin density compared with solid tissue which prohibits its detectability using MRI under thermal equilibrium polarization, thus the process of hyperpolarization is performed. Hyperpolarization is a process by which angular momentum is added to a system. Specifically for noble gases, optical pumping and spin exchange is used to achieve hyperpolarization. Optical pumping involves a circularly polarized laser, with a wavelength corresponding to the electronic orbital transition energy of an alkali metal (i.e. Rb), which serves as the carrier of the angular momentum. The laser is used to excite the electrons of vaporized alkali metal where the excited vapor is within an optical cell also filled with either ^{3}He or ^{129}Xe. The angular momentum of the electrons of the excited alkali metal vapour is transferred to the noble gas nuclei through collisions; this process is known as spin-spin interaction. This method increases the nuclear polarization of the unpaired nuclear proton of the noble gases up to five orders of magnitude compared to thermal equilibrium polarization.[102] It should be noted that the optical cell is maintained in a constant magnetic field; this is performed to reduce the decay rate of the polarized atoms to their ground state. Initially, lung imaging was developed using hyperpolarized ^{129}Xe,[100] but quickly converted to ^{3}He due to the high signal-to-noise ratio that could be achieved because of the inherent properties of the two noble gases. The gyromagnetic ratio of ^{3}He is approximately three times greater than ^{129}Xe (gyromagnetic ratio of -32.3MHz/T for ^{3}He versus -11.8MHz/T for ^{129}Xe) and the achievable polarization of ^{129}Xe is lower than ^{3}He (^{129}Xe: 8-25%; ^{3}He: 30-40%).[103] However, due to the limited supply and increasing price of ^{3}He[104] and recent advances in technology, there has been renewed interest in ^{129}Xe where similar signal-to-noise ratios are becoming more attainable.[105]

Ventilation imaging using noble gas MRI provides a visualization of the spin density of noble gas nuclei within the lung after inhalation, which reflect regions of the lung that are ventilated and those that are not. **Figure 1-11** shows hyperpolarized ^{3}He MR ventilation images (cyan) co-registered to conventional ^{1}H MR images (gray) for a healthy volunteer, an asthmatic, and a subject with COPD. As compared to the healthy volunteer, where there is a homogenous distribution of ^{3}He gas within the lung, the asthmatic and COPD subjects both have visibly obvious regions within the lung that are not gas filled (signal voids); these regions are known as "ventilation defects." These ventilation defects can be quantitatively evaluated using the imaging biomarker known as the ventilation defect percent (VDP), where VDP is the normalized region of the lung that is not participating in ventilation (ventilation defect volume [VDV]) to the whole lung volume (thoracic cavity volume [TCV]),[106] shown below in **Equation 1-3**:

$$VDP = \left(\frac{VDV}{TCV}\right) \times 100\% \tag{1-3}$$

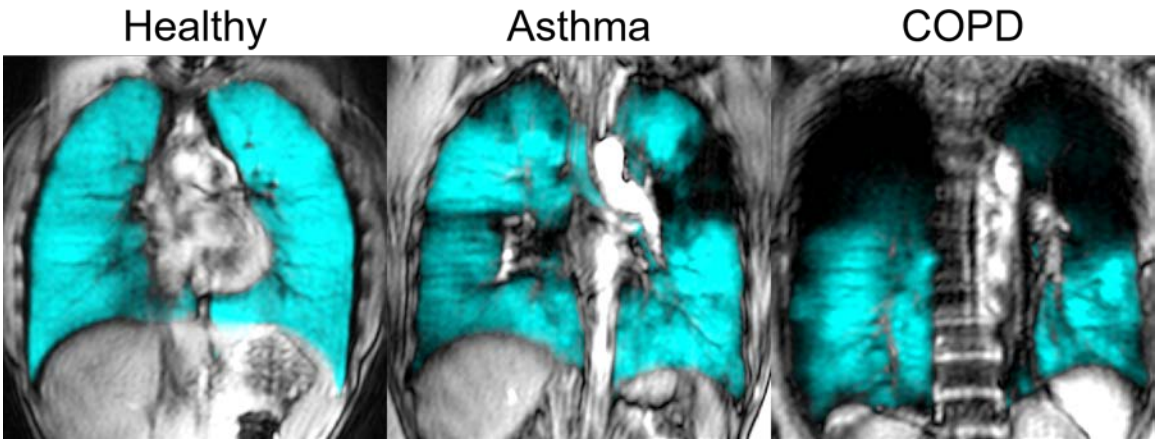

Figure 1-11 Representative Hyperpolarized ^{3}He (cyan) MR Coronal Images Co-registered to Conventional ^{1}H (gray) MR Coronal Images for a Healthy, Asthmatic, and COPD Subject
Homogeneous distribution of ^{3}He MR signal intensities within the lung are observed in the healthy volunteer, while heterogeneous signal intensities (regions or signal void) are seen in both the asthmatic and COPD subject.

This imaging biomarker of ventilation heterogeneity has been shown to be a robust measure that is reproducible[107,108] and related to relevant clinical measurements.[109-111] In asthmatic patients, ventilation defects that appeared in hyperpolarized noble gas MR images have

been shown to be significantly correlate with spirometry,[110-112] disease severity[110] and CT measurements of gas trapping,[111] and are spatially and temporally persistent.[107,113,114] Importantly in asthmatics, ventilation is characteristically heterogeneous as compared with healthy volunteers.[110,115-117] Ventilation defects are larger and more numerous in older asthmatic patients, with greater inflammation and worse airway remodeling[118] and are also related to quality of life and asthma control.[119] In COPD patients, VDP is related to spirometry,[109] symptoms and exercise capacity,[120] CT-derived emphysema measurements,[121] and exacerbations[122] using hyperpolarized ^{3}He and ^{129}Xe gases. Furthermore, for both asthma and COPD patients, ventilation defects are sensitive to bronchodilation,[123,124] while in asthmatics, ventilation defects are also sensitive to bronchoconstriction.[125]

Another application of hyperpolarized noble gas MRI is to probe the microstructure within the lung using diffusion imaging.[126] Diffusion-weighted noble gas MRI, which is sensitive to the self-diffusion of the gases based on the random Brownian motion of the atoms, can be used to measure the apparent diffusion coefficients (ADC) of both hyperpolarized ^{3}He and ^{129}Xe. ADC reflects the restricted diffusion of the gases within the airways and airspaces. As a result, the diffusion time interval can be used as a surrogate measurement of airspace dimension.[127] Accordingly, an increase in ADC value reflects a greater mean square displacement of the gas molecule or an enlarged airspace as a result of, for example, emphysema-related airspace enlargements. ADC measured using hyperpolarized ^{3}He MRI have been validated using histology[23] and shown to be highly reproducible.[128-130] Furthermore, hyperpolarized ^{3}He MRI ADC have been used to validate hyperpolarized ^{129}Xe MRI ADC measurements.[131] In asthma, ADC was significantly elevated in asthmatics as compared to healthy volunteers, potentially suggesting gas-trapping,[132] although other studies have reported otherwise showing no difference.[133,134] ^{3}He MRI ADC has also been used to evaluate the response to methacholine in asthmatics, where ADC values were elevated after bronchoconstriction and decreased following bronchodilation.[135] In patients with COPD, ADC values measured using ^{3}He and ^{129}Xe were elevated compared to age matched healthy volunteers,[109] and correlated with age,[136] lung function tests,[137] smoking history,[136] and CT measurements of emphysema.[109]

Furthermore, ADC measurements were also sensitive to administration of a bronchodilator, suggesting reduction in gas-trapping in patients with COPD.[138]

A number of key limitations have hampered the use of hyperpolarized noble gas MRI in the clinic, which has restricted this technique to a few specialized research centres. These approaches incur relatively high costs due to the need for inhale contrast agents and require access to multinuclear MR hardware and analysis software. Furthermore, except for in the United Kingdom, hyperpolarized noble gas MRI is not yet approved for clinical use in Asia, North America or the rest of the European Union despite numerous demonstrations of safety and efficacy in chronic lung disease patients.[139,140] With this in mind, there has been growing interest for the development and implementation of non-contrast enhanced pulmonary MRI approaches to overcome these challenges specifically with resource accessibility.

1.5.2.2 Non-contrast Enhanced Functional Imaging

As mentioned above, non-contrast enhanced methods to indirectly evaluate lung function can be performed by measuring tissue density or deformation changes as the lungs expand and contract using structural imaging. Ventilation-weighted lung images can be extracted via structural CT or MR images while patients free-breathe or at multiple lung volumes, including full inspiration and full expiration. Ventilation information from structural images is performed by exploiting the aggregate signal changes caused by density variations in the lung during breathing.

Computed Tomography

Thoracic CT images acquired at different phases in the breathing cycle (i.e. full expiration and full inspiration), can be used to generate and quantify the expansion of lung tissue regionally using non-rigid or deformable image registration methods.[141-144] Imaging biomarkers of ventilation using lung deformation information include measures of local volume change, estimates of tissue compliance and deformation biomarkers during breathing. Local volume changes, such as during normal tidal breathing (specific-ventilation),[30] can be measured and generated using a density-based method,[142] which

quantifies the difference in lung tissue density at different lung volumes as air enters and leaves voxels.[145] This measurement reflects the quantity of inhaled gas moving into the lung during normal breathing. Alternatively, local lung tissue expansion can be described using the deformation field maps that are generated from the co-registration of images. More specifically, the determinant of the Jacobian matrix that is generated from the deformation field vector map can be used to quantify specific volume,[146] which has previously been shown to reflect regional ventilation.[147] This imaging biomarker has been evaluated in patients with asthma[148,149] and COPD,[150-152] where abnormal lung biomechanical properties were observed in severe asthmatics, which may be due to gas-trapping.[149] In COPD patients, imaging biomarkers of lung biomechanical properties were related to clinical outcomes,[151] disease severity[150] and progression.[152] The techniques can also be applied to four-dimensional CT (4DCT),[153-155] where images are reconstructed at many different points during the respiratory phase, and changes in volume can be measured throughout the entire process. This technique was used to show that deformation throughout the respiratory cycle is nonlinear[156] and that this deformation is greater in asthmatics than in healthy subjects.[148] In COPD patients, 4DCT ventilation measured using the density and Jacobian based methods were shown to be related to emphysema.[157]

An alternative approach using parametric response maps (PRM) of co-registered inspiratory-expiratory CT, which was first developed as a voxel-based method for improving the sensitivity of diffusion-MRI data for identifying early therapeutic response in glioma patients,[158] has recently been used to evaluate COPD patients.[159] In COPD, co-registered inspiratory-expiratory CT in addition to well-established density thresholds,[61,160,161] can be used to classify lung tissue into normal, emphysematous and gas-trapping regions.[159] In other words, PRM provides a way to classify lung tissue based on the presence of pulmonary air. To generate PRM, voxel-wise comparisons are performed, where co-registered inspiration and expiration images are used to classify lung tissue into four categories based on expiration and inspiration thresholds as previously described:[159] 1) inspiration >-950HU and expiration >-856HU (normal tissue [green]), 2) inspiration >-950HU and expiration <-856HU (gas-trapping [yellow]), 3) inspiration <-950HU and expiration <-856HU (emphysema [red]), and, 4) inspiration <-950HU and expiration >-

856HU, as shown in **Figure 1-12**. The fourth category of voxels was hypothesized to reflect noise in the data due to image registration error.[159] As shown in **Figure 1-12**, with increasing severity of airflow limitation, regions of PRM-normal tissue are reduced while both lung regions of PRM-gas-trapping and PRM-emphysema increase.

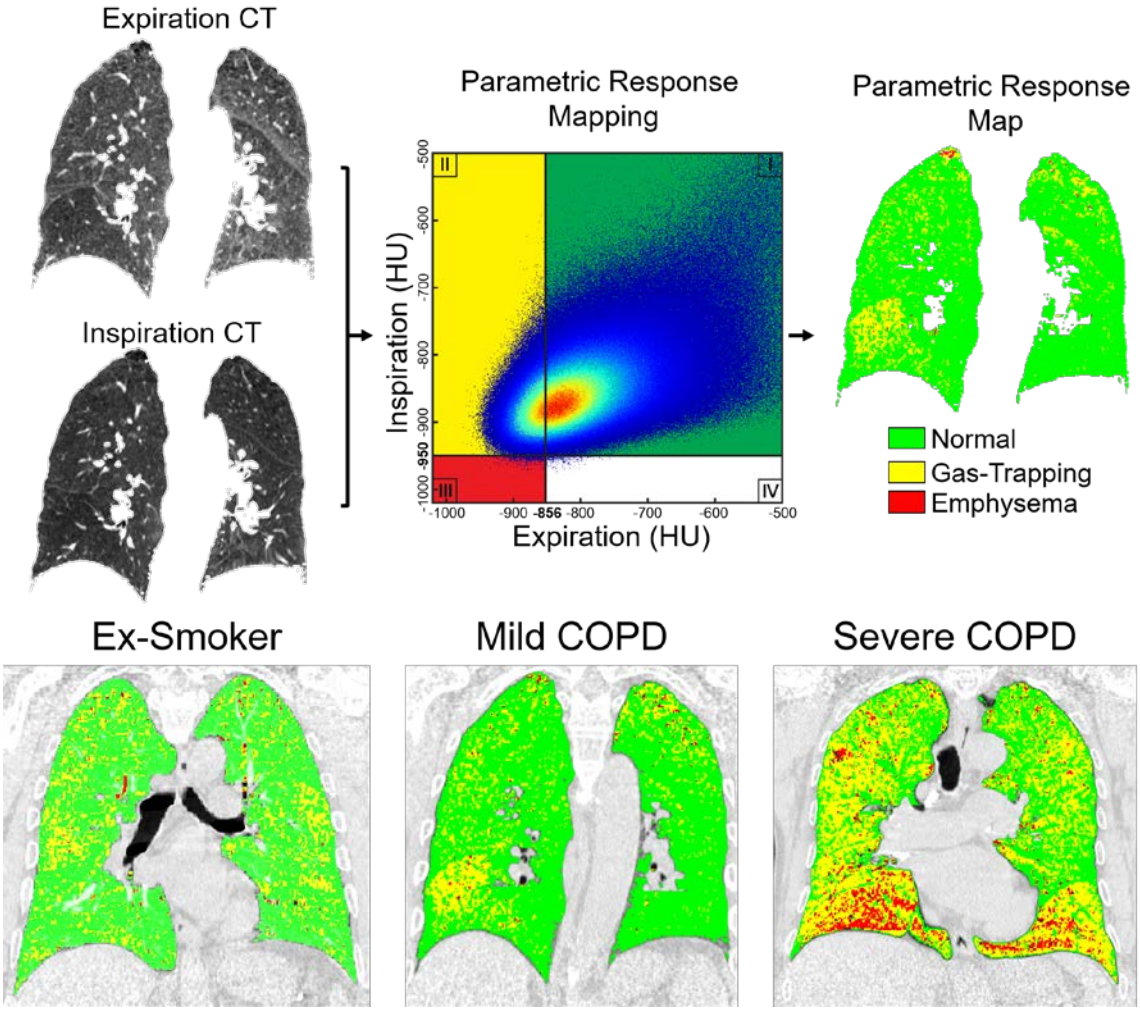

Figure 1-12 Parametric Response Mapping of Co-registered Inspiratory-Expiratory CT Images
Above: A schematic of the generation of PRM. Below: PRM co-registered to CT images of a representative ex-smoker without COPD, mild COPD, and severe COPD subjects.

Although PRM measurements of gas trapping, suggested to be related to "functional" small airway disease, have been shown to be reproducible over short periods of time,[162] differentiated current and former smokers with and without COPD,[163] correlated with pulmonary function,[159] and were associated with longitudinal changes in FEV_1,[164] the

clinical relevance and etiology of this measurement is uncertain and has not yet been pathologically validated.

Magnetic Resonance Imaging

Similar to non-contrast enhanced CT, aggregate signals are extracted from multiple lung volumes of free-breathing ^{1}H MR images to detect changes in air volume regionally within the lung, without the use of ionizing radiation. The first approach, pioneered in 2006, involved a series of coronal images acquired over a time period of one minute during slow, maximum amplitude respiration, where fractional ventilation weighted images of the lung (FV) were generated from signal intensity differences between full inspiration (SI_{insp}) and full expiration (SI_{exp}), as shown below in **Equation 1-4**:[165]

$$FV = \frac{SI_{exp} - SI_{insp}}{SI_{exp}} \tag{1-4}$$

This method was originally developed and used to evaluate healthy volunteers, asthmatics, and cystic fibrosis patients, along with other lung disease patients. Visually obvious ventilation defects appeared in the lung disease patients as compared to the healthy subjects and these ventilation defects were correlated with pulmonary function tests.[165]

Since the original development using ^{1}H MRI to derive surrogate measurements of ventilation, a variety of approaches have been investigated. Multiple lung volumes breath-hold approaches where whole lung MR images are acquired and co-registered to measure signal intensity differences have been developed,[75,166,167] using conventional ^{1}H MRI[167] or UTE MRI.[75,166] Conventional ^{1}H MR signal intensity differences were related to pulmonary function tests in asthma and COPD patients with emphysema, and that these differences were related to ^{3}He MR signal intensities.[167] Furthermore, measurements of ^{1}H MR signal differences generated from dynamic proton maps (DPM) using multi-volume UTE MRI were greater in healthy volunteers as compared to asthma subjects, and correlated with lung function and CT radiodensity measurements.[75]

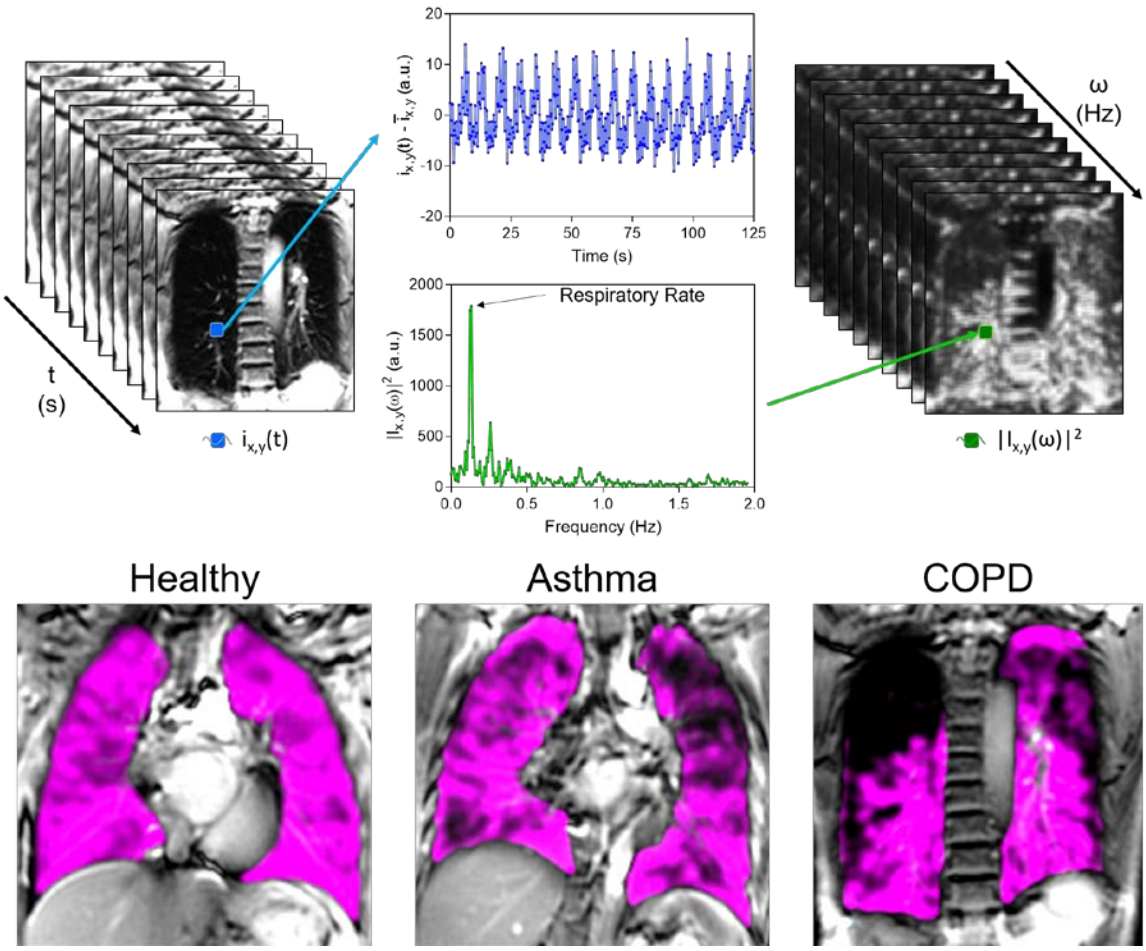

Figure 1-13 Fourier Decomposition of Free-breathing Pulmonary ^{1}H MR Images
Above: A schematic of generating FDMR ventilation-weighted images. Below: FDMR ventilation-weighted images (magenta) co-registered to conventional ^{1}H MR coronal images (gray) for a healthy, asthmatic, and COPD subject.

Fourier-decomposition of free-breathing ^{1}H MRI (FDMRI) is another alternative approach that exploits non-rigid registration and fast pulmonary MR image acquisitions protocols to generate ventilation-weighted images of a single slice coronal image.[168,169] As shown in **Figure 1-13**, this technique involves acquiring a time series of free-breathing ^{1}H MR images and after performing deformable image registration, fast Fourier transforms (FFT) are performed on the signal intensity oscillation pattern (caused by the compression and expansion of the lung parenchyma) generated from the pulmonary voxel intensities in the co-registered free breathing ^{1}H MR images. The magnitude of the first ventilation harmonic (which corresponds to the respiratory rate) is determined for each and every voxel and this is used to generate the ventilation-weighted image. As can be seen when

comparing **Figure 1-11** and **Figure 1-13**, FDMRI methods can provide similar spatial information about ventilation as compared to hyperpolarized noble gas MR methods.

Reproducibility of FDMRI has previously been investigated in healthy volunteers while ventilation abnormalities measured using FDMRI in porcine models have shown to be spatially localized with SPECT-CT[170] and hyperpolarized ^{3}He MRI[171] ventilation defects. Thus far, in asthma and COPD, limited work has been done using FDMRI. Furthermore, while the MRI techniques described above acquire images in breath-hold at multiple lung volumes[166,167] or free-breathing images for a single slice,[168,169] development of approaches that provide a way to generate whole lung functional maps that probe functional abnormalities using conventional equipment and pulse sequences while patients are free-breathing has been limited. These methods, although requiring sophisticated post-processing methods, open the opportunity for functional lung imaging on clinically available MR systems for serial lung function measurements without the dependence of inhaled gases in lung disease patients.

1.6 Thesis Hypotheses and Objectives

The diagnosis and monitoring of pulmonary diseases, such as asthma and COPD, is primarily done using pulmonary function tests. These tests, although inexpensive and easily implemented, are limited because they only provide a measure of global airflow obstruction and provide no regional information, potentially concealing independent underlying pathologies. The limitations of spirometry and current therapies for lung disease patients have motivated the development of pulmonary imaging approaches. Pulmonary imaging has the potential to provide regional measurements of lung function for image-guided treatments and longitudinal monitoring. Inhaled hyperpolarized noble gas MRI has previously been shown to provide a way to quantify pulmonary ventilation by visualizing lung regions accessed by gas during a breath-hold, and alternatively, regions that are not accessed coined “ventilation defects.” Despite the strong foundation and many advantages this contrast enhanced technique has to offer research and patient care, clinical translation has been limited in part due to the need for specialized equipment, including multinuclear-MR hardware and polarizers, and personnel. Thus, the overarching objective

of this thesis was to develop and evaluate imaging biomarkers of pulmonary structure and function using MRI and CT without the use of exogenous contrast agents or specialized equipment. The objectives and hypotheses specific to each chapter are described below.

In **Chapter 2**, our objective was to develop and directly compare CT parametric response maps with ^{3}He MRI ventilation measurements of gas-trapping and emphysema in ex-smokers with and without COPD. We wanted to determine the quantitative and spatial relationships of PRM gas-trapping and PRM emphysema measurements with MRI measurements of parenchymal tissue integrity and ventilation, because these are clinically-important imaging findings and phenotypes of COPD. We hypothesized that ^{3}He ventilation defects would be spatially related to PRM measurements of both gas-trapping and emphysema.

In **Chapter 3**, our objective was to develop and compare pulmonary ventilation abnormalities derived from Fourier decomposition of free-breathing ^{1}H magnetic resonance imaging with ^{3}He MRI in subjects with COPD and bronchiectasis. Based on previous work, we hypothesized that ventilation defects measured using FDMRI and ^{3}He MRI would be spatially and quantitatively correlated in subjects with COPD and those with bronchiectasis.

In **Chapter 4**, based on the FDMR biomarkers developed in patients with COPD and bronchiectasis, our objective was to evaluate ventilation heterogeneity in patients with severe asthma, both pre- and post-salbutamol as well as post-methacholine challenge using FDMRI and ^{3}He MRI. Based on previous work, we hypothesized that FDMRI VDP would be quantitatively related to ^{3}He MRI VDP and show similar responses to both methacholine and salbutamol as compared to baseline measurements in patients with severe asthma.

In **Chapter 5**, based on the free-breathing MR approaches previously developed, our objective was to develop a whole-lung free breathing pulmonary ^{1}H MRI technique to measure regional specific-ventilation and evaluate asthmatics and healthy volunteers. We then wanted to compare ^{1}H MRI specific-ventilation with ^{3}He MRI ventilation in healthy and asthmatic participants, and, determine the relationships between ^{1}H MRI specific-ventilation with both ^{3}He MRI and pulmonary function measurements. We hypothesized

that dynamic whole-lung MR specific-ventilation would be related to static ventilation measurements derived from ^{3}He MRI as well as pulmonary function tests.

In **Chapter 6**, an overview and summary of the important findings and conclusions of **Chapters 2-5** is provided. The study specific and general limitations of these studies will be discussed and some potential solutions are suggested. The thesis concludes with an outline of future studies that can build on the work presented in this thesis.

1.7 References

(1) World Health Organization. Global Health Estimates 2014 Summary Tables: Death by Cause, Age and Sex, 2000-2012. (2014). <http://www.who.int/healthinfo/global_burden_disease/en/>.

(2) Soriano, J. B. *et al.* Global, regional, and national deaths, prevalence, disability-adjusted life years, and years lived with disability for chronic obstructive pulmonary disease and asthma, 1990-2015: a systematic analysis for the Global Burden of Disease Study 2015. *Lancet Respiratory Medicine* 2017; 5: 691-706.

(3) Statistics Canada. (ed CANSIM) (Statistics Canada, Ottawa, Ontario, 2015).

(4) Canadian Institute for Health Information. Health Indicators 2008. (CIHI, Ottawa, 2008).

(5) Mittmann, N. *et al.* The cost of moderate and severe COPD exacerbations to the Canadian healthcare system. *Respir Med* 2008; 102: 413-421.

(6) Ontario Lung Association. Your Lungs, Your Life: Insights and Solutions to Lung Health in Ontario. (Ontario Lung Association, 2011).

(7) Pauwels, R. A. *et al.* Global strategy for the diagnosis, management, and prevention of chronic obstructive pulmonary disease. NHLBI/WHO Global Initiative for Chronic Obstructive Lung Disease (GOLD) Workshop summary. *Am J Respir Crit Care Med* 2001; 163: 1256-1276.

(8) West, J. B. *Respiratory Physiology the Essentials*. Ninth edn, (Lippincott Williams & Wilkins, 2012).

(9) Silverthorn, D. U. *Human Physiology An Integrated Approach 6th Edition*. (Pearson, 2013).

(10) Ochs, M. *et al.* The number of alveoli in the human lung. *Am J Respir Crit Care Med* 2004; 169: 120-124.

(11) Global Initiative for Asthma. *Global Strategy for Asthma Management and Prevention*, <www.ginasthma.org> (2016).

(12) Saetta, M. & Turato, G. Airway pathology in asthma. *Eur Respir J Suppl* 2001; 34: 18s-23s.

(13) Hamid, Q. *et al.* Inflammation of small airways in asthma. *J Allergy Clin Immunol* 1997; 100: 44-51.

(14) Crapo, R. O. *et al.* Guidelines for methacholine and exercise challenge testing-1999. This official statement of the American Thoracic Society was adopted by the

ATS Board of Directors, July 1999. *Am J Respir Crit Care Med* 2000; 161: 309-329.

(15) Health, U. D. o. & Services, H. The health consequences of smoking: a report of the Surgeon General. *Atlanta, GA: US Department of Health and Human Services, Centers for Disease Control and Prevention, National Center for Chronic Disease Prevention and Health Promotion, Office on Smoking and Health* 2004; 62.

(16) Fletcher, C. & Peto, R. The natural history of chronic airflow obstruction. *Br Med J* 1977; 1: 1645-1648.

(17) Vestbo, J. *et al.* Global strategy for the diagnosis, management, and prevention of chronic obstructive pulmonary disease: GOLD executive summary. *Am J Respir Crit Care Med* 2013; 187: 347-365.

(18) Mullen, J. B., Wright, J. L., Wiggs, B. R., Pare, P. D. & Hogg, J. C. Reassessment of inflammation of airways in chronic bronchitis. *Br Med J (Clin Res Ed)* 1985; 291: 1235-1239.

(19) Hogg, J. C. Pathophysiology of airflow limitation in chronic obstructive pulmonary disease. *Lancet* 2004; 364: 709-721.

(20) Saetta, M. *et al.* Inflammatory cells in the bronchial glands of smokers with chronic bronchitis. *Am J Respir Crit Care Med* 1997; 156: 1633-1639.

(21) Hogg, J. C., Macklem, P. T. & Thurlbeck, W. M. Site and nature of airway obstruction in chronic obstructive lung disease. *N Engl J Med* 1968; 278: 1355-1360.

(22) Mead, J. The lung's "quiet zone". *N Engl J Med* 1970; 282: 1318-1319.

(23) Woods, J. C. *et al.* Hyperpolarized 3He diffusion MRI and histology in pulmonary emphysema. *Magn Reson Med* 2006; 56: 1293-1300.

(24) Snider, G. The definition of emphysema; report of a National Heart, Lung and Blood Institute. Division of Lung Diseases. Workshop. *Am Rev Respir Dis* 1985; 132: 182-185.

(25) Thurlbeck, W. M. & Muller, N. L. Emphysema: definition, imaging, and quantification. *AJR Am J Roentgenol* 1994; 163: 1017-1025.

(26) Smith, B. M. *et al.* Pulmonary emphysema subtypes on computed tomography: the MESA COPD study. *Am J Med* 2014; 127: 94 e97-23.

(27) Clayton, N. Review Series: Lung function made easy: Assessing lung size. *Chronic respiratory disease* 2007; 4: 151-157.

(28) Miller, M. R. *et al.* Standardisation of spirometry. *Eur respir J* 2005; 26: 319-338.

(29) Wanger, J. *et al.* Standardisation of the measurement of lung volumes. *European Respiratory Journal* 2005; 26: 511.

(30) Lewis, S. M., Evans, J. W. & Jalowayski, A. A. Continuous distributions of specific ventilation recovered from inert gas washout. *J Appl Physiol Respir Environ Exerc Physiol* 1978; 44: 416-423.

(31) Macintyre, N. *et al.* Standardisation of the single-breath determination of carbon monoxide uptake in the lung. *European Respiratory Journal* 2005; 26: 720-735.

(32) Robertson, J. S., Siri, W. E. & Jones, H. B. Lung ventilation patterns determined by analysis of nitrogen elimination rates; use of mass spectrometer as a continuous gas analyzer. *J Clin Invest* 1950; 29: 577-590.

(33) Becklake, M. R. A new index of the intrapulmonary mixture of inspired air. *Thorax* 1952; 7: 111-116.

(34) Robinson, P. D. *et al.* Consensus statement for inert gas washout measurement using multiple- and single-breath tests. *European Respiratory Journal* 2013; 41: 507-522.

(35) Busse, W. W. Asthma diagnosis and treatment: filling in the information gaps. *J Allergy Clin Immunol* 2011; 128: 740-750.

(36) Celli, B. R. The importance of spirometry in COPD and asthma: effect on approach to management. *Chest* 2000; 117: 15S-19S.

(37) Vestbo, J. *et al.* Evaluation of COPD Longitudinally to Identify Predictive Surrogate End-points (ECLIPSE). *Eur Respir J* 2008; 31: 869-873.

(38) Cerveri, I. *et al.* Underestimation of airflow obstruction among young adults using FEV(1)/FVC < 70% as a fixed cut-off: a longitudinal evaluation of clinical and functional outcomes. *Thorax* 2008; 63: 1040-1045.

(39) Enright, P. L. & Kaminsky, D. A. Strategies for screening for chronic obstructive pulmonary disease. *Respir Care* 2003; 48: 1194-1201; discussion 1201-1193.

(40) Burgel, P. R. The role of small airways in obstructive airway diseases. *Eur Respir Rev* 2011; 20: 23-33.

(41) Macklem, P. T. & Mead, J. Resistance of central and peripheral airways measured by a retrograde catheter. *J Appl Physiol* 1967; 22: 395-401.

(42) Tulic, M. K., Christodoulopoulos, P. & Hamid, Q. Small airway inflammation in asthma. *Respir Res* 2001; 2: 333-339.

(43) Brenner, D. J. & Hall, E. J. Computed tomography--an increasing source of radiation exposure. *N Engl J Med* 2007; 357: 2277-2284.

(44) Hodson, M. E., Simon, G. & Batten, J. C. Radiology of uncomplicated asthma. *Thorax* 1974; 29: 296-303.

(45) Rebuck, A. S. Radiological aspects of severe asthma. *Australas Radiol* 1970; 14: 264-268.

(46) Thurlbeck, W. M. & Simon, G. Radiographic appearance of the chest in emphysema. *AJR Am J Roentgenol* 1978; 130: 429-440.

(47) Pipavath, S. N. J., Schmidt, R. A., Takasugi, J. E. & Godwin, J. D. Chronic Obstructive Pulmonary Disease: Radiology-Pathology Correlation. *Journal of Thoracic Imaging* 2009; 24: 171-180.

(48) Rosenblum, L. J. *et al.* Density patterns in the normal lung as determined by computed tomography. *Radiology* 1980; 137: 409-416.

(49) Haaga, J. R. & Boll, D. *Computed tomography & magnetic resonance imaging of the whole body*. (Elsevier Health Sciences, 2008).

(50) Litmanovich, D. E., Hartwick, K., Silva, M. & Bankier, A. A. Multidetector computed tomographic imaging in chronic obstructive pulmonary disease: emphysema and airways assessment. *Radiol Clin North Am* 2014; 52: 137-154.

(51) Goldman, L. W. Principles of CT and CT technology. *Journal of nuclear medicine technology* 2007; 35: 115-128.

(52) Houndfield, G. N. Computerized Transverse Axial Scanning (Tomography) .1. Description of System. *British Journal of Radiology* 1973; 46: 1016-1022.

(53) Mettler, F. A., Jr., Huda, W., Yoshizumi, T. T. & Mahesh, M. Effective doses in radiology and diagnostic nuclear medicine: a catalog. *Radiology* 2008; 248: 254-263.

(54) Lambert, L., Banerjee, R., Votruba, J., El-Lababidi, N. & Zeman, J. Ultra-low-dose CT Imaging of the Thorax: Decreasing the Radiation Dose by One Order of Magnitude. *Indian J Pediatr* 2016.

(55) Willemink, M. J. *et al.* Iterative reconstruction techniques for computed tomography part 2: initial results in dose reduction and image quality. *Eur Radiol* 2013; 23: 1632-1642.

(56) Newman, K. B., Lynch, D. A., Newman, L. S., Ellegood, D. & Newell, J. D. Quantitative Computed-Tomography Detects Air Trapping Due to Asthma. *Chest* 1994; 106: 105-109.

(57) Aysola, R. S. *et al.* Airway Remodeling Measured by Multidetector CT Is Increased in Severe Asthma and Correlates With Pathology. *Chest* 2008; 134: 1183-1191.

(58) Okazawa, M. *et al.* Human airway narrowing measured using high resolution computed tomography. *Am J Respir Crit Care Med* 1996; 154: 1557-1562.

(59) Little, S. A. *et al.* High resolution computed tomographic assessment of airway wall thickness in chronic asthma: reproducibility and relationship with lung function and severity. *Thorax* 2002; 57: 247-253.

(60) Awadh, N., Muller, N. L., Park, C. S., Abboud, R. T. & FitzGerald, J. M. Airway wall thickness in patients with near fatal asthma and control groups: assessment with high resolution computed tomographic scanning. *Thorax* 1998; 53: 248-253.

(61) Busacker, A. *et al.* A multivariate analysis of risk factors for the air-trapping asthmatic phenotype as measured by quantitative CT analysis. *Chest* 2009; 135: 48-56.

(62) Hackx, M., Bankier, A. A. & Gevenois, P. A. Chronic Obstructive Pulmonary Disease: CT Quantification of Airways Disease. *Radiology* 2012; 265: 34-48.

(63) Nakano, Y. *et al.* Quantitative assessment of airway remodeling using high-resolution CT. *Chest* 2002; 122: 271s-275s.

(64) Hayhurst, M. D. *et al.* Diagnosis of pulmonary emphysema by computerised tomography. *Lancet* 1984; 2: 320-322.

(65) Klein, J. S., Gamsu, G., Webb, W. R., Golden, J. A. & Muller, N. L. High-resolution CT diagnosis of emphysema in symptomatic patients with normal chest radiographs and isolated low diffusing capacity. *Radiology* 1992; 182: 817-821.

(66) Müller, N., Staples, C., Miller, R. & Abboud, R. " Density mask". An objective method to quantitate emphysema using computed tomography. *Chest* 1988; 94: 782.

(67) Uppaluri, R., Mitsa, T., Sonka, M., Hoffman, E. A. & McLennan, G. Quantification of pulmonary emphysema from lung computed tomography images. *Am J Respir Crit Care Med* 1997; 156: 248-254.

(68) Smith-Bindman, R. *et al.* Use of diagnostic imaging studies and associated radiation exposure for patients enrolled in large integrated health care systems, 1996-2010. *JAMA* 2012; 307: 2400-2409.

(69) Albertine, K. Structural organization and quantitative morphology of the lung. *Application of magnetic resonance to the study of lung. Futura, Armonk, New York, USA* 1996; 73-114.

(70) Bergin, C. J., Glover, G. M. & Pauly, J. Magnetic resonance imaging of lung parenchyma. *J Thorac Imaging* 1993; 8: 12-17.

(71) Bergin, C. J., Noll, D. C., Pauly, J. M., Glover, G. H. & Macovski, A. MR imaging of lung parenchyma: a solution to susceptibility. *Radiology* 1992; 183: 673-676.

(72) Ohno, Y. *et al.* T2* measurements of 3-T MRI with ultrashort TEs: capabilities of pulmonary function assessment and clinical stage classification in smokers. *AJR Am J Roentgenol* 2011; 197: W279-285.

(73) Ohno, Y. *et al.* Pulmonary MR imaging with ultra-short TEs: utility for disease severity assessment of connective tissue disease patients. *Eur J Radiol* 2013; 82: 1359-1365.

(74) Ohno, Y. *et al.* Pulmonary High-Resolution Ultrashort TE MR Imaging: Comparison With Thin-Section Standard- and Low-Dose Computed Tomography for the Assessment of Pulmonary Parenchyma Diseases. *Journal of Magnetic Resonance Imaging* 2016; 43: 512-532.

(75) Sheikh, K. *et al.* Ultrashort echo time MRI biomarkers of asthma. *J Magn Reson Imaging* 2017; 45: 1204-1215.

(76) Ma, W. *et al.* Ultra-short echo-time pulmonary MRI: evaluation and reproducibility in COPD subjects with and without bronchiectasis. *J Magn Reson Imaging* 2015; 41: 1465-1474.

(77) Musch, G. & Venegas, J. G. Positron emission tomography imaging of regional lung function. *Minerva Anestesiologica* 2006; 72: 363-367.

(78) King, G. G., Eberl, S., Salome, C. M., Meikle, S. R. & Woolcock, A. J. Airway closure measured by a technegas bolus and SPECT. *Am J Respir Crit Care Med* 1997; 155: 682-688.

(79) Mishkin, F. & Wagner, H. N., Jr. Regional abnormalities in pulmonary arterial blood flow during acute asthmatic attacks. *Radiology* 1967; 88: 142-144.

(80) Farrow, C. E. *et al.* Airway closure on imaging relates to airway hyperresponsiveness and peripheral airway disease in asthma. *J Appl Physiol (1985)* 2012; 113: 958-966.

(81) Sovijarvi, A. R., Poyhonen, L., Kellomaki, L. & Muittari, A. Effects of acute and long-term bronchodilator treatment on regional lung function in asthma assessed with krypton-81m and technetium-99m-labelled macroaggregates. *Thorax* 1982; 37: 516-520.

(82) Venegas, J. G. *et al.* Self-organized patchiness in asthma as a prelude to catastrophic shifts. *Nature* 2005; 434: 777-782.

(83) Bajc, M. *et al.* Grading obstructive lung disease using tomographic pulmonary scintigraphy in patients with chronic obstructive pulmonary disease (COPD) and long-term smokers. *Ann Nucl Med* 2015; 29: 91-99.

(84) Norberg, P. *et al.* Quantitative lung SPECT applied on simulated early COPD and humans with advanced COPD. *EJNMMI Res* 2013; 3: 28.

(85) Suga, K., Iwanaga, H., Tokuda, O., Okada, M. & Matsunaga, N. Intrabullous ventilation in pulmonary emphysema: assessment with dynamic xenon-133 gas SPECT. *Nucl Med Commun* 2012; 33: 371-378.

(86) Brudin, L. H. *et al.* Regional structure-function correlations in chronic obstructive lung disease measured with positron emission tomography. *Thorax* 1992; 47: 914-921.

(87) Kong, X. *et al.* Xenon-Enhanced Dual-Energy CT Lung Ventilation Imaging: Techniques and Clinical Applications. *American Journal of Roentgenology* 2014; 202: 309-317.

(88) Chae, E. J. *et al.* Xenon Ventilation Imaging Using Dual-Energy Computed Tomography in Asthmatics Initial Experience. *Investigative Radiology* 2010; 45: 354-361.

(89) Goo, H. W. & Yu, J. H. Redistributed Regional Ventilation after the Administration of a Bronchodilator Demonstrated on Xenon-Inhaled Dual-Energy CT in a Patient with Asthma. *Korean Journal of Radiology* 2011; 12: 386-389.

(90) Kim, W. W. *et al.* Xenon-Enhanced Dual-Energy CT of Patients With Asthma: Dynamic Ventilation Changes After Methacholine and Salbutamol Inhalation. *American Journal of Roentgenology* 2012; 199: 975-981.

(91) Park, E. A. *et al.* Chronic Obstructive Pulmonary Disease: Quantitative and Visual Ventilation Pattern Analysis at Xenon Ventilation CT Performed by Using a Dual-Energy Technique. *Radiology* 2010; 256: 985-997.

(92) Edelman, R. R., Hatabu, H., Tadamura, E., Li, W. & Prasad, P. V. Noninvasive assessment of regional ventilation in the human lung using oxygen-enhanced magnetic resonance imaging. *Nature Medicine* 1996; 2: 1236-1239.

(93) Ohno, Y. *et al.* Asthma: Comparison of Dynamic Oxygen-enhanced MR Imaging and Quantitative Thin-Section CT for Evaluation of Clinical Treatment. *Radiology* 2014; 273: 907-916.

(94) Ohno, Y. *et al.* Oxygen-enhanced MRI vs. quantitatively assessed thin-section CT: Pulmonary functional loss assessment and clinical stage classification of asthmatics. *European Journal of Radiology* 2011; 77: 85-91.

(95) Ohno, Y. *et al.* Dynamic oxygen-enhanced MRI reflects diffusing capacity of the lung. *Magnetic Resonance in Medicine* 2002; 47: 1139-1144.

(96) Ohno, Y. *et al.* Oxygen-enhanced magnetic resonance imaging versus computed tomography - Multicenter study for clinical stage classification of smoking-related

chronic obstructive pulmonary disease. *American Journal of Respiratory and Critical Care Medicine* 2008; 177: 1095-1102.

(97) Kuethe, D. O., Caprihan, A., Fukushima, E. & Waggoner, R. A. Imaging lungs using inert fluorinated gases. *Magnetic Resonance in Medicine* 1998; 39: 85-88.

(98) Halaweish, A. F. *et al.* Perfluoropropane Gas as a Magnetic Resonance Lung Imaging Contrast Agent in Humans. *Chest* 2013; 144: 1300-1310.

(99) Couch, M. J. *et al.* Pulmonary Ultrashort Echo Time F-19 MR Imaging with Inhaled Fluorinated Gas Mixtures in Healthy Volunteers: Feasibility. *Radiology* 2013; 269: 903-909.

(100) Albert, M. S. *et al.* Biological Magnetic-Resonance-Imaging Using Laser Polarized Xe-129. *Nature* 1994; 370: 199-201.

(101) Kauczor, H. U. *et al.* Normal and abnormal pulmonary ventilation: Visualization at hyperpolarized He-3 MR imaging. *Radiology* 1996; 201: 564-568.

(102) Saam, B. T. Magnetic resonance imaging with laser-polarized noble gases. *Nat Med* 1996; 2: 358-359.

(103) Kauczor, H.-U. *MRI of the Lung*. (2009).

(104) Shea, D. A. & Morgan, D.

(105) Stewart, N. J., Norquay, G., Griffiths, P. D. & Wild, J. M. Feasibility of human lung ventilation imaging using highly polarized naturally abundant xenon and optimized three-dimensional steady-state free precession. *Magnetic Resonance in Medicine* 2015; 74: 346-352.

(106) Kirby, M. *et al.* Hyperpolarized 3He magnetic resonance functional imaging semiautomated segmentation. *Acad Radiol* 2012; 19: 141-152.

(107) de Lange, E. E. *et al.* Changes in regional airflow obstruction over time in the lungs of patients with asthma: evaluation with 3He MR imaging. *Radiology* 2009; 250: 567-575.

(108) Mathew, L. *et al.* Hyperpolarized 3He magnetic resonance imaging of chronic obstructive pulmonary disease: reproducibility at 3.0 tesla. *Acad Radiol* 2008; 15: 1298-1311.

(109) Kirby, M. *et al.* Hyperpolarized 3He and 129Xe MR imaging in healthy volunteers and patients with chronic obstructive pulmonary disease. *Radiology* 2012; 265: 600-610.

(110) de Lange, E. E. *et al.* Evaluation of asthma with hyperpolarized helium-3 MRI: correlation with clinical severity and spirometry. *Chest* 2006; 130: 1055-1062.

(111) Fain, S. B. *et al.* Evaluation of structure-function relationships in asthma using multidetector CT and hyperpolarized He-3 MRI. *Academic Radiology* 2008; 15: 753-762.

(112) Tgavalekos, N. T. *et al.* Relationship between airway narrowing, patchy ventilation and lung mechanics in asthmatics. *European Respiratory Journal* 2007; 29: 1174-1181.

(113) de Lange, E. E. *et al.* The variability of regional airflow obstruction within the lungs of patients with asthma: Assessment with hyperpolarized helium-3 magnetic resonance imaging. *Journal of Allergy and Clinical Immunology* 2007; 119: 1072-1078.

(114) Wheatley, A. *et al.* Hyperpolarized helium-3 magnetic resonance imaging of asthma: Short-term reproducibility - art. no. 69161X. *Medical Imaging 2008: Physiology, Function, and Structure from Medical Images* 2008; 6916: X9161-X9161.

(115) Altes, T. A. *et al.* Hyperpolarized 3He MR lung ventilation imaging in asthmatics: preliminary findings. *J Magn Reson Imaging* 2001; 13: 378-384.

(116) Tzeng, Y. S., Lutchen, K. & Albert, M. The difference in ventilation heterogeneity between asthmatic and healthy subjects quantified using hyperpolarized He-3 MRI. *Journal of Applied Physiology* 2009; 106: 813-822.

(117) Teague, W. G., Tustison, N. J. & Altes, T. A. Ventilation heterogeneity in asthma. *Journal of Asthma* 2014; 51: 677-684.

(118) Svenningsen, S. *et al.* What are ventilation defects in asthma? *Thorax* 2014; 69: 63-71.

(119) Svenningsen, S., Nair, P., Guo, F., McCormack, D. G. & Parraga, G. Is ventilation heterogeneity related to asthma control? *Eur Respir J* 2016.

(120) Kirby, M. *et al.* COPD: Do Imaging Measurements of Emphysema and Airway Disease Explain Symptoms and Exercise Capacity? *Radiology* 2015; 277: 872-880.

(121) Kirby, M. *et al.* Pulmonary ventilation visualized using hyperpolarized helium-3 and xenon-129 magnetic resonance imaging: differences in COPD and relationship to emphysema. *J Appl Physiol (1985)* 2013; 114: 707-715.

(122) Kirby, M., Pike, D., Coxson, H. O., McCormack, D. G. & Parraga, G. Hyperpolarized (3)He ventilation defects used to predict pulmonary exacerbations in mild to moderate chronic obstructive pulmonary disease. *Radiology* 2014; 273: 887-896.

(123) Svenningsen, S. *et al.* Hyperpolarized (3) He and (129) Xe MRI: differences in asthma before bronchodilation. *J Magn Reson Imaging* 2013; 38: 1521-1530.

(124) Kirby, M. *et al.* Chronic obstructive pulmonary disease: quantification of bronchodilator effects by using hyperpolarized (3)He MR imaging. *Radiology* 2011; 261: 283-292.

(125) Samee, S. *et al.* Imaging the lungs in asthmatic patients by using hyperpolarized helium-3 magnetic resonance: assessment of response to methacholine and exercise challenge. *J Allergy Clin Immunol* 2003; 111: 1205-1211.

(126) Mugler III, J. in *Proceedings of the 6th annual meeting of ISMRM, Sydney, Australia.* 1904.

(127) Saam, B. T. *et al.* MR imaging of diffusion of He-3 gas in healthy and diseased lungs. *Magnetic Resonance in Medicine* 2000; 44: 174-179.

(128) Morbach, A. E. *et al.* Diffusion-weighted MRI of the lung with hyperpolarized helium-3: a study of reproducibility. *J Magn Reson Imaging* 2005; 21: 765-774.

(129) Parraga, G. *et al.* Hyperpolarized 3He ventilation defects and apparent diffusion coefficients in chronic obstructive pulmonary disease: preliminary results at 3.0 Tesla. *Invest Radiol* 2007; 42: 384-391.

(130) Diaz, S. *et al.* Validity of apparent diffusion coefficient hyperpolarized 3He-MRI using MSCT and pulmonary function tests as references. *Eur J Radiol* 2009; 71: 257-263.

(131) Kirby, M. *et al.* Hyperpolarized 3He and 129Xe magnetic resonance imaging apparent diffusion coefficients: physiological relevance in older never- and ex-smokers. *Physiol Rep* 2014; 2.

(132) Wang, C. *et al.* Assessment of the lung microstructure in patients with asthma using hyperpolarized 3He diffusion MRI at two time scales: comparison with healthy subjects and patients with COPD. *J Magn Reson Imaging* 2008; 28: 80-88.

(133) Trampel, R. *et al.* Diffusional kurtosis imaging in the lung using hyperpolarized 3He. *Magn Reson Med* 2006; 56: 733-737.

(134) Fain, S. *et al.* in *Proc Intl Soc Mag Reson Med.* 335.

(135) Costella, S. *et al.* Regional pulmonary response to a methacholine challenge using hyperpolarized (3)He magnetic resonance imaging. *Respirology* 2012; 17: 1237-1246.

(136) Fain, S. B. *et al.* Detection of age-dependent changes in healthy adult lungs with diffusion-weighted 3He MRI. *Acad Radiol* 2005; 12: 1385-1393.

(137) Salerno, M. *et al.* Emphysema: Hyperpolarized Helium 3 Diffusion MR Imaging of the Lungs Compared with Spirometric Indexes—Initial Experience 1. *Radiology* 2002; 222: 252-260.

(138) Kirby, M., Heydarian, M., Wheatley, A., McCormack, D. G. & Parraga, G. Evaluating bronchodilator effects in chronic obstructive pulmonary disease using diffusion-weighted hyperpolarized helium-3 magnetic resonance imaging. *J Appl Physiol* 2012; 112: 651-657.

(139) Lutey, B. A. *et al.* Hyperpolarized 3He MR imaging: physiologic monitoring observations and safety considerations in 100 consecutive subjects. *Radiology* 2008; 248: 655-661.

(140) Driehuys, B. *et al.* Chronic obstructive pulmonary disease: safety and tolerability of hyperpolarized 129Xe MR imaging in healthy volunteers and patients. *Radiology* 2012; 262: 279-289.

(141) Guerrero, T. *et al.* Dynamic ventilation imaging from four-dimensional computed tomography. *Physics in medicine and biology* 2006; 51: 777.

(142) Guerrero, T. *et al.* Quantification of regional ventilation from treatment planning CT. *Int J Radiat Oncol Biol Phys* 2005; 62: 630-634.

(143) Yin, Y. B., Hoffman, E. A. & Lin, C. L. Mass preserving nonrigid registration of CT lung images using cubic B-spline. *Medical Physics* 2009; 36: 4213-4222.

(144) Li, B. J., Christensen, G. E., Hoffman, E. A., McLennan, G. & Reinhardt, J. M. Pulmonary CT image registration and warping for tracking tissue deformation during the respiratory cycle through 3D consistent image registration. *Medical Physics* 2008; 35: 5575-5583.

(145) Pan, T., Lee, T. Y., Rietzel, E. & Chen, G. T. Y. 4D-CT imaging of a volume influenced by respiratory motion on multi-slice CT. *Medical Physics* 2004; 31: 333-340.

(146) Reinhardt, J. M. *et al.* Registration-based estimates of local lung tissue expansion compared to xenon CT measures of specific ventilation. *Med Image Anal* 2008; 12: 752-763.

(147) Fuld, M. K. *et al.* CT-measured regional specific volume change reflects regional ventilation in supine sheep. *J Appl Physiol (1985)* 2008; 104: 1177-1184.

(148) Jahani, N. *et al.* A four-dimensional computed tomography comparison of healthy and asthmatic human lungs. *J Biomech* 2017; 56: 102-110.

(149) Choi, S. *et al.* Registration-based assessment of regional lung function via volumetric CT images of normal subjects vs. severe asthmatics. *J Appl Physiol (1985)* 2013; 115: 730-742.

(150) Bodduluri, S., Newell, J. D., Jr., Hoffman, E. A. & Reinhardt, J. M. Registration-based lung mechanical analysis of chronic obstructive pulmonary disease (COPD) using a supervised machine learning framework. *Acad Radiol* 2013; 20: 527-536.

(151) Bodduluri, S. *et al.* Biomechanical CT metrics are associated with patient outcomes in COPD. *Thorax* 2017; 72: 409-414.

(152) Bhatt, S. P. *et al.* CT Measure of Lung At-risk and Lung Function Decline in Chronic Obstructive Pulmonary Disease. *Am J Respir Crit Care Med* 2017.

(153) Seco, J. *et al.* Dosimetric impact of motion in free-breathing and gated lung radiotherapy: a 4D Monte Carlo study of intrafraction and interfraction effects. *Med Phys* 2008; 35: 356-366.

(154) Vedam, S. S. *et al.* Acquiring a four-dimensional computed tomography dataset using an external respiratory signal. *Physics in Medicine and Biology* 2003; 48: 45-62.

(155) Yamamoto, T. *et al.* 4D CT lung ventilation images are affected by the 4D CT sorting method. *Med Phys* 2013; 40: 101907.

(156) Jahani, N. *et al.* Assessment of regional ventilation and deformation using 4D-CT imaging for healthy human lungs during tidal breathing. *J Appl Physiol (1985)* 2015; 119: 1064-1074.

(157) Yamamoto, T. *et al.* Investigation of four-dimensional computed tomography-based pulmonary ventilation imaging in patients with emphysematous lung regions. *Phys Med Biol* 2011; 56: 2279-2298.

(158) Moffat, B. A. *et al.* Functional diffusion map: a noninvasive MRI biomarker for early stratification of clinical brain tumor response. *Proc Natl Acad Sci U S A* 2005; 102: 5524-5529.

(159) Galban, C. J. *et al.* Computed tomography-based biomarker provides unique signature for diagnosis of COPD phenotypes and disease progression. *Nature medicine* 2012; 18: 1711-1715.

(160) Gevenois, P. A. *et al.* Comparison of computed density and microscopic morphometry in pulmonary emphysema. *Am J Respir Crit Care Med* 1996; 154: 187-192.

(161) Gevenois, P. A., de Maertelaer, V., De Vuyst, P., Zanen, J. & Yernault, J. C. Comparison of computed density and macroscopic morphometry in pulmonary emphysema. *Am J Respir Crit Care Med* 1995; 152: 653-657.

(162) Boes, J. L. *et al.* Parametric Response Mapping Monitors Temporal Changes on Lung CT Scans in the Subpopulations and Intermediate Outcome Measures in COPD Study (SPIROMICS). *Academic Radiology* 2015; 22: 186-194.

(163) Pompe, E. *et al.* Parametric Response Mapping Adds Value to Current Computed Tomography Biomarkers in Diagnosing Chronic Obstructive Pulmonary Disease.

American Journal of Respiratory and Critical Care Medicine 2015; 191: 1084-1086.

(164) Bhatt, S. P. *et al.* Association between Functional Small Airway Disease and FEV1 Decline in Chronic Obstructive Pulmonary Disease. *American Journal of Respiratory and Critical Care Medicine* 2016; 194: 178-184.

(165) Zapke, M. *et al.* Magnetic resonance lung function--a breakthrough for lung imaging and functional assessment? A phantom study and clinical trial. *Respir Res* 2006; 7: 106.

(166) Pusterla, O. *et al.* Rapid 3D in vivo 1H human lung respiratory imaging at 1.5 T using ultra-fast balanced steady-state free precession. *Magn Reson Med* 2017; 78: 1059-1069.

(167) Pennati, F. *et al.* Assessment of regional lung function with multivolume (1)H MR imaging in health and obstructive lung disease: comparison with (3)He MR imaging. *Radiology* 2014; 273: 580-590.

(168) Bauman, G. *et al.* Non-contrast-enhanced perfusion and ventilation assessment of the human lung by means of fourier decomposition in proton MRI. *Magn Reson Med* 2009; 62: 656-664.

(169) Deimling, M., Jellus, V., Geiger, B. & Chefd'Hotel, C. in *Proceedings of the Sixteenth Meeting of the International Society for Magnetic Resonance in Medicine. Berkeley, CA: International Society for Magnetic Resonance in Medicine.* 2639.

(170) Bauman, G. *et al.* Pulmonary functional imaging: qualitative comparison of Fourier decomposition MR imaging with SPECT/CT in porcine lung. *Radiology* 2011; 260: 551-559.

(171) Bauman, G. *et al.* Lung ventilation-and perfusion-weighted Fourier decomposition magnetic resonance imaging: In vivo validation with hyperpolarized 3He and dynamic contrast-enhanced MRI. *Magn Reson Med* 2013; 69: 229-237.

CHAPTER 2

2 PULMONARY IMAGING BIOMARKERS OF GAS TRAPPING AND EMPHYSEMA IN COPD: ^{3}HE MR IMAGING AND CT PARAMETRIC RESPONSE MAPS

To better understand the potential of CT parametric response maps (PRM), we directly compared the imaging biomarkers derived from CT PRM with well-established measurements of airways disease and emphysema, including MRI and pulmonary function tests, to provide for the first time a deeper understanding of the relationship between ventilation abnormalities and gas-trapping in COPD.

The contents of this chapter were previously published in the journal Radiology: DPI Capaldi, N Zha, F Guo, D Pike, DG McCormack, M Kirby, and G Parraga. Radiology 2016; 279(2):597-608. Permission to reproduce this article was granted by the Radiological Society of North America (RSNA) and is provided in ***Appendix A****.*

2.1 Introduction

Chronic obstructive pulmonary disease (COPD) is characterized by persistent airflow limitation related to airway remodeling, inflammation and emphysematous destruction[1]. These pathophysiological features can be quantified regionally using high resolution x-ray computed tomography (CT) measurements of the airways[2,3] and parenchyma.[4,5] For example, airways disease can be estimated using CT measurements of airway wall area percent (WA%) and lumen area (LA) while emphysema may be estimated using CT density thresholds such as -950 Hounsfield units (HU)[4] or the 15th percentile value[6] from inspiratory CT. The expiratory CT density-histogram threshold of -856HU also provides a way to estimate gas trapping[7] reflecting the longer time constants for emptying the parenchyma via obstructed airways.

Parametric response mapping (PRM)[8] was recently used to evaluate COPD,[9] breast cancer treatment response[10] and osteoporosis.[11] In COPD patients, co-registered inspiratory and expiratory thoracic CT can be evaluated using well-established density thresholds,[12] resulting in the classification[9] of normal, emphysematous and gas-trapping lung regions. However, the relationship of PRM classified tissue with other established measurements of airways disease and emphysema is not well-understood. Very recently PRM

phenotyping was used to differentiate current and former smokers with and without COPD,[13] but the clinical relevance and etiology of PRM measurements of airways disease is yet uncertain.

Single photon emission computed tomography (SPECT)[14] and positron emission tomography (PET),[15] have also been used to identify pulmonary function abnormalities in COPD patients. In addition, hyperpolarized inhaled noble gas MRI using ^{3}He and ^{129}Xe gases,[16,17] as well as oxygen-enhanced[18] and ^{19}F MRI[19] provide other ways to quantify both functional and structural pulmonary biomarkers of COPD. Hyperpolarized ^{3}He MRI apparent diffusion coefficients (ADC) reflect the size of the lung acinar units. Such values are abnormally elevated in smokers with and without COPD.[20,21] ^{3}He MRI ventilation defects may reflect both airways disease and emphysema in advanced COPD,[22] but in mild COPD and in asthma,[23] ventilation defects reflect airways disease. Despite the potential of ^{3}He MRI, limited and unpredictable global quantities and high cost have hampered clinical translation.

We wanted to determine the quantitative and spatial relationships of PRM-gas-trapping and PRM-emphysema measurements with MRI measurements of parenchymal tissue integrity (i.e. ADC) and ventilation, because these are clinically-important imaging findings and phenotypes of COPD. Thus, our objective was to directly compare magnetic-resonance-imaging and computed-tomography parametric-response-map measurements of gas-trapping and emphysema in ex-smokers with and without chronic obstructive pulmonary disease.

2.2 Materials and Methods

2.2.1 Study Volunteers

Participants provided written-informed-consent to a protocol approved by a local research ethics board and Health Canada and compliant with the Health-Insurance-Portability-Accountability-Act (HIPAA, USA) (IRB-Reg. #00000940), in a prospectively planned study performed from March-December 2014.

2.2.2 MR Imaging

MRI acquisition of conventional proton (^{1}H), ^{3}He static ventilation, and ^{3}He diffusion-weighted images was performed using a whole-body 3T Discovery MR750 system (General Electric Health Care [GEHC], Milwaukee, Wisconsin, USA), as previously described.[24] Polarization was achieved (HeliSpin; Polarean, Durham, North Carolina, USA) to 40%, and the magnetized gas was diluted with medical-grade N_2 gas to 5mL/kg of body weight. Coronal MRI was acquired (multi-slice acquisition with no gaps) in breath-hold from FRC after subjects inhaled a 1L gas mixture ($^{4}He/N_2$ mixture for ^{1}H MRI and $^{3}He/N_2$ mixture for ^{3}He MRI).

^{1}H MRI was acquired using the whole-body radiofrequency coil and fast spoiled gradient-recalled echo (FGRE) sequence with a partial echo (total-data-acquisition-time=12s; repetition-time [TR]/echo-time [TE]/flip-angle=4.3ms/1.0ms/30°; field-of-view [FOV]=40×40cm^2; matrix=128×80 [zero-padded to 128×128]; partial-echo-percent=62.5%; bandwidth [BW]=62.50kHz; number-of-excitations [NEX]=1; number-of-slices=14; slice-thickness=15mm, gap=0).

^{3}He MR static ventilation images were acquired using a fast gradient-recalled echo method with a partial echo (total-data-acquisition-time=10s; TR/TE/flip-angle=3.8ms/1.0ms/7°; FOV=40×40cm^2; matrix=128×80 [zero-padded to 128×128]; partial-echo-percent=62.5%; BW=62.50kHz; NEX=1; number-of-slices=14; slice-thickness=15mm, gap=0). ^{3}He MR diffusion-weighted images were also acquired using an FGRE sequence with centric k-space sampling (total-data-acquisition-time=14s; TR/TE/flip-angle=6.8ms/4.5ms/8°; FOV=40×40cm^2; matrix=128×128; BW=62.50kHz; NEX=1; number-of-slices=7; slice-thickness=30mm, gap=0) with two interleaved images (with and without additional diffusion sensitization) (G=1.94G/cm; b=1.6s/cm^2; rise-and-fall time=0.5ms; gradient duration=0.46ms; diffusion time=1.46ms).

2.2.3 CT Imaging

CT images were acquired with subjects in the supine position, approximately 10 minutes prior to MRI and one hour post-salbutamol administration. A 64 slice Lightspeed VCT

scanner (GEHC) was used to acquire breath-hold images at full-inspiration and at full-expiration using a spiral acquisition approach (detector configuration=64×0.625mm; peak x-ray tube voltage=120kVp; effective x-ray tube current=100mA; x-ray tube rotation time=500ms; pitch=1.0, slice thickness=1.25mm; number of slices=200-250 [patient size dependent]; matrix=512×512), as previously described.[25] CT data were reconstructed using a standard convolution kernel to 1.25mm. The ImPACT CT patient dosimetry calculator (based on the Health Protection Agency [UK] NRPB-SR250) and our manufacturer settings were used to calculate total effective dose (1.8mSv for inspiration and 1.4mSv for expiration CT). The approach of Christener and colleagues[26] was used to calculate the size-specific dose estimate (SSDE)[27] for inspiration CT using volumetric CT dose index ($CTDI_{vol}$) (4.4mGy), total effective dose of 1.8mSv, and size-dependent conversion factor (f_{size}) of 1.00-2.00 and this ranged from 5-9mGy. For expiration CT, the SSDE was 3-7mGy ($CTDI_{vol}$ =3.3mGy, total effective dose =1.4mSv, and f_{size}=1.00-2.00).

2.2.4 MR Image Analysis

^{3}He MRI semi-automated segmentation was performed by a single observer (DP, 3 years experience), as previously described,[28] to generate ventilation defect percent (VDP) – the ventilation defect volume (VDV) normalized to ^{1}H MRI thoracic cavity volume (TCV). A detailed description is provided in the **Supplement**.

2.2.5 CT Image Analysis

CT images were analyzed using Pulmonary Workstation 2.0 (VIDA Diagnostics Inc, Coralville, Iowa, USA) by a single observer (DPIC, 2 years experience) for the measurement of wall area percent and to segment the lung regions; these analyses are fully-automated, as previously described and validated.[29,30] The relative area of the CT density-histogram <−950HU (RA_{950}) and −856HU (RA_{856}) were determined using MATLAB for inspiratory and expiratory CT, respectively.

Briefly, pulmonary PRM results can be generated by co-registering inspiratory and expiratory CT scans and then classifying voxels based on their specific thresholds into

normal, gas-trapping or emphysema tissue components. The specific details are provided in the **Supplement**.

2.2.6 Statistics

Analysis of variance (ANOVA) with post-hoc analysis using the Tukey correction was performed to determine differences in participant characteristics and imaging measurements using SPSS Statistics V22.0 (SPSS Inc., Chicago, Illinois, USA). Pearson correlation coefficients (r) were determined for MRI and PRM measurements and adjusted using the Holm-Bonferroni correction. The agreement between CT-PRM and ^{3}He MRI measurements were evaluated using the Bland-Altman method using GraphPad Prism V6.0 (GraphPad Software Inc., La Jolla, California, USA). Multivariate regression models for both PRM-gas-trapping and PRM-emphysema were determined using the step-wise method; variables were added to the model when $p<0.15$, and removed when $p\geq0.15$, using SPSS.

2.3 Results

2.3.1 Participant Characteristics

Table 2-1 shows demographic and pulmonary function measurements for 58 participants (73±9yrs) including 26 ex-smokers with normal spirometry (70±11yrs) and 32 ex-smokers (74±7yrs) with COPD. The patient subgroups were significantly different with respect to body mass index ($p<.001$), smoking history (pack-years, $p=.01$), FEV_1 ($p<.001$), FEV_1/FVC ($p<.001$), and DL_{CO} ($p<.001$) but not age ($p=.1$).

Table 2-1 Subject Demographics

Parameter Mean (±SD)	Normal Ex-smokers (n=26)	COPD Ex-smokers (n=32)				Sig Dif p
		All (n=32)	GOLD I (n=12)	GOLD II (n=13)	GOLD III/IV (n=7)	
Age yrs	70 (11)	74 (7)	75 (8)	74 (8)	73 (6)	.104
Male n	15	25	11	9	5	--
BMI kg/m^2	30 (4)	26 (3)	26 (3)	27 (3)	26 (4)	<.001
Pack years	28 (16)	43 (26)	31 (17)	50 (28)	51 (30)	.012
FEV_1 $\%_{pred}$	103 (19)	73 (27)	101 (14)	64 (10)	39 (7)	<.001
FEV_1/FVC %	80 (7)	55 (11)	63 (4)	55 (8)	40 (5)	<.001
TLC $\%_{pred}$	96 (13)	110 (16)**	103 (34)*	106 (17)	115 (20)	<.001
IC $\%_{pred}$	103 (23)	91 (27)	100 (23)	94 (32)	70 (10)	.078
RV $\%_{pred}$	100 (21)	140 (39)	123 (16)	134 (33)	180 (53)	<.001
DL_{CO} $\%_{pred}$	89 (18)[#]	68 (23)**	73 (29)*	66 (24)	51 (15)	<.001

Sig Dif: Significant difference between subgroups ($p<.05$) determined by ANOVA with Tukey correction; SD: standard deviation; GOLD: The Global Initiative for Chronic Obstructive Lung Disease; $\%_{pred}$: percent of predicted value; BMI: body mass index; FEV_1: forced expiratory volume in one second; FVC: forced vital capacity; TLC: total lung capacity; IC: inspiratory capacity; RV: residual volume; DL_{CO}: diffusing capacity for carbon monoxide; [#]n=25; *n=11; **n=31.

2.3.2 Qualitative Ventilation and PRM Results

Figure 2-1 shows MRI and CT for a representative ex-smoker without airflow limitation and three COPD ex-smokers. For the two ex-smokers with more advanced COPD (GOLD II: 84yrs-male, $FEV_1=52\%_{pred}$, $FEV_1/FVC=44\%$; GOLD III: 67yrs-female, $FEV_1=33\%_{pred}$, $FEV_1/FVC=39\%$) there was more pronounced ^3He ventilation defects, a greater number of PRM voxels reflective of emphysema, and elevated ADC. Alternatively, for ex-smokers with mild or no disease (ex-smoker: 55yrs-male, $FEV_1=83\%_{pred}$, $FEV_1/FVC=77\%$; GOLD I: 69yrs-male, $FEV_1=89\%_{pred}$, $FEV_1/FVC=69\%$) there was more homogeneous ventilation and greater number of PRM voxels reflective of normal or healthy tissue.

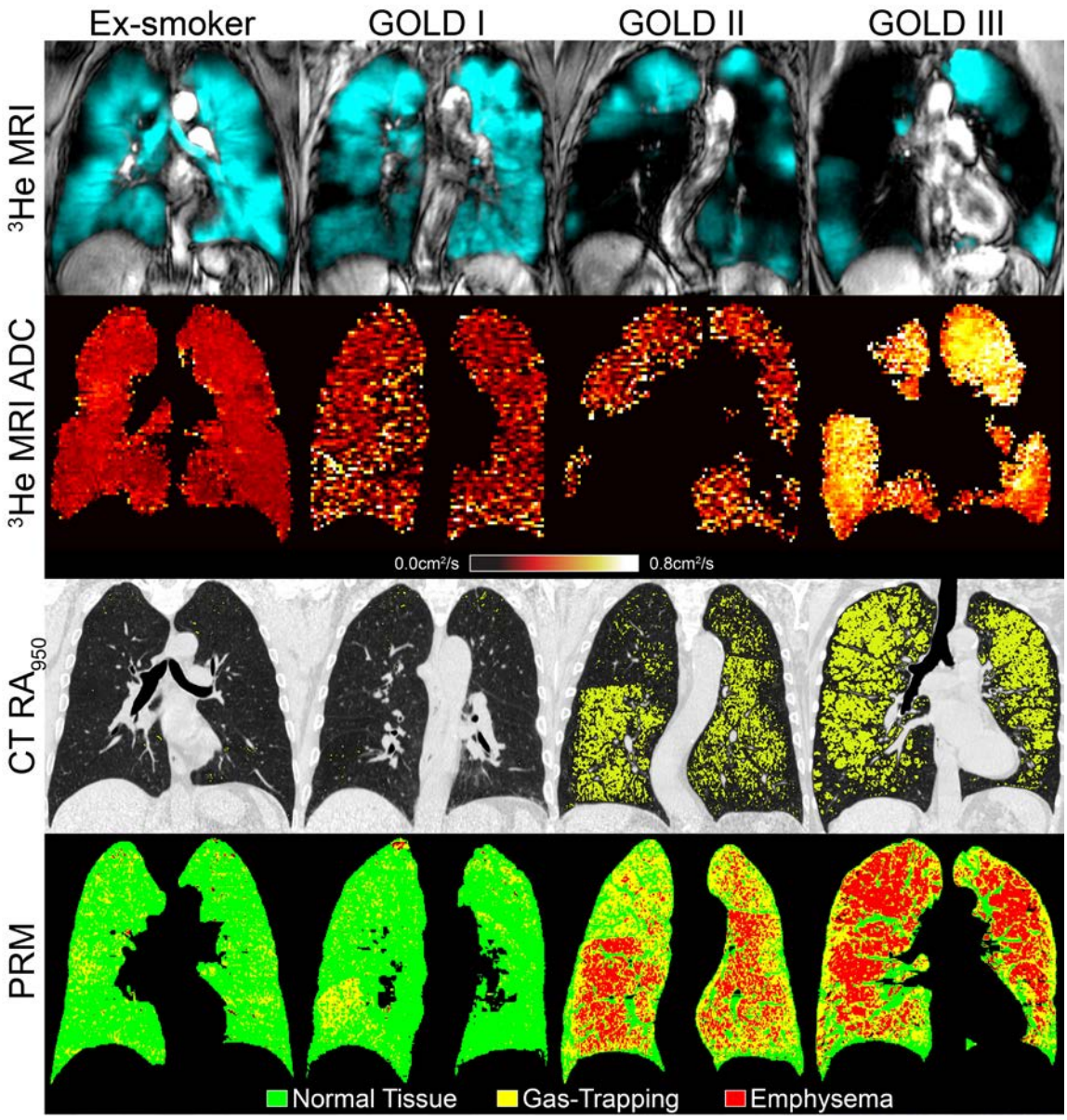

Figure 2-1 Ventilation and Parametric Response Maps for a representative ex-smoker and COPD subjects

Ex-smoker: 55 yrs-male, FEV_1=83%$_{pred}$, FEV_1/FVC=77%, RV/TLC=45%, DL_{CO} not available; GOLD I: 69 yrs-male, FEV_1=89%$_{pred}$, FEV_1/FVC=69%, RV/TLC=39%, DL_{CO}=67%$_{pred}$; GOLD II: 84 yrs-male, FEV_1=52%$_{pred}$, FEV_1/FVC=44%, RV/TLC=62%, DL_{CO}=47%$_{pred}$; GOLD III: 67 yrs-female, FEV_1=33%$_{pred}$, FEV_1/FVC=39%, RV/TLC=72%, DL_{CO}=28%$_{pred}$. Top row: ^{3}He MRI static ventilation in blue co-registered with ^{1}H MRI in grey-scale. Second row: ^{3}He MRI ADC maps (0.0 cm^2/s - 0.8 cm^2/s). Third row: CT density masks where yellow = attenuation < -950 Hounsfield units. Last row: PRM where green=normal tissue, yellow=gas-trapping, and red=emphysema.

2.3.3 Ventilation and PRM Measurements by GOLD Severity

Table 2-2 summarizes MRI ventilation and emphysema measurements as well as CT-derived gas-trapping/emphysema and PRM measurements. COPD ex-smokers reported significantly greater VDP (p<.001), ADC (p<.001), and RA_{950} (p<.001) as well as PRM gas-trapping (p<.001) and emphysema (p<.001) than ex-smokers without airflow limitation. There were no significant differences for CT airway measurement of WA% (p=.9).

Table 2-2 Imaging Measurements

Parameter Mean (±SD)	Normal Ex-smokers (n=26)	COPD Ex-smokers (n=32)				Sig Dif p
		All (n=32)	GOLD I (n=12)	GOLD II (n=13)	GOLD III/IV (n=7)	
CT RA_{950} %	2 (1)	10 (9)	6 (4)	10 (10)	15 (12)	<.001
CT RA_{856} %	14 (10)	37 (18)	34 (13)	35 (20)	53 (16)	<.001
CT 6^{th} gen. WA %	65 (2)	65 (2)	65 (2)	66 (2)	66 (2)	.882
^{3}He MRI Ventilation %	92 (4)	20 (13)	88 (6)	80 (11)	63 (9)	<.001
^{3}He MRI VDP %	8 (4)$^{\#}$	12 (4)	12 (6)	20 (11)	37 (9)	<.001
^{3}He MRI ADC cm^2/s	.29 (.08)$^{\#}$	.36 (.06)*	.34 (.03)**	.36 (.06)$^{\#\#}$	.41 (.05)	<.001
PRM Normal %	85 (11)	60 (18)	64 (13)	63 (20)	46 (17)	<.001
PRM Gas-Trapping %	13 (10)	31 (12)	31 (11)	27 (14)	41 (9)	<.001
PRM-Emphysema %	.5 (.5)	7 (10)	3 (3)	8 (11)	13 (12)	.001

Sig Dif: Significant difference between subgroups (p<.05) determined by ANOVA with Tukey correction; SD: standard deviation; GOLD: The Global Initiative for Chronic Obstructive Lung Disease; RA_{950}: relative area of the lung with attenuation values <-950HU that is in an inspiration CT; RA_{856}: relative area of the lung with attenuation values <-856HU that is in an expiration CT; 6^{th} gen.: sixth generation airway; WA: wall area; VDP: ventilation defect percent; ADC: apparent diffusion coefficient; PRM: parametric response map; $^{\#}$n=24; $^{\#\#}$n=12; *n=30; **n=11.

Figure 2-2 shows that VDP was significantly different between normal ex-smokers (8±4%) and moderate-severe COPD subjects (GOLD II: 20±11%, p<.001; GOLD III/IV: 37±9%, p<.001), but not mild COPD (GOLD I: 11±6%, p=.5). VDP was also significantly different between GOLD I and GOLD II (p=.04), GOLD II and GOLD II/IV (p<.001), and GOLD I and GOLD III/IV (p<.001) ex-smokers. PRM measurements were significantly different for normal ex-smokers (gas-trapping: 13±10%, emphysema: 0.5±0.5%) and moderate-severe COPD subjects (gas-trapping: GOLD II: 27±14%, p=.003; GOLD III/IV: 41±8%, p<.001; emphysema: GOLD II: 8±11%, p=.003; GOLD III/IV: 13±12%, p<.001). PRM gas-trapping was significantly different between ex-smokers and mild COPD (GOLD I: 31±11%, p<.001). PRM emphysema was significantly different between GOLD I and GOLD III/IV (p=.03). ADC was significantly different between normal ex-smokers (.29±.08cm^2/s) and GOLD II (.36±.06cm^2/s, p=.02) GOLD III/IV (.41±.05cm^2/s, p<.001), but not GOLD I (.34±.03cm^2/s, p=.2) COPD.

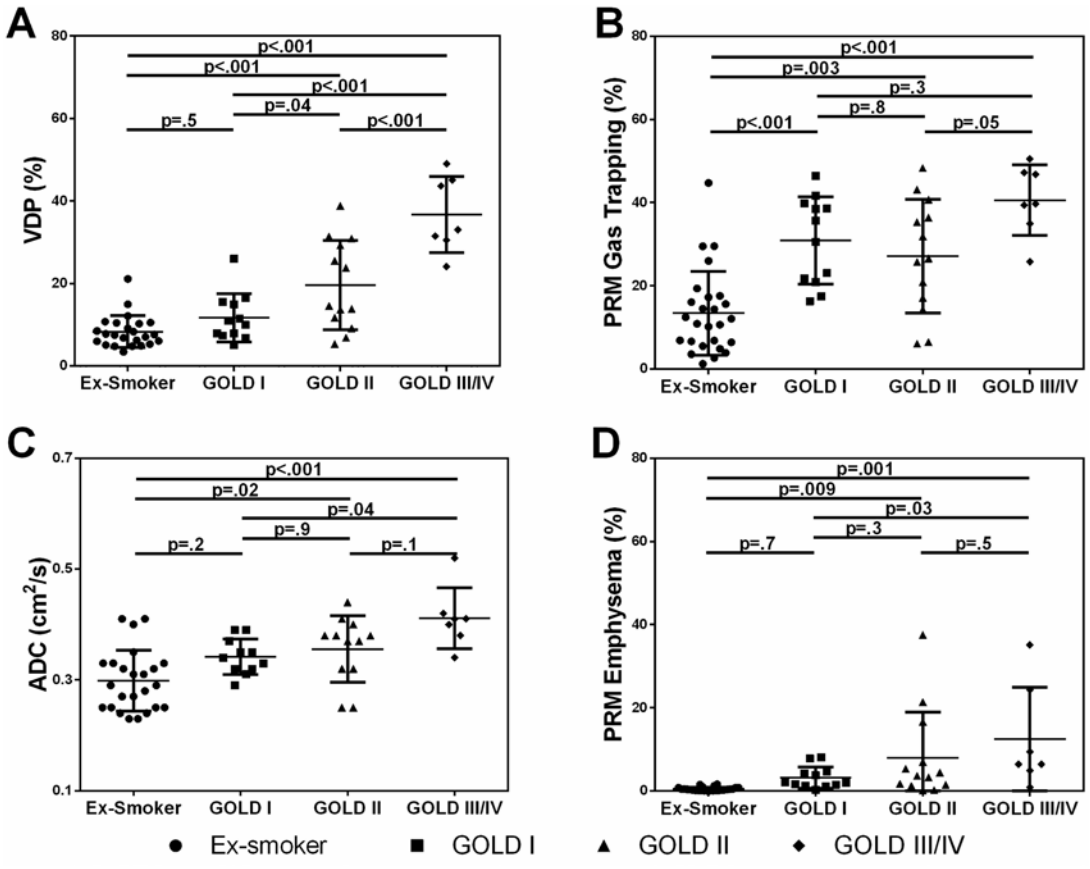

Figure 2-2 ^{3}He MRI ventilation and PRM measurements by COPD grade

A) ^{3}He MRI VDP for ex-smokers=8±4%, GOLD I=11±6%, GOLD II=20±11%, and GOLD III/IV=37±9%. Significant difference for VDP between ex-smokers and GOLD II (p<.001), ex-smokers and GOLD III/IV (p<.001), GOLD I and GOLD II (p=.04), GOLD II and GOLD III/IV (p<.001), and GOLD I and GOLD III/IV (p<.001).

B) PRM-derived gas-trapping voxels for ex-smokers=13±10%, GOLD I=31±11%, GOLD II=27±14%, and GOLD III/IV=41±8%. Significant difference for PRM gas-trapping between ex-smokers and GOLD I (p<.001), ex-smokers and GOLD II (p=.003), and ex-smokers and GOLD III/IV (p<.001).

C) ^{3}He MRI ADC for ex-smokers=.29±.08cm^2/s, GOLD I=.34±.03cm^2/s, GOLD II=.36±.06cm^2/s, and GOLD III/IV=.41±.05cm^2/s. Significant difference for ADC between ex-smokers and GOLD II (p=.02), ex-smokers and GOLD III/IV (p<.001), and GOLD I and GOLD III/IV (p=.04).

D) PRM-derived emphysema voxels for ex-smokers= 0.5±0.5%, GOLD I=3±3%, GOLD II=8±11%, and GOLD III/IV=13±12%. Significant difference for PRM emphysema between ex-smokers and GOLD II (p=.009), ex-smokers and GOLD III/IV (p=.001), and GOLD I and GOLD III/IV (p=.03).

Significant difference between subgroups (p<.05) were determined by ANOVA with a Post-hoc Tukey analysis.

Error bars represent the standard deviation of the data.

2.3.4 Relationships for MR Imaging and PRM Measurements

Table 2-3 shows the Holm-Bonferroni-corrected Pearson correlations as well as multivariate regression model results for CT-derived PRM gas-trapping and emphysema measurements. In ex-smokers with COPD only, PRM gas-trapping was significantly related to FEV_1/FVC (r=-.58, p=.003), ADC (r=.53, p=.01), and VDP (r=.47, p=.03). PRM emphysema was significantly correlated with FEV_1 (r=-.43, p=.03), FEV_1/FVC (r=-.52, p=.008), DL_{CO} (r=-.69, p<.001), ADC (r=.69, p<.001), and VDP (r=.62, p<.001) in COPD ex-smokers. **Figure 2-3** provides linear regressions for PRM-gas-trapping and emphysema and shows that VDP was significantly correlated with PRM-gas-trapping (r=.58, p<.001) and PRM-emphysema (r=.68, p<.001) in all subjects and in the COPD ex-smoker subgroup (gas-trapping: r=.47, p=.03; emphysema: r=.62, p<.001), but not in normal ex-smokers. ADC was also significantly correlated with PRM-gas-trapping (r=.55, p<.001) and PRM-emphysema (r=.62, p<.001) in all subjects, and the COPD ex-smoker subgroup (gas-trapping: r=.53, p=.01; emphysema: r=.69, p<.001), but not in normal ex-smokers. **Figure 2-3** also shows Bland-Altman plot for PRM-gas-trapping and emphysema; in relation to VDP, there was a negative bias for PRM gas-trapping (-9±12% [-32%-15% 95% CI]) and a positive bias for PRM emphysema (11±9% [-6%-28% 95% CI]). **Table 2-3** shows that in the multivariate regression model that explains PRM-gas-trapping, FEV_1/FVC ($ß_S$=-.69, p=.001) and WA% ($ß_S$=-.22, p=.02) make significant contributions, whereas for the PRM-emphysema model, DL_{CO} ($ß_S$=-.29, p=.03) and VDP ($ß_S$=.41, p=.001) were significant.

Table 2-3 Pearson Correlations and Multivariate Regressions for PRM Gas-Trapping and Emphysema Measurements

	Pearson Correlations*				**Multivariate Regressions^**							
	PRM Gas-Trapping		**PRM Emphysema**		**PRM Gas-Trapping**				**PRM Emphysema**			
	Normal (n=26)	**COPD (n=32)**	**Normal (n=26)**	**COPD (n=32)**	**All (n=58)**				**All (n=58)**			
Variables	**r/p**	**r/p**	**r/p**	**r/p**	**ß$_U$**	**ß$_S$**	**Partial R^2**	**p**	**ß$_U$**	**ß$_S$**	**Partial R^2**	**p**
FEV_1 $\%_{pred}$	-.09/.9	-.29/.1	-.11/.9	**-.43/.03**	--	--	--	--	--	--	--	--
FEV_1/FVC %	-.33/.6	**-.58/.003**	-.34/.6	**-.52/.008**	-.65	-.69	.53	.001	--	--	--	--
DL_{CO} $\%_{pred}$	-.06/.8	-.36/.09	-.21/.9	**-.69/<.001**	--	--	--	--	-.10	-.29	.10	.03
ADC cm^2/s	.08/.9	**.53/.01**	.30/.8	**.69/<.001**	--	--	--	--	--	--	--	--
6^{th} WA %	-.16/.9	-.44/.07	-.22/.9	-.14/.4	-1.72	-.22	.08	.02	--	--	--	--
VDP %	.13/.9	**.47/.03**	.10/.7	**.62/<.001**	--	--	--	--	.29	.41	.20	.001

$\%_{pred}$: percent of predicted value; GOLD: The Global Initiative for Chronic Obstructive Lung Disease; FEV_1: forced expiratory volume in one second; FVC: forced vital capacity; DL_{CO}: diffusing capacity for carbon monoxide; ADC: apparent diffusion coefficient; 6^{th}: sixth generation airway; WA: wall area; VDP: ventilation defect percent; PRM: parametric response map; r: Pearson correlation coefficient; ß$_U$: unstandardized regression coefficients; ß$_S$: standardized regression coefficients; *Holm-Bonferroni corrected p-value; ^Adjusted for age, sex, height, weight, and smoking history and all variables in the model significant at the p=0.15 level.

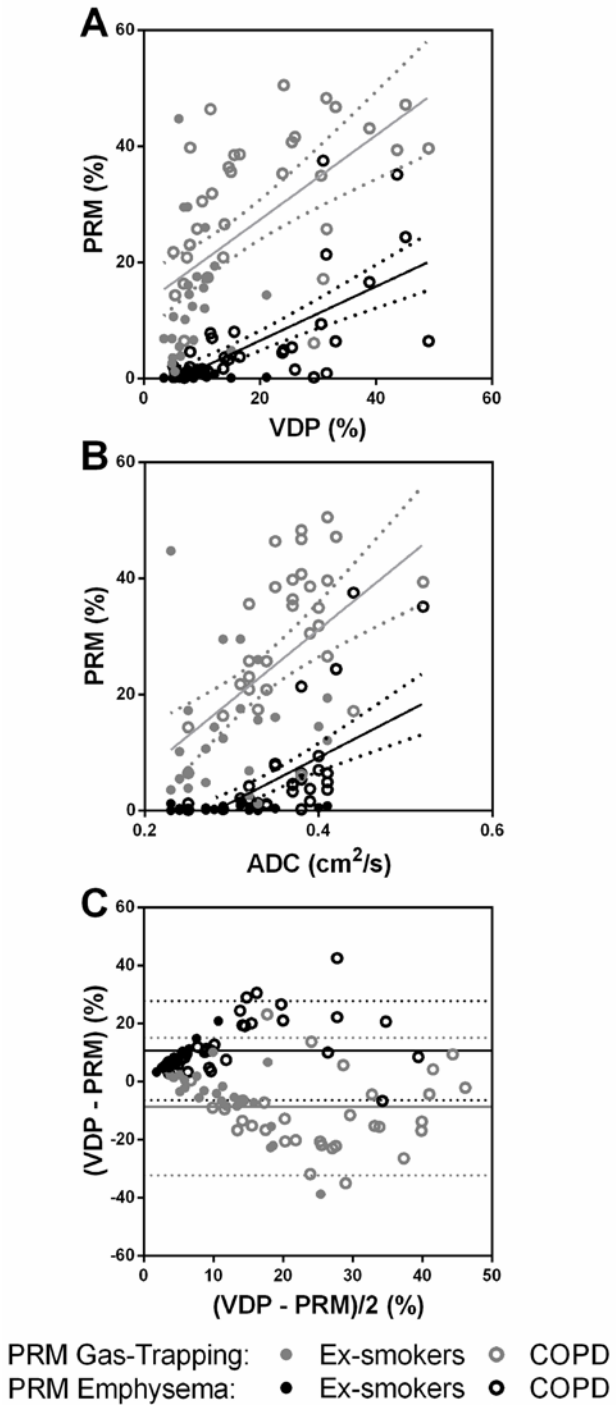

Figure 2-3 Relationships for ^{3}He MRI VDP and ADC with PRM-derived gas-trapping and emphysema voxels

A) Linear regression for ^{3}He MRI VDP with PRM for all subjects (gas-trapping voxels: r=.58, r^2=.34, p<.001, y=0.73x–12.88; emphysema voxels: r=.68, r^2=.47, p<.001, y=0.47x–2.78), normal ex-smokers (gas-trapping voxels: r=.13, r^2=.02, p=.9, y=0.35x+10.92; emphysema voxels: r=.10, r^2=.009, p=.7, y=0.01x+0.39), and COPD subjects (gas-trapping voxels: r=.47, r^2=.23, p=.03, y=0.46x+22.12; emphysema voxels: r=.62, r^2=.38, p<.001, y=0.46x–2.22).

B) Linear regression for ^{3}He MRI ADC with PRM for all subjects (gas-trapping voxels: r=.55, r^2=.30, p<.001, y=122x-17; emphysema voxels: r=.62, r^2=.39, p<.001, y=77x–22), normal ex-smokers (gas-trapping voxels: r=.08, r^2=.006, p=.9, y=14x+10; emphysema voxels: r=.30, r^2=.09, p=.8, y=2.5x–0.3), and COPD subjects (gas-trapping voxels: r=.53, r^2=.28, p=.01, y=119x-12; emphysema voxels: r=.69, r^2=.48, p<.001, y=121x–37).
C) Bland-Altman analysis of agreement for ^{3}He MRI VDP and PRM for all subjects (gas-trapping voxels: bias=-9±12%, lower limit=-32%, upper limit=15%; emphysema voxels: bias=11±9%, lower limit=-6%, upper limit=28%), normal ex-smokers (gas-trapping voxels: bias=-6±10%, lower limit=-26%, upper limit=15%; emphysema voxels: bias=8±4%, lower limit=1%, upper limit=15%), and COPD subjects (gas-trapping voxels: bias=-11±13%, lower limit=-36%, upper limit=14%; emphysema voxels: bias=13±10%, lower limit=-7%, upper limit=33%).
Dotted lines = 95% confidence intervals.

2.3.5 Spatial and Regional Relationships

Given the significant quantitative relationships for MRI and PRM COPD measurements, we evaluated the spatial correlations of ventilation defects with PRM measurements. Qualitative examples are shown in **Figure 2-4** for an ex-smoker with mild COPD and another with GOLD grade III COPD. The spatial relationship for ventilation defects with PRM gas-trapping is more obvious in the ex-smoker with mild disease whereas there is co-localization of PRM emphysema and ventilation defects in the ex-smoker with severe airflow limitation.

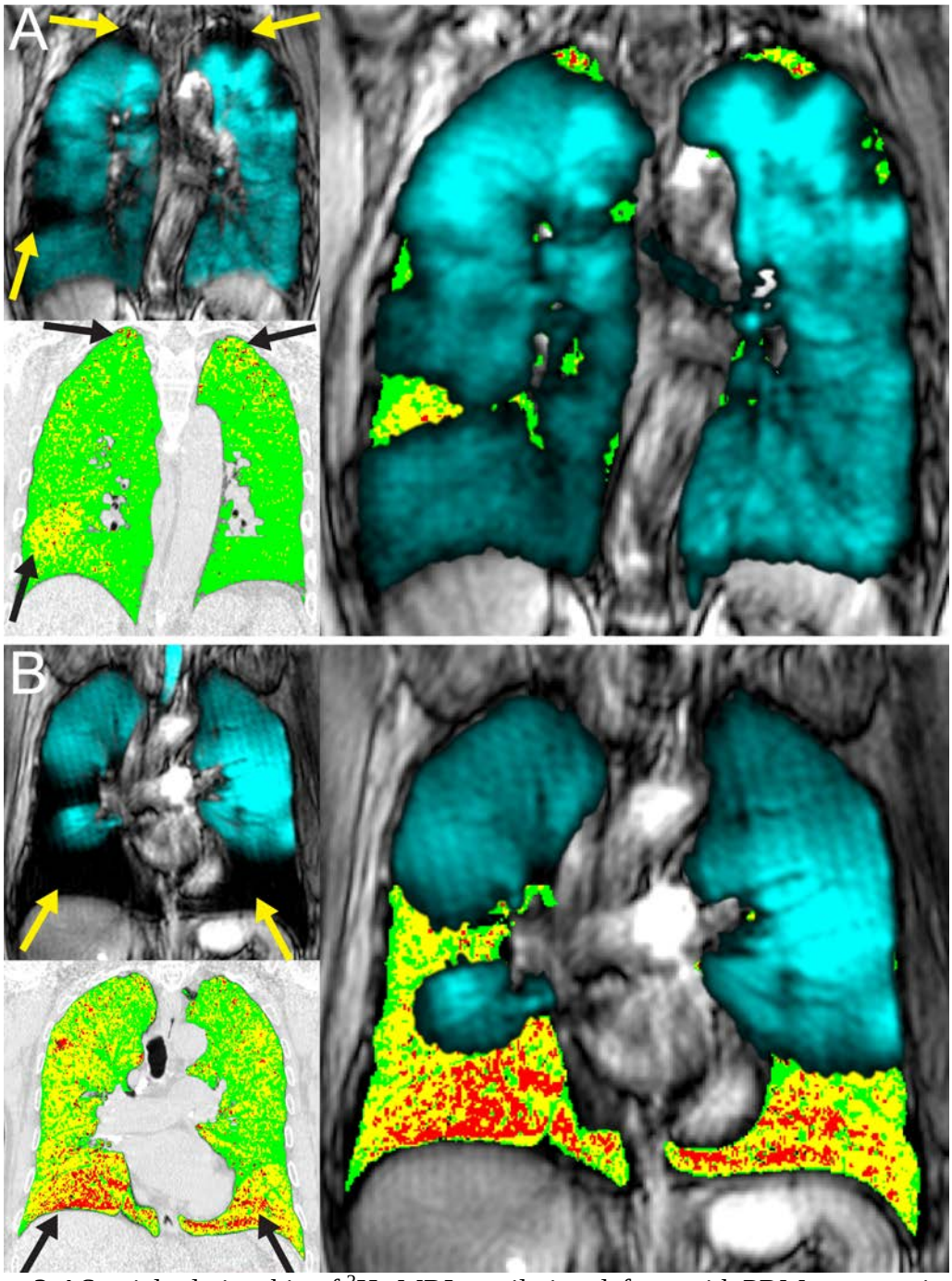

Figure 2-4 Spatial relationship of ^{3}He MRI ventilation defects with PRM gas-trapping and emphysema for a representative (A) mild and (B) severe COPD subject
A) GOLD I: age=69, sex=male, FEV_1=89%$_{pred}$, FEV_1/FVC=69%, RV/TLC=39%, DL_{CO}=67%$_{pred}$;
B) GOLD III: age=78, sex=male, FEV_1=47%$_{pred}$, FEV_1/FVC=37%, RV/TLC=50%, DL_{CO}=57%$_{pred}$. ^{3}He MRI ventilation (blue) co-registered with ^{1}H MRI and PRM normal (green), gas-trapping (yellow) and emphysema (red) tissue co-registered with CT. Arrows show spatial relationship between ventilation defects with PRM gas-trapping and emphysema regions.

To explore these relationships in more detail, we quantitatively evaluated the spatial overlap of PRM gas-trapping and emphysema voxels with ADC (**Figure 2-5**) and ventilation defects (**Table 2-4**). As shown in **Figure 2-5**, ^{3}He ADC was significantly elevated in PRM gas-trapping as compared to normal tissue (normal ex-smoker: p=.004, GOLD I: p=.01, GOLD II: p=.01, GOLD III/IV: p=.03). ^{3}He ADC was also significantly greater in the regions of PRM-emphysema as compared to regions of PRM-gas-trapping for GOLD I (p=.03), but not for normal, GOLD II, or GOLD III/IV ex-smokers. **Table 2-4** shows that in mild and moderate COPD, the spatial overlap coefficient (SOC_{MRI}) for ^{3}He ventilation defects with PRM-gas-trapping tissue (mild: SOC_{MRI}=36±28%; moderate: SOC_{MRI}=34±28%) was significantly greater than for PRM-emphysema voxels (mild: SOC_{MRI}=1±2%, p=.001; moderate: SOC_{MRI}=7±15%, p=.006). Thus for mild and moderate COPD subjects, ^{3}He ventilation defects showed a greater spatial relationship with PRM-gas-trapping versus emphysema voxels. For severe COPD, SOC_{CT} for ^{3}He ventilation defects with PRM-emphysema (SOC_{CT}=64±30%) was significantly greater than for PRM-gas-trapping voxels (SOC_{CT}=36±18; p=.01). Therefore for severe COPD subjects, PRM-emphysema was mainly localized within ^{3}He ventilation defect regions. In addition, in severe COPD, SOC_{MRI} for ^{3}He ventilation defects with PRM-gas-trapping voxels (SOC_{MRI}=62±25%) was significantly greater than with PRM-emphysema (SOC_{MRI}=11±20%, p=.009). Hence, in severe COPD, ^{3}He ventilation defect regions mostly consisted of PRM-gas-trapping voxels, although there was a mixture of PRM-gas-trapping and emphysema.

Table 2-4 Quantitative Spatial Relationships for ^{3}He MRI ventilation defects with CT-PRM Voxels

Mean (±SD)	Normal Ex-smokers (n=26)	COPD Ex-smokers (n=32)				Sig Dif p
		All (n=32)	GOLD I (n=12)	GOLD II (n=13)	GOLD III/IV (n=7)	
Spatial Overlap Coefficient Normalized using CT voxels						
Gas-Trapping-to-VDP (%)	3 (12)	15 (16)	4 (4)	13 (13)	36 (18)	<.001
Emphysema-to-VDP (%)	0 (0)	22 (32)	3 (9)	16 (27)	64 (30)	<.001
Sig Dif*	.2	.06	.5	.5	.01	
Spatial Overlap Coefficient Normalized using MRI voxels						
VDP-to-Gas-Trapping (%)	3 (8)	41 (29)	36 (28)	34 (28)	62 (25)	<.001
VDP-to-Emphysema (%)	0 (0)	6 (14)	1 (2)	7 (15)	11 (20)	.04
Sig Dif*	.09	<.001	.001	.006	.009	

Sig Dif: Significant difference between groups (p<.05) using ANOVA and corrected using Tukey's method; SD: standard deviation; GOLD: The Global Initiative for Chronic Obstructive Lung Disease; VDP: ventilation defect percent; PRM: parametric response map; *Significant difference measured using paired t-test for spatial overlap coefficients of MRI ventilation defects with PRM gas-trapping and emphysema

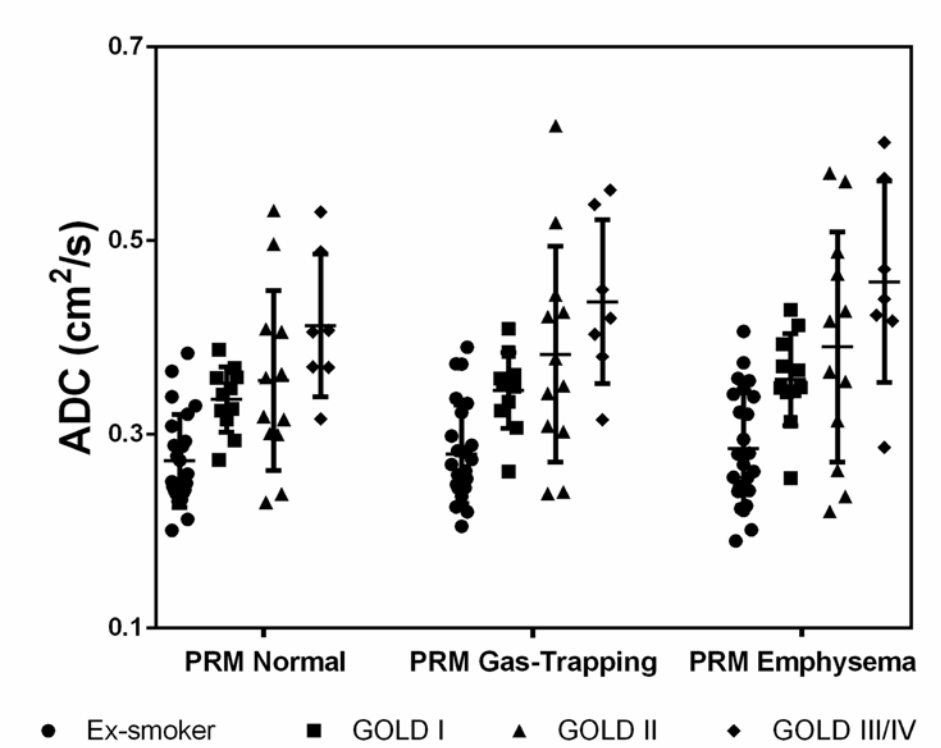

Figure 2-5 ^{3}He MRI apparent diffusion coefficient measurements spatially within PRM regions of normal, gas-trapped, and emphysematous tissue
^{3}He ADC measurements for PRM normal tissue (ex-smokers=.27±.05cm^2/s, GOLD I=.34±.03cm^2/s, GOLD II=.36±.09cm^2/s, GOLD III/IV=.41±.07cm^2/s), gas-trapped (ex-smoker=.28±.05cm^2/s, GOLD II=.35±.04cm^2/s, GOLD II=.38±.11cm^2/s, GOLD III/IV=.44±.08cm^2/s), and emphysema tissue (ex-smoker=.29±.06cm^2/s, GOLD I=.36±.05cm^2/s, GOLD II=.39±.12cm^2/s, GOLD III/IV=.46±.10cm^2/s).
Error bars represent the standard deviation of the data.

2.4 Discussion

We evaluated 58 ex-smokers in the first direct comparison of PRM and MRI measurements of COPD. We acquired inspiration/expiration CT and noble gas MRI within an hour and observed: 1) with increasing severity of airflow limitation, PRM-gas-trapping, PRM-emphysema, ADC and VDP measurements were significantly greater, 2) ^{3}He ventilation and PRM measurements were correlated in COPD, but not in normal ex-smokers, 3) in a multivariate model that predicted PRM-gas-trapping, WA% and FEV_1/FVC were significant, while for PRM-emphysema, VDP and DL_{CO} were significant, and, 4) ^{3}He ADC was significantly elevated in regions of PRM- gas-trapping and there were quantitative and

spatial correlations for both PRM-gas-trapping and emphysema with ^{3}He ventilation defects that differed according to COPD severity.

Parametric-response-mapping[9] classifies lung tissue based on the presence of pulmonary air – either as a consequence of emphysema and gas-trapping due to airways disease and/or emphysema.[9] We were curious about the potential relationships between PRM and MRI phenotypes of COPD, especially because both ventilation defects and PRM-gas trapping have been suggested as biomarkers of small-airways disease. First, we observed that with increasing severity of airflow limitation, PRM-gas-trapping, PRM-emphysema, ADC and VDP measurements were significantly greater. We also noted that ^{3}He VDP and PRM measurements were correlated in COPD ex-smokers but not in ex-smokers with normal pulmonary function. This might be expected because correlations in ex-smokers with mainly normal pulmonary function are statistically difficult to ascertain in small sample sizes since the range of values for normal lung function is small.[31] It is also worth noting that in this study, CT emphysema measurements for normal ex-smokers were in agreement with previously reported values for healthy subjects.[7,32] Importantly, CT may not be adequately sensitive to very mild or subclinical parenchymal[33] and obstructive disease and this may also partially explain the negligible VDP and PRM correlations in normal ex-smokers.

In addition to these bilateral relationships, multivariate modelling identified the parameters that significantly added to the model for PRM-gas-trapping (WA% and FEV_1/FVC) and PRM-emphysema (VDP and DL_{CO}). The PRM-gas-trapping model is intuitive, based on our prior knowledge of the role of airway wall morphology in functional small airways disease.[34] This finding is also consistent with the major pulmonary imaging and clinical phenotypes recently summarized by the Fleischner Society.[35] We note, however, that while the significant contribution of DL_{CO} to PRM-emphysema is also consistent with a large body of previous work,[36] the contribution of PRM-emphysema to ventilation defects is a novel and somewhat surprising result. Strong hints that ventilation defects may stem from emphysematous bullae were previously reported in patients with advanced/severe COPD and numerous exacerbations requiring hospitalization.[22] Together, this information

suggests a role for pulmonary imaging to phenotype COPD patients beyond FEV_1 to help guide therapy to change exacerbations and other outcomes.

These quantitative associations and some obvious qualitative regional relationships led to our exploration of potential spatial correlations. Notably, and unexpectedly, we observed that ^{3}He ADC was significantly elevated in regions of PRM-gas-trapping. This surprising result suggested that PRM 'functional small-airway disease' that leads to gas-trapping may be detected as enlarged airspaces reflected by elevated ADC. This is one of the first studies to spatially compare ^{3}He ADC to gas-trapping measurements. This novel finding is in agreement with other studies that demonstrated gravitational[37,38] and lung volume effects[39] on pulmonary ADC values. This also suggests that abnormally elevated ADC may not always reflect emphysematous abnormalities in COPD patients. There were also spatial correlations in mild and moderate COPD patients in whom ^{3}He MRI ventilation defects were spatially related to PRM-gas-trapping. In contrast, in the small group of seven severe COPD patients, MRI ventilation defects were spatially related to both PRM-gas-trapping and emphysema identified using SOC_{CT} and SOC_{MRI}. The rationale for performing the SOC analysis in both directions was the need to evaluate the overlap of ^{3}He defects within PRM regions (SOC_{CT}) and the overlap of PRM voxels within ^{3}He defects (SOC_{MRI}). While the quantitative results showed differences between the two methods, this was not due to non-symmetry between registering from the fixed to moving image because we performed registration in a symmetric manner to mitigate this potential bias.[40,41] It was important to perform the spatial overlap analysis in both directions because the results showed that in severe COPD, PRM emphysema voxels were mainly occupied by ventilation defect voxels and in contrast, ventilation defect voxels were mainly occupied by PRM gas-trapping voxels. This means that both PRM emphysema and gas-trapping voxels are spatially coincident with ventilation defects. This exciting result provides, for the first time, a deeper understanding of the source of ventilation defects and gas-trapping in COPD. We think these findings underscore the importance of phenotyping COPD patients with quantitative imaging. Future work should aim to determine the spatial relationships between continuous pixel wise data and PRM, as this may provide a better understanding of these relationships.

Numerous studies have used paired inspiratory/expiratory lung CT-images[42-44] to provide COPD phenotypes. In COPD subjects, gas-trapping is influenced by both emphysema and small-airways disease[43,45] for which PRM attempts to differentiate. In addition, severe small-airways disease sometimes appears on CT as emphysema, making it challenging to delineate between the two phenotypes. Regardless, here we determined the different relationships between MRI and CT phenotypes of COPD across GOLD grades of severity. We think these results underscore the need to adopt multimodality approaches to deeply phenotype COPD patients so that the independent contributions of emphysema and airways disease may be ascertained, which may help to optimize COPD therapy and improve outcomes.

In summary, in all ex-smokers, ventilation defects and ADC were correlated with PRM-gas-trapping and emphysema measurements. In a subset of ex-smokers with mild-moderate COPD, ventilation defects were quantitatively and spatially related to PRM-gas-trapping whereas in severe COPD, there were spatial and quantitative relationships for ventilation defects with both PRM-gas-trapping and emphysema.

2.5 References

(1) Vestbo, J. *et al.* Global strategy for the diagnosis, management, and prevention of chronic obstructive pulmonary disease: GOLD executive summary. *Am J Respir Crit Care Med* 2013; 187: 347-365.

(2) Hackx, M., Bankier, A. A. & Gevenois, P. A. Chronic Obstructive Pulmonary Disease: CT Quantification of Airways Disease. *Radiology* 2012; 265: 34-48.

(3) Nakano, Y. *et al.* Quantitative assessment of airway remodeling using high-resolution CT. *Chest* 2002; 122: 271s-275s.

(4) Hayhurst, M. D. *et al.* Diagnosis of pulmonary emphysema by computerised tomography. *Lancet* 1984; 2: 320-322.

(5) Klein, J. S., Gamsu, G., Webb, W. R., Golden, J. A. & Muller, N. L. High-resolution CT diagnosis of emphysema in symptomatic patients with normal chest radiographs and isolated low diffusing capacity. *Radiology* 1992; 182: 817-821.

(6) Dirksen, A. *et al.* A randomized clinical trial of alpha(1)-antitrypsin augmentation therapy. *Am J Respir Crit Care Med* 1999; 160: 1468-1472.

(7) Zach, J. A. *et al.* Quantitative computed tomography of the lungs and airways in healthy nonsmoking adults. *Invest Radiol* 2012; 47: 596-602.

(8) Moffat, B. A. *et al.* Functional diffusion map: a noninvasive MRI biomarker for early stratification of clinical brain tumor response. *Proc Natl Acad Sci U S A* 2005; 102: 5524-5529.

(9) Galban, C. J. *et al.* Computed tomography-based biomarker provides unique signature for diagnosis of COPD phenotypes and disease progression. *Nature medicine* 2012; 18: 1711-1715.

(10) Cho, N. *et al.* Breast cancer: early prediction of response to neoadjuvant chemotherapy using parametric response maps for MR imaging. *Radiology* 2014; 272: 385-396.

(11) Hoff, B. A. *et al.* Parametric response mapping of CT images provides early detection of local bone loss in a rat model of osteoporosis. *Bone* 2012; 51: 78-84.

(12) Gevenois, P. A., de Maertelaer, V., De Vuyst, P., Zanen, J. & Yernault, J. C. Comparison of computed density and macroscopic morphometry in pulmonary emphysema. *Am J Respir Crit Care Med* 1995; 152: 653-657.

(13) Pompe, E. *et al.* Parametric response mapping adds value to current computed tomography biomarkers in diagnosing chronic obstructive pulmonary disease. *Am J Respir Crit Care Med* 2015; 191: 1084-1086.

(14) Jogi, J., Ekberg, M., Jonson, B., Bozovic, G. & Bajc, M. Ventilation/perfusion SPECT in chronic obstructive pulmonary disease: an evaluation by reference to symptoms, spirometric lung function and emphysema, as assessed with HRCT. *Eur J Nucl Med Mol Imaging* 2011; 38: 1344-1352.

(15) Brudin, L. H. *et al.* Regional structure-function correlations in chronic obstructive lung disease measured with positron emission tomography. *Thorax* 1992; 47: 914-921.

(16) Kirby, M. *et al.* Chronic obstructive pulmonary disease: longitudinal hyperpolarized (3)He MR imaging. *Radiology* 2010; 256: 280-289.

(17) Kirby, M. *et al.* Hyperpolarized 3He and 129Xe MR imaging in healthy volunteers and patients with chronic obstructive pulmonary disease. *Radiology* 2012; 265: 600-610.

(18) Ohno, Y. *et al.* Oxygen-enhanced magnetic resonance imaging versus computed tomography: multicenter study for clinical stage classification of smoking-related chronic obstructive pulmonary disease. *Am J Respir Crit Care Med* 2008; 177: 1095-1102.

(19) Couch, M. J. *et al.* Inert fluorinated gas MRI: a new pulmonary imaging modality. *NMR Biomed* 2014; 27: 1525-1534.

(20) Fain, S. B. *et al.* Early emphysematous changes in asymptomatic smokers: detection with 3He MR imaging. *Radiology* 2006; 239: 875-883.

(21) Swift, A. J. *et al.* Emphysematous changes and normal variation in smokers and COPD patients using diffusion 3He MRI. *Eur J Radiol* 2005; 54: 352-358.

(22) Kirby, M., Pike, D., Coxson, H. O., McCormack, D. G. & Parraga, G. Hyperpolarized He Ventilation Defects Used to Predict Pulmonary Exacerbations in Mild to Moderate Chronic Obstructive Pulmonary Disease. *Radiology* 2014; 140161.

(23) Svenningsen, S. *et al.* What are ventilation defects in asthma? *Thorax* 2013.

(24) Parraga, G. *et al.* Hyperpolarized 3He ventilation defects and apparent diffusion coefficients in chronic obstructive pulmonary disease: preliminary results at 3.0 Tesla. *Invest Radiol* 2007; 42: 384-391.

(25) Kirby, M. *et al.* On the role of abnormal DLCO in ex-smokers without airflow limitation: symptoms, exercise capacity and hyperpolarised helium-3 MRI. *Thorax* 2013; thoraxjnl-2012-203108.

(26) Christner, J. A. *et al.* Size-specific Dose Estimates for Adult Patients at CT of the Torso. *Radiology* 2012; 265: 841-847.

(27) Brink, J. A. & Morin, R. L. Size-specific dose estimation for CT: how should it be used and what does it mean? *Radiology* 2012; 265: 666-668.

(28) Kirby, M. *et al.* Hyperpolarized 3He magnetic resonance functional imaging semiautomated segmentation. *Acad Radiol* 2012; 19: 141-152.

(29) Hu, S., Hoffman, E. A. & Reinhardt, J. M. Automatic lung segmentation for accurate quantitation of volumetric X-ray CT images. *IEEE Trans Med Imaging* 2001; 20: 490-498.

(30) Tschirren, J., Hoffman, E. A., McLennan, G. & Sonka, M. Intrathoracic airway trees: segmentation and airway morphology analysis from low-dose CT scans. *IEEE Trans Med Imaging* 2005; 24: 1529-1539.

(31) Sheikh, K. *et al.* Pulmonary ventilation defects in older never-smokers. *J Appl Physiol (1985)* 2014; 117: 297-306.

(32) Schroeder, J. D. *et al.* Relationships between airflow obstruction and quantitative CT measurements of emphysema, air trapping, and airways in subjects with and without chronic obstructive pulmonary disease. *AJR. American journal of roentgenology* 2013; 201: W460.

(33) Miller, R. R., Muller, N. L., Vedal, S., Morrison, N. J. & Staples, C. A. Limitations of computed tomography in the assessment of emphysema. *Am Rev Respir Dis* 1989; 139: 980-983.

(34) Nakano, Y. *et al.* The prediction of small airway dimensions using computed tomography. *Am J Respir Crit Care Med* 2005; 171: 142-146.

(35) Lynch, D. A. *et al.* CT-Definable Subtypes of Chronic Obstructive Pulmonary Disease: A Statement of the Fleischner Society. *Radiology* 2015; 141579.

(36) Nambu, A. *et al.* Relationships between diffusing capacity for carbon monoxide (DLCO), and quantitative computed tomography measurements and visual assessment for chronic obstructive pulmonary disease. *European Journal of Radiology* 2015; 84: 980-985.

(37) Evans, A. *et al.* Anatomical distribution of (3)He apparent diffusion coefficients in severe chronic obstructive pulmonary disease. *J Magn Reson Imaging.* 2007; 26: 1537-1547.

(38) Fichele, S. *et al.* MRI of helium-3 gas in healthy lungs: posture related variations of alveolar size. *J Magn Reson Imaging* 2004; 20: 331-335.

(39) Hajari, A. J. *et al.* Morphometric changes in the human pulmonary acinus during inflation. *J Appl Physiol (1985)* 2012; 112: 937-943.

(40) Heinrich, M. P. *et al.* MIND: Modality independent neighbourhood descriptor for multi-modal deformable registration. *Medical Image Analysis* 2012; 16: 1423-1435.

(41) Modat, M., McClelland, J. & Ourselin, S. Lung registration using the NiftyReg package. *Medical Image Analysis for the Clinic-A Grand Challenge* 2010; 2010: 33-42.

(42) Bommart, S. *et al.* Relationship between CT air trapping criteria and lung function in small airway impairment quantification. *BMC Pulm Med* 2014; 14: 29.

(43) Hersh, C. P. *et al.* Paired inspiratory-expiratory chest CT scans to assess for small airways disease in COPD. *Respir Res* 2013; 14: 42.

(44) Kim, E. Y. *et al.* Detailed analysis of the density change on chest CT of COPD using non-rigid registration of inspiration/expiration CT scans. *Eur Radiol* 2015; 25: 541-549.

(45) Gevenois, P. A. *et al.* Pulmonary emphysema: quantitative CT during expiration. *Radiology* 1996; 199: 825-829.

2.6 Supplement

2.6.1 Materials and Methods

2.6.1.1 Study Subjects

We recruited participants from a local tertiary care centre and by advertisement. Briefly, inclusion criteria comprised ambulatory males and females with a previous clinical diagnosis of COPD, aged 50-90 with a smoking history ≥10 pack-years. Exclusion criteria included claustrophobia, current smoker, body mass index >40 and any MRI contraindications (i.e. metal/electronic/magnetic implants). All participants were 53-88 years (mean age=73±9yrs) of age (male: mean age=73±9yrs, age range=55-88yrs; female: mean age=71±7yrs, age range=53-84yrs; p=.4). In a single two hour visit, participants underwent the following evaluations in the same order: 1) salbutamol administration, 2) spirometry, 3) plethysmography and DL_{CO}, 4) inspiration and expiration CT, and, 5) MRI. COPD subjects were classified according to the Global Initiative for Chronic Obstructive Lung Disease (GOLD) grades.[1]

2.6.1.2 Pulmonary Function

Post-bronchodilator plethysmography and spirometry were performed using a body plethysmograph (MedGraphics Corporation, St. Paul, Minnesota, USA) to measure the forced expiratory volume in one second (FEV_1), forced vital capacity (FVC) and static lung volumes including total lung capacity (TLC), inspiratory capacity (IC), residual volume (RV), and functional residual capacity (FRC). The diffusing capacity of lung for carbon monoxide (DL_{CO}) was also determined using the attached gas analyzer. Measurements were performed according to the American Thoracic Society (ATS) guidelines.[2]

2.6.1.3 MR Image Analysis

^{3}He static ventilation images were segmented using a k-means approach that classifies voxel intensity values into five clusters ranging from signal void (cluster 1[C1] or VDV) and hypo-intense (cluster 2 [C2]) to hyper-intense signal (cluster 5 [C5]), therefore

generating a gas distribution cluster-map. The delineation of the ventilation defect boundaries was performed using a seeded region-growing algorithm that segmented the ^{1}H MRI thoracic cavity, as previously described.[3]

^{3}He MRI ADC values were determined using a custom-built algorithm using MATLAB R2014b (MathWorks, Natick, Massachusetts, USA). To ensure that ADC were generated for voxels corresponding to ventilated lung regions, a k-means clustering algorithm,[3] was applied to the non-diffusion weighted images to obtain a binary mask for each slice. The resulting binary masks were applied to the corresponding non-diffusion weighted images, and the ADC maps were generated on a voxel-by-voxel basis according to **Equation 2-1**:

$$ADC = \frac{1}{b}\ln\left(\frac{S_0}{S}\right) \quad (2\text{-}1)$$

where S_0 is the segmented non-diffusion weighted image, S is the diffusion-weighted image, and b=1.6s/cm^2.

2.6.1.4 CT Image Analysis

PRM measures were generated by co-registering inspiratory and expiratory images using an affine method followed by a deformable step provided in the NiftyReg package[4] which is ranked among the top registration algorithms for thoracic CT.[5] The affine registration step was performed on a coarse-to-fine scheme to achieve both accuracy and computational efficiency. Voxel-wise comparisons were performed, where co-registered inspiration and expiration images were imported into MATLAB and voxels classified into four categories based on expiration and inspiration thresholds as previously described:[6] 1) inspiration >-950HU and expiration >-856HU (normal-tissue), 2) inspiration >-950HU and expiration <-856HU (gas-trapping), 3) inspiration <-950HU and expiration <-856HU (emphysema), and, 4) inspiration <-950HU and expiration >-856HU. As previously described,[6] the fourth category of voxels were hypothesized to reflect noise in the data due to registration error because previously, these did not correlate with FEV_1, FEV_1/FVC, or RA_{950}.

2.6.1.5 MRI-to-CT Spatial Overlap

^{3}He MRI was registered to ^{1}H MRI using a landmark-based approach[3] and ^{1}H MRI was registered to expiratory CT using deformable registration via the modality-independent-neighbourhood-descriptor (MIND) method, previously shown suitable for cross-modality image registration.[7] The deformation field was applied to the ^{3}He MRI slices for MRI-to-CT co-registration. The deformable registration consisted of voxel-wise similarity measurements of MIND of the two images, rather than the image themselves, as well as diffusion regularization of the deformation field and optimization using the Gauss-Newton framework. The registration was performed with three-levels (down-sampling factor of 4, 2, and 1) in a symmetric manner so that the algorithm was not dependent on the choice of moving or fixed image.

Spatial overlap for ^{3}He ventilation defects and PRM voxels was evaluated using the spatial overlap coefficient (SOC), which is the intersection of ^{3}He ventilation defect and PRM voxels expressed as a fraction of the total number of CT PRM voxels (SOC_{CT}) or ^{3}He MRI ventilation defect voxels (SOC_{MRI}). The rationale for performing spatial overlap measurements in this manner was to determine the contribution of ^{3}He defect voxels within PRM gas-trapped or emphysema regions. The spatial overlap of PRM voxels within ^{3}He defect regions (SOC_{MRI}) was also evaluated to determine the contribution of PRM (gas-trapping and/or emphysema) to ^{3}He ventilation defects. CT and ^{3}He images were evaluated once because the CT analysis was fully-automated and MRI semi-automated segmentation method was previously reported[3] to provide high inter- and intra-observer reproducibility. In total, CT and MR image analysis per subject was completed in approximately one hour.

2.6.1.6 Statistics

The variables considered were based on univariate relationships. The unstandardized ß coefficients were reported and show how a single-unit change in the independent variable influenced a change in the dependent variable. We also reported the standardized ß coefficients, expressed in units of standard deviation (SD) and these showed the independent variable with the greatest ß coefficient reflecting the greatest relative effect on the dependent variable. Multi-co-linearity was evaluated using the variance inflation factor

(VIF) and deemed acceptable when <10.[8] For spatial overlap coefficients, significant differences were measured using paired t-tests. Results were considered significant when the probability of two-tailed type I error (α) was less than 5% ($p<.05$).

2.6.2 Discussion

2.6.2.1 Limitations

The limitations of spirometry have motivated us and others to continue developing thoracic imaging methods including ventilation MRI and CT-PRM measurements to better phenotype patients using direct and regional measurements of the underlying disease.[9] Spirometry measurements of FEV_1 and FEV_1/FVC are reproducible and inexpensive, but these provide only a global measure of lung function that is dominated by larger airway function. For this reason, pulmonary function tests are relatively insensitive to early disease stages.[10] In addition, FEV_1 and FEV_1/FVC are relatively poor surrogates of COPD symptoms[11] and other outcomes perhaps because disease heterogeneity derives from the pathological features of COPD, including parenchyma destruction (emphysema) and airway remodeling (airways disease), which also differ in individual patients with the same FEV_1.[1,12]

We recognize that this study has a number of limitations. First, this work was limited by the relatively small study group and the fact that we mainly evaluated ex-smokers with mildly abnormal and normal spirometry. This was prospectively planned and driven by our interest to investigate very early or mild disease, but given our understanding of the heterogeneity of COPD patients, we must be cautious about extrapolating our results. We must also acknowledge that the results generated here were not compared with results stemming from commercially available software such as Apollo Workstation 2.0 (VIDA Diagnostics Inc., Coralville, Iowa, USA) or Lung Density Analysis software (IMBIO, Minneapolis, Minnesota, USA). It should be noted that any potential differences would likely stem from the different image registration/warping algorithms used because the density thresholds used are generally the same. Registration errors pose a challenge that has been previously reported for PRM in the liver[13] and we caution that registration errors

would result in tissue misclassification because PRM analysis relies heavily on voxel-by-voxel comparisons. Notably, in the parametric-response-maps generated here, there was consistent scattering of misclassified voxels and this underscores the need for optimized thoracic CT registration techniques to minimize these effects. We recognize that MRI-CT registration error will certainly affect the analysis of spatial agreement. For this reason, we used a pulmonary MRI-CT deformable registration method[7] previously described as highly suitable for cross-modality image registration and which achieved significantly better results than other methods, such as normalized mutual information.[7] Differences between PRM and ^{3}He may be related to the fact that PRM measurements are inherently more indirect as these are based on the abnormal presence of air due to both emphysema and airways disease. In contrast, inhaled gas methods provide static snapshots of regional ventilation. In advanced COPD, ventilation defects have been previously shown to reflect both emphysema and airways disease,[9] whereas in mild asthma, ventilation defects were shown to be directly related to abnormal airway wall thickening or airways disease.[14] Similar to four-dimensional CT,[15] Fourier decomposition MRI[16] and paired inspiratory/expiratory CT,[17-19] PRM exploits the image signal differences from inspiration and expiration as air moves in and out and tissue contracts and expands. All these approaches rely on either computational or intuitive co-registration of inspiratory and expiratory CT and assume that the abnormal presence of air can be regionally related to emphysema and/or functional small airways disease. Finally, hyperpolarized ^{3}He MRI is still limited to a few research facilities worldwide and is unlikely to be translated clinically due to the depleted global supply of ^{3}He. However, with recent improvements in ^{129}Xe polarization[20] and the development of ^{19}F MRI,[21] inhaled gas MRI may yet be considered for regulatory approval and future clinical workflows.

2.6.3 References

(1) Vestbo, J. *et al.* Global strategy for the diagnosis, management, and prevention of chronic obstructive pulmonary disease: GOLD executive summary. *Am J Respir Crit Care Med* 2013; 187: 347-365.

(2) Miller, M. R. *et al.* Standardisation of spirometry. *Eur Respir J* 2005; 26: 319-338.

(3) Kirby, M. *et al.* Hyperpolarized 3He magnetic resonance functional imaging semiautomated segmentation. *Acad Radiol* 2012; 19: 141-152.

(4) Modat, M., McClelland, J. & Ourselin, S. Lung registration using the NiftyReg package. *Medical Image Analysis for the Clinic-A Grand Challenge* 2010; 2010: 33-42.

(5) Murphy, K. *et al.* Evaluation of registration methods on thoracic CT: the EMPIRE10 challenge. *Medical Imaging, IEEE Transactions on* 2011; 30: 1901-1920.

(6) Galban, C. J. *et al.* Computed tomography-based biomarker provides unique signature for diagnosis of COPD phenotypes and disease progression. *Nature medicine* 2012; 18: 1711-1715.

(7) Heinrich, M. P. *et al.* MIND: Modality independent neighbourhood descriptor for multi-modal deformable registration. *Medical Image Analysis* 2012; 16: 1423-1435.

(8) O'Brien, R. M. A caution regarding rules of thumb for variance inflation factors. *Quality & Quantity* 2007; 41: 673-690.

(9) Kirby, M., Pike, D., Coxson, H. O., McCormack, D. G. & Parraga, G. Hyperpolarized He Ventilation Defects Used to Predict Pulmonary Exacerbations in Mild to Moderate Chronic Obstructive Pulmonary Disease. *Radiology* 2014; 140161.

(10) Vestbo, J. *et al.* Evaluation of COPD Longitudinally to Identify Predictive Surrogate End-points (ECLIPSE). *Eur Respir J* 2008; 31: 869-873.

(11) Agusti, A. *et al.* Characterisation of COPD heterogeneity in the ECLIPSE cohort. *Respir Res* 2010; 11: 122.

(12) Pauwels, R. A. *et al.* Global strategy for the diagnosis, management, and prevention of chronic obstructive pulmonary disease. NHLBI/WHO Global Initiative for Chronic Obstructive Lung Disease (GOLD) Workshop summary. *Am J Respir Crit Care Med* 2001; 163: 1256-1276.

(13) Lausch, A. *et al.* An augmented parametric response map with consideration of image registration error: towards guidance of locally adaptive radiotherapy. *Phys Med Biol* 2014; 59: 7039-7058.

(14) Svenningsen, S. *et al.* What are ventilation defects in asthma? *Thorax* 2014; 69: 63-71.

(15) Guerrero, T. *et al.* Dynamic ventilation imaging from four-dimensional computed tomography. *Physics in medicine and biology* 2006; 51: 777.

(16) Bauman, G. *et al.* Non-contrast-enhanced perfusion and ventilation assessment of the human lung by means of fourier decomposition in proton MRI. *Magn Reson Med* 2009; 62: 656-664.

(17) Bommart, S. *et al.* Relationship between CT air trapping criteria and lung function in small airway impairment quantification. *BMC Pulm Med* 2014; 14: 29.

(18) Hersh, C. P. *et al.* Paired inspiratory-expiratory chest CT scans to assess for small airways disease in COPD. *Respir Res* 2013; 14: 42.

(19) Kim, E. Y. *et al.* Detailed analysis of the density change on chest CT of COPD using non-rigid registration of inspiration/expiration CT scans. *Eur Radiol* 2015; 25: 541-549.

(20) Mugler, J. P., 3rd & Altes, T. A. Hyperpolarized 129Xe MRI of the human lung. *J Magn Reson Imaging* 2013; 37: 313-331.

(21) Ruiz-Cabello, J., Barnett, B. P., Bottomley, P. A. & Bulte, J. W. Fluorine (19F) MRS and MRI in biomedicine. *NMR Biomed* 2011; 24: 114-129.

CHAPTER 3

3 FREE-BREATHING PULMONARY ^{1}H AND HYPERPOLARIZED ^{3}HE MRI: COMPARISON IN COPD AND BRONCHIECTASIS

To better understand the potential for Fourier-decomposition MRI (FDMRI) to provide quantitative endpoints for COPD and bronchiectasis subjects, we developed and evaluated pulmonary ventilation abnormalities derived from free-breathing ^{1}H MRI. We quantitatively and qualitatively compared these measurements to those derived from ^{3}He MRI and pulmonary function tests.

The contents of this chapter were previously published in the journal Academic Radiology: DPI Capaldi, K Sheikh, F Guo, S Svenningsen, R Etemad-Rezai, HO Coxson, JA Leipsic, DG McCormack, and G Parraga. Acad Radiol 2015; 22(3):320-329. Permission to reproduce this article was granted by Elsevier Publishing and is provided in ***Appendix A****.*

3.1 Introduction

Chronic obstructive pulmonary disease (COPD) is diagnosed and disease severity stratified based on not fully reversible airflow obstruction measured using spirometry. Airflow obstruction, symptoms, and exercise capacity measurements in COPD are related to both parenchyma destruction (emphysema) and airway remodeling (airways disease and bronchiectasis).[1,2] While spirometry is relatively easy to implement, reproducible, and inexpensive, it can only provide a global measure of lung function and is weakly predictive of COPD progression, as well as insensitive to early disease stages.[3-5] The limitations of spirometry measurements of COPD have motivated the development of thoracic imaging approaches to provide direct and regional measurements of the underlying pathological features of COPD - airways disease and emphysema.

High resolution computed tomography (HRCT) is the clinical imaging tool of choice for visualizing and quantifying airways disease[6,7] and emphysema[8-10] in COPD patients. Emphysema can be quantified automatically based on thresholds of the CT density histogram (<-950 Hounsfield units [HU]).[8,10,11] Thoracic CT estimates of airways disease can also be generated using measurements of airway wall area percent (WA%) and lumen area (LA). Indirect measurements of airways disease include CT measurements of gas

trapping using densitometry thresholds (-856HU) on expiratory CT images[12] or parametric response maps (PRM) using co-registered inspiratory and expiratory CT.[13] Finally, bronchiectasis can be readily observed in thoracic CT in up to 50% of patients with severe COPD,[14,15] and this is typically identified by enlarged bronchial diameters and evidence of significant mucous plugging.

Pulmonary magnetic resonance imaging (MRI) using inhaled hyperpolarized ^{3}He or ^{129}Xe gas also provides a way to visualize regional ventilation abnormalities and lung microstructure in subjects with COPD.[16-25] Ventilation abnormalities may be quantified using the ventilation defect percent (VDP), that represents the volume of ventilation defects normalized to the thoracic cavity.[24,26] While rapid (8-15s acquisition time) and well-tolerated, inhaled noble gas MRI is dependent on polarized gas and multinuclear MR hardware. An alternative approach that exploits Fourier decomposition of free-breathing pulmonary MRI (FDMRI) was first developed by Bauman and colleagues at 1.5T.[27] This method provides a way to generate quantitative pulmonary maps of ventilation and perfusion using fast pulmonary MRI acquisitions of free-breathing ^{1}H MRI and non-rigid registration.[27-33] FDMRI was recently compared and validated with SPECT-CT[28] and ^{3}He MRI[30] in a porcine model.

Until now, FDMRI has not been evaluated in COPD or bronchiectasis subjects, nor at 3T where there is diminished signal intensity at higher field strengths due to T_2* effects.[34] Hence, our objective was to generate FDMRI (first developed at 1.5T) and ^{3}He MRI ventilation measurements acquired at 3T in subjects with COPD or bronchiectasis. We hypothesized that ventilation defects measured using FDMRI and ^{3}He MRI would be spatially and quantitatively correlated in subjects with COPD and those with bronchiectasis.

3.2 Materials and Methods

3.2.1 Study Subjects

All subjects were previously diagnosed with COPD or bronchiectasis by a pulmonologist and provided written informed consent to the study protocol approved by a local research

ethics board and Health Canada. COPD subjects were classified according to the Global initiative for chronic Obstructive Lung Disease (GOLD) grades.[1] COPD subjects were ex-smokers between 50 to 80 years of age and with a smoking history of ≥ 10 pack-years (the number of packs of cigarettes smoked per day multiplied by the number of years the patient has smoked). Subjects with bronchiectasis were ex-smokers (n=4) and never-smokers (n=10) between 40 to 85 years of age. An expert chest radiologist (>20y experience) qualitatively examined CT data for evidence of bronchiectasis and emphysema.

3.2.2 Pulmonary Function Tests

Spirometry and whole body plethysmography was performed using a body plethysmograph (MedGraphics Corporation, St. Paul, Minnesota, USA) to measure the forced expiratory volume in one second (FEV_1), forced vital capacity (FVC) and static lung volumes including total lung capacity (TLC), inspiratory capacity (IC), residual volume (RV), and functional residual capacity (FRC), airways resistance (R_{AW}), and the diffusing capacity of lung for carbon monoxide (DL_{CO}) using the attached gas analyzer. All measurements were performed according to the American Thoracic Society (ATS) guidelines.[35]

3.2.3 Image Acquisition

MRI was performed with a whole-body 3T Discovery MR750 system (General Electric Health Care [GEHC], Milwaukee, Wisconsin, USA) capable of performing multinuclear imaging. All MR images were acquired in the coronal slice orientation. Conventional ^{1}H MRI was performed 5 minutes prior to hyperpolarized ^{3}He MRI. Subjects were instructed to maintain normal tidal breathing and then from functional residual capacity (FRC) inhale a 1.0L mixture of $^{4}He/N_2$. For the purposes of this study and in order to aid direct comparisons, all MRI and CT images were acquired at FRC+1.0L in order for consistency. By having all subjects inhale 1.0L of gas after passive expiration, we ensured consistent lung volumes across all imaging methods. We also note that in order to truly capture the same lung volume consistently, our approach of using a measured volume for inhalation is straightforward and easily undertaken even supine in the CT or MR scanner. ^{1}H MRI was acquired with subjects in breath-hold position using a whole-body radiofrequency coil and

a ^{1}H fast spoiled gradient-recalled echo (FGRE) sequence with a partial echo (total data acquisition time=12s; repetition time [TR]/echo time [TE]/flip-angle=4.3ms/1.0ms/30°; field-of-view [FOV]=40×40cm^2; matrix=128×80 [zero-padded to 128×128]; partial echo percent=62.5%; bandwidth [BW]=62.50kHz; number of excitations [NEX]=1; number of slices=14; slice thickness=15mm). For all MRI breath-hold maneuvers, oxygen saturation (S_PO_2) was continuously monitored using a digital pulse oximeter.

Hyperpolarized ^{3}He MRI was performed using a single channel rigid elliptical transmit-receive chest coil (RAPID Biomedical, Rimpar, Wuerzburg, Germany). A polarizer system (HeliSpin; Polarean, Durham, North Carolina, USA) was utilized to polarize the ^{3}He gas, which achieved polarization levels of approximately 40%. Doses of 5mL/kg of body weight were diluted with medical-grade N_2 gas (Spectra Gases, Branchburg, New Jersey, USA) and administered in 1.0L Tedlar bags (Jensen Inert Products, Coral Springs, Florida, USA). Hyperpolarized ^{3}He ventilation images were acquired with subjects in breath-hold position after inspiration of a 1.0L ^{3}He/N_2 mixture using a fast gradient-recalled echo method with a partial echo (total data acquisition time=10s; TR/TE/flip-angle=3.8ms/1.0ms/7°; FOV=40×40cm^2; matrix=128×80 [zero-padded to 128×128]; partial echo percent=62.5%; BW=62.50kHz; NEX=1; number of slices=14; slice thickness=15mm). The flip angle was determined using a constant flip angle approach where flip angle (α) depends on the number of phase encoding steps (Y-gradient steps). Thus, $\alpha = \tan^{-1}\sqrt{2/N}$, where N was a number of Y-gradient steps. Therefore for this pulse sequence, where there are 128 Y-gradient steps, a 7.12° flip angle was used. Hyperpolarized ^{3}He diffusion-weighted images were acquired using a FGRE sequence with centric *k*-space sampling (total data acquisition time=14s; TR/TE/flip-angle=6.8ms/4.5ms/8°; FOV=40×40cm^2; matrix=128×128; BW=62.50kHz; NEX=1; number of slices=7; slice thickness=30mm). Two interleaved images were acquired with and without additional diffusion sensitization (G=1.94G/cm; b=1.6s/cm^2; rise-and-fall time=0.5ms; gradient duration=0.46ms; diffusion time=1.46ms).

Dynamic free tidal-breathing ^{1}H MRI was acquired over a period of 125s at a rate of four frames per second using an optimized balanced steady state free precession sequence

(bSSFP) and respiratory bellows. We used a fast imaging employing steady state pulse sequence (FIESTA, GEHC) with total data acquisition time=125s, TE/TR/flip-angle=0.6ms/1.9ms/15°, FOV=40×40cm, matrix = 256×256, BW=250kHz, NEX=1, number of phases=500, slice thickness=15mm, and a 32-channel torso coil (GEHC). A single coronal slice was obtained with slice thickness=15mm. The number of phases refers to the number of images acquired from one specific location over time. In other words, we acquired multiple frames of one single coronal slice over a certain time span. The slice was prescribed on an axial localizer and was positioned slightly posterior to the cardiac silhouette in an effort to eliminate artifacts due to cardiac motion but allow visualization of the aorta.

CT was acquired using a 64 slice Lightspeed VCT scanner (GEHC) at FRC+1.0L of N_2 gas using a spiral acquisition (detector configuration=64×0.625mm; peak x-ray tube voltage=120kVp; effective x-ray tube current=100mA; x-ray tube rotation time=500ms; pitch=1.0). Image reconstruction was performed using a standard convolution kernel for 1.25mm isotropic resolution.

3.2.4 Image Analysis

Segmentation of ^{3}He MRI and FDMRI ventilation was performed using custom software generated using MATLAB R2013a (Mathworks, Natick, Massachusetts, USA), as previously described.[26] ^{3}He MRI apparent diffusion coefficient (ADC) maps were generated as previously described.[36] The relative area of the CT density histogram with attenuation values < -950HU (RA_{950}) was determined using MATLAB R2013a (Mathworks). Pulmonary Workstation 2.0 (VIDA Diagnostics Inc., Coralville, Iowa, USA) was used to quantify WA% and lumen area LA.

Image analysis of dynamic free-breathing ^{1}H MRI was performed using MATLAB R2013a (Mathworks). Non-rigid registration was used to co-register the temporal series of tidal-breathing ^{1}H MRI slices using a modality independent neighbourhood descriptor (MIND) deformable registration method.[37] A specific reference image was used so that the corresponding lung volume was consistent with ^{3}He MRI volumes. Pulmonary voxel intensities from the registered free-breathing ^{1}H MRI were aligned along a time axis and

discrete Fourier transforms were performed on the signal intensity oscillation pattern. The frequency of the first ventilation harmonic (corresponding to the respiratory rate) was determined for every voxel, the magnitude of which was used to generate a ventilation map.

The Dice Similarity Coefficient (DSC)[38] was used to quantify the regional overlap for ^{3}He MRI and FDMRI ventilation as well as the spatial relationship of CT RA_{950} density maps with FDMRI ventilation defect volume.

3.2.5 Statistics

Independent *t*-tests, tests for normality (determined with a Shapiro-Wilk test), and analysis of variance (ANOVA) with post-hoc analysis using the Holm-Bonferroni correction were performed using SPSS Statistics V22.0 (SPSS Inc., Chicago, Illinois, USA). Pearson correlation coefficients (r) were used to determine the correlation between measurements using SPSS Statistics V22.0 (SPSS Inc.). Measurement agreement was evaluated using the Bland-Altman method using GraphPad Prism V6.0 (GraphPad Software Inc., La Jolla, California, USA). Correlation coefficients were compared using the Fisher z′ transformation for each r value.[21] Results were considered significant when the probability of two-tailed type I error (α) was less than 5% ($p<.05$).

3.3 Results

Table 3-1 shows the demographic and pulmonary function test measurements for all subjects (69±10yrs) as well as the 12 COPD (67±9yrs) and 14 bronchiectasis subjects (70±11yrs). For COPD subjects, three were GOLD grade I, four were GOLD grade II, and five were GOLD grades III/IV. CT evidence of emphysema only was reported in seven COPD subjects and there was CT evidence of both emphysema and bronchiectasis in five COPD subjects.

Table 3-1 Subject demographic and pulmonary function measurements

Mean (±SD)	All (n=26)	Bronchiectasis (n=14)	COPD (n=12)	Sig Dif (p)
Age yrs	69 (10)	70 (11)	67 (9)	.5
Male n	11	4	7	--
BMI $kg \cdot m^{-2}$	25 (4)	23 (4)	27 (4)	**.02**
Pack years	31 (40)	4 (10)	63 (39)	**<.001**
FEV_1 $\%_{pred}$	64 (22)	68 (22)	60 (23)	.4
FVC $\%_{pred}$	82 (22)	73 (20)	91 (22)	**.04**
FEV_1/FVC %	60 (16)	70 (12)	50 (14)	**.001**
TLC $\%_{pred}$	107 (18)	98 (14)	117 (16)	**.003**
RV/TLC %	51 (10)	54 (11)	49 (9)	.3
R_{AW} $\%_{pred}$	138 (41)	135 (48)	141 (33)	.7
DL_{CO} $\%_{pred}$	57 (19)	60 (18)	53 (21)	.3

Sig Dif: Significant difference between subgroups ($p<.05$) determined by ANOVA; SD: standard deviation; $\%_{pred}$: percent of predicted value; BMI: body mass index; FEV_1: forced expiratory volume in one second; FVC: forced vital capacity; TLC: total lung capacity; RV: residual volume; R_{AW}: airways resistance; DL_{CO}: diffusing capacity of lung for carbon monoxide.

Figure 3-1 shows coronal FDMRI and ^{3}He MRI ventilation registered to the ^{1}H MRI of the thorax, as well as RA_{950} and ^{3}He ADC maps for two representative COPD and two representative bronchiectasis subjects. As shown in **Figure 3-1**, for all four subjects there were qualitatively similar ventilation patterns derived from FDMRI and ^{3}He MRI. In COPD subjects, regional ventilation defects were also qualitatively similar to regional emphysema apparent in the RA_{950} density maps and the brighter regions of ^{3}He MRI ADC maps.

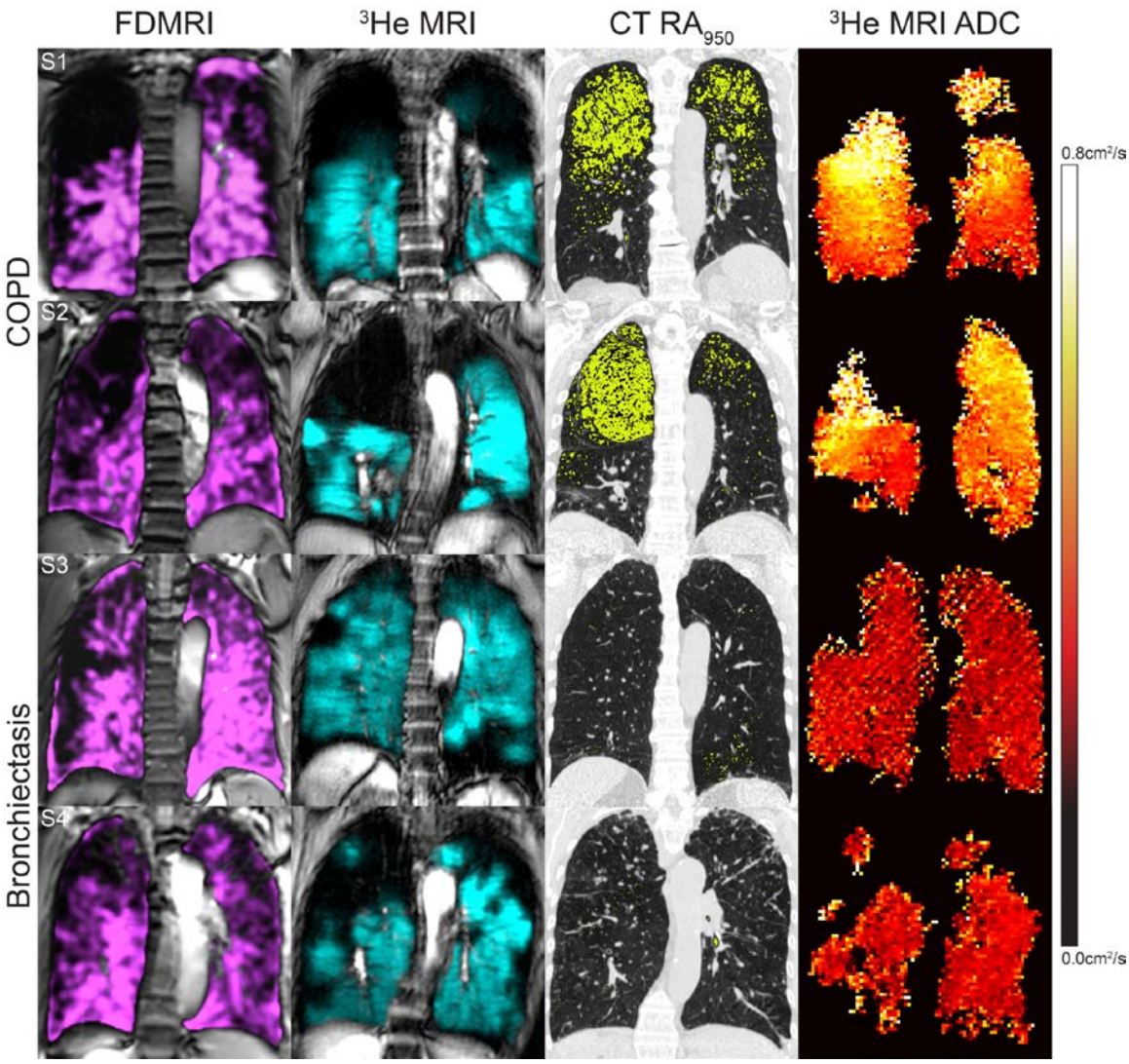

Figure 3-1 Ventilation and CT imaging for representative COPD and bronchiectasis subjects
FDMRI in magenta co-registered with ^{1}H MRI. ^{3}He MRI static ventilation in aqua co-registered with ^{1}H MRI. CT density masks where yellow = attenuation < -950 Hounsfield units (RA_{950}) and ^{3}He MRI ADC maps, both reflective of emphysema for COPD subjects (S1 and S2) and Bronchiectasis subjects (S3 and S4).

Table 3-2 provides imaging measurements for COPD and bronchiectasis subjects. FDMRI (94±4%) and ^{3}He MRI (79±12%) ventilation measurements were significantly different ($p<.001$). FDMRI VDP (6±4%) was also significantly different than ^{3}He MRI VDP (21±12%) ($p<.001$). As expected, ^{3}He MRI ADC was significantly greater in COPD as compared to bronchiectasis subjects ($p<.001$) and all CT measurements (RA_{950}, WA%, and LA) were significantly greater in COPD as compared to bronchiectasis subjects.

Table 3-2 Imaging measurements

Mean (±SD)	All (n=26)	Bronchiectasis (n=14)	COPD (n=12)	Sig Dif (p)
FDMRI Ventilation %	94 (4)	95 (3)	93 (6)	.3
^{3}He MRI Ventilation %	79 (12)	82 (9)	76 (14)	.2
FDMRI VDP %	6 (4)	5 (3)	7 (6)	.3
^{3}He MRI VDP %	21 (12)	18 (9)	24 (14)	.2
^{3}He MRI ADC cm^{2}/s	0.35 (0.13)	0.27 (0.05)	0.43 (0.12)	**<.001**
CT RA_{950} %	5 (7)	2 (3)	9 (8)	**.005**
CT WA %	57 (2)	58 (2)	56 (2)	**.009**
CT LA mm^{2}	46 (14)	40 (10)	53 (15)	**.01**

Sig Dif: significant difference between groups (p<.05) by ANOVA; SD: standard deviation; VDP: ventilation defect percent; ADC: apparent diffusion coefficient; RA_{950}: relative area of the lung with attenuation values <-950HU; WA: wall area; LA: lumen area.

Figure 3-2 shows the linear correlation of FDMRI with ^{3}He MRI VDP and the agreement between measurements for both COPD and bronchiectasis subjects. Although FDMRI and ^{3}He MRI VDP were significantly different, as shown in **Table 3-2**, these measurements were strongly correlated in COPD (r=.88, p=.0001), but not bronchiectasis subjects (r = .1, p>.05). Bland-Altman analysis showed a bias of -16±9% (-35%-5% 95% CI) for FDMRI (**Figure 3-2**) and this bias increased with increasing VDP for COPD subjects. FDMRI VDP was also strongly correlated with RA_{950} (r=.80, p=.002) and ^{3}He MRI ADC (r=.71, p=.01) for COPD subjects, both of which are well-established measurements of emphysema.[8,16]

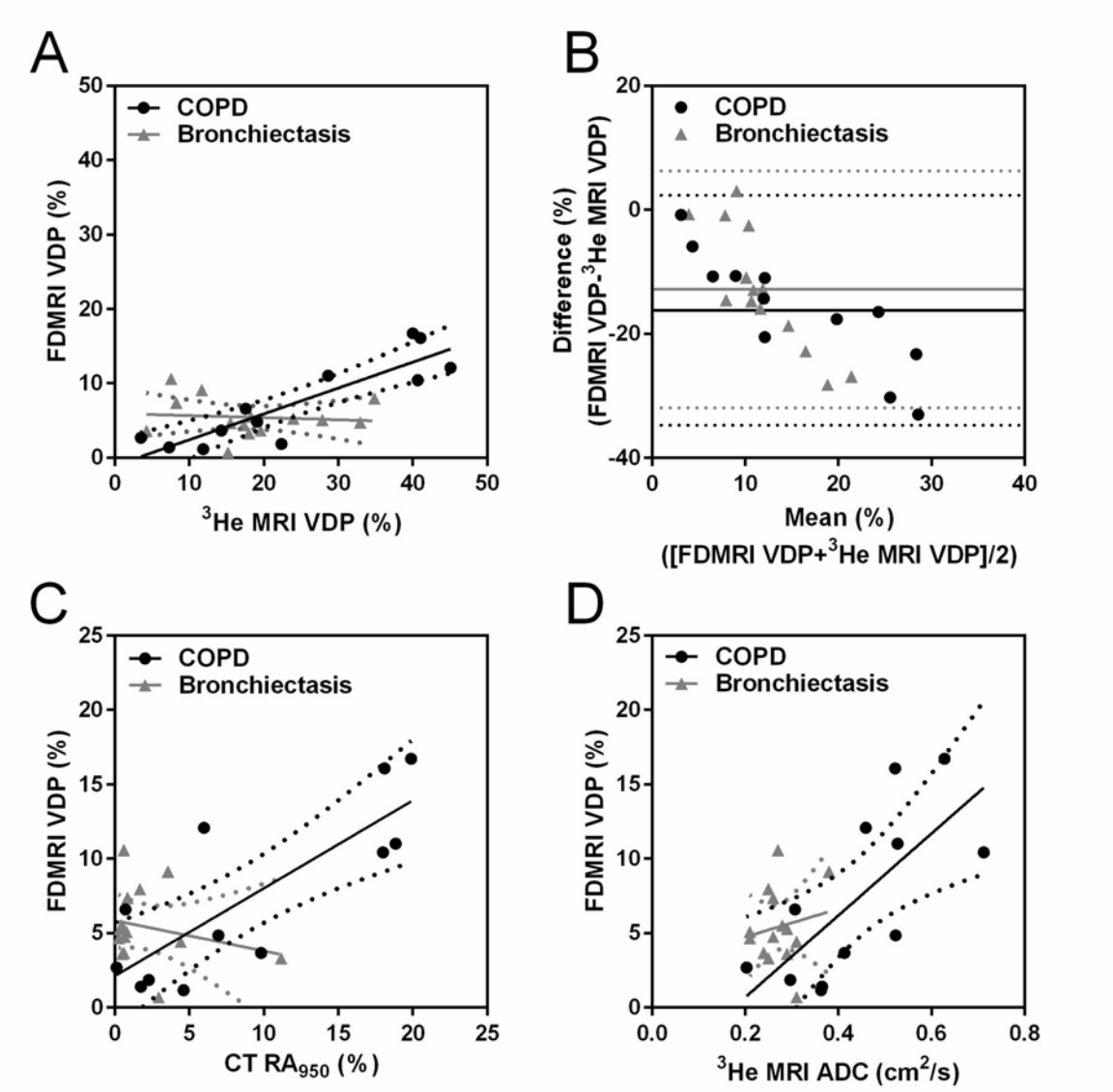

Figure 3-2 Correlations for FDMRI with ^{3}He MRI and CT RA$_{950}$
A) FDMRI VDP linear regression with ^{3}He MRI VDP (COPD: r=.88, r^2=.78, p=.0001, y=0.35x–1.07 and Bronchiectasis: r=-.1, r^2=.009, p>.05, y=-0.03x+5.92)
B) Bland-Altman analysis of agreement for FDMRI and ^{3}He MRI VDP (COPD: bias=-16±9%, lower limit=-35%, upper limit=2%; Bronchiectasis: bias=-13±10%, lower limit=-32%, upper limit=6%).
C) FDMRI VDP linear regression with CT RA$_{950}$ (COPD: r=.80, r^2=.64, p=.002, y=0.59x+2.10; Bronchiectasis: r=-.23, r^2=.05, p>.05, y=-.21x+5.85)
D) FDMRI VDP linear regression with ^{3}He MRI ADC (COPD: r=.71, r^2=.51, p=.01, y=28x+5; Bronchiectasis: r=.16, r^2=.03, p>.05, y=9.4x+2.9).
Dotted lines =95% confidence intervals.

Given the strong correlation between FDMRI and ^{3}He MRI VDP for COPD subjects, we evaluated the spatial relationships for ventilation and ventilation defects derived from using both these methods. These data are shown in **Table 3-3** and for representative COPD (S1 and S2) and bronchiectasis subjects (S3 and S4) in **Figure 3-3**. **Table 3-3** provides mean DSC for FDMRI and ^{3}He MRI ventilation and ventilation defects. The DSC for FDMRI and ^{3}He MRI ventilation was 86% for both subject groups. In a similar fashion, the spatial overlap of FDMRI ventilation with lung regions >-950HU was 92% and 93% for COPD and bronchiectasis subjects respectively. For ventilation defects, the spatial relationship of FDMRI and ^{3}He MRI ventilation defects was 20±17% and 14±9% for COPD and bronchiectasis subjects respectively. In COPD subjects, the DSC for FDMRI ventilation defects with lung regions <-950HU, reflective of emphysema was 19±20%. For bronchiectasis subjects, the spatial overlap of FDMRI and lung regions <-950HU (2±3%) was significantly lower than the spatial overlap of FDMRI and ^{3}He MRI ventilation defects (20±17%) ($p<.001$).

Table 3-3 Quantitative spatial relationships for FDMRI Ventilation and Ventilation defects

Mean DSC (±SD)	All (n=26)	Bronchiectasis (n=14)	COPD (n=12)	Sig Dif (p)
Ventilation				
FDMRI–^{3}He MRI %	86 (5)	86 (4)	86 (7)	.8
FDMRI–$RA_{>950}$ %	92 (3)	93 (2)	92 (3)	.5
Ventilation Defects				
FDMRI–^{3}He MRI %	16 (13)	14 (9)	20 (17)	.2
FDMRI–RA_{950} %	10 (16)	2 (3)	19 (20)	**.005**

Sig Dif: Significant difference between groups ($p<.05$) by ANOVA; DSC: Dice Similarity Coefficient; VDP: ventilation defect percent; ADC: apparent diffusion coefficient; RA_{950}: relative area <-950HU; $RA_{>950}$: relative area >-950HU.

Some of these spatial relationships are also shown in **Figure 3-3**, where the regional similarities of FDMRI with ^{3}He static ventilation images are visually apparent for COPD subjects S1 and S2 and less obvious for bronchiectasis subjects S3 and S4. In particular for the bronchiectasis subjects, there is little evidence of emphysema and therefore there is negligible overlap between RA_{950} and ventilation defects.

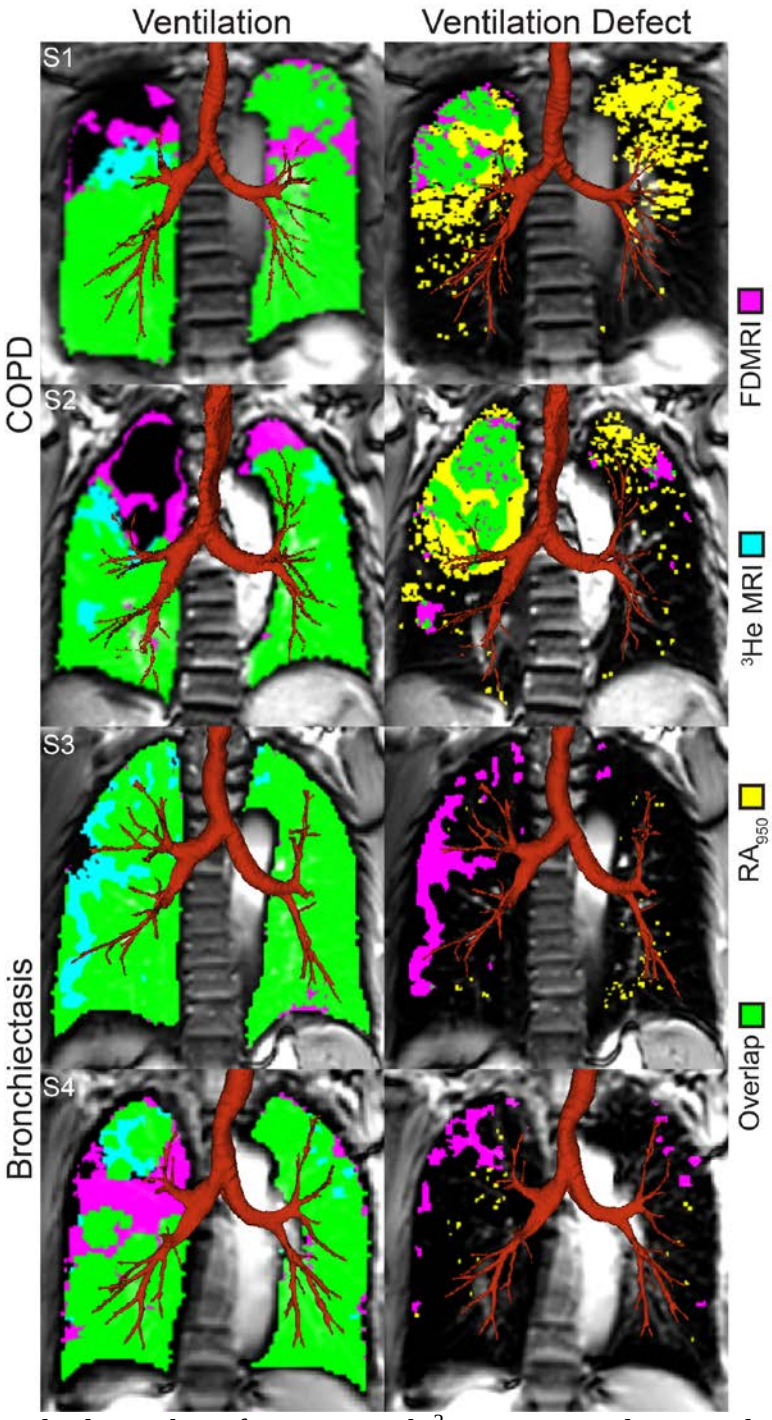

Figure 3-3 Spatial relationship of FDMRI with ^{3}He MRI ventilation and emphysema for representative subjects with COPD and Bronchiectasis

Left panel: Spatial overlap (green) of FDMRI (purple) and ^{3}He MRI (aqua) ventilation co-registered with ^{1}H MRI and airway tree in brown. Right panel: Spatial overlap (green) of FDMRI (purple) ventilation defects and RA_{950} mask (yellow) co-registered with CT for COPD subjects S1 and S2 and Bronchiectasis subjects S3 and S4.

Dice coefficients for FDMRI–^{3}He MRI ventilation: S1=88%, S2=86%, S3=91%, S4=84% and FDMRI defects–RA_{950}: S1=41%, S2=56%, S3=1%, S4=0%.

Table 3-4 summarizes the significant correlations for FDMRI VDP with ^{3}He MRI, CT, and pulmonary function measurements for the COPD and bronchiectasis subgroups. There were significant correlations for FDMRI VDP with ^{3}He MRI VDP and ADC, R_{AW} and RA_{950} ($p<.05$) for COPD subjects. For bronchiectasis subjects there was a significant correlation between FDMRI VDP and LA ($p<.05$). For COPD subjects, the FDMRI and ^{3}He MRI VDP correlations were not significantly different; however, for bronchiectasis subjects, there were significant differences.

Table 3-4 Pearson Correlations for FDMRI and ^{3}He MRI

	FDMRI VDP %		**^{3}He MRI VDP %**		**Fisher z′**	
	Bronchiectasis (n=14) r/p	**COPD (n=12) r/p**	**Bronchiectasis (n=14) r/p**	**COPD (n=12) r/p**	**B p**	**C p**
FEV_1 $\%_{pred}$	.41/.1	-.22/.5	**-.73/.003**	-.42/.2	**.001**	.6
FVC $\%_{pred}$	.31/.3	.20/.5	**-.60/.02**	-.04/.9	**.02**	.7
RV/TLC %	-.31/.3	-.19/.6	**.65/.02**	-.07/.8	**.01**	.8
R_{AW} $\%_{pred}$	-.23/.4	**.60/.04**	.47/.09	.56/.06	.08	.9
DL_{CO} $\%_{pred}$	.08/.8	-.57/.05	-.36/.2	**-.61/.04**	.3	.9
FDMRI Ventilation %	**~-1/<.001**	**~-1/<.001**	.1/.7	**-.88/<.001**	**<.001**	**<.001**
FDMRI VDP %	--/--	--/--	-.1/.7	**.88/<.001**	--	--
^{3}He MRI Ventilation %	.1/.7	**-.88/<.001**	**~-1/<.001**	**~-1/<.001**	**<.001**	**<.001**
^{3}He MRI VDP %	-.10/.7	**.88/<.001**	--/--	--/--	--	--
^{3}He MRI ADC (cm^2/s)	.16/.6	**.71/.01**	.35/.2	**.76/.004**	.6	.8
CT RA_{950} %	-.23/.4	**.80/.002**	-.04/.9	**.72/.008**	.6	.7
CT WA %	-.35/.2	-.07/.8	.29/.3	-.18/.6	.1	.8
CT LA mm^2	**.58/.03**	.43/.2	-.09/.7	**.59/.04**	.08	.6

r: Pearson correlation coefficients; $\%_{pred}$: percent of predicted value; FEV_1: forced expiratory volume in one second; FVC: forced vital capacity; RV/TLC: residual volume/total lung capacity; R_{AW}: airways resistance; DL_{CO}: Diffusing capacity for carbon monoxide; VDP: ventilation defect percent; ADC: apparent diffusion coefficient; RA_{950}: relative area of the lung with attenuation < -950HU; WA: wall area; LA: lumen area.

3.4 Discussion

In this proof-of-concept study, we evaluated 26 patients including 12 subjects with COPD and another 14 with bronchiectasis and observed: 1) in all subjects, FDMRI VDP was significantly less than ^{3}He MRI VDP, 2) in COPD but not bronchiectasis subjects, FDMRI and ^{3}He MRI ventilation and VDP were quantitatively correlated and these values showed strong spatial relationships with one another and with RA_{950} maps, and, 3) in COPD subjects only there were significant and similar correlations for FDMRI and ^{3}He MRI VDP with pulmonary function test and CT measurements.

In all subjects, FDMRI VDP was significantly less than ^{3}He MRI VDP. It is difficult to completely understand why FDMRI VDP was significantly less and FDMRI ventilation was significantly greater than ^{3}He MRI measurements in all subjects. However, one explanation may be derived from the underlying principles of the two methods and how they generate or capture ventilation information. Inhaled contrast gas methods provide static breath-hold snapshots of where the high contrast inhaled gas travels to and resides during the scanning period of 8-15s. In this manner, very high contrast and signal-to-noise ventilation images can be easily generated and processed. In contrast, but similar to four-dimensional CT (4DCT) which produces three-dimensional image datasets through time,[39,40] FDMRI generates ventilation contrast based on image signal differences during the breathing cycle as air enters and leaves the pulmonary system and tissue contracts and expands. This is a more indirect approach that relies on robust and accurate image processing methods to co-register the dynamic free tidal-breathing ^{1}H MRI. This method also relies on the inherent image signal intensity and signal-to-noise ratios of pulmonary images from a system that is inherently air-filled. In CT, the attenuation values for air as compared to tissue provide significant contrast. However, the contrast derived from the ^{1}H signal changes are inherently weak, and this certainly necessitates that the image processing methods used must be more complex and robust. Previous work[41] explored the spatial and quantitative relationship of ^{3}He MRI and 4DCT ventilation measurements in a proof of concept demonstration in a small number of non-small cell lung cancer patients. There was excellent spatial correspondence for the ventilation maps derived using static MRI and free-breathing CT imaging approaches with no significant differences in ventilation. These results provided good evidence that ventilation maps and measurements generated using vastly different image acquisition and analysis methods as well as breathing maneuvers provided similar regional and quantitative ventilation information.

It is important to note that ^{3}He MRI ventilation percent and VDP are not independent measurements since these simply sum to 100%. However, because here we are directly comparing VDP which is a relatively small volume and ventilation which is a large volume for both FD and ^{3}He MRI, we think it's important to use and compare both values. This is especially important in order to show spatial relationships such as the Dice coefficient that

is highly dependent on the relative size of the comparators. We think this is also important because the ^{3}He ventilation MRI depicts gas distribution, whereas, FDMRI ventilation reflects the ventilation fundamental frequency and signal intensity changes related to this value. Because of this, spatial overlap analyses were conducted for both ventilation maps and ventilation defect maps obtained using both ^{3}He and FDMRI.

In COPD, but not bronchiectasis subjects, FDMRI and ^{3}He MRI ventilation were quantitatively and spatially related. In addition, FDMRI and ^{3}He MRI VDP were quantitatively correlated and showed strong spatial relationships with RA_{950} maps – those regions that reflected emphysematous destruction or air in CT images. We were surprised to observe such differences in the spatial and quantitative correlations for FDMRI and ^{3}He MRI in COPD as compared to bronchiectasis subjects. One explanation can be derived from the presence of thick mucus (which appears as greater ^{1}H signal intensity relative to that of parenchyma tissue) in the airways and parenchyma in bronchiectasis that may lead to registration error. To generate FDMRI ventilation images, registration algorithms must account for the movement of the diaphragm and any registration error will result in regions of high signal intensity (e.g. mucus pooling in bronchiectasis subjects) oscillating at the same frequency as respiration. This registration error can result in apparently increased ventilation, which may or may not accurately reflect truly ventilated regions. Thus, in bronchiectasis subjects, there may be regions that appear as ventilated in FDMRI that are in fact not ventilated due to misalignment of the mucus' boundaries via the deformable registration process. We must acknowledge that all three imaging methods measure very different physical parameters. For example, while CT provides a measurement of regional lung tissue density, ^{3}He MRI provides a functional estimate of pulmonary ventilation and alveolar dimensions using diffusion-weighted imaging. FDMRI on the other hand, provides an estimate of ventilation by quantifying the signal intensity contributions throughout the compression and expansion of the lung parenchyma via the cardiac and the respiratory cycles. However, we recently showed that in COPD subjects, ^{3}He MRI ventilation defects often co-localize with large emphysematous bullae.[42] In fact, we previously observed this in patients with advanced emphysema and because of this work hypothesized that this spatial co-localization was related to the long time constants for

filling of emphysematous bullae and not airways disease. Here and in light of these previous findings, we directly evaluated the spatial co-localization of emphysematous regions with FDMRI and ^{3}He MRI ventilation defects. The spatial relationships observed for FDMRI and ^{3}He MRI ventilation defects with RA_{950} in the current study suggest that in patients with emphysema, ventilation defects generated using FDMRI may also be derived to the long time-constants for lung filling. Our findings further support the notion that these methods (i.e. FDMRI, ^{3}He MRI, and CT), though very different, are probing and interrogating similar functional but likely not structural information in COPD subjects. It appears that a free-breathing method like FDMRI, shows some dependence on the very long time constants for filling emphysematous bullae, and this finding should be considered when using FDMRI for COPD imaging.

Finally, in COPD subjects only, there were significant and similar correlations for FDMRI and ^{3}He MRI VDP with pulmonary function test and CT measurements. These are important findings that further support and suggest that both methods provide similar functional information in COPD subjects even though they are different methods. In contrast, for bronchiectasis subjects, there was a significant correlation between FDMRI VDP and airway lumen area. This suggests that elevated lumen area (corresponding to dilated airways) may be related to low proton density.

We recognize and acknowledge that this work was limited by the relatively small sample size. In addition, we studied mainly subjects with moderate COPD (8/12 subjects with GOLD grade II or III) and given our understanding of the heterogeneity of COPD patients, caution should be used when extrapolating our results to a broader COPD group. Fourier decomposition has recently emerged as a pulmonary functional MRI method, with the promise of serial lung function measurements without a dependence on polarized or other inhaled gases or multinuclear capabilities. This opens up the opportunity for functional lung imaging on conventional MRI scanners - available more universally, albeit the final measurements are dependent on more sophisticated image processing methods. It should be noted that one of the challenges associated with pulmonary proton MRI methods, is the weak pulmonary proton signal intensity that is further diminished at higher field strengths because of the relationship between field-strength and T_2* effects. Previous pilot and

development studies at 1.5T, have shown qualitative agreement for regional ventilation and perfusion measurements with the clinical reference standard SPECT/CT.[28] Moreover, recent studies have also demonstrated the reproducibility of FDMRI ventilation- and perfusion-weighted images in healthy volunteers.[32] Finally FDMRI-to-^{3}He MRI comparisons in animals showed similar regional abnormalities including pulmonary embolism, atelectasis, and air trapping.[30]

To our knowledge, there has been no prospective comparison of FDMRI with ^{3}He MRI at 3T in subjects with COPD and bronchiectasis. Consistent with previous studies we showed similar regional ventilation abnormalities using FDMRI and ^{3}He MRI in COPD subjects and these appear to be dominated by the presence of regional emphysematous bullae. In summary, FDMRI and ^{3}He MRI ventilation and VDP were strongly correlated in COPD, but not bronchiectasis subjects. In COPD subjects only, FDMRI ventilation defects were also spatially related with ^{3}He MRI ventilation defects and CT measurements of emphysema.

3.5 References

(1) Vestbo, J. *et al.* Global strategy for the diagnosis, management, and prevention of chronic obstructive pulmonary disease: GOLD executive summary. *Am J Respir Crit Care Med* 2013; 187: 347-365.

(2) Pauwels, R. A. *et al.* Global strategy for the diagnosis, management, and prevention of chronic obstructive pulmonary disease. NHLBI/WHO Global Initiative for Chronic Obstructive Lung Disease (GOLD) Workshop summary. *Am J Respir Crit Care Med* 2001; 163: 1256-1276.

(3) Vestbo, J. *et al.* Evaluation of COPD Longitudinally to Identify Predictive Surrogate End-points (ECLIPSE). *Eur Respir J* 2008; 31: 869-873.

(4) Cerveri, I. *et al.* Underestimation of airflow obstruction among young adults using FEV(1)/FVC < 70% as a fixed cut-off: a longitudinal evaluation of clinical and functional outcomes. *Thorax* 2008; 63: 1040-1045.

(5) Enright, P. L. & Kaminsky, D. A. Strategies for screening for chronic obstructive pulmonary disease. *Respir Care* 2003; 48: 1194-1201; discussion 1201-1193.

(6) Hackx, M., Bankier, A. A. & Gevenois, P. A. Chronic Obstructive Pulmonary Disease: CT Quantification of Airways Disease. *Radiology* 2012; 265: 34-48.

(7) Nakano, Y. *et al.* Quantitative assessment of airway remodeling using high-resolution CT. *Chest* 2002; 122: 271s-275s.

(8) Hayhurst, M. D. *et al.* Diagnosis of pulmonary emphysema by computerised tomography. *Lancet* 1984; 2: 320-322.

(9) Klein, J. S., Gamsu, G., Webb, W. R., Golden, J. A. & Muller, N. L. High-resolution CT diagnosis of emphysema in symptomatic patients with normal chest radiographs and isolated low diffusing capacity. *Radiology* 1992; 182: 817-821.

(10) Müller, N., Staples, C., Miller, R. & Abboud, R. " Density mask". An objective method to quantitate emphysema using computed tomography. *Chest* 1988; 94: 782.

(11) Uppaluri, R., Mitsa, T., Sonka, M., Hoffman, E. A. & McLennan, G. Quantification of pulmonary emphysema from lung computed tomography images. *Am J Respir Crit Care Med* 1997; 156: 248-254.

(12) Zach, J. A. *et al.* Quantitative computed tomography of the lungs and airways in healthy nonsmoking adults. *Invest Radiol* 2012; 47: 596-602.

(13) Galban, C. J. *et al.* Computed tomography-based biomarker provides unique signature for diagnosis of COPD phenotypes and disease progression. *Nature medicine* 2012; 18: 1711-1715.

(14) O'Brien, C., Guest, P. J., Hill, S. L. & Stockley, R. A. Physiological and radiological characterisation of patients diagnosed with chronic obstructive pulmonary disease in primary care. *Thorax* 2000; 55: 635-642.

(15) Patel, I. S. *et al.* Bronchiectasis, exacerbation indices, and inflammation in chronic obstructive pulmonary disease. *Am J Respir Crit Care Med* 2004; 170: 400-407.

(16) de Lange, E. E. *et al.* Lung air spaces: MR imaging evaluation with hyperpolarized 3He gas. *Radiology* 1999; 210: 851-857.

(17) Kauczor, H. U. *et al.* Normal and abnormal pulmonary ventilation: Visualization at hyperpolarized He-3 MR imaging. *Radiology* 1996; 201: 564-568.

(18) Albert, M. S. *et al.* Biological Magnetic-Resonance-Imaging Using Laser Polarized Xe-129. *Nature* 1994; 370: 199-201.

(19) Mathew, L. *et al.* Hyperpolarized (3)He magnetic resonance imaging: preliminary evaluation of phenotyping potential in chronic obstructive pulmonary disease. *Eur J Radiol* 2011; 79: 140-146.

(20) Kirby, M. *et al.* Pulmonary ventilation visualized using hyperpolarized helium-3 and xenon-129 magnetic resonance imaging: differences in COPD and relationship to emphysema. *Journal of Applied Physiology* 2013; 114: 707-715.

(21) Kirby, M. *et al.* Hyperpolarized 3He and 129Xe MR imaging in healthy volunteers and patients with chronic obstructive pulmonary disease. *Radiology* 2012; 265: 600-610.

(22) Driehuys, B. *et al.* Chronic obstructive pulmonary disease: safety and tolerability of hyperpolarized 129Xe MR imaging in healthy volunteers and patients. *Radiology* 2012; 262: 279-289.

(23) Kaushik, S. S. *et al.* Diffusion-weighted hyperpolarized 129Xe MRI in healthy volunteers and subjects with chronic obstructive pulmonary disease. *Magn Reson Med* 2011; 65: 1154-1165.

(24) Parraga, G. *et al.* Hyperpolarized 3He ventilation defects and apparent diffusion coefficients in chronic obstructive pulmonary disease: preliminary results at 3.0 Tesla. *Invest Radiol* 2007; 42: 384-391.

(25) Kirby, M. *et al.* Chronic obstructive pulmonary disease: longitudinal hyperpolarized (3)He MR imaging. *Radiology* 2010; 256: 280-289.

(26) Kirby, M. *et al.* Hyperpolarized 3He magnetic resonance functional imaging semiautomated segmentation. *Acad Radiol* 2012; 19: 141-152.

(27) Bauman, G. *et al.* Non-contrast-enhanced perfusion and ventilation assessment of the human lung by means of fourier decomposition in proton MRI. *Magn Reson Med* 2009; 62: 656-664.

(28) Bauman, G. *et al.* Pulmonary functional imaging: qualitative comparison of Fourier decomposition MR imaging with SPECT/CT in porcine lung. *Radiology* 2011; 260: 551-559.

(29) Bauman, G. *et al.* Validation of Fourier decomposition MRI with dynamic contrast-enhanced MRI using visual and automated scoring of pulmonary perfusion in young cystic fibrosis patients. *European journal of radiology* 2013; 82: 2371-2377.

(30) Bauman, G. *et al.* Lung ventilation-and perfusion-weighted Fourier decomposition magnetic resonance imaging: In vivo validation with hyperpolarized 3He and dynamic contrast-enhanced MRI. *Magn Reson Med* 2013; 69: 229-237.

(31) Kjørstad, Å. *et al.* Quantitative lung perfusion evaluation using fourier decomposition perfusion MRI. *Magnetic Resonance in Medicine* 2013.

(32) Lederlin, M. *et al.* Functional MRI using Fourier decomposition of lung signal: Reproducibility of ventilation-and perfusion-weighted imaging in healthy volunteers. *European journal of radiology* 2013.

(33) Sommer, G. *et al.* Non-contrast-enhanced preoperative assessment of lung perfusion in patients with non-small-cell lung cancer using Fourier decomposition magnetic resonance imaging. *Eur J Radiol* 2013; 82: e879-887.

(34) Yu, J., Xue, Y. & Song, H. K. Comparison of lung T2* during free-breathing at 1.5 T and 3.0 T with ultrashort echo time imaging. *Magnetic Resonance in Medicine* 2011; 66: 248-254.

(35) Miller, M. R. *et al.* Standardisation of spirometry. *Eur Respir J* 2005; 26: 319-338.

(36) Kirby, M., Heydarian, M., Wheatley, A., McCormack, D. G. & Parraga, G. Evaluating bronchodilator effects in chronic obstructive pulmonary disease using diffusion-weighted hyperpolarized helium-3 magnetic resonance imaging. *J Appl Physiol (1985)* 2012; 112: 651-657.

(37) Heinrich, M. P. *et al.* MIND: Modality independent neighbourhood descriptor for multi-modal deformable registration. *Medical Image Analysis* 2012; 16: 1423-1435.

(38) Dice, L. R. Measures of the Amount of Ecologic Association between Species. *Ecology* 1945; 26: 297-302.

(39) Guerrero, T. *et al.* Dynamic ventilation imaging from four-dimensional computed tomography. *Phys Med Biol* 2006; 51: 777-791.

(40) Castillo, R., Castillo, E., Martinez, J. & Guerrero, T. Ventilation from four-dimensional computed tomography: density versus Jacobian methods. *Phys Med Biol* 2010; 55: 4661-4685.

(41) Mathew, L. *et al.* Hyperpolarized (3)He magnetic resonance imaging: comparison with four-dimensional x-ray computed tomography imaging in lung cancer. *Acad Radiol* 2012; 19: 1546-1553.

(42) Kirby, M., Pike, D., Coxson, H. O., McCormack, D. G. & Parraga, G. Hyperpolarized He Ventilation Defects Used to Predict Pulmonary Exacerbations in Mild to Moderate Chronic Obstructive Pulmonary Disease. *Radiology* 2014; 140161.

CHAPTER 4

4 FREE-BREATHING FUNCTIONAL PULMONARY MRI: RESPONSE TO BRONCHODILATOR AND BRONCHOPROVOCATION IN SEVERE ASTHMA

*Based on the free-breathing pulmonary ^{1}H MRI approach developed in **Chapter 3**, we wanted to determine the potential application for Fourier-decomposition MRI in evaluating ventilation heterogeneity in patients with severe asthma, both pre- and post-salbutamol as well as post-methacholine challenge. We qualitatively and quantitatively compared these measurements to those derived from ^{3}He MRI.*

*The contents of this chapter were previously published in the journal Academic Radiology: DPI Capaldi, K Sheikh, RL Eddy, F Guo, S Svenningsen, P Nair, DG McCormack, and G Parraga for the Canadian Respiratory Research Network. Acad Radiol 2017; 24(10):1268-1276. Permission to reproduce this article was granted by Elsevier Publishing and is provided in **Appendix A**.*

4.1 Introduction

Asthma is a chronic and often debilitating airways disease, characterized by intermittent worsening of breathlessness, cough, chest-tightness and wheeze and is typically diagnosed based on spirometry measurements of bronchodilator reversibility[1] or response to methacholine challenge[2] using the forced expiratory volume in one second (FEV_1).[3] While current asthma therapies were developed based on FEV_1 improvements,[4] this measurement of airflow limitation is relatively insensitive to small airway obstruction,[5,6] which is believed to be the main sight of inflammation and airway remodeling (or pre modeling) in asthma.[7] For many children and adults with asthma, disease control remains elusive and a recent survey identified that over 90% of Canadian asthmatics reported poorly-controlled disease and nearly half did not participate in any exercise of any type due to asthma symptoms.[8] This unacceptable disease morbidity and the large and growing number of asthma patients of all ages has motivated the development of pulmonary imaging approaches to generate new and more sensitive biomarkers of small airway dysfunction. To date however, it has been complex to utilize such imaging biomarkers in the development of new therapies in clinical trials[9] or to guide therapy decisions in individual patients.

In asthmatics, thoracic computed tomography (CT) can be used to provide asthma biomarkers of gas-trapping,[10] airway remodeling[11] such as airway wall thickening and lumen narrowing,[12] and dynamic changes in ventilation using xenon-enhanced dual energy CT.[13] Although ultra-low dose CT methods using iterative adaptive reconstruction methods are now under development,[14] because of radiation dose concerns, the clinical use of CT in asthmatics has been limited, especially in mild disease and in children.[15-17] Other examples include positron emission tomography (PET)[18] and single photon emission computed tomography (SPECT),[19,20] both of which have been used in the research setting to evaluate regional ventilation heterogeneity in asthmatics.[18-20]

Magnetic resonance imaging (MRI) methods also provide a way to measure lung structure and function. In particular, inhaled-noble gas MRI ventilation defects[21-27] were shown to be spatially persistent over time,[21] related to airway abnormalities,[22] worsened in response to bronchoconstriction[23] and improve post-bronchodilator.[24] Inhaled-gas MRI ventilation defects also correlate with pulmonary function measurements,[25,26] CT evidence of gas-trapping,[26] disease severity,[22,25] inflammation,[22] and asthma control.[27] Other examples include oxygen-enhanced T_1 mapping of ventilation patterns in asthmatics[28,29] and a number of conventional ^{1}H MRI methods.[30-35] For example, ^{1}H signal intensity at different lung volumes may be used to estimate regional ventilation[30] and was recently compared with hyperpolarized ^{3}He MRI.[31] Fourier decomposition ^{1}H MRI (FDMRI) is another approach[32] that generates ventilation and perfusion maps in free-breathing participants in about two minutes using balanced steady state free precession pulse sequences without cardiac or respiratory gating. FDMRI ventilation defects were previously observed to be spatially related to SPECT-CT defects[33] and ^{3}He MRI ventilation defects in animal models[34] and COPD patients.[35]

To our knowledge, FDMRI has not been evaluated in patients with severe asthma, and this is important because FDMRI may be an important tool for evaluating ventilation and perfusion abnormalities in asthmatics in whom repeated CT is not clinically acceptable and at centres where multinuclear MRI is not available. Therefore, here our objective was to directly compare FDMRI with ^{3}He MRI VDP in severe and poorly controlled asthmatics. Based on previous results,[24,35] we hypothesized that FDMRI VDP would be quantitatively

related to ^{3}He MRI VDP and show similar responses to both methacholine and salbutamol in patients with severe asthma.

4.2 Materials and Methods

4.2.1 Study Logistics and Participants

Sixteen asthmatics (49±10yrs) provided written informed consent to ethics board approved and Health Insurance Portability and Accountability Act compliant protocols (https://clinicaltrials.gov NCT02351141, NCT02263794). We enrolled patients between 18 and 70 years of age with a diagnosis of severe asthma, according to the Global Initiative for Asthma (GINA),[1] from two academic tertiary care centres (Robarts Research Institute, Western University, London, Canada; Firestone Institute for Respiratory Health, McMaster University, Hamilton, Canada). All participants underwent pulmonary function tests, multiple breath gas washout, dynamic free-breathing ^{1}H, static ^{1}H and hyperpolarized ^{3}He MRI, at baseline and 20 minutes after salbutamol administration, within a single two-hour visit. Asthmatics with $FEV_1 > 70\%_{predicted}$ also underwent methacholine challenge (MCh), as per American Thoracic Society (ATS) guidelines[2] with MRI performed at the provocative concentration that lowered FEV_1 by 20% (PC_{20}) and 20 minutes post-salbutamol after MCh test completion.

4.2.2 Spirometry, Plethysmography and Multiple Breath Nitrogen Washout

Spirometry and whole body plethysmography were performed using a *MedGraphics Elite Series* plethysmograph (MedGraphics Corporation, St. Paul, Minnesota, USA), according to ATS guidelines[36] before and after administration of four separate doses of 100μg of salbutamol (Apo-Salvent CRC Free Inhalation Aerosol Apotex, Toronto, Ontario, Canada) through a pressurized metered dose inhaler using an *AeroChamber Plus* spacer (Trudell Medical International, London, Canada). Methacholine challenge was performed according to ATS guidelines[2] using the two-minute tidal breathing method up to and including PC_{20} using an *AeroEclipse II* Breath Actuated Nebulizer (Trudell Medical

International). After PC_{20} imaging was completed, salbutamol was administered. During MCh only, spirometry was performed using a handheld *ndd EasyOne* spirometer (ndd Medizintechnik AG, Zurich, Switzerland). Multiple breath gas washout was performed using the *ndd EasyOne Pro LAB* system (ndd Medizintechnik AG, Zurich, Switzerland) equipped with an ultrasonic flow and molar mass sensor to measure the lung clearance index (LCI), as previously described.[27]

4.2.3 Image Acquisition

MRI was performed in a single two-hour visit at baseline, post-MCh and post-salbutamol in those participants in whom MCh could be safely completed; in all others, MRI was performed at baseline and post-salbutamol. MRI was performed on a whole body 3 Tesla Discovery MR750 (General Electric Health Care [GEHC], Milwaukee, Wisconsin, USA) system with broadband imaging capability.[37] All images were acquired in the coronal plane. Static breath hold ^{1}H MRI was acquired with subjects in breath hold using a whole body radiofrequency coil[38] and fast spoiled gradient recalled echo (FGRE) sequence with a partial echo (total-acquisition-time=16s; repetition-time[TR]/echo-time[TE]/flip-angle=4.7ms/1.2ms/30°;field-of-view [FOV]=40×40cm^2, bandwidth[BW]=24.4kHz; matrix=128×80 [zero-padded to 128×128]; partial-echo-percent=62.5%; number-of-slices=15-17; slice-thickness=15mm, 0-gap). Hyperpolarized ^{3}He static ventilation MRI was performed using a single channel, rigid elliptical transmit/receive chest coil (RAPID Biomedical GmbH, Wuerzburg, Germany) and two dimensional multi-slice FGRE sequence with a partial echo during a single breath-hold (total-acquisition-time=10s; TR/TE/flip-angle=3.8ms/1.0ms/7°; FOV=40×40cm^2, BW=48.8kHz; matrix=128×80 [zero-padded to 128×128]; partial-echo-percent=62.5%; number-of-slices=15-17; slice-thickness=15mm, 0-gap). Polarization was approximately 40% using a commercial polarizer system (HeliSpin, Polarean, Durham, North Carolina, USA. All breath hold maneuvers were performed with the subject instructed to inhale a 1.0L gas mixture from a Tedlar® bags (Jensen Inert Products, Coral Springs, Florida, USA) after passive expiration (functional residual capacity [FRC]).[37] Hyperpolarized ^{3}He gas was diluted with medical grade N_2 (Spectra Gases, Newark, New Jersey, USA) and delivered in a 1.0L Tedlar® bag.

Oxygen saturation (S_PO_2) was continuously monitored using a digital pulse oximeter for all breath hold maneuvers.

Dynamic free breathing ^{1}H MRI was acquired for a single coronal slice using a 32 channel torso coil (GEHC) including respiratory bellows to monitor the patient's respiratory rate using an optimized balanced steady state free precession (bSSFP) sequence (total-acquisition-time=125s; TR/TE/flip-angle=1.9ms/0.6ms/15°; FOV=40×40cm^2; BW=250kHz; matrix=256×256; number-of-slices=1; slice-thickness=15mm; number-of-excitations=1; number-of-phases=500).[35]

4.2.4 Image Analysis

Ventilation abnormalities were quantified using the ventilation defect percent (VDP) which is the ventilation defect volume (VDV) normalized to the thoracic cavity volume (TCV). Hyperpolarized inhaled noble gas MR ventilation images were segmented and registered to the ^{1}H MRI thoracic cavity as previously described[38] by a single observer with four years segmentation experience. Briefly, ^{3}He MR static ventilation images were segmented using a k-means approach that classified voxel intensity values into five clusters (signal void=cluster 1 [C1] or VDV, hypo-intense=cluster 2 [C2] to hyper-intense signal=cluster 5 [C5]) to generate cluster maps.

Figure 4-1 provides a schematic of the approach used to generate and quantify FDMR ventilation images using MATLAB R2016a (Mathworks).[35] Dynamic free breathing ^{1}H MR images were co-registered to a reference with lung volume consistent with inhaled-gas MRI volume (FRC+1L) using a modality independent neighbourhood descriptor (MIND) deformable registration method.[39] Discrete fast Fourier transforms were performed on the signal intensity oscillation pattern generated from the pulmonary voxel intensities in the co-registered free breathing ^{1}H images. The magnitude of the first ventilation harmonic (which corresponded to the respiratory rate) was determined for each and every voxel and this was used to generate the FDMR ventilation image. **Figure 4-1** also shows the schematic of FDMRI semi-automated segmentation method where the reference ^{1}H MRI was segmented to generate the thoracic volume using a continuous max-flow segmentation algorithm and hierarchical k-means clustering was used to segment the FDMR ventilation

images into the same five clusters used to segment the hyperpolarized inhaled noble gas ventilation images.[38]

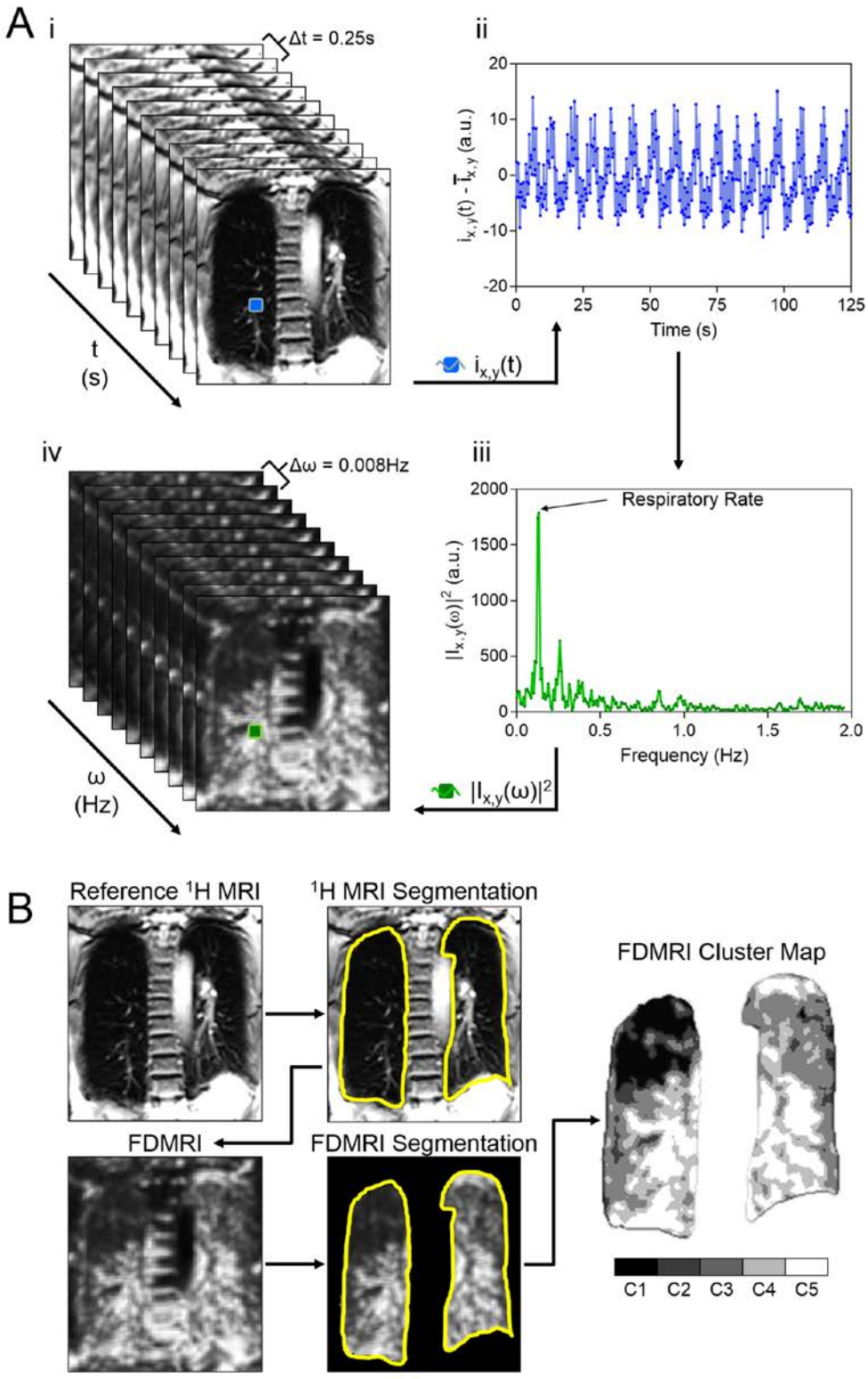

Figure 4-1 FDMRI ventilation map and analysis pipelines

A) Schematic for FDMRI ventilation map generation: i) co-registered MRI aligned along the time axis; ii) oscillating signal intensity pattern upon which discrete fast Fourier transforms performed; iii) magnitude of the frequency of the first ventilation harmonic determined for every voxel; iv) FDMRI ventilation maps generated.
B) Schematic of FDMRI VDP semi-automated segmentation: Anatomical ^{1}H MRI segmented, k-means VDP segmentation where cluster 1 (C1) = ventilation-defects, clusters 2-to-5 (C2-C5) = hypo-intense-to-hyper-intense ventilation.

4.2.5 Statistics

The Shapiro-Wilk test was used to determine the normality of the data and when data were not normally distributed, non-parametric tests were performed. Differences between time-points were determined using Wilcoxon signed rank paired t-test for non-parametric data. A repeated measures ANOVA was performed to investigate treatment (baseline, post MCh, and post salbutamol) and measurement (^{3}He MRI and FDMRI) effects and the Mauchly's test of sphericity was used to test the assumption of sphericity. Relationships were determined using Spearman coefficients (ρ). Agreement between imaging methods were determined using the Bland-Altman method.[40] All statistics were performed using SPSS Statistics V24.0 (SPSS Inc., Chicago, Illinois, USA). Results were considered significant when the probability of two-tailed type I error (α) was less than 5% ($p<.05$)

4.3 Results

4.3.1 Patient Characteristics

Table 4-1 shows participant demographic information as well as pulmonary function test measurements, asthma medication, and asthma control measurements for 16 asthmatics (49±10yrs) including seven patients with severe disease (50±10yrs) and nine patients with severe and uncontrolled[1] disease (49±11yrs). For the nine patients with poorly-controlled disease, ACQ score was significantly greater ($p=.01$), although they were prescribed maximal, guideline-based therapies including long acting β2 agonists (LABA) and high-dose inhaled corticosteroids (ICS).[1]

Table 4-1 Asthma demographics, medication, control and pulmonary function tests

Mean (±SD)	Asthma		
	All (n=16)	**Severe (n=7)**	**Severe Uncontrolled (n=9)**
Age yrs	49 (10)	50 (10)	49 (11)
Male n	6	2	4
BMI $kg \cdot m^{-2}$	28 (4)	28 (5)	28 (4)
FEV_1 $\%_{pred}$	66 (24)	64 (19)	68 (28)
FVC $\%_{pred}$	84 (14)	85 (12)	83 (16)
FEV_1/FVC %	61 (15)	59 (14)	63 (17)
RV $\%_{pred}$	140 (35)	142 (27)	139 (42)
TLC $\%_{pred}$	106 (13)	104 (13)	108 (14)
RV/TLC %	43 (10)	46 (7)	41 (11)
FRC $\%_{pred}$	115 (25)	120 (20)	111 (29)
R_{AW} $\%_{pred}$	170 (61)	161 (45)	176 (74)
LCI	9.2 (2.6)†	9.8 (2.6)	8.6 (3.7)$^{\sim}$
ACQ score	2.0 ± 1.2†	1.2 (0.6)	2.6 (1.2)$^{\sim}$
AQLQ score	5.0 ± 1.4†	5.8 (0.8)	4.4 (1.5)$^{\sim}$
mMRC dyspnea score	0.9 ± 0.7	0.7 (0.8)	1.0 (0.8)
Borg dyspnea	1.4 ± 1.5	0.6 (0.7)	2.1 (1.7)
ICS n [%]	16 [100]	7 [100]	9 [100]
OCS n [%]	6 [40]	2 [29]	4 [44]
SABA n [%]	14 [93]	6 [86]	8 [89]
LABA n [%]	16 [100]	7 [100]	9 [100]
SAMA n [%]	3 [20]	1 [14]	2 [22]
LAMA n [%]	4 [27]	1 [14]	3 [33]
Anti-IgE n [%]	3 [20]	1 [14]	2 [22]
LTRA n [%]	7 [47]	3 [43]	4 [44]

$\%_{pred}$=percent-of-predicted-value; BMI=body-mass-index; FEV_1=forced-expiratory-volume-in-one-second; FVC=forced-vital-capacity; RV=residual-volume; TLC=total-lung-capacity; FRC=functional-residual-capacity; R_{AW}=airways-resistance; LCI=lung-clearance-index; ICS=Inhaled Corticosteroids; OCS=Oral Corticosteroid; SABA=Short-Acting β2-Agonist; LABA=Long-Acting β2-Agonist; SAMA=Short-Acting Anticholinergic; LAMA=Long-Acting Anticholinergic; Anti-IgE=Anti-immunoglobulin E; LTRA=Leukotriene Receptor Antagonists; ACQ=Asthma Control Questionnaire; AQLQ=Asthma Quality of Life Questionnaire; mMRC=modified Medical Research Council; †n=15; $^{\sim}$n=8.

4.3.2 Ventilation Response to Salbutamol

Figure 4-2 shows centre coronal ^{3}He MRI and FDMRI slices for participant S8 with severe uncontrolled asthma (56yr old male, FEV_1=37%$_{pred}$) and another participant, S4 with severe asthma (57yr old female, FEV_1=52%$_{pred}$). Pre-salbutamol, there were numerous and large inhaled gas MRI and FDMRI ventilation defects in both patients and these qualitatively improved, post-salbutamol. As shown in **Table 4-2** and **Figure 4-2**, for all asthmatics, VDP significantly decreased (^{3}He MRI p=.02 and FDMRI; p=.02) post-

salbutamol. **Table 4-2** also provides lung clearance index as well as MRI VDP measurements for all 16 patients.

Table 4-2 Subject listing of hyperpolarized inhaled gas MRI, FDMRI and multiple breath gas washout measurements for each time-point

	Pre-Salbutamol			**PC_{20}**			**Post-Salbutamol**		
	^{3}He VDP (%)	**FD VDP (%)**	**LCI**	**^{3}He VDP (%)**	**FD VDP (%)**	**LCI**	**^{3}He VDP (%)**	**FD VDP (%)**	**LCI**
Severe									
S1	3.6	0.7	7.7	5.2	1.6	--	2.6	1.5	7.3
S2	7.0	7.6	9.5	--	--	--	3.3	5.5	10.1
S3	2.2	0.6	6.7	--	--	--	2.4	1.7	6.1
S4	9.1	4.9	13.5	--	--	--	7.4	2.6	13.2
S5	17.0	1.6	11.7	--	--	--	17.5	1.2	9.7
S6	10.3	2.3	11.9	--	--	--	9.6	1.3	10.8
S7	1.0	0.6	7.4	--	--	--	0.5	0.7	7.7
Mean	7.2	2.6	9.8	5.2	1.6	--	6.2	2.1	9.3
±SD	5.6	2.7	2.6	--	--	--	5.9	1.6	2.4
Severe-Uncontrolled									
S8	27.7	7.9	17.5	--	--	--	24.2	5.4	15.5
S9	5.2	0.2	8.6	6.0	8.1	--	7.0	1.5	8.2
S10	1.9	0.2	7.1	8.0	5.3	--	1.8	1.5	7.7
S11	2.9	4.9	7.1	--	--	--	2.4	3.3	6.6
S12	2.1	1.2	6.2	15.8	5.9	--	1.2	0.2	6.5
S13	3.2	1.5	6.4	--	--	--	3.1	0.7	6.4
S14	32.1	4.7	--	--	--	--	17.2	5.1	--
S15	5.7	9.0	7.5	--	--	--	5.7	6.1	7.4
S16	14.6	1.6	8.7	--	--	--	3.5	0.3	8.8
Mean	10.6	3.5	8.6	10.0	6.4	--	7.4	2.7	8.4
±SD	11.6	3.3	3.7	5.1	1.5	--	8.0	2.3	3.0

LCI=lung-clearance-index; VDP=ventilation-defect-percent: PC_{20}=Provocative-concentration that decreased the forced-expiratory-volume-in-one-second (FEV_1) by 20%.

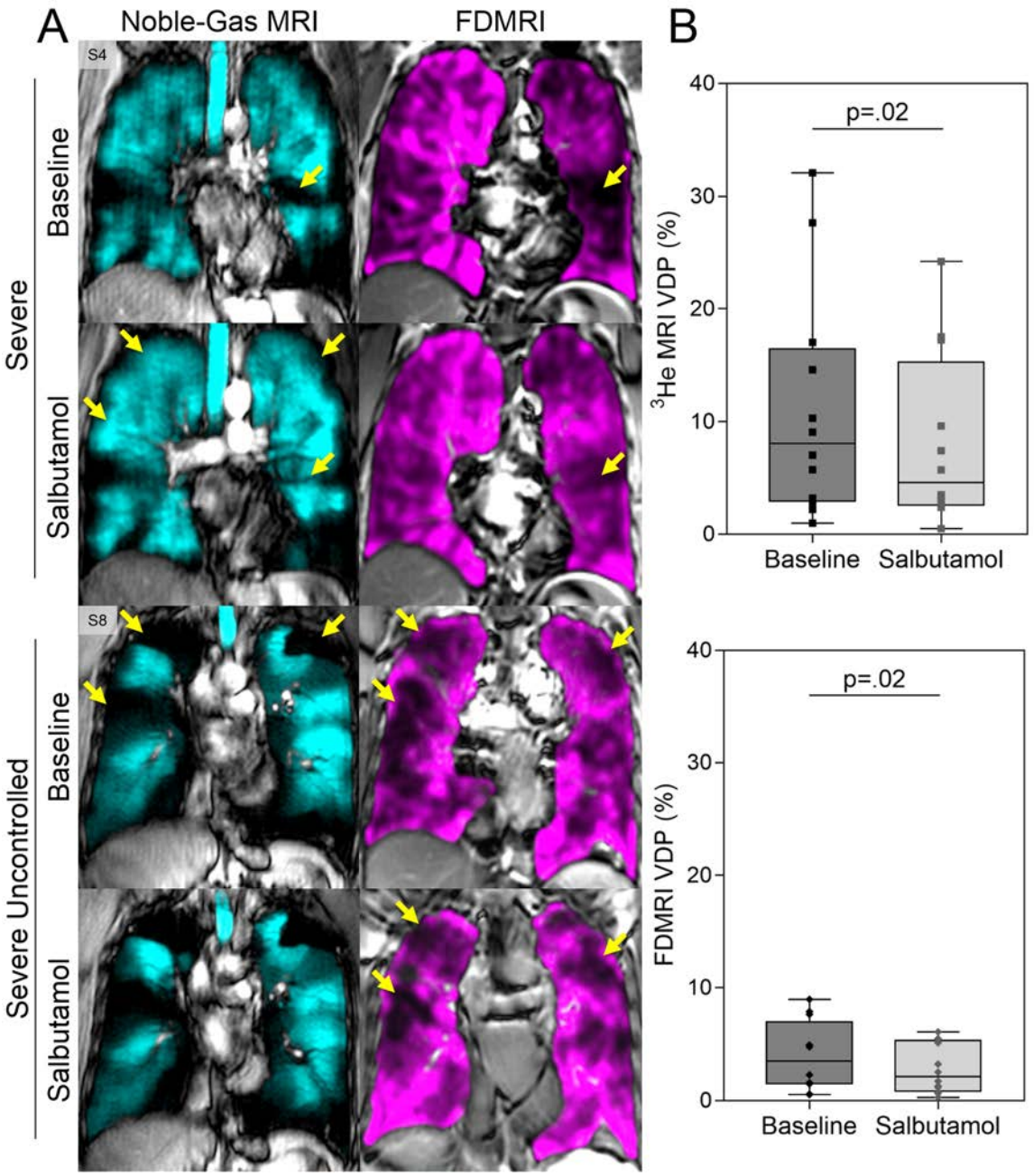

Figure 4-2 Ventilation MRI for severe and severe-uncontrolled asthmatics
A) Hyperpolarized inhaled gas (cyan) and FDMRI (magenta) for a representative severe asthmatic (female, age=57yrs, baseline FEV_1=52%$_{pred}$, post-salbutamol FEV_1=60%$_{pred}$) and severe-uncontrolled asthmatic (male, age=56yrs, baseline FEV_1=37%$_{pred}$, post-salbutamol FEV_1=36%$_{pred}$) at baseline and post-salbutamol. Yellow arrows show ventilation defect spatial relationships.
B) Box and whisker plot (box=25th to 75th percentile; whiskers=minimum to maximum) for VDP baseline and post-salbutamol for ^{3}He MRI (n=12, baseline VDP=11.1±10.1%, post-salbutamol VDP=8.1±7.6%, p=.02) and FDMRI (n=12, baseline VDP=3.9±3.0%, post-salbutamol VDP=2.8±2.1%, p=.02).

4.3.3 Ventilation Response to Methacholine Challenge and Salbutamol Rescue

Figure 4-3 shows centre coronal MRI slices for a representative participant S1 (45yr old female, FEV_1=95%$_{pred}$, severe uncontrolled asthma) who underwent MCh. There was qualitatively greater ^{3}He MR and FDMR ventilation abnormalities post-MCh and these decreased post-salbutamol. It is also important to point out that FDMRI ventilation defects were qualitatively less visibly obvious compared to ^{3}He MRI defects. As shown in **Table 4-2**, ^{3}He VDP and FDMRI VDP significantly increased (worsened) at PC_{20} (n=4; baseline: ^{3}He VDP=3±1%, FDMRI VDP=1±0.2%; methacholine: ^{3}He VDP=9±2%, FDMRI VDP=5±2%) and significantly decreased post-salbutamol (^{3}He VDP=3±1%, FDMRI VDP=2±1%, all p=.02), and there was a significant difference between imaging methods for these VDP differences (p=.01).

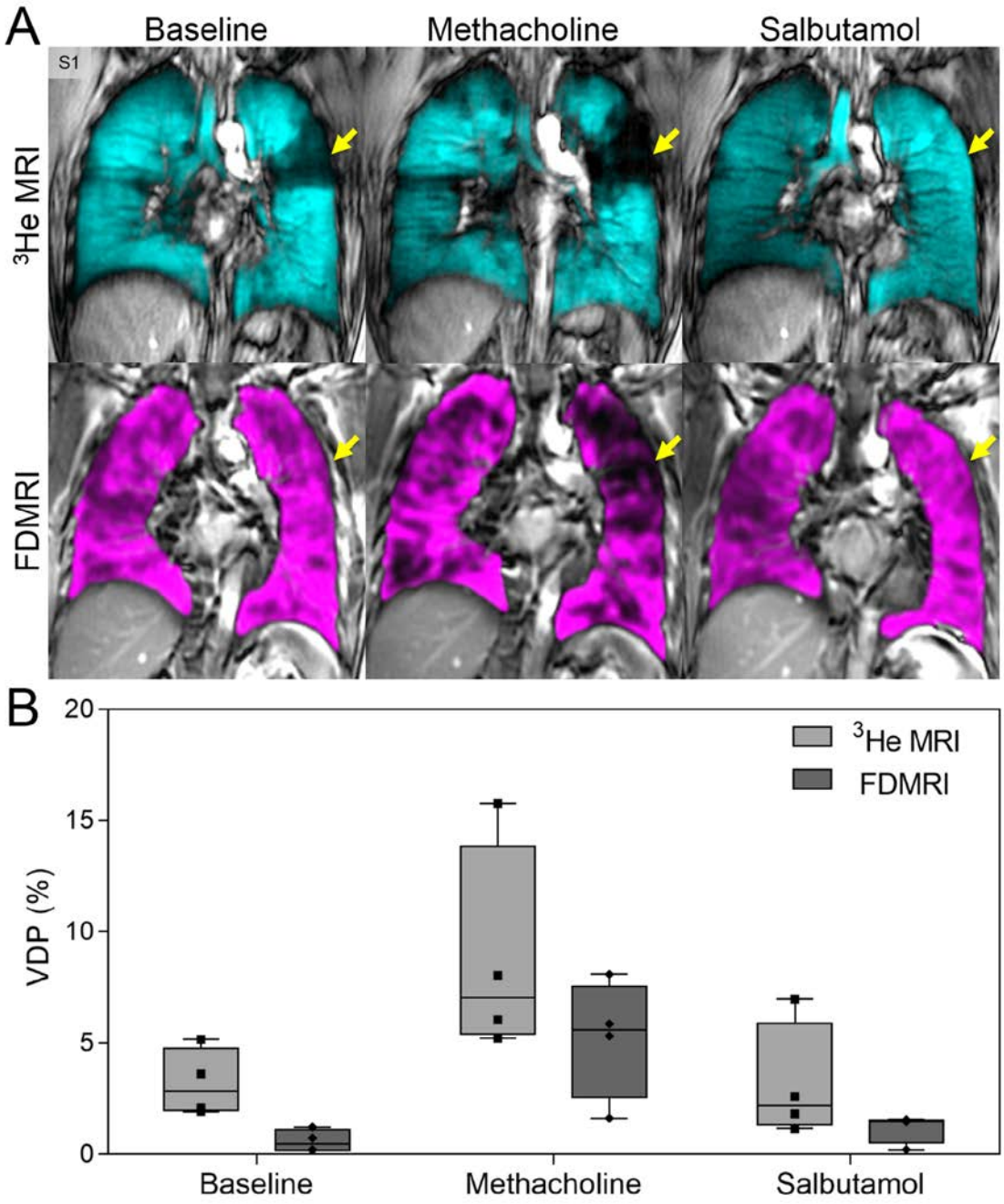

Figure 4-3 Methacholine Challenge

A) Representative severe asthmatic centre coronal slice ^{3}He MRI (cyan) and FDMRI (magenta) female, age=45yrs, baseline FEV_1=95%$_{pred}$, PC_{20}=0.123mg/mL, post-salbutamol FEV_1=101%$_{pred}$ at baseline (^{3}He VDP=3.6%, FDMRI VDP=0.7%), post-MCh (^{3}He VDP=5.2%, FDMRI VDP=1.6%), and post-salbutamol (^{3}He VDP=2.6%, FDMRI VDP=1.5%).

B) Box and whisker plot (box=25th to 75th percentile; whiskers=minimum to maximum) for ^{3}He MRI VDP and FDMRI VDP at baseline (n=4, ^{3}He VDP=3.2±0.8%, FDMRI VDP=0.6±0.2%), post-MCh (n=4, ^{3}He VDP=8.8±2.4%, FDMRI VDP=5.1±1.5%) and post-salbutamol (n=4, ^{3}He VDP=3.1±1.3%, FDMRI VDP=1.2±0.7%).

4.3.4 Relationships and Agreement

Figure 4-4 shows the relationships of FDMRI and ^{3}He MRI VDP and their agreement. While FDMRI VDP was correlated with ^{3}He MRI VDP (ρ=.61, p=.01), Bland-Altman analysis showed a significant bias of -6.0±8.6% (95% limit of agreement: -23% to 11%). **Table 4-3** summarizes the significant correlations for ^{3}He MRI and FDMRI VDP with LCI and other pulmonary function measurements. There were significant relationships for FDMRI VDP with ^{3}He MRI VDP (ρ=.61, p=.01) as well as with FRC (ρ=.61, p=.01), RV (ρ=.54, p=.04), and R_{AW} (ρ=.57, p=.02) but not with LCI (ρ=.49, p=.06), FEV_1 (ρ=-.45, p=.08), or FEV_1/FVC (ρ=-.43, p=.09).

Table 4-3 Relationship for hyperpolarized inhaled gas MRI and FDMRI with pulmonary function and LCI

	Spearman ρ (p)	
	^{3}He MRI VDP % (n=16)	**FDMRI VDP % (n=16)**
FEV_1 $\%_{pred}$	**-.78 (.0006)**	-.45 (.08)
FVC $\%_{pred}$	**-.53 (.03)**	-.43 (.09)
FEV_1/FVC %	**-.75 (.001)**	-.38 (.1)
RV $\%_{pred}$	.45 (.08)	**.51 (.04)**
TLC $\%_{pred}$	.19 (.5)	.35 (.2)
RV/TLC %	.46 (.07)	.28 (.3)
FRC $\%_{pred}$	**.72 (.002)**	**.61 (.01)**
R_{AW} $\%_{pred}$	**.80 (.0004)**	**.57 (.02)**
LCI	**.85 (.0001)**[#]	.49 (.06)[#]
^{3}He MRI VDP %	--	**.61 (.01)**
FDMRI VDP %	**.61 (.01)**	--

ρ=Spearman-correlation-coefficients; $\%_{pred}$=percent-of-predicted-value; FEV_1=forced-expiratory-volume-in-one-second; FVC=forced-vital-capacity; RV=residual-volume; TLC=total-lung-capacity; FRC=functional-residual-capacity; R_{AW}=airways-resistance; LCI=lung-clearance-index; VDP=ventilation-defect-percent; [#]n=15.

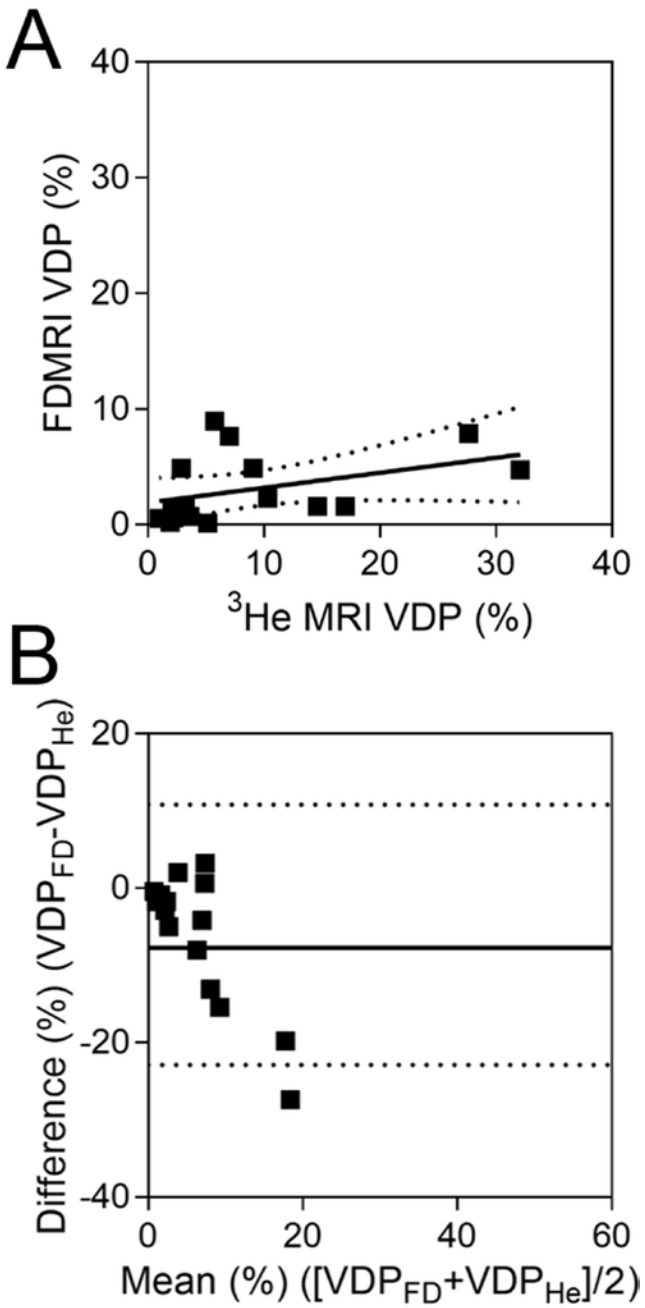

Figure 4-4 Relationships for FDMRI with ^{3}He MRI
A) FDMRI VDP was significantly correlated with ^{3}He MRI VDP (n=16, ρ=.61, p=.01, y=0.1x+1.9).
B) Bland-Altman analysis of agreement for FDMRI with ^{3}He MRI VDP (n=16, bias=-6.0±8.6%, lower limit=-22.9%, upper limit=10.8%).
Dotted lines indicate the 95% confidence intervals.

4.4 Discussion

In a recent survey,[8] the vast majority of asthma patients described their asthma as poorly controlled and nearly half reported that asthma symptom severity limited day-to-day activities or regular exercise. This dire situation reflects a lack of sensitive and specific asthma biomarkers that may be used to guide asthma treatment in individual patients or used as intermediate endpoints in clinical trials of new treatments. We and others[9] think that biomarkers of ventilation heterogeneity and imaging biomarkers in particular may provide one solution to this challenging problem. In this regard, here we evaluated ventilation heterogeneity in a proof-of-concept study in 16 patients with severe and severe with poorly-controlled asthma and observed: 1) FDMRI and ^{3}He MRI VDP significantly decreased post-salbutamol, 2) both FDMRI and ^{3}He MRI VDP significantly increased in response to methacholine and decreased post-bronchodilator, and, 3) FDMRI VDP was significantly correlated with ^{3}He MRI VDP but also significantly underestimated VDP relative to ^{3}He MRI VDP.

Ventilation defect measurements generated using FDMRI and ^{3}He MRI significantly responded to salbutamol and methacholine. Previous work also showed that ^{3}He MRI VDP significantly improved post-salbutamol in mild to moderate asthmatics.[24] However, to our knowledge, this is the first study to investigate FDMRI, ^{3}He MRI and LCI measurements of ventilation heterogeneity in asthmatics with severe disease. Salbutamol-dependent airway smooth muscle relaxation and dilation is reflected by increased asthmatic airway calibre and this is believed to result in decreased ventilation heterogeneity measured using LCI and inhaled gas MRI.[24] Importantly, FDMRI results observed here suggest that the inhaled-gas MRI static ventilation maps and dynamic free breathing FDMRI ventilation maps provide similar but not the same functional information in asthmatics. Differences in the functional information measured using inhaled-gas MRI and FDMRI may stem from the airway abnormalities themselves and the different time constants for lung filling that are the consequence of these airway abnormalities. For example, in asthmatics, inhaled-gas MRI ventilation defects reflect lung regions with long time constants for filling that are beyond the 10-15s acquisition time of scanning. In contrast, multi-breath free-breathing

FDMRI ventilation defects reflect airway and parenchyma abnormalities[35] that do not fill during a much longer, two minute acquisition window, similar to previous work using multi-breath wash-in inhaled gas MRI.[41]

In four patients who could safely undergo methacholine challenge, FDMRI and ^{3}He MRI VDP significantly changed in response to both methacholine and salbutamol. To our knowledge, this is the first time FDMRI ventilation maps have been evaluated during methacholine challenge and the responses were comparable with ^{3}He MRI VDP measured here, and previously described.[23] Previous work in mild-moderate asthmatics using diffusion-weighted ^{3}He MRI suggested that ventilation defects captured at PC_{20} may be due to air trapping induced by methacholine.[42] To support this notion, in another study, air trapping induced using a balloon catheter in a porcine model was also detected using both FDMRI and ^{3}He MRI.[34] Based on these previous results[34] and the current investigation, FDMRI ventilation defects measured post-methacholine challenge, likely stem from hyper-responsive and constricted airways which is an important translational finding for asthma centres that don't have access to inhaled-gas MRI.

While FDMRI and ^{3}He MRI VDP were correlated, there was a bias toward lower FDMRI VDP and this was also previously observed in COPD patients.[35] Given what we know about the time constants for lung filling and the fact that the inhaled gas methods capture a 10-15s snapshot and free breathing MRI methods capture abnormalities over at least two minutes of breathing, these differences are intuitively reasonable.[35] The bias or underestimate of FDMRI VDP relative to ^{3}He MRI VDP may be a result of the differences in how these two methods generate or capture ventilation information. Inhaled gas methods capture a 10-15s snapshot where very high contrast and signal-to-noise ventilation images can be easily generated. In contrast, free breathing MRI methods capture abnormalities over at least two minutes of breathing where the ventilation contrast is generated by the signal differences during the breathing cycle as tissue contracts and expands due to air entering and leaving the pulmonary system. These results provide evidence that these two different methods of generating MR ventilation maps, although different, may probe and interrogate similar lung functional information related to regions of airway remodeling/hyper-responsiveness and gas-trapping. Regardless, MR ventilation

maps, generated using different methods, provide similar lung functional information related to regions of airway remodeling/hyper-responsiveness and gas trapping.

We recognize a number of study limitations, including the small number of patients evaluated. We also focused on severe asthmatics and those with poor control in order to capture information relevant to an important clinical problem and, because of this, the vast majority of patients were unable to perform methacholine challenge. An inherent limitation of pulmonary ^{1}H MRI is the low signal intensity due to intrinsically low proton density and T_2^* effects[43] but recent research[44] that exploits shorter echo times may overcome this challenge. We also acknowledge that different imaging parameters (FDMRI=single 2D slice time series and ^{3}He MRI=multi-slice 2D acquisition) may limit the generalizability of a direct comparison between methods. While complex image-processing methods are required for FDMRI and these still require standardization and validation, newly developed MR acquisition methods[44] will enhance translational potential.

In summary, FDMRI VDP was less sensitive to methacholine and salbutamol, and under-estimated VDP as compared to ^{3}He MRI. While newly improved MR acquisition methods[44] will enhance translational potential, FDMRI is currently limited to single slice acquisitions and the complex image-processing methods needed still require standardization and validation. Nevertheless, new functional biomarkers of asthma that can be acquired on conventional MR scanners are crucially needed to help understand and guide treatment decisions in those asthmatics in whom maximal, guideline based care has not improved disease severity or control.

4.5 References

(1) Global Initiative for Asthma. *Global Strategy for Asthma Management and Prevention*, <www.ginasthma.org> (2016).

(2) Crapo, R. O. *et al.* Guidelines for methacholine and exercise challenge testing-1999. This official statement of the American Thoracic Society was adopted by the ATS Board of Directors, July 1999. *Am J Respir Crit Care Med* 2000; 161: 309-329.

(3) Busse, W. W. Asthma diagnosis and treatment: filling in the information gaps. *J Allergy Clin Immunol* 2011; 128: 740-750.

(4) Gjevre, J. A., Hurst, T. S., Taylor-Gjevre, R. M. & Cockcroft, D. W. The American Thoracic Society's spirometric criteria alone is inadequate in asthma diagnosis. *Can Respir J* 2006; 13: 433-437.

(5) Burgel, P. R. The role of small airways in obstructive airway diseases. *Eur Respir Rev* 2011; 20: 23-33.

(6) Macklem, P. T. & Mead, J. Resistance of central and peripheral airways measured by a retrograde catheter. *J Appl Physiol* 1967; 22: 395-401.

(7) Tulic, M. K., Christodoulopoulos, P. & Hamid, Q. Small airway inflammation in asthma. *Respir Res* 2001; 2: 333-339.

(8) The Lung Association. *Asthma Control in Canada™ Survey 2016*, <http://mb.lung.ca/file_download/2c91f259-3586-48d9-8496-63530f7f4c9a> (2016).

(9) Trivedi, A. *et al.* Using imaging as a biomarker for asthma. *Journal of Allergy and Clinical Immunology* 2017; 139: 1-10.

(10) Newman, K. B., Lynch, D. A., Newman, L. S., Ellegood, D. & Newell, J. D. Quantitative Computed-Tomography Detects Air Trapping Due to Asthma. *Chest* 1994; 106: 105-109.

(11) Aysola, R. S. *et al.* Airway Remodeling Measured by Multidetector CT Is Increased in Severe Asthma and Correlates With Pathology. *Chest* 2008; 134: 1183-1191.

(12) Little, S. A. *et al.* High resolution computed tomographic assessment of airway wall thickness in chronic asthma: reproducibility and relationship with lung function and severity. *Thorax* 2002; 57: 247-253.

(13) Kim, W. W. *et al.* Xenon-enhanced dual-energy CT of patients with asthma: dynamic ventilation changes after methacholine and salbutamol inhalation. *AJR Am J Roentgenol* 2012; 199: 975-981.

(14) Gordic, S. *et al.* Ultralow-dose chest computed tomography for pulmonary nodule detection: first performance evaluation of single energy scanning with spectral shaping. *Invest Radiol* 2014; 49: 465-473.

(15) Smith-Bindman, R. *et al.* Use of Diagnostic Imaging Studies and Associated Radiation Exposure for Patients Enrolled in Large Integrated Health Care Systems, 1996-2010. *Jama-Journal of the American Medical Association* 2012; 307: 2400-2409.

(16) de Gonzalez, A. B. *et al.* Projected Cancer Risks From Computed Tomographic Scans Performed in the United States in 2007. *Archives of Internal Medicine* 2009; 169: 2071-2077.

(17) Smith-Bindman, R. *et al.* Radiation Dose Associated With Common Computed Tomography Examinations and the Associated Lifetime Attributable Risk of Cancer. *Archives of Internal Medicine* 2009; 169: 2078-2086.

(18) Venegas, J. G. *et al.* Self-organized patchiness in asthma as a prelude to catastrophic shifts. *Nature* 2005; 434: 777-782.

(19) King, G. G., Eberl, S., Salome, C. M., Meikle, S. R. & Woolcock, A. J. Airway closure measured by a Technegas bolus and SPECT. *American Journal of Respiratory and Critical Care Medicine* 1997; 155: 682-688.

(20) King, G. G., Eberl, S., Salome, C. M., Young, I. H. & Woolcock, A. J. Differences in airway closure between normal and asthmatic subjects measured with single-photon emission computed tomography and technegas. *American Journal of Respiratory and Critical Care Medicine* 1998; 158: 1900-1906.

(21) de Lange, E. E. *et al.* Changes in regional airflow obstruction over time in the lungs of patients with asthma: evaluation with 3He MR imaging. *Radiology* 2009; 250: 567-575.

(22) Svenningsen, S. *et al.* What are ventilation defects in asthma? *Thorax* 2014; 69: 63-71.

(23) Samee, S. *et al.* Imaging the lungs in asthmatic patients by using hyperpolarized helium-3 magnetic resonance: assessment of response to methacholine and exercise challenge. *J Allergy Clin Immunol* 2003; 111: 1205-1211.

(24) Svenningsen, S. *et al.* Hyperpolarized (3) He and (129) Xe MRI: differences in asthma before bronchodilation. *J Magn Reson Imaging* 2013; 38: 1521-1530.

(25) de Lange, E. E. *et al.* Evaluation of asthma with hyperpolarized helium-3 MRI: correlation with clinical severity and spirometry. *Chest* 2006; 130: 1055-1062.

(26) Fain, S. B. *et al.* Evaluation of structure-function relationships in asthma using multidetector CT and hyperpolarized He-3 MRI. *Acad Radiol* 2008; 15: 753-762.

(27) Svenningsen, S., Nair, P., Guo, F., McCormack, D. G. & Parraga, G. Is ventilation heterogeneity related to asthma control? *Eur Respir J* 2016; 48: 370-379.

(28) Ohno, Y. *et al.* Oxygen-enhanced MRI vs. quantitatively assessed thin-section CT: pulmonary functional loss assessment and clinical stage classification of asthmatics. *Eur J Radiol* 2011; 77: 85-91.

(29) Zhang, W. J. *et al.* Dynamic oxygen-enhanced magnetic resonance imaging of the lung in asthma -- initial experience. *Eur J Radiol* 2015; 84: 318-326.

(30) Zapke, M. *et al.* Magnetic resonance lung function--a breakthrough for lung imaging and functional assessment? A phantom study and clinical trial. *Respir Res* 2006; 7: 106.

(31) Pennati, F. *et al.* Assessment of regional lung function with multivolume (1)H MR imaging in health and obstructive lung disease: comparison with (3)He MR imaging. *Radiology* 2014; 273: 580-590.

(32) Bauman, G. *et al.* Non-contrast-enhanced perfusion and ventilation assessment of the human lung by means of fourier decomposition in proton MRI. *Magn Reson Med* 2009; 62: 656-664.

(33) Bauman, G. *et al.* Pulmonary functional imaging: qualitative comparison of Fourier decomposition MR imaging with SPECT/CT in porcine lung. *Radiology* 2011; 260: 551-559.

(34) Bauman, G. *et al.* Lung ventilation-and perfusion-weighted Fourier decomposition magnetic resonance imaging: In vivo validation with hyperpolarized 3He and dynamic contrast-enhanced MRI. *Magn Reson Med* 2013; 69: 229-237.

(35) Capaldi, D. P. *et al.* Free-breathing Pulmonary (1)H and Hyperpolarized (3)He MRI: Comparison in COPD and Bronchiectasis. *Acad Radiol* 2015; 22: 320-329.

(36) Miller, M. R. *et al.* Standardisation of spirometry. *Eur Respir J* 2005; 26: 319-338.

(37) Parraga, G. *et al.* Hyperpolarized 3He ventilation defects and apparent diffusion coefficients in chronic obstructive pulmonary disease: preliminary results at 3.0 Tesla. *Invest Radiol* 2007; 42: 384-391.

(38) Kirby, M. *et al.* Hyperpolarized 3He magnetic resonance functional imaging semiautomated segmentation. *Acad Radiol* 2012; 19: 141-152.

(39) Heinrich, M. P. *et al.* MIND: Modality independent neighbourhood descriptor for multi-modal deformable registration. *Medical Image Analysis* 2012; 16: 1423-1435.

(40) Altman, D. G. *Practical statistics for medical research.* (CRC press, 1990).

(41) Hamedani, H. *et al.* Regional Fractional Ventilation by Using Multibreath Wash-in (3)He MR Imaging. *Radiology* 2016; 279: 917-924.

(42) Costella, S. *et al.* Regional pulmonary response to a methacholine challenge using hyperpolarized (3)He magnetic resonance imaging. *Respirology* 2012; 17: 1237-1246.

(43) Yu, J., Xue, Y. & Song, H. K. Comparison of lung T2* during free-breathing at 1.5 T and 3.0 T with ultrashort echo time imaging. *Magn Reson Med* 2011; 66: 248-254.

(44) Bauman, G., Pusterla, O. & Bieri, O. Ultra-fast Steady-State Free Precession Pulse Sequence for Fourier Decomposition Pulmonary MRI. *Magn Reson Med* 2016; 75: 1647-1653.

CHAPTER 5

5 FREE-BREATHING PULMONARY MR IMAGING TO QUANTIFY REGIONAL VENTILATION

To further the potential application of free-breathing ^{1}H MRI, we developed a whole-lung free-breathing pulmonary ^{1}H MRI technique to measure regional specific-ventilation in patients with asthma and healthy-volunteers. We compared these specific-ventilation measurements with hyperpolarized ^{3}He MRI ventilation in healthy and asthmatic participants, and, determined the relationships between ^{1}H MRI specific-ventilation and hyperpolarized ^{3}He MRI and pulmonary function measurements.

The contents of this chapter have been submitted to the journal Radiology: DPI Capaldi, RL Eddy, S Svenningsen, F Guo, JSH Baxter, AJ McLeod, P Nair, DG McCormack, and G Parraga and is accepted for publication in Radiology 2018 (in-press).

5.1 Introduction

Asthma is a chronic inflammatory airway disease,[1] characterized clinically by an intermittent and unpredictable worsening of severe dyspnea and wheezing. Asthma is diagnosed and monitored using the spirometry measurement of the forced-expiratory-volume-in-one-second (FEV_1).[2] Although relatively inexpensive and straightforward to implement, spirometry only measures global airflow-obstruction, cannot provide regional information[2,3] and it is inherently insensitive to the structural and functional abnormalities in the small airways[4] where inflammation and remodeling occur.[5] These limitations have motivated the development of pulmonary functional imaging approaches.

To overcome some of these limitations, multi-detector computed-tomography (MDCT) of the chest has been used to quantify air-trapping[6] and airway-remodeling[7] in asthmatics.[8-11] Four-dimensional (4D) CT has also been used to quantify specific-ventilation,[12] which is defined as tidal-volume normalized to functional-residual-capacity.[13] 4DCT specific-ventilation,[12] is measured based on the difference in lung-tissue-density at tidal inspiration and expiration as air enters and leaves voxels. Magnetic resonance (MR) imaging has also been exploited to measure both lung structure and function in asthmatics.[14] For example, hyperpolarized ^{3}He MRI measures inhaled gas distribution[15] while oxygen-enhanced ^{1}H MRI also provides maps of signal enhancement due to oxygen[16-18] by exploiting

differences in T_1-weighted images acquired whilst breathing pure oxygen and room air. ^{1}H MR imaging ventilation maps may also be generated without exogenous-contrast[19-23] by measuring differences in ^{1}H signal intensity at different lung volumes.[19,20] Free-breathing Fourier-decomposition ^{1}H MR imaging (FDMR imaging) is another approach that uses deformable-registration to generate ventilation-weighted images[21,22] that are sensitive to bronchoconstriction in asthmatics.[23]

In this proof-of-concept investigation, our objective was to: 1) develop a way to generate specific-ventilation measurements, based on conventional, free-breathing ^{1}H MRI without exogenous contrast, 2) compare ^{1}H MRI specific-ventilation with hyperpolarized ^{3}He MRI ventilation in healthy and asthmatic participants, and 3) determine the relationships between ^{1}H MRI specific-ventilation and hyperpolarized ^{3}He MRI and pulmonary-function measurements.

5.2 Materials and Methods

5.2.1 Participants and Pulmonary Function Tests

Participants aged 18-85, provided written-informed-consent to an ethics-board approved prospectively-planned investigation that was Health-Insurance-Portability-and-Accountability-Act (HIPAA) compliant (healthy-volunteers: NCT03169673; asthmatics: NCT02351141 and NCT02263794); participants were consecutively recruited between January and June 2017 based on inclusion/exclusion criteria provided in the **Supplement** that also provides a description of the pulmonary function tests performed.

5.2.2 Image Acquisition

All MR imaging acquisitions were performed in the coronal plane using a whole body 3.0 Tesla Discovery MR750 (General-Electric-Health-Care [GEHC], Milwaukee, WI, USA) system as follows: 1) static breath-hold ^{1}H MR imaging, 2) static breath-hold hyperpolarized ^{3}He MR imaging, and, 3) free-breathing ^{1}H MR imaging. Static breath hold ^{1}H MR imaging was acquired using a whole body radiofrequency coil and fast spoiled gradient-recalled-echo (FGRE) sequence (partial-echo-acquisition; total-acquisition-

time=16s; TR/TE/flip-angle[FA]=4.7ms/1.2ms/30°; FOV=40×40cm^2, BW=24.4kHz; matrix=128×80 [zero-padded to 128×128]; partial-echo-percent=62.5%; number-of-slices[NS]= 15-17; slice-thickness[ST]=15mm, 0-gap). Hyperpolarized ^{3}He static ventilation MR imaging was performed using a single channel, rigid elliptical transmit/receive chest coil (RAPID Biomedical GmbH, Wuerzburg, Germany) and 2D multi-slice FGRE sequence (partial-echo-acquisition; total-acquisition-time=10s; TR/TE/FA=3.8ms/1.0ms/7°; FOV=40×40cm^2, BW=48.8kHz; matrix=128×80 [zero-padded to 128×128]; partial-echo-percent=62.5%; NS=15-17; ST=15mm, 0-gap). A commercial polarizer (HeliSpin, Polarean, Durham, North Carolina, USA) was used to polarize ^{3}He to 40%. Participants inhaled a 1.0L gas mixture (30%/70% by volume hyperpolarized ^{3}He/ultrahigh pure N_2) after passive expiration to FRC. As shown in **Figure 5-1**, free-breathing ^{1}H MR imaging was acquired using a 32-channel torso coil (GEHC), with respiratory bellows to monitor respiratory rate and an optimized balanced-steady-state-free-precession sequence (total-acquisition-time=160-200s; TE/TR/FA=0.6ms/1.9ms/15°; FOV=40×40cm^2; BW=250kHz; matrix=256×256; NS=13-15; ST=15mm; number-of-excitations=1; number-of-phases=51, 0-gap).

5.2.3 Image Analysis

Image processing was performed using MATLAB R2016a (Mathworks, Natick, Massachusetts, USA). Hyperpolarized ^{3}He MRI was quantified as previously described[24] with details provided in the **Supplement** (DPIC with 4 years of experience).

As shown in **Figure 5-1**, the free-breathing images acquired were used to generate ^{1}H MR imaging specific ventilation maps, and the Hilbert transform was used to identify the respiratory signal $B(t)$, in the respiratory bellow data with both real and imaginary components. Using the phase component of $B(t)$, each imaging time point t was linked to respiratory phase (from -π to π). For each free-breathing ^{1}H MR coronal slice time series, a 3D dataset for a single respiratory cycle was created via weighted interpolation, where the third dimension is respiratory phase θ. Each free-breathing ^{1}H MR image at time t contributed to the corresponding slice in the interpolated image at phase θ with weight:

$$w(t,\theta) \propto e^{-\beta|\angle B(t)-\theta|} \tag{5-1}$$

where $B(t)$ is the respiratory bellow signal and β is the exponential decay parameter ($\beta = \frac{\pi}{10}$). Ten θ values were used to reflect the number of phases, as previously described for 4DCT.[25,26] Optical-flow deformable-registration was used to co-register each 2D multi-slice interpolated dataset into coordinate space[27] so that spatially corresponding voxels were determined in the inspiration and expiration phases. Each interpolated dataset was registered to its neighbouring interpolated dataset in the direction of increasing θ, creating a series of dense deformation fields. All images were registered to a single phase by compounding these deformation fields, creating a dataset with lung/cardiac motion removed. The reference phase was halfway between the tidal inspiration and expiration volumes.[21] Specific-ventilation (SV) is expressed without units and represents the proportion of inhaled gas moving into the lung during normal breathing as follows:

$$SV = \frac{\Delta V}{V_{air_{exp}}} = \frac{V_{air_{insp}} - V_{air_{exp}}}{V_{air_{exp}}} \tag{5-2}$$

where $V_{air_{insp}}$and $V_{air_{exp}}$are the air volume fractions at inspiration and expiration, respectively. Since MR imaging signal-intensity (SI) is approximately inversely proportional to lung air volume:[19]

$$SI \approx \frac{1}{V_{air}} \tag{5-3}$$

We know, by substituting **Equation 5-3** into **Equation 5-2**, that:

$$SV \approx \frac{SI_{exp} - SI_{insp}}{SI_{insp}} \tag{5-4}$$

where $SI_{insp}$and SI_{exp} are the MR signal-intensities at inspiration and expiration, respectively. Using the co-registered tidal inspiration and expiration volumes, specific-ventilation maps were generated as shown in **Figure 5-1**. The reference phase used to register the interpolated dataset was segmented using a multiregional segmentation

approach, as previously described.[28] A primal-dual optimization technique was implemented to solve the convex segmentation optimization problem,[28] resulting in the segmented lung. The segmented lung region was then applied to the 4DMR imaging specific-ventilation maps and the mean value was calculated.

To interrogate the spatial relationship between specific-ventilation and hyperpolarized ^{3}He MR imaging ventilation, hyperpolarized ^{3}He MR imaging was registered to ^{1}H MR imaging using landmarks[24] and ^{1}H MR imaging was registered via modality-independent-neighborhood-descriptor (MIND) deformable registration[29] to the reference phase of the interpolated dataset. The deformation field was applied to hyperpolarized ^{3}He MR imaging using voxel-wise similarity measurements of the two images, as well as diffusion-regularization of the deformation field and optimization using the Gauss-Newton framework.[29] Finally, the mean ^{1}H MR imaging specific-ventilation was calculated within well-ventilated and ventilation defected regions. Images were evaluated once because the segmentation approaches have high reproducibility.[24,28]

In each subject, 4DMRI specific-ventilation was partitioned in five regions of equal vertical extent and the mean values were computed and is provided in the **Supplement**. To perform statistical analysis in larger lung regions and to evaluate regional gravitational differences, lung maps were segmented into two equal lung regions in the anterior-posterior direction, representing the gravitational dependent and independent regions for supine participants; mean 4DMRI specific-ventilation was calculated in both lung regions.

5.2.4 Statistics

Non-parametric statistical tests were used due to the small sample sizes.[30] Differences between groups were determined using Mann-Whitney tests and relationships were determined using Spearman (ρ) correlation coefficients. Significant differences for specific-ventilation measurements in well-ventilated versus poorly ventilated lung regions and anterior versus posterior lung regions of interest were measured using paired t-tests. All statistics were performed using GraphPad Prism 7.00 (GraphPad Software Inc., San

Diego, CA, USA) and results considered significant when the probability of two-tailed type I error (α) was less than 5% ($p<.05$).

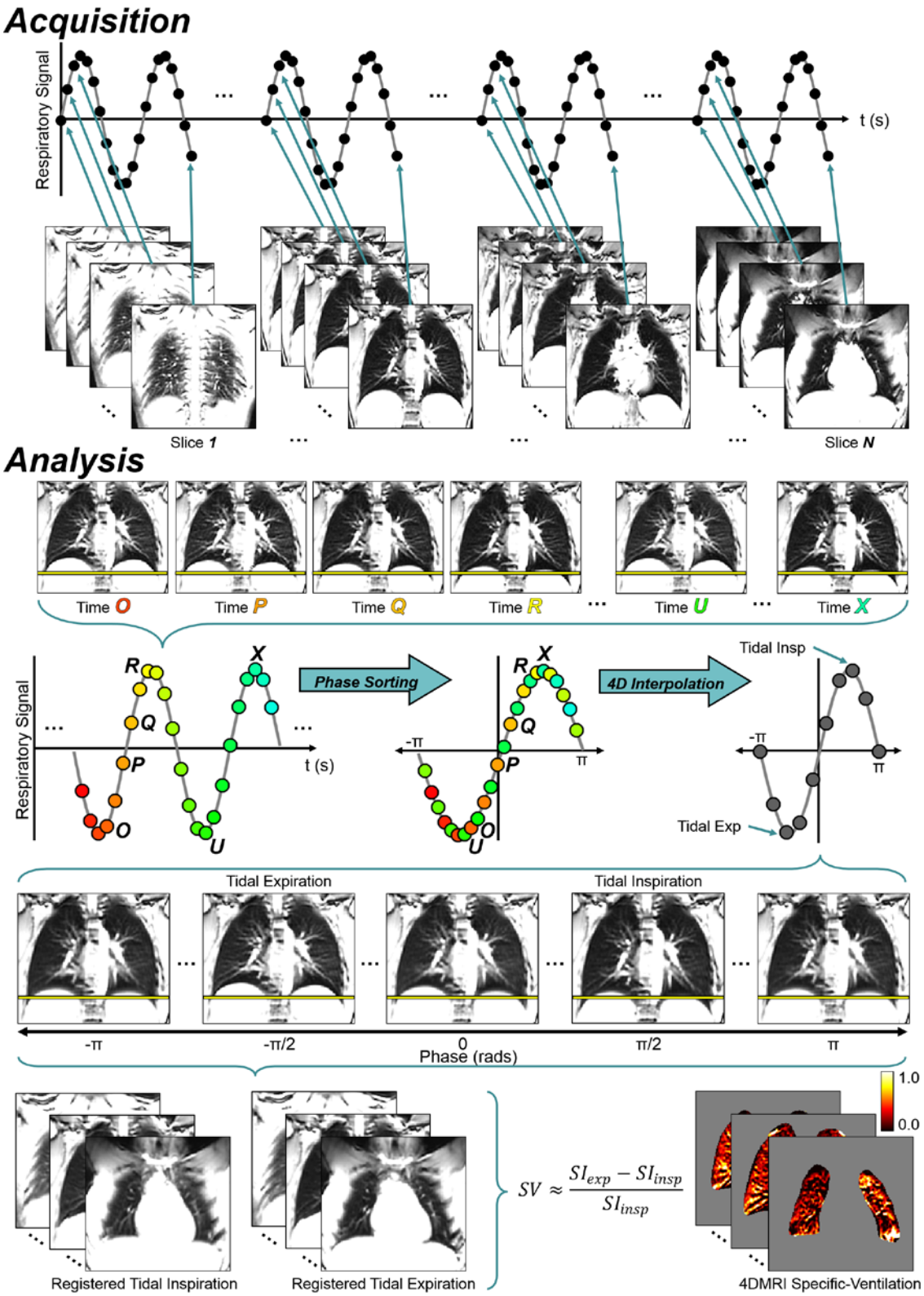

Figure 5-1 4DMR Imaging Specific-Ventilation Acquisition and Analysis Pipeline

Acquisition: Multi-slice free-breathing ^{1}H MR imaging acquired in the posterior-to-anterior direction for whole lung coverage with corresponding respiratory bellow data trace.
Analysis: Respiratory phase sorting for a single slice over time where the colors are associated with the time that each image (time *O*-*X*) is acquired corresponding to the color points on the respiratory bellow trace. Four-dimensional interpolation was performed on the respiratory phase sorted images to generate respiratory phase binned images. Yellow bar indicates the level of the diaphragm on tidal inspiration image. MR imaging specific-ventilation heat-maps were generated on a voxel-by-voxel basis after co-registration of tidal inspiratory and tidal expiratory MR imaging volumes to provide a local distribution of specific ventilation shown for a representative healthy volunteer.

5.3 Results

5.3.1 Participants

Thirty participants (15M/15F; 48[34]yrs/51[27]yrs; p=.9) were evaluated, including 23 asthmatics (11M/12F; 57[18]yrs/53[18]yrs; p=.7) and seven healthy volunteers (4M/3F; 26[4]yrs/23[9]yrs; p=.9) with no history of chronic or acute respiratory disease. **Table 5-1** shows subject demographics, pulmonary-function-tests and imaging measurements. Healthy volunteers were significantly younger and reported greater FEV_1 (p<.0001), FVC (p=.01), and FEV_1/FVC (p<.0001) as well as lower BMI (p=.003), RV (p=.008), RV/TLC (p<.0001), and R_{AW} (p<.0001) than asthmatics.

Table 5-1 Participant Demographics and MRI Findings

Parameter Median (IQR)	Healthy (n=7)	Asthma (n=23)	Sig Dif p
Age yrs	25 (4)	54 (17)	<.0001
Male n	4	11	--
Male age yrs	26 (4)	57 (18)	.002
Female n	3	12	--
Female age yrs	23 (9)	53 (18)	.009
BMI kg/m^2	21 (4)	28 (6)	.003
FEV_1 $\%_{pred}$	96 (10)	73 (22)	<.0001
FVC $\%_{pred}$	99 (8)	85 (22)	.01
FEV_1/FVC %	82 (9)	67 (18)	<.0001
RV $\%_{pred}$	104 (37)	134 (29)	.008
TLC $\%_{pred}$	101 (13)	104 (12)	.6
RV/TLC %	25 (11)	41 (10)	<.0001
R_{AW} $\%_{pred}$	61 (30)	167 (117)	<.0001

Sig Dif: Significant difference between subgroups ($p<.05$) determined using Mann-Whitney test; IQR=interquartile range; $\%_{pred}$=percent of predicted value; FEV_1=forced expiratory volume in one second; FVC=forced vital capacity; RV=residual volume; TLC=total lung capacity; R_{AW}=airways resistance.

5.3.2 Hyperpolarized ^{3}He MR Imaging Ventilation and ^{1}H MR Imaging Specific-Ventilation

Figure 5-2 and **Figure 5-3** shows representative ^{1}H MR imaging specific-ventilation and hyperpolarized ^{3}He MR imaging static ventilation (anterior-center-posterior) maps for an asthmatic and healthy volunteer. As shown in **Table 5-1**, there was significantly larger ^{1}H MR imaging specific-ventilation for healthy (0.14[0.05]) as compared to asthmatic volunteers (0.08[0.06], $p<.0001$); hyperpolarized ^{3}He MR imaging ventilation-percent was also significantly greater for healthy (99[1]%) versus asthmatic (94[5]%, $p<.0001$) participants.

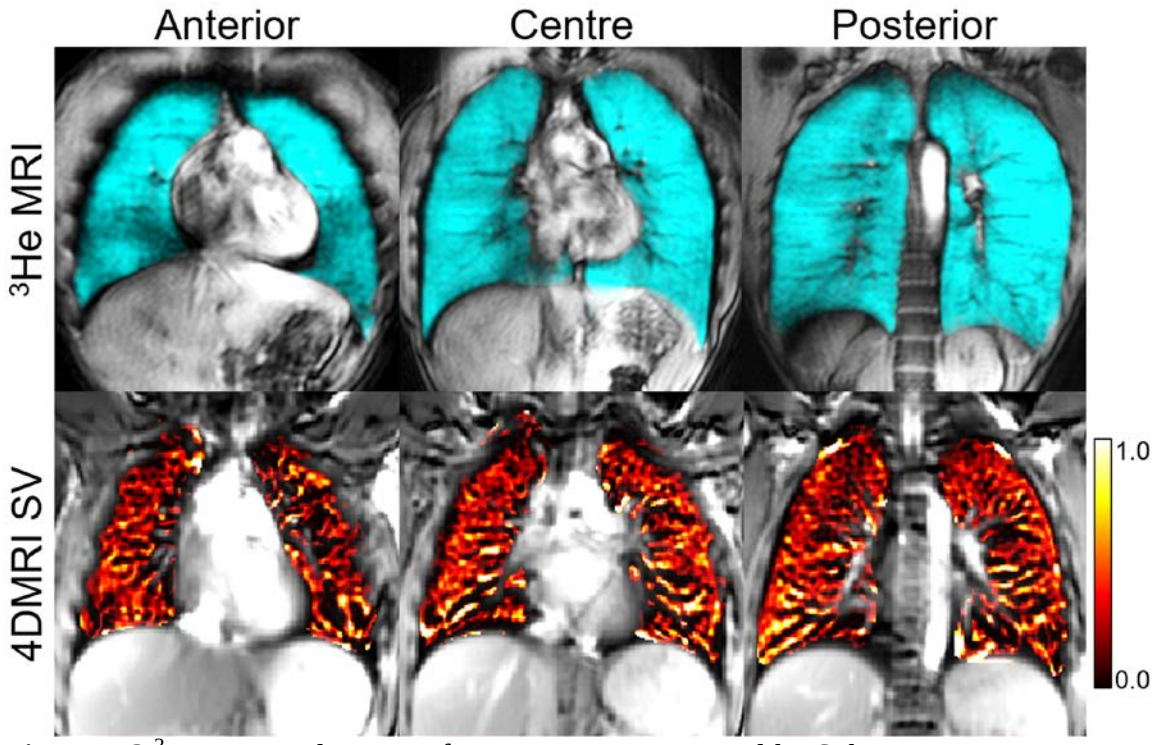

Figure 5-2 ^{3}He MRI and 4DMRI for a Representative Healthy Subject
Hyperpolarized ^{3}He MRI static-ventilation (cyan) and 4DMRI specific-ventilation (heat-map) co-registered to anatomical ^{1}H MRI (grey-scale) for anterior, center and posterior coronal slices for healthy female: age=22yrs, FEV_1=111%$_{pred}$, RV/TLC=17%, ^{3}He MRI ventilation-percent=100%, 4DMRI specific-ventilation=0.18, plethysmography specific-ventilation=0.43.

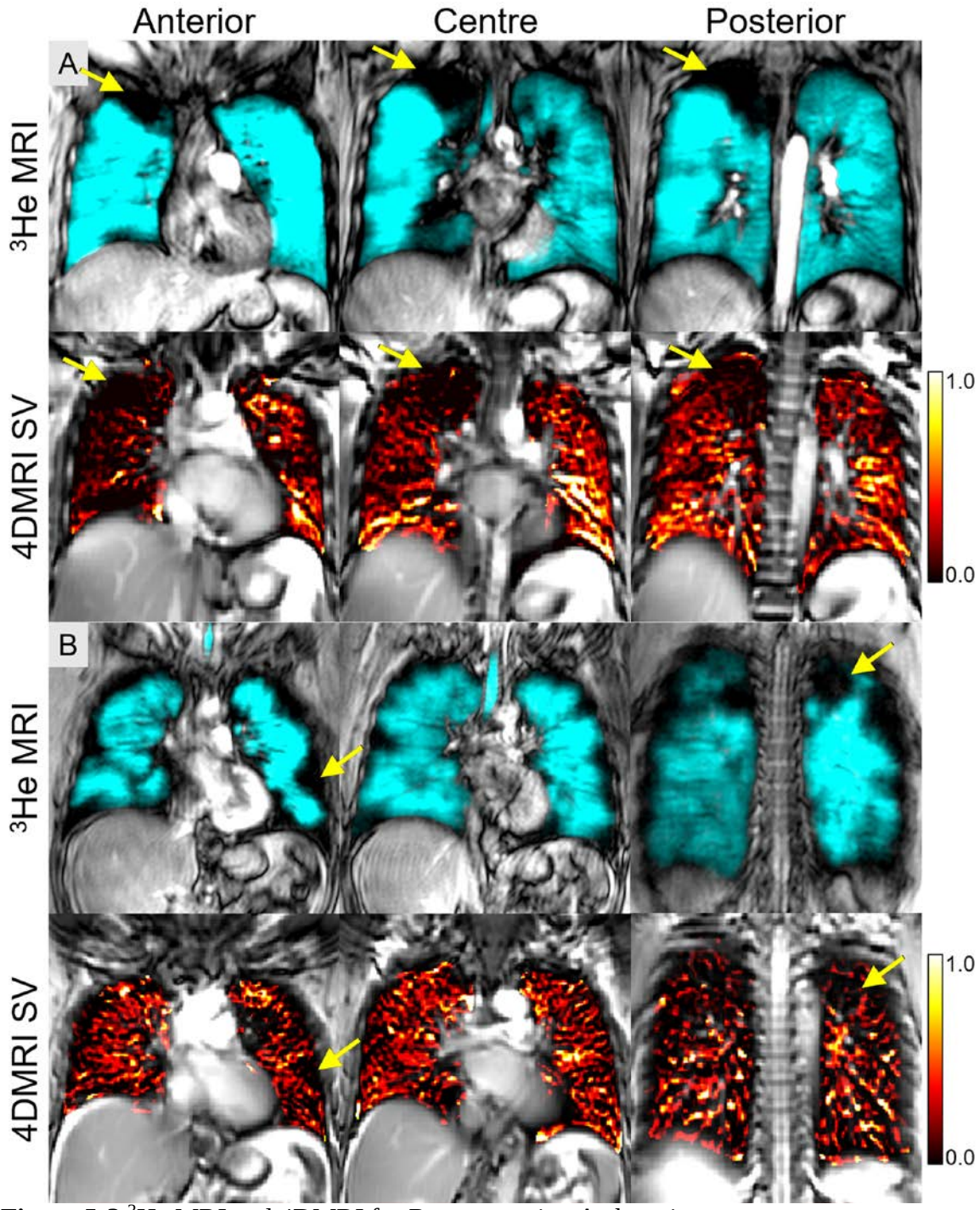

Figure 5-3 ^{3}He MRI and 4DMRI for Representative Asthmatics
Hyperpolarized ^{3}He MRI static-ventilation (cyan) and 4DMRI specific-ventilation (heat-map) co-registered to anatomical ^{1}H MRI (grey-scale) for anterior, center and posterior coronal slices for A) female with asthma: age=27yrs, FEV_1=71%$_{pred}$, RV/TLC=34%, ^{3}He MRI ventilation-percent=97%, 4DMRI specific-ventilation=0.08, plethysmography specific-ventilation=0.21; and B) female with asthma: age=42yrs, FEV_1=75%$_{pred}$, RV/TLC=40%, ^{3}He MRI ventilation-percent=93%, 4DMRI specific-ventilation=0.13, plethysmography specific-ventilation=0.14. Yellow arrows identify ventilation defects.

5.3.3 Correlations

Figure 5-4 and **Table 5-2** show that ^{1}H MRI specific-ventilation was significantly correlated with hyperpolarized ^{3}He MRI ventilation-percent (ρ=.67, p<.0001) and plethysmography specific-ventilation (ρ=.54, p=.002). **Table 5-2** reveals that MRI measurements were significantly correlated with FEV_1 (specific-ventilation: ρ=.65, p=.0001; ventilation-percent: ρ=.52, p=.003), FEV_1/FVC (specific-ventilation: ρ=.75, p<.0001; ventilation-percent: ρ=.64, p=.001), and RV/TLC (specific-ventilation: ρ=-.68, p<.0001; ventilation-percent: ρ=-.66, p<.0001).

Table 5-2 ^{3}He MRI Ventilation and ^{1}H MRI Specific-Ventilation Correlations with Pulmonary Function

	Spearman Correlation Coefficient ρ (p) [CI]	
	^{3}He MRI Ventilation-Percent % (n=30)	**4DMRI Specific-Ventilation (n=30)**
FEV_1 $\%_{pred}$	.52 (.003) [.19 - .75]	.65 (.0001) [.36 - .82]
FEV_1/FVC %	.64 (.0001) [.35 - .82]	.75 (<.0001) [.52 - .88]
RV $\%_{pred}$	-.52 (.003) [-.75 - -.19]	-.55 (.002) [-.77 - -.23]
RV/TLC %	-.66 (<.0001) [-.83 - -.39]	-.68 (<.0001) [-.84 - -42]
R_{AW} $\%_{pred}$	-.58 (.0008) [-.78 - -.27]	-.51 (.004) [-.74 - -.17]
Specific-Ventilation	.32 (.08) [-.05 - .62]	.54 (.002) [.21 - .76]
^{3}He MRI Ventilation-Percent %	--	.67 (<.0001) [.40 - .83]
4DMRI Specific-Ventilation	.67 (<.0001) [.40 - .83]	--

CI=confidence interval; $\%_{pred}$=percent of predicted value; FEV_1=forced expiratory volume in one second; FVC=forced vital capacity; RV=residual volume; TLC=total lung capacity; R_{AW}=airways resistance; Specific-Ventilation=plethysmography measurement of specific-ventilation.

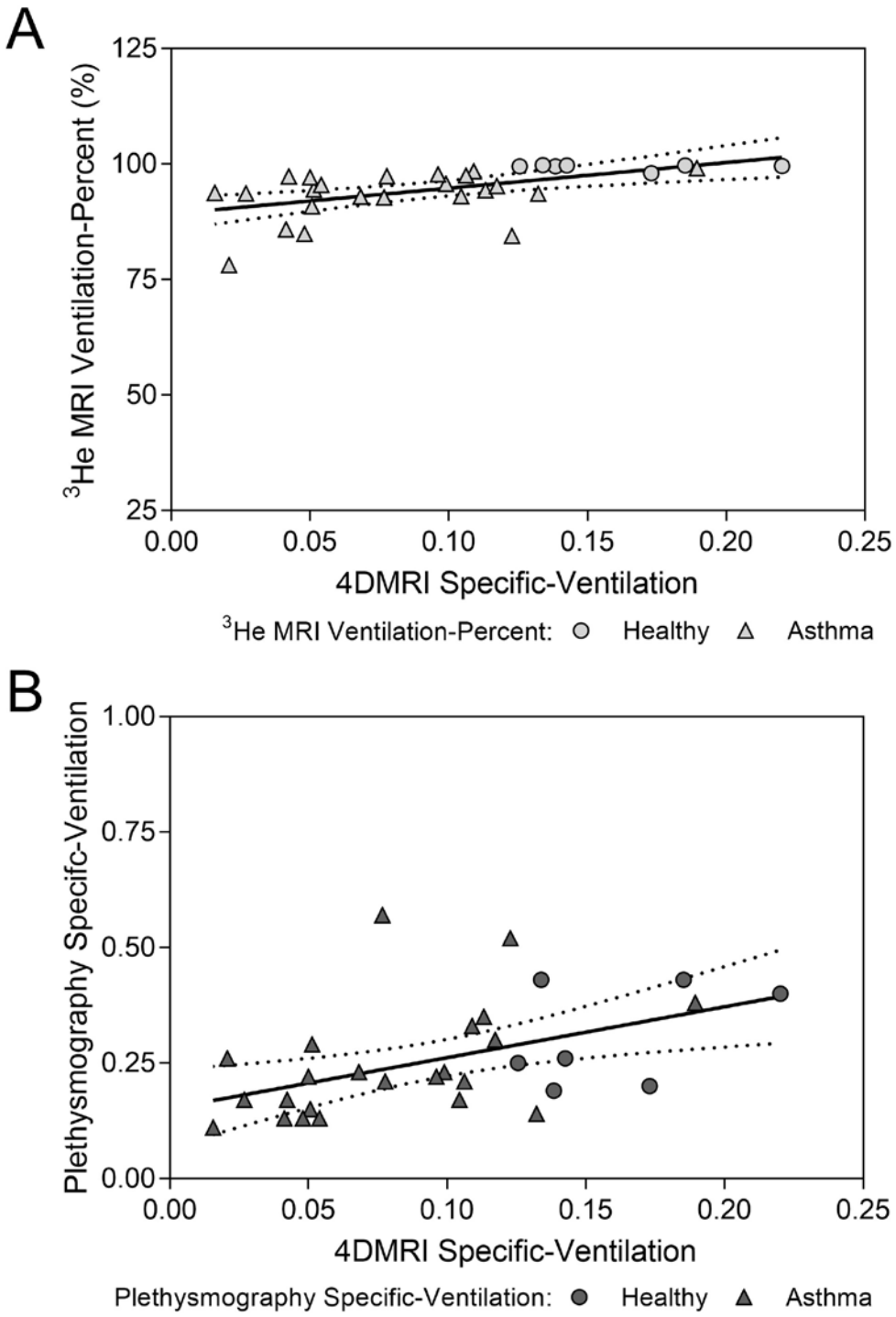

Figure 5-4 Relationships for 4DMRI Specific-Ventilation with ^{3}He MRI Ventilation-Percent and Plethysmography Specific-Ventilation

A) ^{3}He MRI ventilation-percent and 4DMRI specific-ventilation were significantly correlated (ρ=.67, p<.0001, y=55x+89).

B) Plethysmography specific-ventilation and 4DMRI specific-ventilation were significantly correlated (ρ=.54, p=.002, y=1.09x+0.15).

Dotted lines indicate the 95% confidence intervals.

Figure 5-5 shows co-registered hyperpolarized ^{3}He MR imaging and ^{1}H MR imaging for a representative asthmatic with a focal right upper lobe ventilation defect and the spatial relationship with a specific-ventilation void. Non-rigid co-registration of hyperpolarized ^{3}He and ^{1}H MR imaging maps showed that ^{1}H MR imaging specific-ventilation was significantly worse in hyperpolarized ^{3}He MR imaging ventilation-defects (0.05±0.04) as compared to well-ventilated lung regions (0.09±0.05; p<.0001) in asthmatics. **Figure 5-5** also shows that specific-ventilation was significantly larger in the gravitational dependent (0.20±0.07) versus independent (0.12±0.03; p=.02) lung regions in healthy participants, but not in asthmatics (dependent=0.09±0.05, independent=0.07±0.05; p=.1).

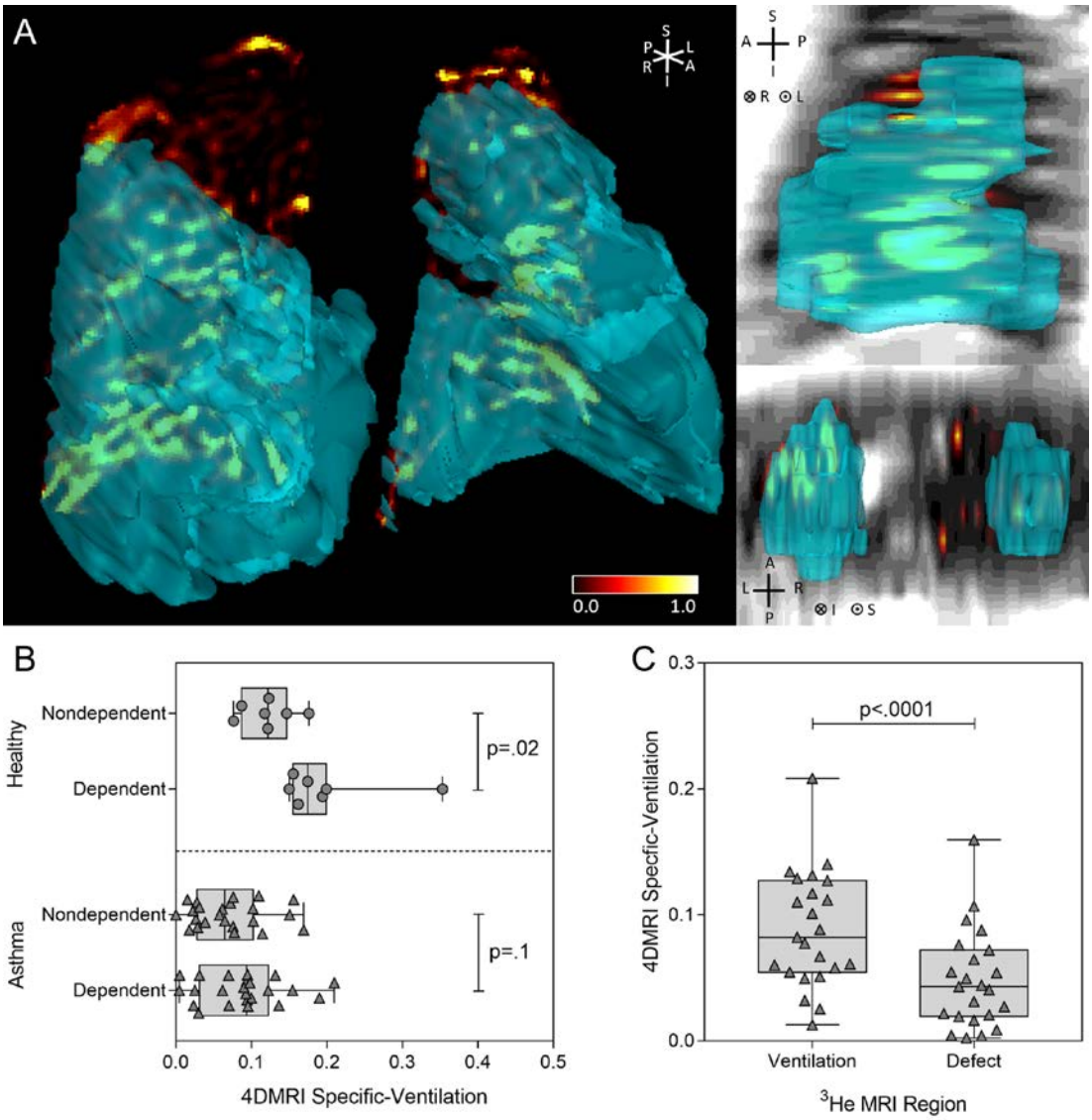

Figure 5-5 Spatial Correspondence of free-breathing 4DMRI Specific-Ventilation and ^{3}He MRI Static Ventilation Maps

A) Three-dimensional co-registration of 4DMR imaging specific-ventilation (heat-map) and static ^{3}He MR imaging ventilation (transparent cyan), with Coronal on left panel, Sagittal (right upper panel) and Axial views (right lower panel) showing anatomical ^{1}H MR imaging in grey-scale (in the sagittal and coronal panels) for a female with asthma: age=27yrs, FEV_1=71%$_{pred}$, RV/TLC=34%, ^{3}He MR imaging ventilation-percent=97%, specific-ventilation=0.21, 4DMR imaging specific-ventilation whole-lung/ventilated-region/ventilation-defect-region=0.08/0.08/0.02.

B) 4DMR imaging specific-ventilation was significantly increased in the dependent (0.20±0.07) versus the nondependent (0.12±0.03) region of the lung (p=.02) in the healthy subjects. In the asthmatics, no gravitational dependence was observed (dependent=0.09±0.05, nondependent=0.07±0.05, p=.1).

C) 4DMR imaging specific-ventilation was significantly less in the ^{3}He MR ventilation-defects (0.05±0.04) versus the ventilated (0.09±0.05) regions of the lung (p<.0001) in the asthmatic subjects.

5.4 Discussion

In a proof-of-concept demonstration in 30 participants, conventional free-breathing ^{1}H MR imaging and retrospective respiratory phase co-registration and interpolation was used to generate ^{1}H MR imaging specific-ventilation measurements. Our results showed: 1) ^{1}H MR imaging specific-ventilation was significantly diminished in asthmatics compared to healthy volunteers, 2) quantitative and spatial correlations with static breath-hold hyperpolarized ^{3}He MR imaging ventilation and a significant correlation with plethysmography specific-ventilation, and, 3) a significant difference in ^{1}H MR imaging specific-ventilation in the gravitational dependent lung region in healthy volunteers but not asthmatics.

As expected, MR imaging ventilation and specific-ventilation measurements were significantly greater in healthy participants as compared to asthmatics. This is consistent with static multi-volume ^{1}H MR imaging signal-intensity measurements in asthmatic and healthy participants.[20] Diminished MR imaging specific-ventilation in the asthmatic lung may reflect gas-trapping, airway-remodeling or inflammation, similar to previously described studies that showed CT radio-density[6] and ultra-short echo-time (UTE) MR imaging signal intensity differences[31] in asthma patients compared to healthy volunteers.

^{1}H MR imaging specific-ventilation was significantly related to plethysmography specific-ventilation and FEV_1/FVC, indicating a relationship with airflow obstruction. Correlations with RV and RV/TLC were consistent with the notion that gas-trapping reduced specific-ventilation, similar to previous work that showed multi-volume UTE MR imaging was related to pulmonary-function-tests in asthmatics.[31] The relationship between ^{1}H MR imaging and plethysmography-measured specific-ventilation was consistent with a previous investigation using oxygen-enhanced MR imaging with multiple-breath washout.[32]

In asthmatics, ^{1}H MR imaging specific-ventilation was significantly diminished within ventilation defects as compared to well-ventilated regions. This suggests that different static breath-hold and dynamic MR imaging methods may interrogate similar airway

abnormalities that influence the time constants for lung filling or ventilation. Hyperpolarized ^{3}He MR imaging measures inhaled gas distribution during a 10-15s breath-hold, while ^{1}H MR imaging specific-ventilation maps are generated, (like 4DCT specific-ventilation[12]) over a few minutes of tidal breathing. This important difference suggests that both methods may also reflect the different time-constants for lung filling, which we think can be exploited clinically and in research studies. We also observed gravitational differences in healthy participants,[18,32] but not in asthmatics, similar to previous findings.[20] Although other studies using static breath-hold ^{1}H MRI observed differences in asthmatics,[20] 4D modeling of airflow demonstrated differences between breath-hold and dynamic breathing when evaluating ventilation heterogeneity in asthmatics,[33] which may explain some of our results. Gravitational differences in ^{3}He MRI have also been observed whereby ventilation defects were larger in posterior regions of interest in asthmatics, suggestive of gas-trapping.[34,35]

We acknowledge a number of study limitations including the relatively small sample size and modest correlations between our ^{1}H MRI specific-ventilation measurement compared to both the reference plethysmography specific-ventilation measurement (ρ=.54, p=.002) and hyperpolarized ^{3}He MRI (ρ=.67, p<.0001). We must also acknowledge that because all of these measurements were performed in the same small subject group, caution must be taken when extending these results to a general population. Free-breathing protocols may be influenced by irregular breathing patterns, previously observed using 4DCT,[36] so some patients will require coaching or support.[37] There was also a significant age difference between healthy and asthmatic volunteers (p<.0001), as a result of consecutive recruitment between January and June 2017 based on inclusion/exclusion criteria (provided in the **Supplement**), which is important to consider because lung aging has been shown to influence lung ventilation.[38] Furthermore, other confounding factors, such as the differences in the demographics, may contribute to the overall differences observed between the two subject groups. The difference between MRI specific-ventilation and plethysmography specific-ventilation may stem from a number of issues. For example, MR imaging specific-ventilation is based on the difference in signal-intensities between co-registered volumes, which may be biased by poor co-registration. Moreover,

differences in position are important to consider since previous studies showed the effect of body position on lung volumes.[39,40] While supine, FRC and tidal-volume are lower than when upright but to different extents;[39] this would result in greater specific-ventilation in the supine position, which we did not observe. These measurements are also influenced by arm position[40] and may have influenced our results. ^{1}H MRI specific-ventilation was significantly diminished within ventilation defects as compared to well-ventilated regions, which provides some preliminary evidence that in these patients the time constants for filling were dominated by longer timescales, although a voxel-wise comparison may help to better ascertain spatial differences. Unfortunately, while it is theoretically possible to measure ^{3}He MRI specific ventilation in free-breathing human subjects, it is not feasible because of the exorbitant cost of ^{3}He gas and the safety concerns related to repeated breathing of anoxic gas mixtures (mixtures with O_2 are not possible because this accelerates polarization signal decay). ^{3}He MRI measures gas distribution during a 10-15s breath-hold,[41] while 4DMR specific-ventilation images are generated, (like 4DCT[12]) over two to three minutes of tidal breathing. As such, the two methods are not measuring the same quantity and they likely interrogate different lung functional information related to airway calibre that influence the time constants for lung filling and emptying. It is important to point out that the current approach is based on the assumption that changes in signal intensity during tidal breathing were due to air volume changes. However, both blood and tissue contribute to the MRI signal and it is likely that heart rate/blood flow influences were captured during the two minutes of breathing. We have not explicitly accounted for this in our calculations because of the dominant role that the movement of air in and out of the lungs plays in the MRI signal intensity fluctuations. We also note that here we observed changes in signal density distributions that were very similar to what was observed using UTE MRI[42] that is a proton density sensitive method and CT[43] -the clinical gold standard for lung density measurements.

Regional specific-ventilation imaging was demonstrated in a small group of participants using free-breathing ^{1}H MR imaging without exogenous contrast. While other MRI techniques acquire images in breath-hold at multiple lung volumes[20,44] or free-breathing images for a single slice,[19,22,23,45] this approach provides another way to generate whole

lung functional maps that probe functional abnormalities using conventional equipment and pulse sequences while patients are free-breathing. This method may be useful for younger asthmatics who are difficult to treat and may need interventional procedures.

In summary, using conventional ^{1}H MRI without exogenous contrast, we developed a way to rapidly generate regional specific-ventilation measurements that correlate with plethysmography specific-ventilation and static breath-hold hyperpolarized ^{3}He MRI ventilation measurements. This method may offer new diagnostic approaches for pulmonary medicine in more typical clinical settings.

5.5 References

(1) Reddel, H. K. *et al.* A summary of the new GINA strategy: a roadmap to asthma control. *The European respiratory journal* 2015; 46: 622-639.

(2) Busse, W. W. Asthma diagnosis and treatment: filling in the information gaps. *J Allergy Clin Immunol* 2011; 128: 740-750.

(3) Celli, B. R. The importance of spirometry in COPD and asthma: effect on approach to management. *Chest* 2000; 117: 15S-19S.

(4) Burgel, P. R. The role of small airways in obstructive airway diseases. *Eur Respir Rev* 2011; 20: 23-33.

(5) Tulic, M. K., Christodoulopoulos, P. & Hamid, Q. Small airway inflammation in asthma. *Respir Res* 2001; 2: 333-339.

(6) Newman, K. B., Lynch, D. A., Newman, L. S., Ellegood, D. & Newell, J. D. Quantitative Computed-Tomography Detects Air Trapping Due to Asthma. *Chest* 1994; 106: 105-109.

(7) Awadh, N., Muller, N. L., Park, C. S., Abboud, R. T. & FitzGerald, J. M. Airway wall thickness in patients with near fatal asthma and control groups: assessment with high resolution computed tomographic scanning. *Thorax* 1998; 53: 248-253.

(8) Trivedi, A. *et al.* Using imaging as a biomarker for asthma. *Journal of Allergy and Clinical Immunology* 2017; 139: 1-10.

(9) Choi, S. *et al.* Registration-based assessment of regional lung function via volumetric CT images of normal subjects vs. severe asthmatics. *J Appl Physiol (1985)* 2013; 115: 730-742.

(10) Busacker, A. *et al.* A Multivariate Analysis of Risk Factors for the Air-Trapping Asthmatic Phenotype as Measured by Quantitative CT Analysis. *Chest* 2009; 135: 48-56.

(11) Aysola, R. S. *et al.* Airway Remodeling Measured by Multidetector CT Is Increased in Severe Asthma and Correlates With Pathology. *Chest* 2008; 134: 1183-1191.

(12) Guerrero, T. *et al.* Quantification of regional ventilation from treatment planning CT. *Int J Radiat Oncol Biol Phys* 2005; 62: 630-634.

(13) Lewis, S. M., Evans, J. W. & Jalowayski, A. A. Continuous distributions of specific ventilation recovered from inert gas washout. *J Appl Physiol Respir Environ Exerc Physiol* 1978; 44: 416-423.

(14) Fain, S., Schiebler, M. L., McCormack, D. G. & Parraga, G. Imaging of Lung Function Using Hyperpolarized Helium-3 Magnetic Resonance Imaging: Review of Current and Emerging Translational Methods and Applications. *Journal of Magnetic Resonance Imaging* 2010; 32: 1398-1408.

(15) Samee, S. *et al.* Imaging the lungs in asthmatic patients by using hyperpolarized helium-3 magnetic resonance: assessment of response to methacholine and exercise challenge. *J Allergy Clin Immunol* 2003; 111: 1205-1211.

(16) Edelman, R. R., Hatabu, H., Tadamura, E., Li, W. & Prasad, P. V. Noninvasive assessment of regional ventilation in the human lung using oxygen-enhanced magnetic resonance imaging. *Nature Medicine* 1996; 2: 1236-1239.

(17) Ohno, Y. *et al.* Oxygen-enhanced MRI vs. quantitatively assessed thin-section CT: pulmonary functional loss assessment and clinical stage classification of asthmatics. *Eur J Radiol* 2011; 77: 85-91.

(18) Sa, R. C. *et al.* Vertical distribution of specific ventilation in normal supine humans measured by oxygen-enhanced proton MRI. *J Appl Physiol (1985)* 2010; 109: 1950-1959.

(19) Zapke, M. *et al.* Magnetic resonance lung function--a breakthrough for lung imaging and functional assessment? A phantom study and clinical trial. *Respir Res* 2006; 7: 106.

(20) Pennati, F. *et al.* Assessment of regional lung function with multivolume (1)H MR imaging in health and obstructive lung disease: comparison with (3)He MR imaging. *Radiology* 2014; 273: 580-590.

(21) Kjorstad, A. *et al.* Quantitative lung ventilation using Fourier decomposition MRI; comparison and initial study. *Magnetic Resonance Materials in Physics Biology and Medicine* 2014; 27: 467-476.

(22) Bauman, G. *et al.* Non-contrast-enhanced perfusion and ventilation assessment of the human lung by means of fourier decomposition in proton MRI. *Magn Reson Med* 2009; 62: 656-664.

(23) Capaldi, D. P. I. *et al.* Free-breathing Functional Pulmonary MRI: Response to Bronchodilator and Bronchoprovocation in Severe Asthma. *Acad Radiol* 2017; 24: 1268-1276.

(24) Kirby, M. *et al.* Hyperpolarized 3He magnetic resonance functional imaging semiautomated segmentation. *Acad Radiol* 2012; 19: 141-152.

(25) Vedam, S. S. *et al.* Acquiring a four-dimensional computed tomography dataset using an external respiratory signal. *Physics in Medicine and Biology* 2003; 48: 45-62.

(26) Yamamoto, T. *et al.* 4D CT lung ventilation images are affected by the 4D CT sorting method. *Med Phys* 2013; 40: 101907.

(27) Lucas, B. D. & Kanade, T. An iterative image registration technique with an application to stereo vision. 1981.

(28) Guo, F. *et al.* Anatomical pulmonary magnetic resonance imaging segmentation for regional structure-function measurements of asthma. *Med Phys* 2016; 43: 2911.

(29) Heinrich, M. P. *et al.* MIND: Modality independent neighbourhood descriptor for multi-modal deformable registration. *Medical Image Analysis* 2012; 16: 1423-1435.

(30) Nahm, F. S. Nonparametric statistical tests for the continuous data: the basic concept and the practical use. *Korean Journal of Anesthesiology* 2016; 69: 8-14.

(31) Sheikh, K. *et al.* Ultrashort echo time MRI biomarkers of asthma. *J Magn Reson Imaging* 2017; 45: 1204-1215.

(32) Sa, R. C. *et al.* Validating the distribution of specific ventilation in healthy humans measured using proton MR imaging. *Journal of Applied Physiology* 2014; 116: 1048-1056.

(33) Jahani, N. *et al.* A four-dimensional computed tomography comparison of healthy and asthmatic human lungs. *J Biomech* 2017; 56: 102-110.

(34) Altes, T. A. *et al.* Hyperpolarized 3He MR lung ventilation imaging in asthmatics: preliminary findings. *J Magn Reson Imaging* 2001; 13: 378-384.

(35) Costella, S. *et al.* Regional pulmonary response to a methacholine challenge using hyperpolarized (3)He magnetic resonance imaging. *Respirology* 2012; 17: 1237-1246.

(36) Mutaf, Y. D., Antolak, J. A. & Brinkmann, D. H. The impact of temporal inaccuracies on 4DCT image quality. *Med Phys* 2007; 34: 1615-1622.

(37) Pollock, S., Kipritidis, J., Lee, D., Bernatowicz, K. & Keall, P. The impact of breathing guidance and prospective gating during thoracic 4DCT imaging: an XCAT study utilizing lung cancer patient motion. *Phys Med Biol* 2016; 61: 6485-6501.

(38) Fletcher, C. & Peto, R. The natural history of chronic airflow obstruction. *Br Med J* 1977; 1: 1645-1648.

(39) Moreno, F. & Lyons, H. A. Effect of Body Posture on Lung Volumes. *Journal of Applied Physiology* 1961; 16: 27-&.

(40) Lumb, A. B. & Nunn, J. F. Respiratory-Function and Ribcage Contribution to Ventilation in Body Positions Commonly Used during Anesthesia. *Anesthesia and Analgesia* 1991; 73: 422-426.

(41) Middleton, H. *et al.* MR imaging with hyperpolarized 3He gas. *Magn Reson Med* 1995; 33: 271-275.

(42) Ma, W. *et al.* Ultra-short echo-time pulmonary MRI: evaluation and reproducibility in COPD subjects with and without bronchiectasis. *J Magn Reson Imaging* 2015; 41: 1465-1474.

(43) Wegener, O. H., Koeppe, P. & Oeser, H. Measurement of lung density by computed tomography. *J Comput Assist Tomogr* 1978; 2: 263-273.

(44) Pusterla, O. *et al.* Rapid 3D in vivo 1H human lung respiratory imaging at 1.5 T using ultra-fast balanced steady-state free precession. *Magn Reson Med* 2017; 78: 1059-1069.

(45) Capaldi, D. P. *et al.* Free-breathing pulmonary 1H and Hyperpolarized 3He MRI: comparison in COPD and bronchiectasis. *Acad Radiol* 2015; 22: 320-329.

5.6 Supplement

5.6.1 Materials and Methods

5.6.1.1 Study Participants

We recruited participants from a local tertiary care center and by advertisement. For all participants, the exclusion criteria consisted of: 1) serious claustrophobia, 2) unable to perform spirometry, 3) body mass index >40, and, 4) any MR imaging contraindications (i.e. metal/electronic/magnetic implants). Inclusion criteria for healthy volunteers consisted of: 1) medical history with no chronic or acute respiratory disease and stable health, 2) age 18-75, and, 3) smoking history <1 pack-years. Inclusion criteria for asthmatics consisted of: 1) clinical diagnosis of asthma with β2-agonist reversibility of FEV_1>12%, or methacholine FEV_1 provocative concentration that decreased FEV_1 by 20% (PC_{20}) ≤ 8 mg/ml if not administered inhaled corticosteroid (ICS), or ≤ 16mg/ml if administered ICS, 2) no history of other chronic disease, 3) age 18-85, and, 4) smoking history < 1 pack-years.

5.6.1.2 Pulmonary Function Tests

Spirometry and plethysmography were performed using a *MedGraphics Elite Series* plethysmograph (MedGraphics Corporation, St. Paul, Minnesota, USA) according to the American-Thoracic-Society/European-Respiratory-Society guidelines[1] to measure FEV_1, forced-vital-capacity (FVC), total-lung-capacity (TLC), residual-volume (RV), tidal-volume (TV), functional-residual-capacity (FRC) and airways resistance (R_{AW}). Plethysmography-derived specific-ventilation was calculated as TV divided by FRC, as previously described.[2]

5.6.1.3 Hyperpolarized ^{3}He MR Image Processing

Hyperpolarized ^{3}He MR static ventilation images were segmented using a k-means approach that classified voxel intensity values into five clusters as follows: 1) signal-void = cluster 1 (C1) or ventilation defect volume, and 2) ventilation volume = cluster 2-5.

Ventilation boundaries were segmented using a seeded region-growing algorithm of the ^{1}H MR imaging thoracic cavity, as previously described.[3]

5.6.2 Results

Figure 5-6 shows the 4DMRI specific-ventilation maps and signal-intensity distributions for the two lung volumes used to generate 4DMR specific-ventilation images (tidal-inspiration and tidal-expiration volumes) for a representative healthy-volunteer and asthmatic. The signal-intensity distributions for the healthy volunteer demonstrated a shift towards lower signal-intensities and narrowed distribution at the greater lung volume. For the asthmatic, the qualitative difference between tidal inspiration and tidal expiration was smaller.

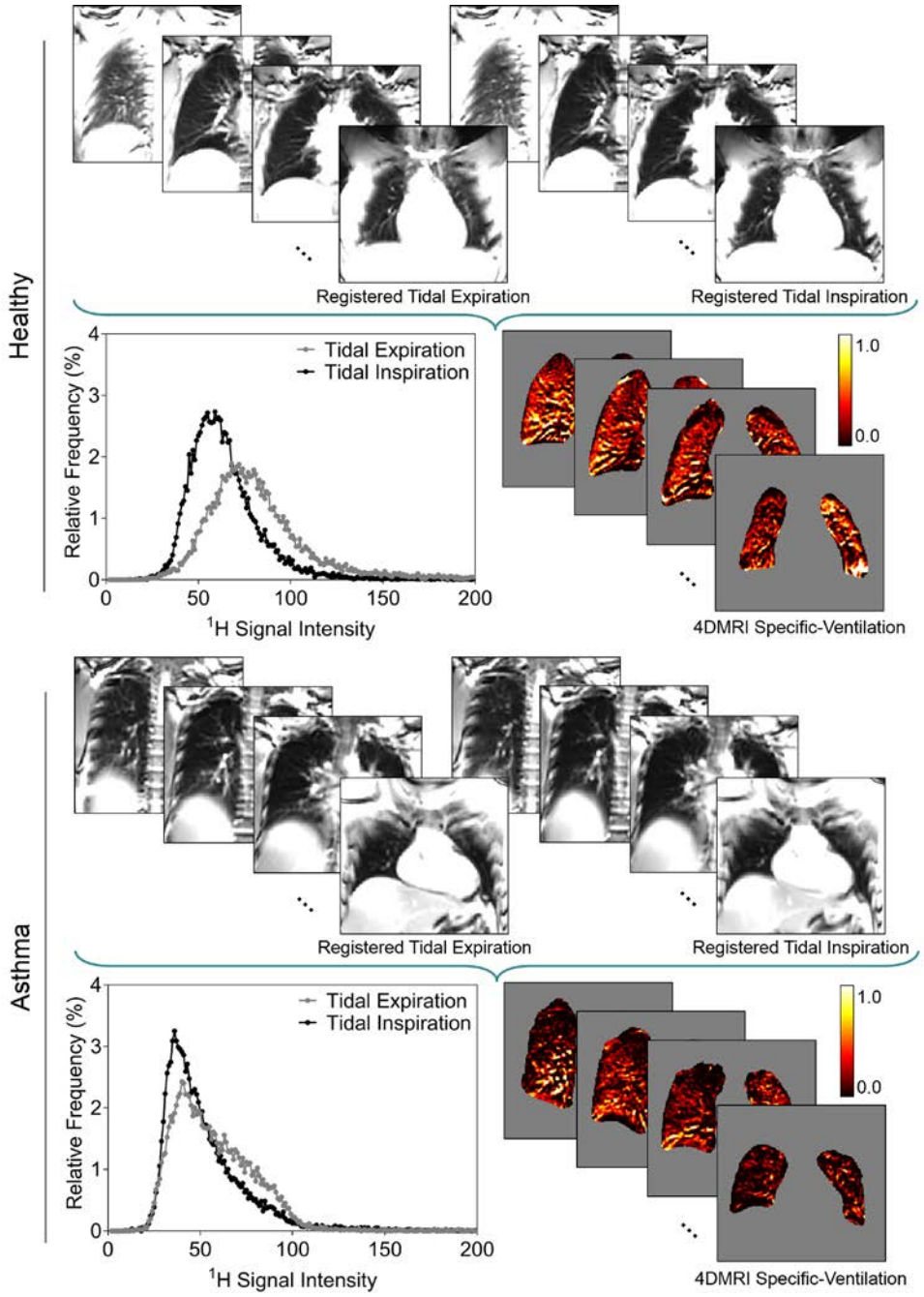

Figure 5-6 Generation of 4DMR Specific-Ventilation Images
4DMRI specific-ventilation heat-maps (black=low-specific-ventilation to yellow=high-specific-ventilation), which is a dimensionless physical quantity that reflects the proportion of inhaled gas moving into the lung during normal breathing, were generated on a voxel-by-voxel basis after co-registration of tidal inspiratory and tidal expiratory MRI volumes to provide a local distribution of specific-ventilation, as shown for a representative healthy volunteer and an asthmatic. Signal intensity histograms are also shown at two lung volumes (tidal inspiration [black] and tidal expiration [gray]), and shows a shift toward lower signal intensities and narrowed distribution at a higher lung volume.

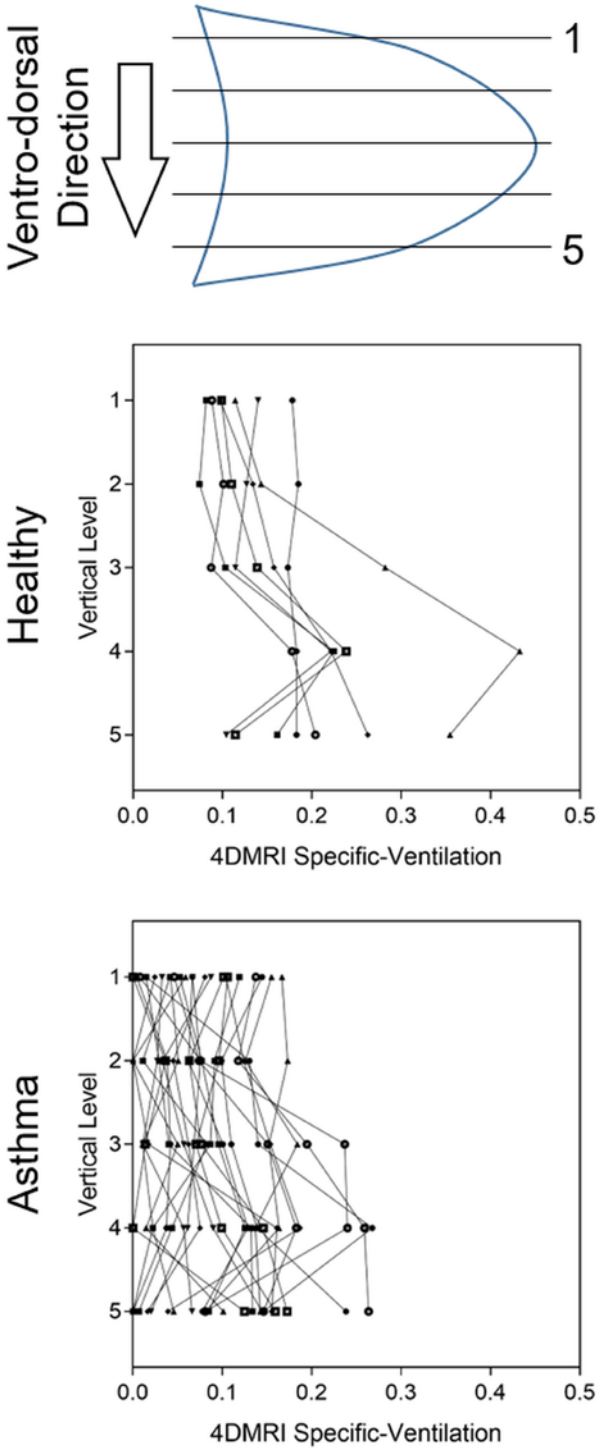

Figure 5-7 Gravity-dependence Analysis in Healthy Volunteer and Patients with Asthma
Individual variations of mean values of 4DMRI specific-ventilation along ventro-dorsal direction (vertical axis) from the least (one) to the most (five) gravity-dependent levels. Each piecewise line represents a single subject.

5.6.3 References

(1) Miller, M. R. *et al.* Standardisation of spirometry. *Eur Respir J* 2005; 26: 319-338.

(2) Lewis, S. M., Evans, J. W. & Jalowayski, A. A. Continuous distributions of specific ventilation recovered from inert gas washout. *J Appl Physiol Respir Environ Exerc Physiol* 1978; 44: 416-423.

(3) Kirby, M. *et al.* Hyperpolarized 3He magnetic resonance functional imaging semiautomated segmentation. *Acad Radiol* 2012; 19: 141-152.

CHAPTER 6

6 CONCLUSIONS AND FUTURE DIRECTIONS

*In this final chapter, I will provide a summary and overview of the important findings and conclusions presented in **Chapters 2-5**. The limitations specific to each study and general limitations will also be provided with some potential solutions. Finally, I will end with some future directions based on what we observed using non-contrast enhanced pulmonary imaging.*

6.1 Overview and Research Questions

COPD and asthma affect hundreds of millions of people throughout the world[1] and this number is projected to increase. Ultimately, this will overwhelm the healthcare system and result in a substantial economic burden.[2] Despite the many years of research, current therapies are lacking,[3,4] leaving patients with dismal prognoses. Clearly, the management and treatment of lung disease patients is inadequate and this is in part due to the way in which these patients are currently diagnosed and monitored using measurements of airflow obstruction. Although these global measurements of airflow limitation are easy to implement and reproducible,[5] they do not provide any regional information about the different underlying pathophysiology in lung disease patients. Accordingly, this has motivated the development and research of other approaches to regionally evaluate lung function using pulmonary imaging for longitudinal monitoring and image-guided treatments.

Numerous pulmonary imaging techniques are being developed to quantify structure and function regionally within the lungs. However, they are not all well suited for longitudinal monitoring because of the potential risks associated with exposure to ionizing radiation,[6-8] specifically for CT and nuclear medicine imaging, which is particularly concerning for young adults and pediatric populations. In contrast, pulmonary MRI is not limited by radiation exposure and provides regional measurements of lung function with the potential for longitudinal monitoring of patients and image-guided treatment. Specifically with the use of inhaled hyperpolarized noble gases (^{3}He and ^{129}Xe), one can regionally quantify pulmonary ventilation by visualizing lung regions accessed by gas during a breath-hold,

and alternatively, regions that are not accessed. The ventilation images that appear in hyperpolarized noble gas MRI have been shown to be reproducible,[9,10] related to relevant clinical measurements,[11-13] and sensitive to treatment response,[14,15] in both asthma and COPD patients. Despite numerous studies, clinical translation of these imaging approaches have been hampered due to a number of key limitations including: 1) relatively high cost associated with inhaled gas contrast; and, 2) requirement of multi-nuclear MR hardware and analysis software and specialized personal, restricting these techniques to a few specialized research centres. With this in mind, there has been growing interest in the development of pulmonary MRI and CT approaches that do not depend on inhaled gas contrast agents to overcome the challenges associated with resource accessibility. The development and validation of these clinically meaningful non-contrast enhanced pulmonary MR and CT imaging biomarkers is critically required to accelerate pulmonary MRI and CT translation from the research workbench to the clinical workflow for patient care.

The overarching objective of this thesis was to develop and evaluate patients with lung disease using MR and CT imaging biomarkers of pulmonary structure and function without the use of inhaled exogenous contrast agents or specialized equipment. The specific research questions addressed were: 1) Do measurements of emphysema and gas-trapping derived from parametric response maps of co-registered inspiratory-expiratory CT images relate to ventilation heterogeneity quantified using hyperpolarized ^{3}He MRI? (**Chapter 2**); 2) Can non-contrast enhanced free-breathing pulmonary ^{1}H MRI measurements of ventilation heterogeneity be developed to measure ventilation abnormalities in subjects with COPD and bronchiectasis, and are these measurements related to pulmonary function tests and ^{3}He MRI ventilation defects? (**Chapter 3**); 3) Can we apply the developed method in **Chapter 3** to patients with severe asthma to evaluate ventilation heterogeneity, both pre- and post-salbutamol as well as post-methacholine challenge? (**Chapter 4**); and, 4) Can we extend the free-breathing pulmonary ^{1}H MRI approach developed in **Chapter 3** to capture whole-lung measurements of regional specific-ventilation in healthy volunteers and patients with asthma? (**Chapter 5**)

6.2 Summary and Conclusions

In **Chapter 2** we developed and directly compared CT PRM with ^{3}He MRI ventilation measurements of gas-trapping and emphysema in ex-smokers with and without COPD. We determined the quantitative and spatial relationships of PRM gas-trapping and PRM emphysema measurements with MRI measurements of parenchymal tissue integrity and ventilation. We found that in 58 ex-smokers with (n=32) and without (n=26) COPD, ^{3}He MRI ventilation defect percent was significantly correlated with CT PRM measurements of gas-trapping (r=.58, p<.001) and emphysema (r=.68, p<.001). ^{3}He MRI ADC measurements were also significantly correlated with PRM gas-trapping (r=.55, p<.001) and PRM emphysema (r=.62, p<.001). Spatial CT-MRI relationships in all ex-smokers showed that ^{3}He MRI ADC was significantly elevated in regions of PRM gas-trapping as compared to normal tissue (p<.05). In patients with mild and moderate COPD (n=25), ^{3}He MRI ventilation defects were quantitatively and spatially related to PRM gas-trapping (mild COPD - gas-trapping: SOC=36±28%, emphysema: SOC=1±2%, p=.001; moderate COPD - gas-trapping: SOC=34±28%, emphysema: SOC=7±15%, p=.006), while in severe COPD (n=7), MRI ventilation defects were quantitatively and spatially related to both PRM-gas-trapping and emphysema (gas-trapping: SOC=36±18%, emphysema: SOC=64±30%, p=.01). These observations are important because while ^{3}He MRI is unlikely to be translated clinically, this information may be used to help better understand PRM gas-trapping measurements, which may be more widely adopted for clinical phenotyping of COPD patients.

We then developed and compared pulmonary ventilation abnormalities derived from FDMRI with ^{3}He MRI in subjects with COPD and bronchiectasis in **Chapter 3**. We observed that in 26 subjects, including 12 COPD subjects and 14 bronchiectasis subjects, that for the COPD subjects, FDMRI and ^{3}He MRI VDP was 7±6% and 24±14%, respectively (p<.001, bias=-16±9%). In COPD subjects, FDMRI was significantly correlated with ^{3}He MRI VDP (r=.88, p=.0001), ^{3}He MRI ADC (r=.71, p<.05), and R_{AW} (r=.60, p<.05). In subjects with bronchiectasis, FDMRI (5±3%) and ^{3}He MRI VDP (18±9%) were significantly different (p<.001) and not correlated (p>.05). The Dice

Similarity Coefficient for FDMRI and ^{3}He MRI ventilation was 86±7% for COPD and 86±4% for bronchiectasis subjects ($p>.05$). This work showed similar regional ventilation abnormalities using FDMRI and ^{3}He MRI in COPD subjects and these appear to be dominated by the presence of regional emphysematous bullae. This work demonstrated that FDMRI and ^{3}He MRI ventilation defects were strongly correlated in COPD, but not bronchiectasis subjects.

In **Chapter 4** we evaluated ventilation heterogeneity in patients with severe asthma, both pre- and post-salbutamol as well as post-methacholine challenge, using FDMRI and ^{3}He MRI. We observed in 16 severe asthmatics that hyperpolarized ^{3}He MRI ($p=.02$) and FDMRI ($p=.02$) VDP significantly improved post-salbutamol and for four asthmatics who could perform MCh ($n=4$), ^{3}He and FDMRI VDP significantly increased at the provocative concentration of methacholine resulting in a 20% decrease in FEV_1 and decreased post-bronchodilator ($p=.02$), with a significant difference between methods ($p=.01$). FDMRI VDP was moderately correlated with ^{3}He VDP ($\rho=.61$, $p=.01$), but under-estimated VDP relative to ^{3}He VDP (-6±9%). While ^{3}He MRI VDP was significantly correlated with the lung-clearance-index, FDMRI was not ($\rho=.49$, $p=.06$). This work demonstrated that FDMRI VDP generated in free-breathing asthmatic patients was correlated with static inspiratory breath-hold ^{3}He MRI VDP, but under-estimated VDP relative to ^{3}He MRI VDP. Although less sensitive to salbutamol and MCh, FDMRI VDP may be considered for asthma patient evaluations at centres without inhaled-gas MRI.

In **Chapter 5** of this thesis, we developed a whole-lung free breathing pulmonary ^{1}H MRI technique to measure regional specific-ventilation and evaluated asthmatics and healthy volunteers. We compared ^{1}H MRI specific-ventilation with hyperpolarized ^{3}He MRI ventilation in healthy and asthmatic participants, and, determined the relationships between ^{1}H MRI specific-ventilation and hyperpolarized ^{3}He MRI and pulmonary-function measurements. We observed in 30 participants, including seven healthy volunteers and 23 asthmatics, ^{1}H MR imaging specific-ventilation ($p<.0001$) and hyperpolarized ^{3}He MR imaging ventilation-percent ($p<.0001$) were both significantly greater in healthy volunteers as compared to asthmatics. For all subjects, ^{1}H MRI specific-ventilation was also correlated with plethysmography specific-ventilation ($\rho=.54$, $p=.002$) and hyperpolarized

^{3}He MRI ventilation-percent (ρ=.67, p<.0001), as well as FEV_1 (ρ=.65, p=.0001), FEV_1/FVC (ρ=.75, p<.0001), RV/TLC (ρ=-.68, p<.0001) and R_{AW} (ρ=-.51, p=.004). ^{1}H MRI specific-ventilation was significantly greater in the gravitational-dependent versus non-dependent lung in healthy volunteers (p=.02), but not in the asthmatics (p=.1). In asthmatics, co-registered ^{1}H MRI specific-ventilation and hyperpolarized ^{3}He MRI maps showed that specific-ventilation was diminished in corresponding ^{3}He MRI ventilation-defects as compared to well-ventilated regions (p<.0001). We demonstrated in this study that using conventional ^{1}H MRI without exogenous contrast, could rapidly generate whole-lung regional specific-ventilation measurements, which correlated with plethysmography specific-ventilation and static breath-hold hyperpolarized ^{3}He MRI ventilation measurements. This method may offer new diagnostic approaches for pulmonary medicine in more typical clinical settings.

In summary, we provided: 1) evidence that CT parametric response maps were quantitatively and spatially related to ventilation measurements using ^{3}He MRI in ex-smokers with and without airflow limitation; 2) evidence that the ventilation defect measurements derived from non-contrast enhanced free-breathing MRI are related to ventilation abnormalities generated from ^{3}He MRI in patients with COPD; 3) evidence that the measurements derived from non-contrast enhanced free-breathing MRI are sensitive to treatment response to bronchodilation and bronchoconstriction in patients with severe asthma; and, 4) a new non-contrast enhanced whole-lung free-breathing ^{1}H MRI method to evaluate regional specific-ventilation in patients with asthma.

6.3 Limitations

The significant limitations from **Chapters 2-5** will be discussed in this section of the thesis. The study specific limitations are also provided in the Discussion section of each of the respective Chapters.

6.3.1 Study Specific Limitations

Chapter 2: *Pulmonary Imaging Biomarkers of Gas-trapping and Emphysema in COPD: ^{3}He MR Imaging and CT Parametric Response Maps*

In the study presented in **Chapter 2**, we sought to better understand the quantitative and spatial relationships between CT PRM and ^{3}He MRI imaging biomarkers in ex-smokers with and without COPD. This work was limited by the relatively small study group and the fact that we mainly evaluated ex-smokers with mildly abnormal and normal spirometry, which was prospectively planned and driven by our interest to investigate very early or mild disease. Given our understanding of the heterogeneity of COPD patients, we must be cautious about extrapolating our results.

Another limitation is the influence of deformable registration error on the results presented in this study. Similar to 4DCT,[16] Fourier decomposition MRI,[17] and paired inspiratory/expiratory CT,[18-20] PRM exploits the image signal differences as the lung tissue expands and contracts from inspiration to expiration. All these approaches rely on either computational or intuitive co-registration of inspiratory and expiratory CT and assume that the abnormal presence of air can be regionally related to emphysema and/or functional small airways disease. Thus, deformable image registration errors pose a challenge, which has been previously reported for PRM in the liver.[21] A direct comparison of the results generated here with results stemming from commercially available software, such as Apollo Workstation 2.0 (VIDA Diagnostics Inc., Coralville, Iowa, USA) or Lung Density Analysis software (IMBIO, Minneapolis, Minnesota, USA), would allow for a better understanding on how image registration influences CT parametric response maps. Any potential differences between the generated maps would likely stem from the different image registration/warping algorithms used to register the inspiratory and expiratory CT volumes since the density thresholds used are generally the same.

Finally, hyperpolarized ^{3}He MRI is still limited to a few research facilities worldwide and is unlikely to be translated clinically due to the depleted global supply of ^{3}He gas. However, with recent improvements in ^{129}Xe polarization[22] and the development of ^{19}F

MRI,[23] inhaled gas MRI may yet be considered for regulatory approval and future clinical workflow.

Chapter 3: *Free-breathing Pulmonary ^{1}H and Hyperpolarized ^{3}He MRI: Comparison in COPD and Bronchiectasis*

In the study presented in **Chapter 3**, we developed a free-breathing ^{1}H MRI method to evaluate pulmonary ventilation abnormalities in subjects with COPD and bronchiectasis. First, we only acquired a single free-breathing ^{1}H MR image. This limited our ability to directly compare the ventilation measurements derived from FDMRI with those generated from ^{3}He MRI.

One of the challenges associated with pulmonary ^{1}H MRI methods, is the weak pulmonary ^{1}H signal intensity that is further diminished at higher field strengths because of the relationship between field-strength and T_2^* effects. Furthermore, MR signal intensity is dependent on positioning the patient within the RF coil, resulting in potential inter-scan variability. Previous pilot and development studies at 1.5T have shown qualitative agreement for regional ventilation and perfusion measurements with the SPECT/CT.[24] Moreover, recent studies have also demonstrated the reproducibility of FDMRI ventilation- and perfusion-weighted images in healthy volunteers.[25]

Finally, Fourier decomposition has recently emerged as a pulmonary functional MRI method, albeit the ventilation measurements are dependent on more sophisticated image processing methods. FDMRI generates ventilation contrast based on image signal differences during the breathing cycle as air enters and leaves the pulmonary system and tissue contracts and expands. This relies on robust and accurate image registration methods to co-register the free tidal-breathing ^{1}H MR image data. Consequently, deformable registration error poses a challenge when generating FDMR ventilation weighted images. To generate FDMR ventilation-weighted images, registration algorithms must account for the movement of the diaphragm and any registration error will result in regions of high signal intensity (e.g. mucus pooling in bronchiectasis subjects) oscillating at the same frequency as respiration. Accordingly, this registration error can result in apparently increased ventilation, which may or may not accurately reflect truly ventilated regions.

Thus, there may be regions that appear as ventilation in FDMRI that are in fact not ventilated due to misalignment of these regions of high signal intensity via the deformable registration process.

Chapter 4: *Free-breathing Functional Pulmonary MRI: Response to Bronchodilator and Bronchoprovocation in Severe Asthma*

In **Chapter 4**, we applied the developed FDMRI approach in **Chapter 3** in patients with severe asthma to evaluate treatment response to bronchodilation as well as bronchoconstriction. We also focused on severe asthmatics and those with poor control in order to capture information relevant to an important clinical problem and, because of this, the vast majority of patients were unable to perform methacholine challenge (n=4).

As mentioned before, an inherent limitation of pulmonary ^{1}H MRI is the low signal intensity due to intrinsically low proton density and T_2* effects,[26] but recent research[27] that exploits shorter echo times may overcome this challenge. FDMRI is also currently limited to single slice acquisitions and this limits the generalizability of a direct comparison between this method and hyperpolarized ^{3}He MRI (FDMRI=single 2D slice time series and ^{3}He MRI=multi-slice 2D acquisition). Furthermore, there is no standardization of the complex image-processing methods used to generate FDMR ventilation-weighted images.

Finally, inhaled hyperpolarized ^{3}He MRI static ventilation maps and dynamic free breathing FDMRI ventilation maps provide similar but not the same functional information, making it challenging to perform a direct comparison between the two imaging techniques. The differences in the functional information measured using inhaled-gas MRI and FDMRI may stem from the different time constants for lung filling that are the consequence of different airway abnormalities. For example, in asthmatics, ^{3}He MRI ventilation defects reflect lung regions with long time constants for filling that are beyond the 10-15s acquisition time of scanning. In contrast, multi-breath free-breathing FDMRI ventilation defects reflect airway and parenchyma abnormalities[28] that do not fill during a much longer, two minute acquisition window. A comparison between FDMRI and previous work using multi-breath wash-in inhaled gas MRI[29] may be better suited in

probing the relationship of inhaled noble gas MRI and non-contrast enhanced MRI ventilation measurements.

Chapter 5: *Free-breathing Pulmonary MR Imaging to Quantify Regional Ventilation*

In **Chapter 5**, we developed a whole lung free-breathing pulmonary ^{1}H MRI approach to generate regional measurements of specific-ventilation and evaluated asthmatics and healthy volunteers. There was a significant age difference between healthy and asthmatic volunteers, as a result of consecutive recruitment between January and June 2017. This is important to consider because lung aging has been shown to influence lung ventilation.[30] Furthermore, other confounding factors, such as the differences in the demographics, may contribute to the overall differences observed between the two subject groups.

As mentioned before, image registration error poses a challenge when measuring MRI specific-ventilation since this imaging biomarker is based on the voxel-wise difference in signal-intensities between co-registered volumes. It should be noted that we did not acquire specific-ventilation measurements in the same body position using plethysmography (sitting upright) and imaging (supine). Differences in body position, as well as arm position, have been shown in previous studies to influence lung volumes involved in calculating specific-ventilation (FRC and TV).[31,32]

Another limitation is that ^{3}He MRI measures gas distribution during a 10-15s breath-hold,[33] while ^{1}H MR specific-ventilation images are generated, (like 4DCT[34]) over two to three minutes of tidal breathing. Accordingly, the two methods are not measuring the same quantity and they likely interrogate different lung functional information related to airway calibre that influence the time constants for lung filling and emptying. Furthermore, free-breathing protocols may be influenced by irregular breathing patterns, previously observed using 4DCT,[35] so some patients will require coaching or support.[36]

It is important to point out that we did not explicitly account for heart rate/blood flow contribution to the MRI signal intensity in our calculations because of the dominant role that the movement of air in and out of the lungs plays in the MRI signal intensity fluctuations. The current approach is based on the assumption that changes in signal

intensity during tidal breathing were due to air volume changes. Although the observed changes in signal density distributions were very similar to what was observed using UTE MRI[37] and CT,[38] ideally, a mass correction to correct for respiratory-induced changes in tissue perfusion (applied previously to 4DCT[16]) could be applied here to account for changes in blood distribution between the exhale and inhale phases.

6.3.2 General Limitations

In **Chapters 2-5**, there was a small number of subjects evaluated in each study. This was due in part because of the design of the studies and the inability to perform rigorous power calculations since there was little prior knowledge of the imaging biomarkers generated from non-contrast enhanced imaging data. Caution must be taken when extrapolating the results presented in these studies to the broader population of asthmatic and COPD patients. Regardless, these exploratory studies provide the foundation for future studies which should be aimed in evaluating larger groups of patients to confirm the results observed.

One limitation to the studies presented in **Chapters 2-5** was the use of whole lung imaging biomarkers of signal intensity, relative areas of diseased lung, or ventilation to evaluate pulmonary abnormalities in asthma and COPD patients. These global measurements of lung function, although suitable for comparison and validation with other global measures of airflow obstruction (i.e. spirometry), tend to eliminate the heterogeneity in regional ventilation abnormalities visible on images. It is well known that static ventilation images generated from hyperpolarized noble gas MRI are not binary (i.e. 0=non-ventilated vs 1=ventilated); they provide a gradient of signal intensities from hyper-intense to signal void regions within the lungs, as shown in **Figure 1-11**. Analysis methods that were implemented to generate the ventilation defect percent can also be used to generate clusters of signal intensities, as shown in **Figure 4-1**, to quantify hyper-intense, normal, and hypo-intense signal regions.[39] Further studies should be performed to investigate these regions in addition to the non-ventilated regions in both asthma and COPD patients. Furthermore, threshold methods, such as those implemented in **Chapter 2**, either under[40] or over[41] estimate disease depending on the choice of threshold value. Alternative approaches have

been proposed that leverage principal component analysis (PCA) to overcome the use of a single predefined threshold.[42,43]

Another important limitation to the studies presented in **Chapters 2-5** was the use of ^{3}He gas and the limited availability of this gas for medical imaging. The high cost of ^{3}He gas, due to the depleting global supply of ^{3}He,[44] has limited hyperpolarized ^{3}He MRI to a few research facilities worldwide and is unlikely to be translated clinically. As mentioned in **Section 1.5.2.1**, the transition to ^{129}Xe and ^{19}F gases has been the focus of the inhaled gas MRI community, where with recent improvements in ^{129}Xe polarization[22] and the development of ^{19}F MRI,[23] inhaled gas MRI may yet be considered for regulatory approval and future clinical workflows. Regardless, future studies involving ^{19}F and hyperpolarized ^{129}Xe MRI are required to validate the results presented using ^{3}He MRI and how these results may differ when comparing to the non-contrast enhanced imaging techniques presented in this thesis.

Finally, all the non-contrast enhanced imaging methods developed in **Chapters 2-5** rely on sophisticated image processing methods, which may limit clinical translation. Furthermore, there is a dependence on these image analysis methods to be robust, accurate, and reproducible. Consequently, any error in the image analysis pipeline, such as deformable registration error, poses a challenge when generating these imaging biomarkers of pulmonary disease. Thus, future studies should focus on the standardization and validation of software used to analyze these images. This will be important moving forward since the advancement of pulmonary imaging toward clinical implementations requires large-scale and multi-centre evaluation of clinically-relevant biomarkers.

6.4 Future Directions

6.4.1 Regional Ventilation Heterogeneity: Three Dimensional Ventilation Clustering of Hyperpolarized Noble Gas MRI

In **Chapters 2-5**, we evaluated lung disease using the ventilation defect percent generated from hyperpolarized ^{3}He MRI. Although VDP is a robust measure that is reproducible[9,10] and related to relevant clinical measurements,[11-13] the ventilation defect percent does not fully exploit the rich information and spatial content that is inherent to the hyperpolarized noble-gas MR ventilation images, as mentioned in **Section 6.3.2**.[45] As shown in **Figure 6-1**, specific cases can be identified whereby the VDP for two subjects is the same, but the ventilation patterns are visibly different. This may suggest that there are measureable differences in ventilation heterogeneity that are not reflected by VDP. Hence, the objective of this proof-of-concept study was to develop an automated algorithm that quantifies the ventilation heterogeneity readily displayed in pulmonary functional inhaled noble-gas MRI. We hypothesize that the incorporation of both the magnitude and spatial location of ventilation defects when analyzing inhaled noble-gas MR ventilation images could provide further clinically relevant information that would be complementary to VDP and reflect clinical measurements of ventilation heterogeneity, such as LCI.

The proposed three-dimensional clustering algorithm iteratively traces the non-ventilated volumes until the maximum sphere (or multiple spheres of the same size) that can be filled within the volume are found. Once the largest sphere (or multiple spheres of the same size) was identified, this volume(s) was removed from the non-ventilated volume. This was iteratively repeated until the non-ventilated volume was replaced by spheres. Thus, the algorithm determines the minimum number of spheres of unequal sizes required to fill a specified volume. This is similar to previous work where unequal sphere packing was investigated in connection with radiosurgical treatment planning.[46]

Mathematically, this approach can be implemented using a naïve greedy algorithm. Let $S = \{b_1, b_2, \dots, b_n\}$, be a set with n elements where each element $b_n = B_n(r, l)$ is an open sphere of radius r at locations l. Our goal is to determine the minimum number of spheres of unequal sizes, thus resulting in the following minimization problem:

$$\min_{S}\{\|S\|_0\} \; : \; S \in \mathbf{R}^n \tag{6-1}$$

where we want to minimize the cardinality of the set S and $\forall\ (b \in S)\ \exists\ (r, l)$.

To insure that the spheres are filling the specified volume R, a constraint was implemented so that the intersection between the region that is being packed with spheres R and the spheres b is just b:

$$b \cap R = b \tag{6-2}$$

Furthermore, to prevent overlapping between spheres, the overlap between two spheres (b and b') would result in the null set:

$$b \cap b' = \emptyset \tag{6-3}$$

A volume constraint was imposed so that the total volume of spheres is equal to the volume of the specified region R:

$$\sum_{b \in S} V(b) = V(R) \tag{6-4}$$

To further simplify the problem, there is no location constraint with regards to where the spheres are positioned.

Computationally, MATLAB R2016a (Mathworks) was used to solve the minimization problem. In the discrete case, three-dimensional matrices were used to store visual information of where the volumes are located using binary values (0=background; 1=foreground). We resampled the segmented ^{3}He MRI from 3.125x3.125x15mm^3 into approximately 5x5x5mm^3 voxel space to ensure isotropic resolution prior to implementation. The ventilation defect regions were completely packed with spheres, where the minimum sphere diameter was equal to one voxel.

Figure 6-1 shows the output from the proposed algorithm with ventilation defects and ventilated regions being clustered for two representative subjects (COPD and bronchiectasis) with the same VDP. For the ventilation defect clustering, ventilation is shown in blue and ventilation defects are shown as spheres with different volumes shown in colour (red=13-voxels-diameter to yellow=3-voxels-diameter). The COPD subject had a large upper lobe ventilation defect that was reflected by larger sphere sizes that corresponded to 25% of the total defect volume. In contrast, the bronchiectasis subject had ventilation defect regions that mostly consisted of smaller spheres.

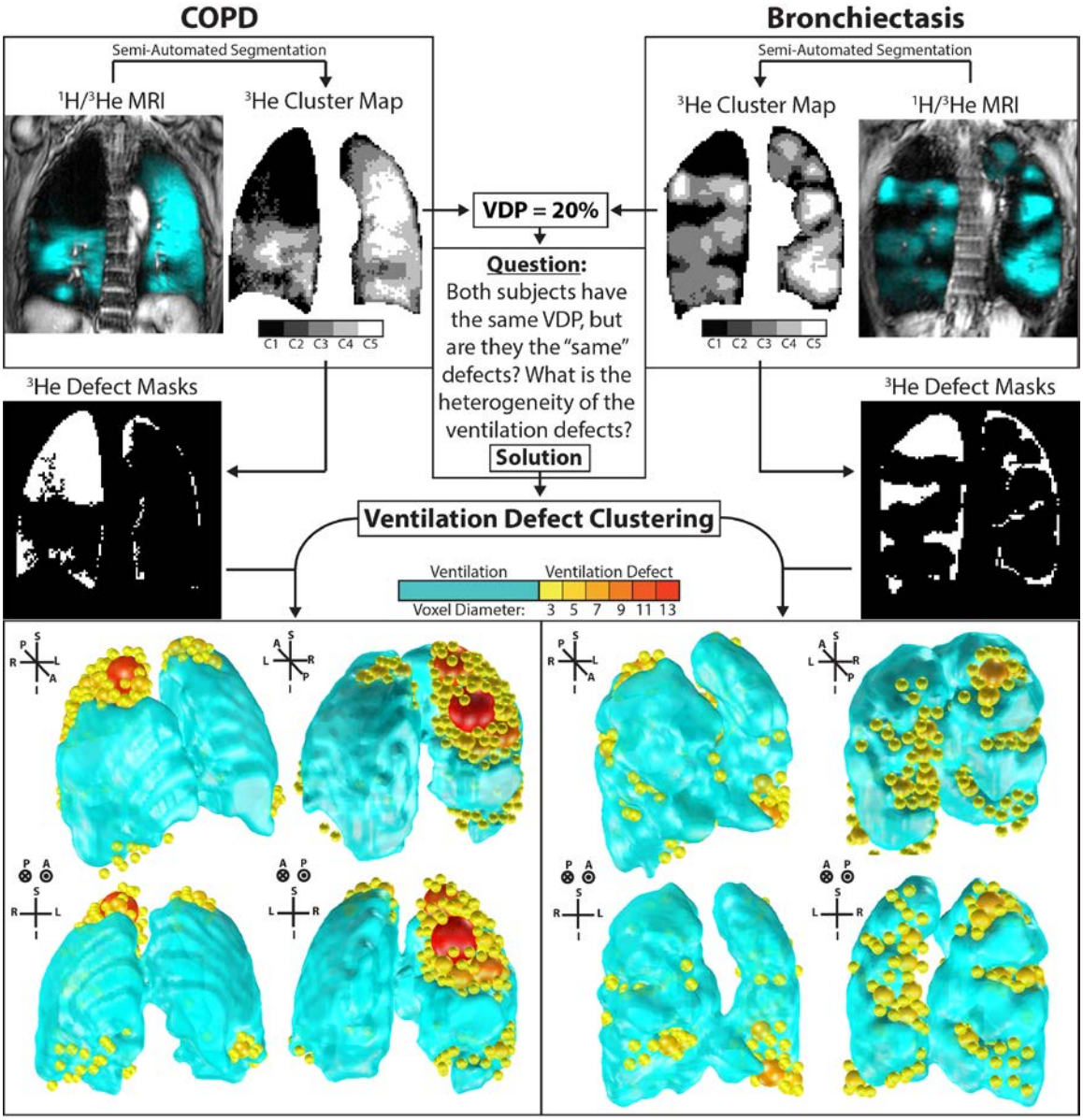

Figure 6-1 Ventilation defect clusters for two subjects (COPD and bronchiectasis) with the same ventilation defect percent

For ventilation defect clusters, the algorithm outputs a three-dimensional volume of ventilation in aqua and ventilation defects represented by spheres ranging in voxel diameters of 3-5 voxels (yellow) to voxel diameters of 9-13 voxels (red). Voxel= $5x5x5mm^3$.

Figure 6-2 shows a cumulative volume sum for each sphere normalized to the total lung volume (cluster ventilation defect percent) and this was performed to better demonstrate what was visually observed in **Figure 6-1**. When cluster voxel diameter is plotted in relation to normalized volume, there are numerous smaller spheres, and no large

homogeneous regions in the non-ventilated volume for the bronchiectasis subject. Alternatively, for the COPD subject, there is a mixture of small and large spheres in the non-ventilated volume. To complement the results generated using the algorithm, the lung clearance index, which reports a global measure of ventilation heterogeneity made at the mouth, was also greater in the bronchiectasis (LCI=20.8) as compared with the COPD subject (LCI=14.6).

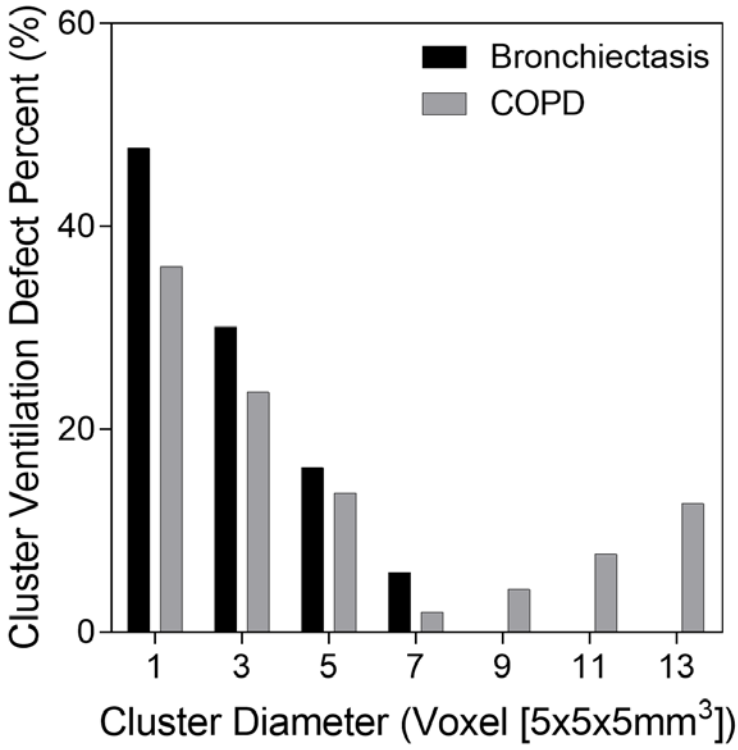

Figure 6-2 Cluster ventilation defect percent for the same two subjects in **Figure 6-1** Ventilation defect volume normalized to the total ventilation defect volume (cluster ventilation defect percent) by cluster (sphere) size for COPD (gray) and bronchiectasis (black) subjects. Voxel= 5x5x5mm^3.

The proposed ventilation defect cluster algorithm provides a way to identify and quantify differences in regional ventilation heterogeneity a measurement that is similar to LCI, an established global measure of ventilation inhomogeneity made at the mouth.

6.4.2 Free-breathing Pulmonary ^{1}H MRI in Non-small Cell Lung Cancer: Relationships with 4DCT and Noble Gas MRI Measurements of Ventilation

Hyperpolarized ^{3}He MRI has previously been investigated as a way to identify well-functioning lung regions in patients with non-small-cell lung cancer (NSCLC) for functional avoidance targets in radiotherapy.[47] For a number of reasons, the clinical translation of this approach to guide radiotherapy planning has been limited. As an alternative, FDMRI using clinically available MRI systems and pulse sequences provides a non-contrast enhanced method to generate ventilation-weighted maps. Free-breathing ^{1}H MRI exploits Fourier decomposition of MRI signal intensity differences and non-rigid registration to generate ventilation-weighted functional maps.[17] Similarly, 4DCT has been proposed to generate ventilation-weighted maps to serve as functional avoidance maps, and has been implemented in clinical trials (i.e., NCT02528942). Here, our objective was to generate free-breathing ^{1}H MRI ventilation in patients with NSCLC as an alternative way to guide radiation therapy, and compare it to both hyperpolarized ^{3}He MRI and 4DCT ventilation maps.

We have performed preliminary analysis in a small proof-of-concept study in which stage IIIA/IIIB NSCLC patients (n=9, 67±7yr) provided written informed consent to a double-blinded randomized controlled clinical trial (NCT02002052) that aimed to compare outcomes related to MR image-guided versus conventional radiation therapy planning. Hyperpolarized ^{3}He MRI, FDMRI, and 4DCT ventilation maps were generated as previously described,[28,48,49] and semi-automated segmentation was used to generate the VDP for all three imaging methods.[39]

Figure 6-3 shows FDMRI, hyperpolarized ^{3}He MRI and 4DCT ventilation maps for a representative NSCLC patient. There was strong qualitative spatial agreement for ventilation defects in the left lung where the tumour mass has partially stunted the ventilation resulting in a ventilation defect.

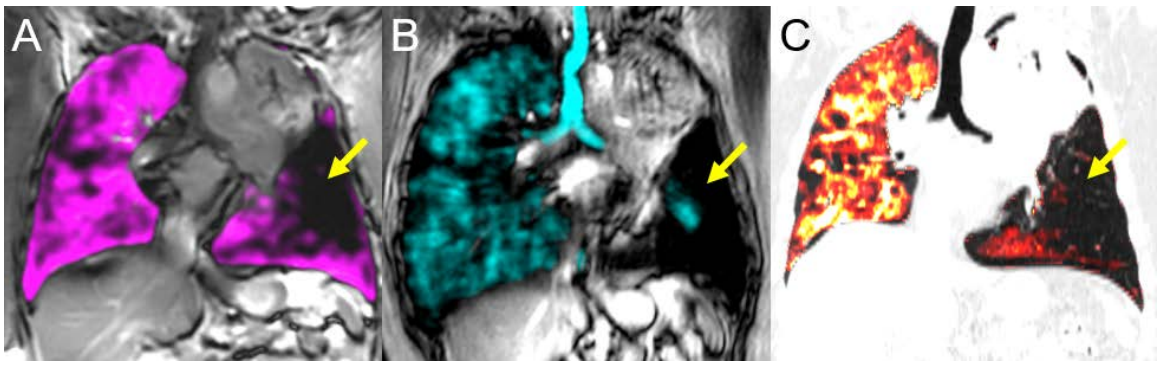

Figure 6-3 MRI and 4DCT ventilations images of a representative patient with stage III non-small-cell lung cancer
For a 74yrs female; pack year=12yrs; FEV_1=61%$_{pred}$; DL_{CO}=54%$_{pred}$; FDMRI VDP=15%; ^{3}He MRI VDP=26%; 4DCT VDP=51%.
A) FDMRI in magenta co-registered to anatomical ^{1}H MRI in gray-scale.
B) Hyperpolarized ^{3}He MRI in blue co-registered to anatomical ^{1}H MRI in gray-scale.
C) 4DCT ventilation in hot co-registered to anatomical CT in gray-scale.
The yellow arrows indicate corresponding regions of ventilation defect visible across all imaging techniques.

Figure 6-4 shows the relationships and agreement for MRI and 4DCT measurements. FDMRI VDP was correlated with ^{3}He MRI VDP (r=.69, p=.04) and 4DCT VDP (r=.73, p=.02), although Bland-Altman analysis indicated that there were biases of -10±8% [-26%, 7%] and -19±8% [-35%, -3%] for ^{3}He and 4DCT, respectively.

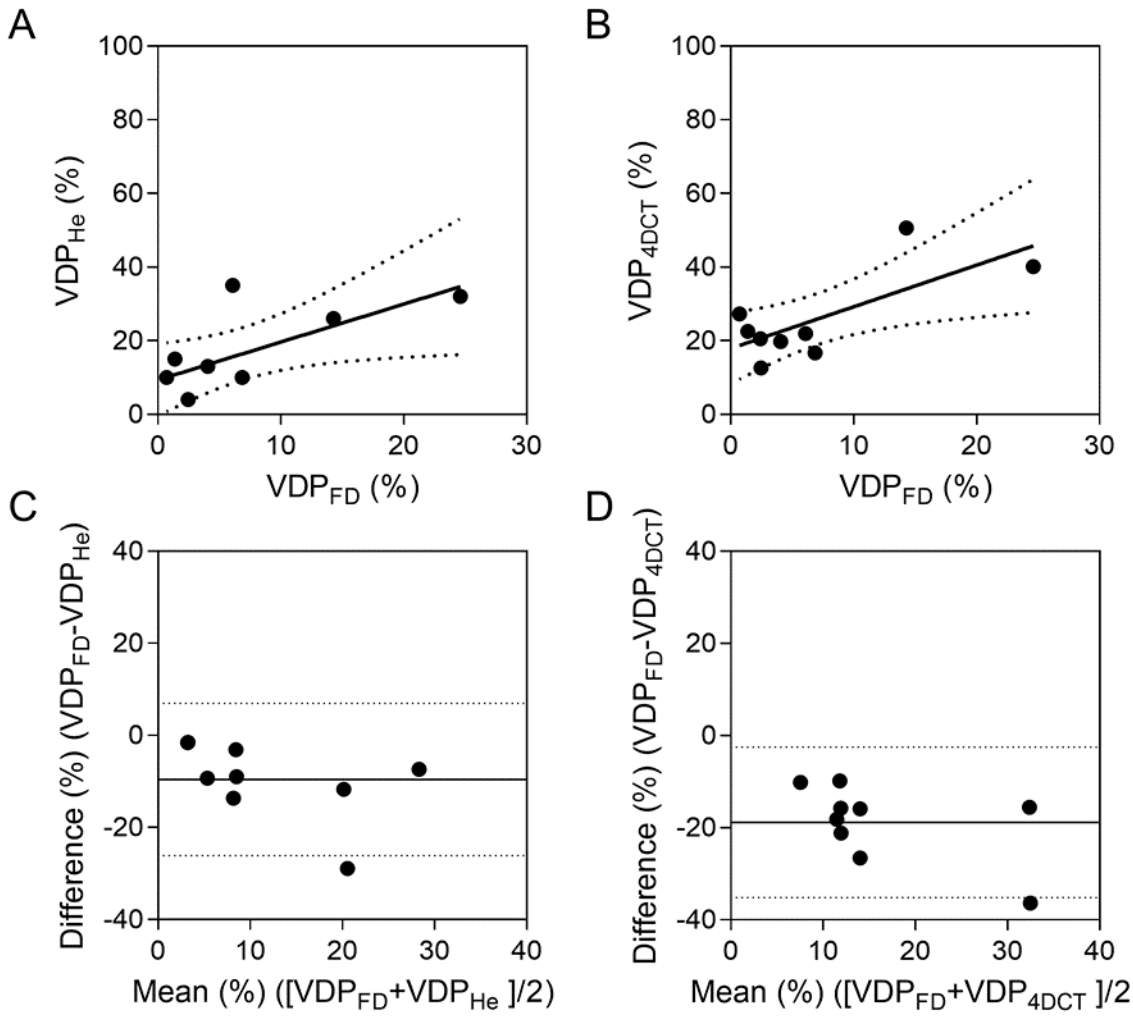

Figure 6-4 Relationships for FDMRI with ^{3}He MRI and 4DCT
A) FDMRI VDP was significantly correlated with ^{3}He MRI VDP (r=.69, p=.04).
B) FDMRI VDP was significantly correlated with 4DCT VDP (r=.73, p=.02).
C) Bland-Altman analysis of agreement for FDMRI VDP with ^{3}He MRI VDP (bias=-10±8%, [-26%, 7%]).
D) Bland-Altman analysis of agreement for FDMRI with 4DCT VDP (bias=-19±8%, [-35%, -3%]).
Dotted lines indicate the 95% confidence intervals.

While FDMRI ventilation imaging is currently limited to only a single slice and is therefore inherently two-dimensional, results showed that regional FDMRI ventilation abnormalities were spatially related to inhaled gas MRI ventilation defects as well as 4DCT-derived ventilation. Importantly, this result suggests that free-breathing pulmonary ^{1}H MRI provides similar functional information compared to hyperpolarized noble-gas MRI and free-breathing CT techniques that are currently implemented in clinical trials for functional

lung avoidance. This may allow for clinical translation of MRI-guided radiotherapy planning since this technique does not require exogenous contrast agents and can be easily implemented using clinically available MRI systems and pulse sequences.

6.4.3 Pulmonary Imaging Platform - Graphical User Interface to Evaluate and Generate Lung Imaging Biomarkers

In all of the studies presented in **Chapters 2-5**, image processing methods were developed and evaluated to generate imaging biomarkers of pulmonary structure and function in asthma and COPD patients. As mentioned in **Section 6.3.2**, the complexity of these image processing methods may limit clinical translation. Accordingly, there is a need for an easy-to-use, standardized, and validated pulmonary image processing and analysis toolbox for broad research use and clinical translation.[50,51] This will be important moving forward since the advancement of pulmonary MRI and CT toward clinical implementations requires large-scale and multi-centre evaluation of clinically-relevant biomarkers.

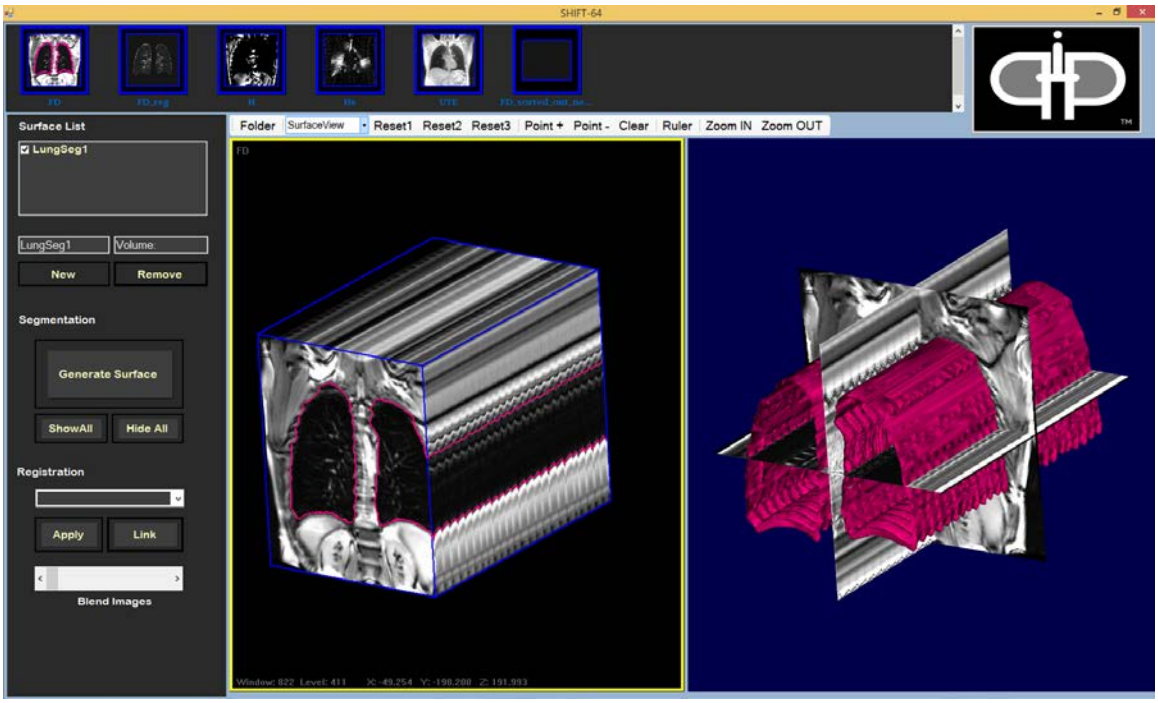

Figure 6-5 Pulmonary Imaging Platform (PIP™) graphical user interface
Image datasets are imported into the software where users will have access to the image processing methods developed to generate the imaging biomarkers of lung structure and function.

As shown in **Figure 6-5**, the Pulmonary Imaging Platform (PIP™) is a graphical user interface (GUI) oriented software with a number of features, including: 1) multi-view three-dimensional volume rendering;[52] 2) surface rendering (using Visualization Toolkit); 3) fiducial placing; 4) image seeding; and, 5) blending/overlapping. The GUI will integrate all of the individual image analysis processes presented in **Chapters 2-5**, including: 1) inspiration-expiration CT parametric response mapping analysis (**Chapter 2**); 2) whole lung and regional noble gas MRI measurements (**Chapters 2-5**); 3) two-dimensional free-breathing ^{1}H MRI ventilation weighted maps (**Chapter 3** and **Chapter 4**); and, 4) three-dimensional free-breathing ^{1}H MRI specific-ventilation measurements (**Chapter 5**). While PIP™ only currently provides a set of commonly used lung imaging biomarkers, the software is flexible and sustainable to be expanded to include currently developing analyses. Once validated, new imaging biomarkers may be easily incorporated to PIP™ and distributed to end users. Future work will involve dissemination of PIP™ to the pulmonary imaging research community to further validate and improve the imaging biomarkers generated from this software.

6.5 Significance and Impact

Unfortunately, hospitalization, mortality rates, and costs associated with lung disease patients continue to rise, and health economists warn that this upward trend will continue and will very soon overwhelm the global healthcare system.[53] In light of this dire situation, new management strategies are urgently required to combat this growing healthcare crisis. For patients with chronic lung disease, pulmonary function tests provide a global measurement of lung function, which are easy to implement and reproducible.[5] As a result, these tests are universally accepted for clinical use and are considered the clinical standard for the diagnosis and evaluation of response to treatment. The limitations of spirometry, including: 1) only providing a global measurement of lung function; 2) the relative insensitivity to early disease stages;[3] and, 3) weakly related to important clinical outcomes,[54,55] has motivated the development of alternative approaches to evaluate pulmonary diseases. Specifically, pulmonary imaging methods, such as MRI and CT, have been proposed to provide objective measurements of regional lung pathologies in asthma

and COPD. Until now, pulmonary MRI has focused on hyperpolarized noble gas MRI, which has yet to be translated clinically and is restricted to a few specialized research centres. To facilitate broad clinical applications of pulmonary imaging techniques, it is urgent to develop new diagnostic approaches for pulmonary medicine using clinically available equipment.

In this thesis, we have developed and evaluated methods of obtaining imaging biomarkers of pulmonary structure and function without the use of exogenous contrast agents or specialized equipment. The work presented here confirms that there are qualitative and quantitative similarities between the non-contrast enhanced methods and those generated from inhaled noble gas MRI in identifying regional lung disease. Armed with this knowledge, there is enormous potential for these imaging methods to be implemented at any imaging centre around the world and be used as intermediate endpoints in clinical trials to evaluate novel therapies and possibly guide treatment. The development and validation of these clinically meaningful non-contrast enhanced pulmonary MR and CT imaging biomarkers will accelerate the translation of pulmonary imaging from “the benchtop to the bedside” where imaging will play an integral part of the clinical workflow for patients with lung disease.

6.6 References

(1) Soriano, J. B. *et al.* Global, regional, and national deaths, prevalence, disability-adjusted life years, and years lived with disability for chronic obstructive pulmonary disease and asthma, 1990-2015: a systematic analysis for the Global Burden of Disease Study 2015. *Lancet Respiratory Medicine* 2017; 5: 691-706.

(2) Louis Theriault, G. H., Danielle Goldfarb, Carole Stonebridge, Fares Bounajm. Cost Risk Analysis for Chronic Lung Disease in Canada. (Ottawa, Canada, 2012).

(3) Vestbo, J. *et al.* Global strategy for the diagnosis, management, and prevention of chronic obstructive pulmonary disease: GOLD executive summary. *Am J Respir Crit Care Med* 2013; 187: 347-365.

(4) Reddel, H. K. *et al.* A summary of the new GINA strategy: a roadmap to asthma control. *Eur Respir J* 2015; 46: 622-639.

(5) Pauwels, R. A. *et al.* Global strategy for the diagnosis, management, and prevention of chronic obstructive pulmonary disease. NHLBI/WHO Global Initiative for Chronic Obstructive Lung Disease (GOLD) Workshop summary. *Am J Respir Crit Care Med* 2001; 163: 1256-1276.

(6) Smith-Bindman, R. *et al.* Use of Diagnostic Imaging Studies and Associated Radiation Exposure for Patients Enrolled in Large Integrated Health Care Systems, 1996-2010. *Jama-Journal of the American Medical Association* 2012; 307: 2400-2409.

(7) de Gonzalez, A. B. *et al.* Projected Cancer Risks From Computed Tomographic Scans Performed in the United States in 2007. *Archives of Internal Medicine* 2009; 169: 2071-2077.

(8) Smith-Bindman, R. *et al.* Radiation Dose Associated With Common Computed Tomography Examinations and the Associated Lifetime Attributable Risk of Cancer. *Archives of Internal Medicine* 2009; 169: 2078-2086.

(9) de Lange, E. E. *et al.* Changes in regional airflow obstruction over time in the lungs of patients with asthma: evaluation with 3He MR imaging. *Radiology* 2009; 250: 567-575.

(10) Mathew, L. *et al.* Hyperpolarized 3He magnetic resonance imaging of chronic obstructive pulmonary disease: reproducibility at 3.0 tesla. *Acad Radiol* 2008; 15: 1298-1311.

(11) Kirby, M. *et al.* Hyperpolarized 3He and 129Xe MR imaging in healthy volunteers and patients with chronic obstructive pulmonary disease. *Radiology* 2012; 265: 600-610.

(12) de Lange, E. E. *et al.* Evaluation of asthma with hyperpolarized helium-3 MRI: correlation with clinical severity and spirometry. *Chest* 2006; 130: 1055-1062.

(13) Fain, S. B. *et al.* Evaluation of structure-function relationships in asthma using multidetector CT and hyperpolarized He-3 MRI. *Academic Radiology* 2008; 15: 753-762.

(14) Svenningsen, S. *et al.* Hyperpolarized (3) He and (129) Xe MRI: differences in asthma before bronchodilation. *J Magn Reson Imaging* 2013; 38: 1521-1530.

(15) Kirby, M. *et al.* Chronic obstructive pulmonary disease: quantification of bronchodilator effects by using hyperpolarized (3)He MR imaging. *Radiology* 2011; 261: 283-292.

(16) Guerrero, T. *et al.* Dynamic ventilation imaging from four-dimensional computed tomography. *Physics in medicine and biology* 2006; 51: 777.

(17) Bauman, G. *et al.* Non-contrast-enhanced perfusion and ventilation assessment of the human lung by means of fourier decomposition in proton MRI. *Magn Reson Med* 2009; 62: 656-664.

(18) Bommart, S. *et al.* Relationship between CT air trapping criteria and lung function in small airway impairment quantification. *BMC Pulm Med* 2014; 14: 29.

(19) Hersh, C. P. *et al.* Paired inspiratory-expiratory chest CT scans to assess for small airways disease in COPD. *Respir Res* 2013; 14: 42.

(20) Kim, E. Y. *et al.* Detailed analysis of the density change on chest CT of COPD using non-rigid registration of inspiration/expiration CT scans. *Eur Radiol* 2015; 25: 541-549.

(21) Lausch, A. *et al.* An augmented parametric response map with consideration of image registration error: towards guidance of locally adaptive radiotherapy. *Phys Med Biol* 2014; 59: 7039-7058.

(22) Mugler, J. P., 3rd & Altes, T. A. Hyperpolarized 129Xe MRI of the human lung. *J Magn Reson Imaging* 2013; 37: 313-331.

(23) Ruiz-Cabello, J., Barnett, B. P., Bottomley, P. A. & Bulte, J. W. Fluorine (19F) MRS and MRI in biomedicine. *NMR Biomed* 2011; 24: 114-129.

(24) Bauman, G. *et al.* Pulmonary functional imaging: qualitative comparison of Fourier decomposition MR imaging with SPECT/CT in porcine lung. *Radiology* 2011; 260: 551-559.

(25) Lederlin, M. *et al.* Functional MRI using Fourier decomposition of lung signal: Reproducibility of ventilation-and perfusion-weighted imaging in healthy volunteers. *European journal of radiology* 2013.

(26) Yu, J., Xue, Y. & Song, H. K. Comparison of lung T2* during free-breathing at 1.5 T and 3.0 T with ultrashort echo time imaging. *Magn Reson Med* 2011; 66: 248-254.

(27) Bauman, G., Pusterla, O. & Bieri, O. Ultra-fast Steady-State Free Precession Pulse Sequence for Fourier Decomposition Pulmonary MRI. *Magn Reson Med* 2016; 75: 1647-1653.

(28) Capaldi, D. P. *et al.* Free-breathing Pulmonary (1)H and Hyperpolarized (3)He MRI: Comparison in COPD and Bronchiectasis. *Acad Radiol* 2015; 22: 320-329.

(29) Hamedani, H. *et al.* Regional Fractional Ventilation by Using Multibreath Wash-in (3)He MR Imaging. *Radiology* 2016; 279: 917-924.

(30) Fletcher, C. & Peto, R. The natural history of chronic airflow obstruction. *Br Med J* 1977; 1: 1645-1648.

(31) Moreno, F. & Lyons, H. A. Effect of Body Posture on Lung Volumes. *Journal of Applied Physiology* 1961; 16: 27-&.

(32) Lumb, A. B. & Nunn, J. F. Respiratory-Function and Ribcage Contribution to Ventilation in Body Positions Commonly Used during Anesthesia. *Anesthesia and Analgesia* 1991; 73: 422-426.

(33) Middleton, H. *et al.* MR imaging with hyperpolarized 3He gas. *Magn Reson Med* 1995; 33: 271-275.

(34) Guerrero, T. *et al.* Quantification of regional ventilation from treatment planning CT. *Int J Radiat Oncol Biol Phys* 2005; 62: 630-634.

(35) Mutaf, Y. D., Antolak, J. A. & Brinkmann, D. H. The impact of temporal inaccuracies on 4DCT image quality. *Med Phys* 2007; 34: 1615-1622.

(36) Pollock, S., Kipritidis, J., Lee, D., Bernatowicz, K. & Keall, P. The impact of breathing guidance and prospective gating during thoracic 4DCT imaging: an XCAT study utilizing lung cancer patient motion. *Phys Med Biol* 2016; 61: 6485-6501.

(37) Ma, W. *et al.* Ultra-short echo-time pulmonary MRI: evaluation and reproducibility in COPD subjects with and without bronchiectasis. *J Magn Reson Imaging* 2015; 41: 1465-1474.

(38) Wegener, O. H., Koeppe, P. & Oeser, H. Measurement of lung density by computed tomography. *J Comput Assist Tomogr* 1978; 2: 263-273.

(39) Kirby, M. *et al.* Hyperpolarized 3He magnetic resonance functional imaging semiautomated segmentation. *Acad Radiol* 2012; 19: 141-152.

(40) Muller, N. L., Staples, C. A., Miller, R. R. & Abboud, R. T. "Density mask". An objective method to quantitate emphysema using computed tomography. *Chest* 1988; 94: 782-787.

(41) Coxson, H. O. *et al.* A quantification of the lung surface area in emphysema using computed tomography. *Am J Respir Crit Care Med* 1999; 159: 851-856.

(42) Owrangi, A. M., Etemad-Rezai, R., McCormack, D. G., Cunningham, I. A. & Parraga, G. Computed tomography density histogram analysis to evaluate pulmonary emphysema in ex-smokers. *Acad Radiol* 2013; 20: 537-545.

(43) Zha, N. *et al.* Principal Component Analysis of the CT Density Histogram to Generate Parametric Response Maps of COPD. *Medical Imaging 2015: Biomedical Applications in Molecular, Structural, and Functional Imaging* 2015; 9417.

(44) Shea, D. A. & Morgan, D.

(45) Prisk, G. K. & Sa, R. C. It's about numbers, not pictures. *J Appl Physiol (1985)* 2014; 116: 127-128.

(46) Wang, J. Packing of unequal spheres and automated radiosurgical treatment planning. *Journal of Combinatorial Optimization* 1999; 3: 453-463.

(47) Hoover, D. A. *et al.* Functional lung avoidance for individualized radiotherapy (FLAIR): study protocol for a randomized, double-blind clinical trial. *BMC Cancer* 2014; 14: 934.

(48) Sheikh, K. *et al.* Magnetic resonance imaging biomarkers of chronic obstructive pulmonary disease prior to radiation therapy for non-small cell lung cancer. *Eur J Radiol Open* 2015; 2: 81-89.

(49) Castillo, R., Castillo, E., Martinez, J. & Guerrero, T. Ventilation from four-dimensional computed tomography: density versus Jacobian methods. *Physics in medicine and biology* 2010; 55: 4661.

(50) Hoffman, E. A., Lynch, D. A., Barr, R. G., van Beek, E. J. & Parraga, G. Pulmonary CT and MRI phenotypes that help explain chronic pulmonary obstruction disease pathophysiology and outcomes. *Journal of Magnetic Resonance Imaging* 2016; 43: 544-557.

(51) Capaldi, D. P., Eddy, R. L. & Parraga, G. Pulmonary MRI in Clinical Trials. 2016.

(52) Fenster, A., Dunne, S. & Larsen, J. T. (Google Patents, 1998).

(53) Khakban, A. *et al.* Ten-Year Trends in Direct Costs of COPD: A Population-Based Study. *Chest* 2015; 148: 640-646.

(54) Jones, P. W. Health status and the spiral of decline. *COPD* 2009; 6: 59-63.

(55) Agusti, A. *et al.* Characterisation of COPD heterogeneity in the ECLIPSE cohort. *Respir Res* 2010; 11: 122.

APPENDIX

Appendix A – Permission for Reproduction of Scientific Articles

Dear Dante Capaldi:

The Radiological Society of North America (RSNA®) is pleased to grant you permission to reproduce the following article in print, electronic, and web formats for educational, non-profit use in your dissertation/thesis, provided you give full credit to the authors of the original publication.

> Capaldi D P.I., Zha N, Guo F, et al. Pulmonary imaging biomarkers of gas trapping and emphysema in COPD: ^{3}He MR imaging and CT parametric response. *Radiology* 2016;279:597-608.

This permission is a one-time, non-exclusive grant for English-language use and is exclusively limited to the usage stated and underlined above. The requestor guarantees to reproduce the material as originally published. Permission is granted under the condition that a full credit line is prominently placed (i.e. author name(s), journal name, copyright year, volume #, inclusive pages and copyright holder).

This permission becomes effective upon receipt of this signed contract. Please sign a copy of this agreement, return a signed copy to me and retain a copy for your files. Thank you for your interest in our publication.

Appendix B – Health Science Research Ethics Board Approval Notices

Western Research

Research Ethics

Western University Health Science Research Ethics Board
HSREB Annual Continuing Ethics Approval Notice

Date: August 16, 2017
Principal Investigator: Dr. Grace Parraga
Department & Institution: Schulich School of Medicine and Dentistry\Imaging,Robarts Research Institute

Review Type: Full Board
HSREB File Number: 2970
Study Title: Development of 3 Tesla MRI Hardware and Software for 3He gas imaging of the Lung: Healthy Volunteer Development Study (REB #11750)
Sponsor: Internal Research fund UWO

HSREB Renewal Due Date & HSREB Expiry Date:
Renewal Due -2018/08/31
Expiry Date -2018/09/13

The Western University Health Science Research Ethics Board (HSREB) has reviewed the Continuing Ethics Review (CER) Form and is re-issuing approval for the above noted study.

The Western University HSREB operates in compliance with the Tri-Council Policy Statement Ethical Conduct for Research Involving Humans (TCPS2), the International Conference on Harmonization of Technical Requirements for Registration of Pharmaceuticals for Human Use Guideline for Good Clinical Practice (ICH E6 R1), the Ontario Freedom of Information and Protection of Privacy Act (FIPPA, 1990), the Ontario Personal Health Information Protection Act (PHIPA, 2004), Part 4 of the Natural Health Product Regulations, Health Canada Medical Device Regulations and Part C, Division 5, of the Food and Drug Regulations of Health Canada.

Members of the HSREB who are named as Investigators in research studies do not participate in discussions related to, nor vote on such studies when they are presented to the REB.

Western Research

Research Ethics

Western University Health Science Research Ethics Board
HSREB Amendment Approval Notice

Principal Investigator: Dr. Grace Parraga
Department & Institution: Schulich School of Medicine and Dentistry\Imaging,Robarts Research Institute

Review Type: Full Board
HSREB File Number: 6014
Study Title: Longitudinal Study of Helium-3 Magnetic Resonance Imaging of COPD (REB #15930)
Sponsor: UWO Internal Research Fund

HSREB Amendment Approval Date: June 07, 2017
HSREB Expiry Date: February 10, 2018

Documents Approved and/or Received for Information:

Document Name	Comments	Version Date
Revised Western University Protocol		2017/05/02
Letter of Information & Consent		2017/05/02

The Western University Health Science Research Ethics Board (HSREB) has reviewed and approved the amendment to the above named study, as of the HSREB Initial Approval Date noted above.

HSREB approval for this study remains valid until the HSREB Expiry Date noted above, conditional to timely submission and acceptance of HSREB Continuing Ethics Review.

The Western University HSREB operates in compliance with the Tri-Council Policy Statement Ethical Conduct for Research Involving Humans (TCPS2), the International Conference on Harmonization of Technical Requirements for Registration of Pharmaceuticals for Human Use Guideline for Good Clinical Practice Practices (ICH E6 R1), the Ontario Personal Health Information Protection Act (PHIPA, 2004), Part 4 of the Natural Health Product Regulations, Health Canada Medical Device Regulations and Part C, Division 5, of the Food and Drug Regulations of Health Canada.

Members of the HSREB who are named as Investigators in research studies do not participate in discussions related to, nor vote on such studies when they are presented to the REB.

Western Research

Western University Health Science Research Ethics Board
HSREB Amendment Approval Notice

Principal Investigator: Dr. Grace Parraga
Department & Institution: Schulich School of Medicine and Dentistry\Imaging, Robarts Research Institute

Review Type: Full Board
HSREB File Number: 103516
Study Title: Structure and Function MRI of Asthma

HSREB Amendment Approval Date: May 19, 2017
HSREB Expiry Date: February 19, 2018

Documents Approved and/or Received for Information:

Document Name	Comments	Version Date
Other	Attestation Form	2017/05/04
Increase in number of local Participants	PDF Protocol ROB0037	2017/05/04
Revised Letter of Information & Consent	Clean Copy	2017/05/19
Revised Western University Protocol	Clean Copy	2017/05/19

The Western University Health Science Research Ethics Board (HSREB) has reviewed and approved the amendment to the above named study, as of the HSREB Initial Approval Date noted above.

HSREB approval for this study remains valid until the HSREB Expiry Date noted above, conditional to timely submission and acceptance of HSREB Continuing Ethics Review.

The Western University HSREB operates in compliance with the Tri-Council Policy Statement Ethical Conduct for Research Involving Humans (TCPS2), the International Conference on Harmonization of Technical Requirements for Registration of Pharmaceuticals for Human Use Guideline for Good Clinical Practice Practices (ICH E6 R1), the Ontario Personal Health Information Protection Act (PHIPA, 2004), Part 4 of the Natural Health Product Regulations, Health Canada Medical Device Regulations and Part C, Division 5, of the Food and Drug Regulations of Health Canada.

Members of the HSREB who are named as Investigators in research studies do not participate in discussions related to, nor vote on such studies when they are presented to the REB.

Western Research

Research Ethics

Use of Human Participants - Ethics Approval Notice

Principal Investigator: Dr. Grace Parraga
File Number:103969
Review Level: Full Board
Approved Local Adult Participants:30
Approved Local Minor Participants:0
Protocol Title: Evaluation of Oscillatory Positive Expiratory Pressure (oPEP) in Bronchiectasis and COPD
Department & Institution: Schulich School of Medicine and Dentistry\Imaging,Robarts Research Institute
Sponsor:
Ethics Approval Date: July 30, 2013
Ethics Expiry Date: September 30, 2014

Documents Reviewed & Approved & Documents Received for Information:

Document Name	Comments	Version Date
Protocol	Robarts Protocol - Received for information	2013/06/12
Other	Instructions for Aerobika device	
Response to Board Recommendations	Response to Board Recommendations	2013/07/10
Health Canada Correspondence	Health Canada MDL	
Letter of Information & Consent	Letter of Information V2 Clean	2013/07/10
Instruments	Study Diary,Patient Evaluation Questionnaire, St. George's Respiratory Questionnaire and BORG Scale	
Western University Protocol		

This is to notify you that the University of Western Ontario Health Sciences Research Ethics Board (HSREB) which is organized and operates according to the Tri-Council Policy Statement: Ethical Conduct of Research Involving Humans and the Health Canada/ICH Good Clinical Practice Practices: Consolidated Guidelines; and the applicable laws and regulations of Ontario has reviewed and granted approval to the above referenced study on the approval date noted above. The membership of this HSREB also complies with the membership requirements for REB's as defined in Division 5 of the Food and Drug Regulations.

The ethics approval for this study shall remain valid until the expiry date noted above assuming timely and acceptable responses to the HSREB's periodic requests for surveillance and monitoring information. If you require an updated approval notice prior to that time you must request it using the University of Western Ontario Updated Approval Request form.

Member of the HSREB that are named as investigators in research studies, or declare a conflict of interest, do not participate in discussions related to, nor vote on, such studies when they are presented to the HSREB.

Western Research

Research Ethics

Western University Health Science Research Ethics Board
HSREB Amendment Approval Notice

Principal Investigator: Dr. Grace Parraga
Department & Institution: Schulich School of Medicine and Dentistry\Imaging, Robarts Research Institute

Review Type: Full Board
HSREB File Number: 104200
Study Title: Hyperpolarized Magnetic Resonance Imaging in Asthma Pre- and Post-Bronchial Thermoplasty
Sponsor: Lawson Health Research Institute

HSREB Amendment Approval Date: June 26, 2017
HSREB Expiry Date: September 03, 2017

Documents Approved and/or Received for Information:

Document Name	Comments	Version Date
Revised Western University Protocol		2017/06/26
Revised Letter of Information & Consent		2017/06/05
Other	Site Protocol Version 5	2017/06/08

The Western University Health Science Research Ethics Board (HSREB) has reviewed and approved the amendment to the above named study, as of the HSREB Initial Approval Date noted above.

HSREB approval for this study remains valid until the HSREB Expiry Date noted above, conditional to timely submission and acceptance of HSREB Continuing Ethics Review.

The Western University HSREB operates in compliance with the Tri-Council Policy Statement Ethical Conduct for Research Involving Humans (TCPS2), the International Conference on Harmonization of Technical Requirements for Registration of Pharmaceuticals for Human Use Guideline for Good Clinical Practice Practices (ICH E6 R1), the Ontario Personal Health Information Protection Act (PHIPA, 2004), Part 4 of the Natural Health Product Regulations, Health Canada Medical Device Regulations and Part C, Division 5, of the Food and Drug Regulations of Health Canada.

Members of the HSREB who are named as Investigators in research studies do not participate in discussions related to, nor vote on such studies when they are presented to the REB.

Western Research

Research Ethics

Western University Health Science Research Ethics Board
HSREB Annual Continuing Ethics Approval Notice

Date: January 13, 2017
Principal Investigator: Dr. Brian Yaremko
Department & Institution: Schulich School of Medicine and Dentistry\Oncology,London Health Sciences Centre

Review Type: Full Board
HSREB File Number: 104834
Study Title: Functional Lung Avoidance for Individualized Radiotherapy (FLAIR): A Randomized, Double-Blind Clinical Trial
Sponsor: Ontario Institute for Cancer Research

HSREB Renewal Due Date & HSREB Expiry Date:
Renewal Due -2018/01/31
Expiry Date -2018/02/11

The Western University Health Science Research Ethics Board (HSREB) has reviewed the Continuing Ethics Review (CER) Form and is re-issuing approval for the above noted study.

The Western University HSREB operates in compliance with the Tri-Council Policy Statement Ethical Conduct for Research Involving Humans (TCPS2), the International Conference on Harmonization of Technical Requirements for Registration of Pharmaceuticals for Human Use Guideline for Good Clinical Practice (ICH E6 R1), the Ontario Freedom of Information and Protection of Privacy Act (FIPPA, 1990), the Ontario Personal Health Information Protection Act (PHIPA, 2004), Part 4 of the Natural Health Product Regulations, Health Canada Medical Device Regulations and Part C, Division 5, of the Food and Drug Regulations of Health Canada.

Members of the HSREB who are named as Investigators in research studies do not participate in discussions related to, nor vote on such studies when they are presented to the REB.

Appendix C – Curriculum Vitae

EDUCATION

2013-2018 Doctor of Philosophy in Medical Biophysics (Candidate)
Department of Medical Biophysics
The University of Western Ontario, London, Canada
Supervisor: Dr. Grace Parraga
Thesis: Imaging Biomarkers of Pulmonary Structure and Function

2013-2018 Master of Science in Clinical Physics (Candidate)
CAMPEP accredited
Department of Medical Biophysics
The University of Western Ontario, London, Canada
Supervisor: Dr. Grace Parraga

2009-2013 Bachelor of Science
Honours Physics [Medical Physics] with Thesis Co-op
Minor in Mathematics
Department of Physics
University of Windsor, Windsor, Canada
Supervisor: Dr. Roman G. Maev
Thesis: Finite Element Analysis of Percussion Models: Modeling Different Complex Structures to Determine Acoustical Properties

POSITIONS

2017 **Robarts Research Institute**
Research Assistant
The University of Western Ontario, London, Canada
Supervisor: Dr. Grace Parraga
Project: Maintenance and Management of Polarization Facility

2016 **London Regional Cancer Program**
Quality Assurance Internship
London Health Science Centre, London, Canada
Supervisor: Dr. Jerry Battista
Project: Performing Weekly, Bi-Weekly, and Monthly Quality Assurance on the Linear Accelerators at Victoria Hospital

2016 **Robarts Research Institute**
Research Assistant
The University of Western Ontario, London, Canada
Supervisor: Dr. Grace Parraga
Project: Maintenance and Management of Polarization Facility

2014 **London Regional Cancer Program**
Quality Assurance Internship
London Health Science Centre, London, Canada
Supervisor: Dr. Jerry Battista
Project: Performing Weekly, Bi-Weekly, and Monthly Quality Assurance on the Linear Accelerators at Victoria Hospital

2012-2013 **Institute for Diagnostic Imaging Research**
Outstanding Scholar
Department of Physics, University of Windsor
Supervisor: Dr. Roman G. Maev
Project: Portable Pulmonary Injury Diagnostic Device Testing and Development

2012 **BC Cancer Agency**
Coop Student
Department of Medical Physics
Supervisor: Dr. Parminder Basran
Project: Automate the Analysis of a High Precision Image Quality Phantom Manufactured for CT Imaging

Institute for Diagnostic Imaging Research
Researcher
Department of Physics, University of Windsor
Supervisor: Dr. Roman G. Maev
Project: Finite Element Analysis of Percussion Models: Modeling Different Complex Structures to Determine Acoustical Properties

Institute for Diagnostic Imaging Research
Coop Student
Department of Physics, University of Windsor
Supervisor: Dr. Roman G. Maev
Project: Investigating Experimental Approaches to Determine Attributes of the Portable Pulmonary Injury Diagnostic Device (PPIDD)

2011 **Institute for Diagnostic Imaging Research**
Coop Student
Department of Physics, University of Windsor
Supervisor: Dr. Roman G. Maev
Project: Developing Input Method Editors for Medical Devices

2010 **University of Windsor**
Student Developer
Department of Physics, University of Windsor
Supervisor: Dr. Roman G. Maev

Project: Chest Percussion Devices: Designing, Manufacturing & Testing Prototypes

HONOURS AND AWARDS

2018-2020 **Postdoctoral Fellowship (PDF)**
Natural Science and Engineering Research Council of Canada (NSERC)
Awarded to highly qualified Canadians with leading edge scientific and research skills for Canadian industry, government and universities
National ($90,000)

2017 **Radiological Society of North America (RSNA) Trainee Research Prize**
Radiological Society of North America Annual Scientific Meeting 2017
Awarded to honor the most outstanding scientific contribution submitted and accepted to the RSNA international meeting for presentation
International (USD $1,000)

2017-2018 **Doctoral Excellence Research Awards**
Schulich School of Medicine and Dentistry, Western University
Recognized for having a tri-agency doctoral scholarship (NSERC)
Institutional ($5,000)

2017-2018 **Western Graduate Research Scholarship**
Department of Medical Biophysics, Western University
Awarded to a full time graduate student for stipend support who has maintained an average of 80% or more
Institutional ($7,600)

2017 **Nellie Farthing Fellowship in the Medical Sciences**
Schulich School of Medicine and Dentistry, Western University
Established in 1960 with money bequeathed by Nellie Farthing to Western University to create a Fellowship for full-time doctoral students in the Medical Sciences that recognized and rewarded excellence in research
Institutional ($3,000)

2017 **Alfred Jay Award for Translational Research**
Department of Medical Biophysics, Western University
Awarded annually to a graduate student demonstrating innovation in the development of a clinical diagnostic or therapeutic procedure during their studies
Institutional ($2,000)

2017 **1st Place - Best Oral Presentation Award**
Imaging Network of Ontario Meeting

Recognized for having the top oral presentation out of all participates at the annual meeting
National ($350)

2017 **Best Scientific Exhibition Award**
International Workshop on Pulmonary Functional Imaging Meeting
Selected as one of ten awardees of IWPFI 2017 for the best scientific exhibition works
International

2016-2017 **Western Graduate Research Scholarship**
Department of Medical Biophysics, Western University
Awarded to a full time graduate student for stipend support who has maintained an average of 80% or more
Institutional ($7,600)

2016-2017 **Doctoral Excellence Research Awards**
Schulich School of Medicine and Dentistry, Western University
Recognized for having a tri-agency doctoral scholarship (NSERC)
Institutional ($5,000)

2016 **Canadian Student Health Research Forum Funding Competition**
Canadian Institutes of Health Research (CIHR)
Selected by CIHR to receive funding to reimburse travel and accommodations for
participation in the 2014 Canadian Student Health Research Forum
National ($1,000)

2016 **Publication of the Month**
Schulich School of Medicine and Dentistry, Western University
Recognized for having the top publication at the Schulich School of Medicine and Dentistry for the month of April 2016
Institutional

2016 **Drs. Madge and Charles Macklin Fellowship for Publication Nominee**
Schulich School of Medicine and Dentistry, Western University
Selected by the Department of Medical Biophysics to compete for an award based on the significance of the candidate's 1st author publication in a high impact peer reviewed journal
Institutional

2016 **Canadian Student Health Research Forum National Student Research Poster Competition Participant**
Canadian Institutes of Health Research (CIHR)
Nominated by the University of Western Ontario as being within the top 5% of doctoral students in the field of health sciences

National

2016 **1st Place - The Lucille & Norton Wolf Trainee Publication Award**
London Health Research Day 2016
Awarded to the top peer-reviewed publication from a trainee or medical residents and fellows of the Schulich School of Medicine & Dentistry working in labs across Schulich Medicine & Dentistry
Regional ($2,000)

2016 **Trainee (Educational) Stipend**
International Society for Magnetic Resonance in Medicine Annual Meeting
Awarded to support the attendance of students, postdoctoral and clinical trainees to present abstracts at the international scientific meeting held in Singapore, Singapore
International (USD $475)

2015-2016 **Western Graduate Research Scholarship**
Department of Medical Biophysics, Western University
Awarded to a full time graduate student for stipend support who has maintained an average of 80% or more
Institutional ($7,600)

2015 **Magna Cum Laude Merit Award**
International Society for Magnetic Resonance in Medicine Annual Meeting
Awarded to those whose abstract score was in the top 15% of those submitted for review to be presented at the annual international meeting
International

2015 **The Queen Elizabeth II Graduate Scholarship in Science and Technology**
Ontario Graduate Scholarship (OGS)
A merit based scholarship (based on academic standing) that encourages excellence in graduate studies and is available to students in all disciplines of academic study
Provincial ($15,000) *declined*

2015-2018 **Postgraduate Scholarship – Doctoral (PGSD3)**
Natural Science and Engineering Research Council of Canada (NSERC)
Awarded to high-calibre students who are engaged in doctoral programs in the natural sciences or engineering
National ($63,000)

2015 **Top 80 Posters: Judges' Selection**
London Health Research Day 2015
Awarded to those whose abstract score was in the top 80 abstracts submitted

Regional

2015 **Trainee (Educational) Stipend**
International Society for Magnetic Resonance in Medicine Annual Meeting
Awarded to support the attendance of students, postdoctoral and clinical trainees to present abstracts at the international scientific meeting held in Toronto, Canada
International (USD $360)

2014-2015 **Western Graduate Research Scholarship**
Department of Medical Biophysics, Western University
Awarded to a full time graduate student for stipend support who has maintained an average of 80% or more
Institutional ($7,800)

2014 **Radiological Society of North America Trainee Research Prize Finalist**
Radiological Society of North America Annual Scientific Meeting 2014
Awarded to one of the highest ranked abstracts submitted for the Trainee Research Prize
International

2014 **Trainee (Educational) Stipend**
International Society for Magnetic Resonance in Medicine Annual Meeting
Awarded to support the attendance of students, postdoctoral and clinical trainees to present abstracts at the international scientific meeting held in Milan, Italy
International (USD $540)

2013-2014 **Western Graduate Research Scholarship**
Department of Medical Biophysics, Western University
Awarded to a full time graduate student for stipend support who has maintained an average of 80% or more
Institutional ($7,800)

2012-2013 **University of Windsor Outstanding Scholars Award in Physics**
Department of Physics, University of Windsor
Awarded to students with exceptional cumulative averages who are enrolled in Physics
Institutional ($4,000)

2009 **University of Windsor Entrance Scholarship**
University of Windsor
Awarded to students with exceptional high school entrance averages
Institutional ($1,250)

2009 **University of Windsor Outstanding Scholars Award in Physics**

Department of Physics, University of Windsor
Awarded to students with exceptional cumulative averages who are enrolled in Physics
Institutional ($2,000)

ACADEMIC RESPONSIBILITIES

2017 **Graduate Research Assistant (3 term contract)**
Maintenance and Management of Polarization Facility
Robarts Research Institute, Western University

2016 **Graduate Research Assistant (1 term contract)**
Physics Quality Assurance Radiation therapy infrastructure
London Regional Cancer Centre and Department of Oncology
Western University

Graduate Research Assistant (3 term contract)
Maintenance and Management of Polarization Facility
Robarts Research Institute, Western University

Cancer Program Clinical Observership (1 term)
Shadowed Radiation Oncologists in Clinic
London Regional Cancer Centre and Department of Oncology
Western University

Medical Resident Research Trainee Supervision
Resident (PGY-2 Internal Medicine): Colin J. Adams, MD
Project: A comparison of MRI and CT for targeting areas for lung volume reduction procedures
Abstract: MRI Stratification of COPD Patients for Bronchoscopic Lung Volume Reduction: A Cautionary Note
Manuscript: On the potential role of MRI Biomarkers of COPD to Guide Bronchoscopic Lung Volume Reduction

Undergraduate Research Project Mentoring
Robert DiCesare (3rd year UG BMSc, Western University)
Project: MRI ventilation used for targeting areas for lung volume reduction procedures
Ryan Yip (3rd year UG BMSc, Western University - 6 week rotation project)
Project: Reproducibility of ^{3}He MRI segmentation
Matthew Schweers (1st year UG BSc, Western University)
Project: Database management and clerical duties

2015 **Undergraduate Research Project Mentoring**
Robert DiCesare (2nd year UG BMSc, Western University)

Project: Reproducibility of ^{3}He MRI segmentation
Nanxi Zha BEng (2nd year MD, Schulich Research Opportunities Funded Project, Western University)
Project: Second order texture analysis of noble gas MRI
Manuscript: Second-Order Texture Measurements of ^{3}He Ventilation MRI: Proof of Concept Evaluation of Asthma Bronchodilator Response

2014 **Graduate Research Assistant (1 term contract)**
Physics Quality Assurance Radiation therapy infrastructure
London Regional Cancer Centre and Department of Oncology
Western University

Undergraduate Research Project Mentoring
Nanxi Zha BEng (1st year MD, Schulich Research Opportunities Funded Project, Western University)
Project: Parametric response mapping of co-registered inspiratory/expiratory CT
Conference Paper: Principal component analysis of the CT density histogram to generate parametric response maps of COPD

2013 **Introductory Physics II (University of Windsor: 03-64-141)**
Proctored Exams and Laboratory Instructor (3 Labs)

Introduction to Astronomy II (University of Windsor: 03-64-191)
Proctored Exams

2012 **Introductory Physics II (University of Windsor: 03-64-141)**
Proctored Exams and Laboratory Instructor (1 Lab)

Theoretical Methods (University of Windsor: 03-64-151)
Proctored Exams and Marked Assignments

PUBLICATIONS AND PRESENTATIONS

Peer-Reviewed Journal Manuscripts (17 published/in-press)

Published and In-Press **(17 total; 8 first author)**

1. **D.P.I. Capaldi**, R.L. Eddy, S. Svenningsen, F. Guo, J.S.H. Baxter, A.J. McLeod, P. Nair, D.G. McCormack, G. Parraga. Free-breathing Pulmonary MR Imaging to Quantify Regional Specific-Ventilation. *Radiology*. February 22, 2018. doi.org/10.1148/radiol.2018171993

2. C.J. Adams*, **D.P.I. Capaldi***, R. Di Cesare, D.G. McCormack, G. Parraga, CRRN Investigators. On the potential role of MRI Biomarkers of COPD to Guide

Bronchoscopic Lung Volume Reduction. *Academic Radiology*. October 2017. doi.org/10.1016/j.acra.2017.08.010 (* Co-first Author)

3. **D.P.I. Capaldi**, G. Parraga. Through the Looking Glass and What was Found There: More Imaging Biomarkers of COPD. *American Journal of Respiratory and Critical Care Medicine*. August 2017. doi.org/10.1164/rccm.201707-1473ED

4. **D.P.I. Capaldi**, K. Sheikh, R.L. Eddy, F. Guo, S. Svenningsen, P. Nair, D.G. McCormack, G. Parraga. Free-breathing Pulmonary MRI Ventilation Response to Bronchodilator and Provocation in Severe Asthma. *Academic Radiology*. May 2017. dx.doi.org/10.1016/j.acra.2017.04.012

5. F. Guo, S. Svenningsen, M. Kirby, **D.P.I. Capaldi**, K. Sheikh, A. Fenster, G. Parraga. Thoracic CT-MRI Co-Registration for Regional Pulmonary Structure-Function Measurements of Obstructive Lung Disease. *Medical Physics*. February 2017. doi.org/10.1002/mp.12160. ***This manuscript was featured on the cover of the journal (May 2017)***

6. A. Dasgupta, M. Kjarsgaard, **D.P.I. Capaldi**, K. Radford, F. Aleman, C. Boylan, L.C. Altman, T. Wight, G. Parraga, P.M. O'Byrne, P. Nair. A pilot randomized clinical trial of mepolizumab in COPD with eosinophilic bronchitis. *European Respiratory Journal*. March 2017. doi.org/10.1183/13993003.02486-2016

7. K. Sheikh, F. Guo, **D.P.I Capaldi**, A. Ouriadov, R.L. Eddy, S. Svenningsen, G. Parraga, CRRN Investigators. Ultra-short Echo Time Magnetic Resonance Imaging Biomarkers of Asthma. *Journal of Magnetic Resonance Imaging*. October 2016. doi.org/10.1002/jmri.25503

8. F. Guo, S. Svenningsen, R.L. Eddy, **D.P.I. Capaldi**, K. Sheikh, A. Fenster, G. Parraga. Anatomical Pulmonary MRI Multi-Region Segmentation using a Convex Optimization-Based Approach and Volume Proportion Prior. *Medical Physics*. May 2016. doi.org/10.1118/1.4948999

9. **D.P.I. Capaldi**, F. Guo, G. Parraga. Imaging How and Where We Breathe Oxygen: Another Big Short? *Journal of Thoracic Disease*. March 2016. doi.org/10.21037/jtd.2016.01.83

10. N. Zha, D. Pike, S. Svenningsen, **D.P.I. Capaldi**, D.G. McCormack, G. Parraga. Second-Order Texture Measurements of ^{3}He Ventilation MRI: Proof of Concept Evaluation of Asthma Bronchodilator Response. *Academic Radiology*. February 2016. doi.org/10.1016/j.acra.2015.10.010

11. **D.P.I. Capaldi**, N. Zha, F. Guo, D. Pike, D.G. McCormack, M. Kirby, G. Parraga. Pulmonary Imaging Biomarkers of Gas Trapping and Emphysema in COPD: ^{3}He MR Imaging and CT Parametric Response Maps. *Radiology*. January 2016.

doi.org/10.1148/radiol.2015151484. ***This manuscript was featured on the cover of the journal (May 2016)***

12. D. Pike, M. Kirby, R.L. Eddy, F. Guo, **D.P.I. Capaldi**, A. Ouriadov, D.G. McCormack, G. Parraga. Regional Heterogeneity of Chronic Obstructive Pulmonary Disease Phenotypes: Pulmonary ^{3}He Magnetic Resonance Imaging and Computed Tomography. *Journal of Chronic Obstructive Pulmonary Disease.* January 2016. doi.org/10.3109/15412555.2015.1123682

13. K. Sheikh*, **D.P.I. Capaldi***, D.A. Hoover, G. Parraga, D.A. Palma, B.P. Yaremko. Magnetic resonance imaging biomarkers of chronic obstructive pulmonary disease prior to radiation therapy for non-small cell lung cancer. *European Journal of Radiology Open*. December 2015. doi.org/10.1016/j.ejro.2015.05.003 (* Co-first Author)

14. F. Guo, J. Yuan, M. Rajchl, S. Svenningsen, **D.P.I. Capaldi**, K. Sheikh, A. Fenster, G. Parraga. Globally Optimal Joint Segmentation of Three-dimensional Pulmonary ^{1}H and Hyperpolarized ^{3}He MRI with Spatial Consistence Prior. *Medical Image Analysis*. July 2015. doi.org/10.1016/j.media.2015.04.001

15. **D.P.I. Capaldi**, K. Sheikh, F. Guo, S. Svenningsen, R. Etemad-Rezai, H.O. Coxson, J. Leipsic, D.G. McCormack, G. Parraga. Free-breathing Pulmonary ^{1}H and Hyperpolarized ^{3}He MRI: Comparison in COPD and Bronchiectasis. *Academic Radiology*. March 2015. doi.org/10.1016/j.acra.2014.10.003

16. M. Bhuiyan, E.V. Malyarenko, M.A. Pantea, **D.P.I. Capaldi**, A.E. Baylor, R.G. Maev. Time-Frequency Analysis of Clinical Percussion Signals using Matrix Pencil Method. *Journal of Electrical and Computer Engineering*. January 2015. doi.org/10.1155/2015/274541

17. D.A. Hoover, **D.P.I. Capaldi**, K. Sheikh, D.A. Palma, G.B. Rodrigues, R. Dar, E. Yu, B. Dingle, M. Landis, W. Kocha, M. Sanatani, M. Vincent, J. Younus, S. Gaede, G. Parraga, B.P. Yaremko. Functional lung avoidance for individualized radiotherapy (FLAIR): Study protocol for a randomized, double-blind clinical trial. *BMC Cancer*. December 2014. doi.org/10.1186/1471-2407-14-934

Under Review **(1 total)**

1. F. Guo, **D.P.I. Capaldi**, M. Kirby, K. Sheikh, S. Svenningsen, D.G. McCormack, A. Fenster, G. Parraga. Pulmonary Imaging Platform: A New Toolbox for Chronic Lung Disease Management using Pulmonary Magnetic Resonance Imaging. *Journal of Medical Imaging.* Submitted - December 12 2017 (Manuscript ID: JMI 17360)

In Preparation **(3 total; 2 first author)**

1. **D.P.I. Capaldi**, K. Sheikh, S. Svenningsen, D.G. McCormack, G. Parraga. Magnetic Resonance Measurements of Regional Ventilation Heterogeneity: Three Dimensional Ventilation Clustering of Hyperpolarized Noble Gas MRI. *Academic Radiology*.

2. **D.P.I. Capaldi**, K. Sheikh, D.A. Hoover, T. Yamamoto, D.A. Palma, M. Daly, A. Warner, S. Kabus, M. Bal, B.P. Yaremko, G. Parraga. Lung Expansion to Measure Ventilation in Non-Small Cell Lung Cancer Patients: Comparison between Fourier-Decomposition Free-breathing Pulmonary ^{1}H MRI and Four-Dimensional CT. *International Journal of Radiation Oncology • Biology • Physics*.

3. A. Ouriadov, **D.P.I. Capaldi**, E. Lessard, F. Guo, H.M. Young, D.G. McCormack, G. Parraga. Undersampled Diffusion-weighted ^{129}Xe MRI Morphometry of Airspace Enlargement: Feasibility in Chronic Obstructive Pulmonary Disease. *Magnetic Resonance in Medicine.*

Book Chapters (1 total; 1 first author)

1. **D.P.I Capaldi**, R.L. Eddy, G. Parraga. Pulmonary MRI in Clinical Trials. MRI of the Lung. 2nd Edition. *Springer*. November 2016. doi.org/10.1007/174_2016_81

Peer-Reviewed Conference Manuscript Proceedings (4 total; 1 first author)

1. A.J. McLeod, **D.P.I. Capaldi**, J.S.H. Baxter, G. Parraga, X. Luo, T.M. Peters. Analysis of Periodicity in Video Sequences through Dynamic Linear Modeling. *Medical Image Computing and Computer Assisted Intervention (MICCAI) 2017*. doi.org/10.1007/978-3-319-66185-8_44

2. F. Guo, **D.P.I. Capaldi**, R. Di Cesare, A. Fenster, G. Parraga. Registration Pipeline for Pulmonary Free-Breathing ^{1}H MRI Ventilation Measurements. *Proceedings of the Society for Photo-optical Instrumentation Engineers (SPIE) 2017*. doi.org/10.1117/12.2253879

3. **D.P.I. Capaldi**, S. Svenningsen, I.A. Cunningham, G. Parraga. Fourier-Based Linear Systems Description of Free-Breathing Pulmonary Magnetic Resonance Imaging. *Proceedings of the Society for Photo-optical Instrumentation Engineers (SPIE) 2015*. doi.org/10.1117/12.2081503

4. N. Zha, **D.P.I. Capaldi**, D. Pike, D.G. McCormack, I.A. Cunningham, G. Parraga. Principal component analysis of the CT density histogram to generate parametric response maps of COPD. *Proceedings of the Society for Photo-optical Instrumentation Engineers (SPIE) 2015*. doi.org/10.1117/12.2076396

Peer-Reviewed Conference Abstracts (55 total; 24 first author; 5 submitted)

1. A. Ouriadov, **D.P.I. Capaldi**, H. Young, M. Kirby, H.O. Coxson, D.G. McCormack, G. Parraga. Development of the Emphysema Biomarkers in COPD and Alpha-1 Antitrypsin Deficiency Based on the Accelerated ^{129}Xe MRI Morphometry Approach. *International Conference of the American Thoracic Society Meeting Proceedings 2018* (submitted)

2. S. Svenningsen, R.L. Eddy, **D.P.I. Capaldi**, M. Kjarsgaard, K. Radford, G. Parraga, P. Nair. Effect of anti-Th2 Therapy on MRI Ventilation Heterogeneity in Prednisone Dependent Asthma. *International Conference of the American Thoracic Society Meeting Proceedings 2018* (submitted)

3. R.L. Eddy, H. Young, A. Kassay, **D.P.I. Capaldi**, S. Svenningsen, D.G. McCormack, G. Parraga. Contributions of Large Versus Small Airways to MRI Ventilation Heterogeneity in Asthmatics. *International Society for Magnetic Resonance in Medicine Meeting Proceedings 2018* (submitted)

4. A. Westcott, R.L. Eddy, **D.P.I. Capaldi**, H. Young, D.G. McCormack, G. Parraga. Novel Quantification of Ventilation Heterogeneity Patterns in Hyperpolarized ^{3}He MRI. *International Society for Magnetic Resonance in Medicine Meeting Proceedings 2018* (submitted)

5. A. Ouriadov, **D.P.I. Capaldi**, D.G. McCormack, G. Parraga. A Single Shot Whole Lung Method of Acquiring a Complete set of the Hyperpolarized Gas MRI-based Emphysema Biomarkers. *International Society for Magnetic Resonance in Medicine Meeting Proceedings 2018* (submitted)

6. B.P. Yaremko, D.A. Hoover, **D.P.I. Capaldi**, K. Sheikh, G.B. Rodrigues, A.R. Dar, E. Yu, S. Gaede, J. Chen, A. Erickson, A. Warner, B. Dingle, M. Landis, W. Kocha, M. Sanatani, M. Vincent, J. Younus, S. Kuruvilla, D.A. Palma, G. Parraga. Functional Lung Avoidance for Individualized Radiotherapy (FLAIR): Results of a Randomized, Double-Blind Clinical Trial. *American Society for Radiation Oncology 2017*

7. **D.P.I. Capaldi**, J.S.H. Baxter, A.J. McLeod, R.L. Eddy, S. Svenningsen, F. Guo, D.G. McCormack, G. Parraga. Measuring Specific Ventilation using Four-dimensional Magnetic Resonance Ventilation Imaging: A Novel Physiological Biomarker of Asthma. *Radiological Society of North America Annual Meeting 2017* (Trainee Prize Winner)

8. D.A. Hoover, T. Yamamoto, K. Sheikh, **D.P.I. Capaldi**, G. Parraga, D.A. Palma, M. Daly, A. Warner, S. Kabus, M. Bal, B.P. Yaremko. Comparison of Hyperpolarized ^{3}He MRI and CT Ventilation From a Cohort of Patients On the FLAIR Double-Blind, Randomized Trial. *American Association of Physicist in Medicine Proceedings 2017*

9. **D.P.I. Capaldi**, K. Sheikh, R.L. Eddy, S. Svenningsen, M. Kirby, D.G. McCormack, G. Parraga, Canadian Respiratory Research Network. Asthma Ventilation Abnormalities Measured using Fourier-Decomposition Free-breathing Pulmonary ^{1}H MRI. *International Workshop for Pulmonary Functional Imaging 2017* (Best Scientific Exhibition Award)

10. **D.P.I. Capaldi**, K. Sheikh, R.L. Eddy, S. Svenningsen, M. Kirby, D.G. McCormack, G. Parraga, Canadian Respiratory Research Network. Asthma Ventilation Abnormalities Measured using Fourier-Decomposition Free-breathing Pulmonary ^{1}H MRI. *Canadian Respiratory Research Network Annual General Meeting 2017*

11. **D.P.I. Capaldi**, K. Sheikh, R.L. Eddy, S. Svenningsen, M. Kirby, D.G. McCormack, G. Parraga, Canadian Respiratory Research Network. Asthma Ventilation Abnormalities Measured using Fourier-Decomposition Free-breathing Pulmonary Proton Magnetic Resonance Imaging. *London Health Research Day 2017*

12. **D.P.I. Capaldi**, K. Sheikh, R.L. Eddy, S. Svenningsen, M. Kirby, D.G. McCormack, G. Parraga, Canadian Respiratory Research Network. Asthma Ventilation Abnormalities Measured using Fourier-Decomposition Free-breathing Pulmonary ^{1}H MRI. *Imaging Network Ontario Symposium 2017* (1st Place - Best Oral Presentation Award)

13. **D.P.I. Capaldi**, K. Sheikh, R.L. Eddy, S. Svenningsen, M. Kirby, D.G. McCormack, G. Parraga, Canadian Respiratory Research Network. Asthma Ventilation Abnormalities Measured using Fourier-Decomposition Free-breathing Pulmonary ^{1}H MRI. *International Society for Magnetic Resonance in Medicine Meeting Proceedings 2017*

14. H.M. Young, **D.P.I. Capaldi**, K. Sheikh, D.G. McCormack, C.M. Yamashita, G. Parraga. Ultra-Short Echo Time MRI Quantification of Airspace Enlargement in Bronchopulmonary Dysplasia and Alpha-1 Antitrypsin Deficiency: Parenchyma Destruction, Air trapping or Both? *International Society for Magnetic Resonance in Medicine Meeting Proceedings 2017*

15. R.L. Eddy, **D.P.I. Capaldi**, K. Sheikh, S. Svenningsen, D.G. McCormack, G. Parraga. Pulmonary MRI Ventilation Defects in Asthma: Stochastic or Deterministic? *International Society for Magnetic Resonance in Medicine Meeting Proceedings 2017*

16. **D.P.I. Capaldi**, K. Sheikh, R. Di Cesare, D.A. Palma, G. Parraga. Is Ventilation Heterogeneity Related to Quality of Life Scores Post-Radiation Therapy in Non-Small Cell Lung Cancer Patients? *International Conference of the American Thoracic Society Meeting Proceedings 2017*

17. R.L. Eddy, K. Sheikh, **D.P.I. Capaldi**, S. Svenningsen, C. Licskai, D.G. McCormack, G. Parraga. Ventilation Heterogeneity Reversibility: Asthma, COPD or ACOS? *International Conference of the American Thoracic Society Meeting Proceedings 2017*

18. R.L. Eddy, **D.P.I. Capaldi**, K. Sheikh, S. Svenningsen, D.G. McCormack, G. Parraga. Probability Mapping of Lung Functional Abnormalities in Asthma using MRI: Lung Atlas Explorations of Non-randomness. *International Conference of the American Thoracic Society Meeting Proceedings 2017*

19. C.J. Adams, **D.P.I. Capaldi**, R. Di Cesare, D.G. McCormack, G. Parraga. MRI Stratification of COPD Patients for Bronchoscopic Lung Volume Reduction: A Cautionary Note. *International Conference of the American Thoracic Society Meeting Proceedings 2017*

20. **D.P.I. Capaldi**, K. Sheikh, D.A. Hoover, B.P. Yaremko, D.A. Palma, G. Parraga. Free-Breathing Proton MRI Functional Lung Avoidance Maps to Guide Radiation Therapy. *American Association of Physicist in Medicine Proceedings 2016*

21. K. Sheikh, **D.P.I. Capaldi**, D.A. Hoover, B.P. Yaremko, D.A. Palma, G. Parraga. Pulmonary Functional Imaging Biomarkers of NSCLC to Guide and Optimize Functional Lung Avoidance Radiotherapy. *American Association of Physicist in Medicine Proceedings 2016*

22. **D.P.I. Capaldi**, N. Zha, F. Guo, D. Pike, D.G. McCormack, M. Kirby, G. Parraga. Pulmonary Imaging Biomarkers of Gas Trapping and Emphysema in COPD: ^{3}He MR Imaging and CT Parametric Response Maps. *Canadian Student Health Research Forum 2016* (Canadian Student Health Research Forum Participant and Funding Competition Winner)

23. A. Dasgupta, M. Kjarsgaard, **D.P.I. Capaldi**, K. Radford, F. Aleman, G. Parraga, P.M. O'Byrne, P. Nair. Mepolizumab in COPD with eosinophilic bronchitis: A Randomized Clinical Trial. *European Respiratory Society 2016*

24. F. Guo, K. Sheikh, R. Eddy, **D.P.I. Capaldi**, D.G. McCormack, A. Fenster, G. Parraga. A Segmentation Pipeline for Measuring Pulmonary Ventilation Suitable for Clinical Workflows and Decision-making. *International Society for Magnetic Resonance in Medicine Meeting Proceedings 2016*

25. K. Sheikh, F. Guo, A. Ouriadov, **D.P.I. Capaldi**, S. Svenningsen, M. Kirby, D.G. McCormack, H.O. Coxson, G. Parraga. Ventilation Estimates in Severe Uncontrolled Asthma using 3D Single breath-hold Ultra-short Echo Time MRI. *International Society for Magnetic Resonance in Medicine Meeting Proceedings 2016*

26. **D.P.I. Capaldi**, A. Lausch, K. Sheikh, F. Guo, D.G. McCormack, G. Parraga. Pulmonary Imaging Biomarkers of COPD for Personalized Treatment and Better Outcomes. *International Society for Magnetic Resonance in Medicine Meeting Proceedings 2016*

27. **D.P.I. Capaldi**, K. Sheikh, S. Svenningsen, M. Kirby, H.O. Coxson, D.G. McCormack, G. Parraga. Measurement of Asthma Treatment Response using Free-breathing ^{1}H Ventilation MRI. *International Conference of the American Thoracic Society Meeting Proceedings 2016*

28. E. Lessard, A. Ouriadov, D. Pike, **D.P.I. Capaldi**, D.G. McCormack, G. Parraga. Novel Biomarkers of Lung Parenchyma Destruction and Emphysema Progression in COPD Using Inhaled Gas MRI Morphometry. *International Conference of the American Thoracic Society Meeting Proceedings 2016*

29. K. Sheikh, F. Guo, S. Svenningsen, A. Ouriadov, **D.P.I. Capaldi**, R.L. Eddy, D.G. McCormack, G. Parraga. What does Magnetic Resonance Imaging Signal-Intensity mean in Asthma? *International Conference of the American Thoracic Society Meeting Proceedings 2016*

30. M. Fennema, **D.P.I. Capaldi**, K. Sheikh, S. Svenningsen, R.L. Eddy, C. Licskai, D.G. McCormack, G. Parraga. The Abnormal Airways that Dominate Asthma Attack: New clues using ventilation MRI during Exercise- and Methacholine-Challenge. *International Conference of the American Thoracic Society Meeting Proceedings 2016*

31. **D.P.I. Capaldi**, K. Sheikh, S. Svenningsen, M. Kirby, H.O. Coxson, D.G. McCormack, G. Parraga. Measurement of Asthma Treatment Response using Free-breathing Proton Ventilation MRI. *London Health Research Day 2016*

32. A. Dasgupta, M. Kjarsgaard, **D.P.I. Capaldi**, K. Radford, F. Aleman, G. Parraga, P.M. O'Byrne, P. Nair. Mepolizumab in COPD with eosinophilic bronchitis: A Randomized Clinical Trial. *American Academy of Allergy, Asthma & Immunology 2016*

33. K. Sheikh, A. Ouriadov, F. Guo, **D.P.I. Capaldi**, D.G. McCormack, G. Parraga. Functional and Structural Magnetic Resonance Imaging of an Ex-Preterm Young Adult. *International Workshop for Pulmonary Functional Imaging 2015*

34. S. Svenningsen, **D.P.I. Capaldi**, P. Nair, D.G. McCormack, G. Parraga. Linking Ventilation Heterogeneity and Asthma Control: Out with the Old and in with the New? *International Workshop for Pulmonary Functional Imaging 2015*

35. **D.P.I. Capaldi**, K. Sheikh, D.A. Hoover, D.A. Palma, B.P. Yaremko, G. Parraga. Free-breathing MRI Ventilation Defects in Non-Small Cell Lung Cancer: Comparison with Hyperpolarized ^{3}He MRI and Pulmonary Function Tests. *International Workshop for Pulmonary Functional Imaging 2015*

36. B.P. Yaremko, D.A. Palma, G. Parraga, **D.P.I. Capaldi**, K. Sheikh, G.B. Rodrigues, A.R. Dar, A.V. Louie, E. Yu, S. Gaede, D.A. Hoover. Functional Lung Avoidance Radiotherapy for Stage III Non-Small Cell Lung Cancer: A double-blind randomized phase II trial. *American Society for Radiation Oncology 2015*

37. **D.P.I. Capaldi**, K. Sheikh, S. Svenningsen, D. Pike, D.G. McCormack, G. Parraga. MRI Measurements of Regional Ventilation Heterogeneity: Ventilation Defect Clusters. *International Society for Magnetic Resonance in Medicine Meeting Proceedings 2015*

38. **D.P.I. Capaldi**, N. Zha, D. Pike, K. Sheikh, D.G. McCormack, G. Parraga. ^{3}He MRI and CT Parametric Response Mapping of Small Airways Disease: The Battle-Ground for Ground Truth. *International Society for Magnetic Resonance in Medicine Meeting Proceedings 2015* (Magna Cum Laude Award)

39. K. Sheikh, **D.P.I. Capaldi**, S. Svenningsen, D.G. McCormack, G. Parraga. Ultra-short echo time MRI Measurements of Emphysema using Principal Component Analysis. *International Society for Magnetic Resonance in Medicine Meeting Proceedings 2015*

40. D. Pike, **D.P.I. Capaldi**, S. Mattonen, F. Guo, A. Ward, D.G. McCormack, G. Parraga. Second-Order Texture Analysis of Hyperpolarized ^{3}He MRI - Beyond the Ventilation Defect. *International Society for Magnetic Resonance in Medicine Meeting Proceedings 2015*

41. **D.P.I. Capaldi**, S. Svenningsen, P. Nair, D.G. McCormack, G. Parraga. Ventilation Heterogeneity in Severe Asthma: Effects of Prednisone and Salbutamol before Bronchial Thermoplasty. *International Conference of the American Thoracic Society Meeting Proceedings 2015*

42. S. Svenningsen**, D.P.I. Capaldi**, E. Bluemke, G. Paulin, C. Davis, K. Sheikh, D.G. McCormack, G. Parraga. Lung Clearance Index and Hyperpolarized ^{3}He MRI Ventilation Heterogeneity Measurements in non-CF Bronchiectasis and COPD. *International Conference of the American Thoracic Society Meeting Proceedings 2015*

43. D. Pike, M. Kirby, **D.P.I. Capaldi**, N. Zha, D.G. McCormack, H.O. Coxson, G. Parraga. Differences in Pulmonary Ventilation in COPD Ex-smokers after Three years: Longitudinal results of the TINCan Cohort. *International Conference of the American Thoracic Society Meeting Proceedings 2015*

44. **D.P.I. Capaldi**, N. Zha, D. Pike, K. Sheikh, D.G. McCormack, G. Parraga. Pulmonary Magnetic Resonance Imaging and CT Parametric Response Mapping Phenotypes in Ex-smokers with and without Chronic Obstructive Pulmonary Disease. *London Health Research Day 2015* (Judges' Selection)

45. N. Zha, **D.P.I. Capaldi**, D. Pike, D.G. McCormack, I.A. Cunningham, G. Parraga. Principal component analysis of the CT density histogram to generate parametric response maps of COPD. *London Health Research Day 2015*

46. D. Pike, M. Kirby, **D.P.I. Capaldi**, N. Zha, D.G. McCormack, H.O. Coxson, G. Parraga. Differences in Pulmonary Ventilation in COPD Ex-smokers after Three years: Longitudinal results of the TINCan Cohort. *London Health Research Day 2015*

47. N. Zha, **D.P.I. Capaldi**, D. Pike, D.G. McCormack, I.A. Cunningham, G. Parraga. Principal component analysis of the CT density histogram to generate parametric response maps of COPD. *Imaging Network Ontario Symposium 2015*

48. D. Pike, M. Kirby, **D.P.I. Capaldi**, N. Zha, D.G. McCormack, H.O. Coxson, G. Parraga. Differences in Pulmonary Ventilation in COPD Ex-smokers after Three years: Longitudinal results of the TINCan Cohort. *Imaging Network Ontario Symposium 2015*

49. **D.P.I. Capaldi**, K. Sheikh, S. Svenningsen, D. Pike, D.G. McCormack, G. Parraga. Ventilation Defect Clusters: MRI Measurements of Regional Ventilation Heterogeneity. *Imaging Network Ontario Symposium 2015*

50. **D.P.I. Capaldi**, K. Sheikh, F. Guo, S. Svenningsen, D.G. McCormack, G. Parraga. Fourier-decomposition Pulmonary Magnetic Resonance Imaging Ventilation Defects in Ex-smokers: Relationship to Emphysema and ^{3}He ventilation defects. *Radiological Society of North America Annual Meeting 2014* (Trainee Prize Finalist)

51. **D.P.I. Capaldi**, K. Sheikh, G. Paulin, S. Svenningsen, H.O. Coxson, D.G. McCormack, G. Parraga. Conventional non-contrast MRI of Ventilation Abnormalities in Bronchiectasis: New Tools and Measurements for an old Disease. *London Health Research Day 2014*

52. **D.P.I. Capaldi**, K. Sheikh, G. Paulin, S. Svenningsen, H.O. Coxson, D.G. McCormack, G. Parraga. Conventional non-contrast MRI of Ventilation Abnormalities in Bronchiectasis: New Tools and Measurements for an old Disease. *Imaging Network Ontario Symposium 2014*

53. **D.P.I. Capaldi**, K. Sheikh, G. Paulin, S. Svenningsen, H.O. Coxson, D.G. McCormack, G. Parraga. Conventional non-contrast MRI of Ventilation Abnormalities in Bronchiectasis: New Tools and Measurements for an old Disease. *International Conference of the American Thoracic Society Meeting Proceedings 2014*

54. **D.P.I. Capaldi**, F. Guo, S. Svenningsen, W. Ma, K. Sheikh, R. Etemad-Rezai, J. Leipsic, H.O. Coxson, D.G. McCormack, G. Parraga. Comparison of Pulmonary ^{1}H non-contrast and Hyperpolarized ^{3}He MRI Ventilation Abnormalities in Bronchiectasis and COPD. *International Society for Magnetic Resonance in Medicine Meeting Proceedings 2014*

55. P.S. Basran, **D.P.I. Capaldi**. On Quantitative Assessment of Deformable CT-CT Registration. Dosimetry and Treatment Planning. *Canadian association of Radiation Oncology and the Canadian Organization of Medical Physicists 2013 Joint Scientific Meeting Proceedings 2013*

Poster Presentations (32 total; 16 first-author) **presenter*

1. B.P. Yaremko*, D.A. Hoover , **D.P.I. Capaldi**, K. Sheikh, G.B. Rodrigues, A.R. Dar, E. Yu, S. Gaede, J. Chen, A. Erickson, A. Warner, B. Dingle, M. Landis, W. Kocha, M. Sanatani, M. Vincent, J. Younus, S. Kuruvilla, D.A. Palma, G. Parraga. Functional Lung Avoidance for Individualized Radiotherapy (FLAIR): Results of a Randomized, Double-Blind Clinical Trial. *American Society for Radiation Oncology 2017*, San Diego, California, USA, September 26, 2017

2. A.J. McLeod*, **D.P.I. Capaldi**, J.S.H. Baxter, G. Parraga, X. Luo, T.M. Peters. Analysis of Periodicity in Video Sequences through Dynamic Linear Modeling. *Medical Image Computing and Computer Assisted Intervention (MICCAI) 2017*, Quebec City, Quebec, Canada, September 12, 2017

3. **D.P.I. Capaldi***, K. Sheikh, R.L. Eddy, S. Svenningsen, M. Kirby, D.G. McCormack, G. Parraga, Canadian Respiratory Research Network. Asthma Ventilation Abnormalities Measured using Fourier-Decomposition Free-breathing Pulmonary Proton Magnetic Resonance Imaging. *London Health Research Day 2017*, London, Ontario, Canada, March 28, 2017 (traditional poster)

4. **D.P.I. Capaldi**, K. Sheikh, R.L. Eddy, S. Svenningsen, M. Kirby, D.G. McCormack, G. Parraga*, Canadian Respiratory Research Network. Asthma Ventilation Abnormalities Measured using Fourier-Decomposition Free-breathing Pulmonary ^{1}H MRI. *International Society for Magnetic Resonance in Medicine Meeting Proceedings 2017*, Honolulu, Hawaii, USA, April 26, 2017 (electronic poster)

5. H.M. Young, **D.P.I. Capaldi**, K. Sheikh, D.G. McCormack, C.M. Yamashita, G. Parraga*. Ultra-Short Echo Time MRI Quantification of Airspace Enlargement in Bronchopulmonary Dysplasia and Alpha-1 Antitrypsin Deficiency: Parenchyma Destruction, Air trapping or Both? *International Society for Magnetic Resonance in Medicine Meeting Proceedings 2017*, Honolulu, Hawaii, USA, April 24, 2017 (electronic poster)

6. **D.P.I. Capaldi**, K. Sheikh, R. Di Cesare, D.A. Palma, G. Parraga*. Is Ventilation Heterogeneity Related to Quality of Life Scores Post-Radiation Therapy in Non-Small Cell Lung Cancer Patients? *International Conference of the American Thoracic Society Meeting Proceedings 2017*, Washington, District of Columbia, USA, May 23, 2017 (poster discussion)

7. R.L. Eddy, K. Sheikh, **D.P.I. Capaldi**, S. Svenningsen, C. Licskai, D.G. McCormack, G. Parraga*. Ventilation Heterogeneity Reversibility: Asthma, COPD or ACOS? *International Conference of the American Thoracic Society Meeting Proceedings 2017*, Washington, District of Columbia, USA, May 23, 2017 (poster discussion)

8. R.L. Eddy, **D.P.I. Capaldi**, K. Sheikh, S. Svenningsen, D.G. McCormack, G. Parraga*. Probability Mapping of Lung Functional Abnormalities in Asthma using MRI: Lung

Atlas Explorations of Non-randomness. *International Conference of the American Thoracic Society Meeting Proceedings 2017*, Washington, District of Columbia, USA, May 23, 2017 (poster discussion)

9. C.J. Adams*, **D.P.I. Capaldi**, R. Di Cesare, D.G. McCormack, G. Parraga. MRI Stratification of COPD Patients for Bronchoscopic Lung Volume Reduction: A Cautionary Note. *International Conference of the American Thoracic Society Meeting Proceedings 2017*, Washington, District of Columbia, USA, May 23, 2017 (poster discussion)

10. **D.P.I. Capaldi***, K. Sheikh, R.L. Eddy, S. Svenningsen, M. Kirby, D.G. McCormack, G. Parraga, Canadian Respiratory Research Network. Asthma Ventilation Abnormalities Measured using Fourier-Decomposition Free-breathing Pulmonary ^{1}H MRI. *International Workshop for Pulmonary Functional Imaging 2017*, Seoul, South Korea, March 25, 2017 (electronic poster - Best Scientific Exhibition Award)

11. **D.P.I. Capaldi***, N. Zha, F. Guo, D. Pike, D.G. McCormack, M. Kirby, G. Parraga. Pulmonary Imaging Biomarkers of Gas Trapping and Emphysema in COPD: ^{3}He MR Imaging and CT Parametric Response Maps. *Canadian Student Health Research Forum*, Winnipeg, Manitoba, Canada, June 7, 2016 (traditional poster - Canadian Student Health Research Forum Participant and Funding Competition Winner)

12. F. Guo, K. Sheikh, R. Eddy, **D.P.I. Capaldi***, D.G. McCormack, A. Fenster, G. Parraga. A Segmentation Pipeline for Measuring Pulmonary Ventilation Suitable for Clinical Workflows and Decision-making. *International Society for Magnetic Resonance in Medicine Meeting Proceedings 2016*, Singapore, Singapore, May 10, 2016 (traditional poster)

13. **D.P.I. Capaldi***, A. Lausch, K. Sheikh, F. Guo, D.G. McCormack, G. Parraga. Pulmonary Imaging Biomarkers of COPD for Personalized Treatment and Better Outcomes. *International Society for Magnetic Resonance in Medicine Meeting Proceedings 2016*, Singapore, Singapore, May 12, 2016 (electronic poster)

14. M. Fennema, **D.P.I. Capaldi**, K. Sheikh*, S. Svenningsen, R.L. Eddy, C. Licskai, D.G. McCormack, G. Parraga. The Abnormal Airways that Dominate Asthma Attack: New clues using ventilation MRI during Exercise- and Methacholine-Challenge. *International Conference of the American Thoracic Society Meeting Proceedings 2016*, San Francisco, California, USA, May 18, 2016 (traditional poster)

15. **D.P.I. Capaldi***, K. Sheikh, S. Svenningsen, M. Kirby, H.O. Coxson, D.G. McCormack, G. Parraga. Measurement of Asthma Treatment Response using Free-breathing Proton Ventilation MRI. *London Health Research Day 2016*, London, Ontario, Canada, March 29, 2016 (traditional poster)

16. K. Sheikh, A. Ouriadov, F. Guo, **D.P.I. Capaldi**, D.G. McCormack, G. Parraga*. Functional and Structural Magnetic Resonance Imaging of an Ex-Preterm Young

Adult. *International Workshop for Pulmonary Functional Imaging 2015*, Edinburgh, Scotland, September 29, 2015 (rapid fire poster)

17. **D.P.I. Capaldi**, K. Sheikh, D.A. Hoover, D.A. Palma, B.P. Yaremko, G. Parraga*. Free-breathing MRI Ventilation Defects in Non-Small Cell Lung Cancer: Comparison with Hyperpolarized ^{3}He MRI and Pulmonary Function Tests. *International Workshop for Pulmonary Functional Imaging 2015*, Edinburgh, Scotland, September 29, 2015 (rapid fire poster)

18. **D.P.I. Capaldi***, K. Sheikh, S. Svenningsen, D. Pike, D.G. McCormack, G. Parraga. MRI Measurements of Regional Ventilation Heterogeneity: Ventilation Defect Clusters. *International Society for Magnetic Resonance in Medicine Meeting Proceedings 2015*, Toronto, Ontario, Canada, June 3, 2015 (electronic poster)

19. K. Sheikh*, **D.P.I. Capaldi**, S. Svenningsen, D.G. McCormack, G. Parraga. Ultra-short echo time MRI Measurements of Emphysema using Principal Component Analysis. *International Society for Magnetic Resonance in Medicine Meeting Proceedings 2015*, Toronto, Ontario, Canada, June 2, 2015 (traditional poster)

20. D. Pike, **D.P.I. Capaldi***, S. Mattonen, F. Guo, A. Ward, D.G. McCormack, G. Parraga. Second-Order Texture Analysis of Hyperpolarized ^{3}He MRI - Beyond the Ventilation Defect. *International Society for Magnetic Resonance in Medicine Meeting Proceedings 2015*, Toronto, Ontario, Canada, June 3, 2015 (electronic poster)

21. **D.P.I. Capaldi**, S. Svenningsen*, P. Nair, D.G. McCormack, G. Parraga. Ventilation Heterogeneity in Severe Asthma: Effects of Prednisone and Salbutamol before Bronchial Thermoplasty. *International Conference of the American Thoracic Society Meeting Proceedings 2015*, Denver, Colarado, USA, May 17, 2015 (poster discussion)

22. S. Svenningsen***, D.P.I. Capaldi**, E. Bluemke, G. Paulin, C. Davis, K. Sheikh, D.G. McCormack, G. Parraga. Lung Clearance Index and Hyperpolarized ^{3}He MRI Ventilation Heterogeneity Measurements in non-CF Bronchiectasis and COPD. *International Conference of the American Thoracic Society Meeting Proceedings 2015*, Denver, Colarado, USA, May 17, 2015 (poster discussion)

23. D. Pike, M. Kirby*, **D.P.I. Capaldi**, N. Zha, D.G. McCormack, H.O. Coxson, G. Parraga. Differences in Pulmonary Ventilation in COPD Ex-smokers after Three years: Longitudinal results of the TINCan Cohort. *International Conference of the American Thoracic Society Meeting Proceedings 2015*, Denver, Colarado, USA, May 17, 2015 (poster discussion)

24. **D.P.I. Capaldi***, N. Zha, D. Pike, K. Sheikh, D.G. McCormack, G. Parraga. Pulmonary Magnetic Resonance Imaging and CT Parametric Response Mapping Phenotypes in Ex-smokers with and without Chronic Obstructive Pulmonary Disease. *London Health Research Day 2015*, London, Ontario, Canada, April 1, 2015 (traditional poster - Judges' Selection)

25. N. Zha*, **D.P.I. Capaldi**, D. Pike, D.G. McCormack, I.A. Cunningham, G. Parraga. Principal component analysis of the CT density histogram to generate parametric response maps of COPD. *London Health Research Day 2015*, London, Ontario, Canada, April 1, 2015 (traditional poster)

26. D. Pike*, M. Kirby, **D.P.I. Capaldi**, N. Zha, D.G. McCormack, H.O. Coxson, G. Parraga. Differences in Pulmonary Ventilation in COPD Ex-smokers after Three years: Longitudinal results of the TINCan Cohort. *London Health Research Day 2015*, London, Ontario, Canada, April 1, 2015 (traditional poster)

27. D. Pike*, M. Kirby, **D.P.I. Capaldi**, N. Zha, D.G. McCormack, H.O. Coxson, G. Parraga. Differences in Pulmonary Ventilation in COPD Ex-smokers after Three years: Longitudinal results of the TINCan Cohort. *Imaging Network Ontario Symposium 2015*, London, Ontario, Canada, March 30 & 31, 2015 (traditional poster)

28. **D.P.I. Capaldi***, K. Sheikh, G. Paulin, S. Svenningsen, H.O. Coxson, D.G. McCormack, G. Parraga. Conventional non-contrast MRI of Ventilation Abnormalities in Bronchiectasis: New Tools and Measurements for an old Disease. *International Conference of the American Thoracic Society Meeting Proceedings 2014*, San Diego, California, USA, May 18, 2014 (poster discussion)

29. **D.P.I. Capaldi***, F. Guo, S. Svenningsen, W. Ma, K. Sheikh, R. Etemad-Rezai, J. Leipsic, H.O. Coxson, D.G. McCormack, G. Parraga. Comparison of Pulmonary ^{1}H non-contrast and Hyperpolarized ^{3}He MRI Ventilation Abnormalities in Bronchiectasis and COPD. *International Society for Magnetic Resonance in Medicine Meeting Proceedings 2014*, Milan, Milan, Italy, May 14, 2014 (traditional poster)

30. **D.P.I. Capaldi***, K. Sheikh, G. Paulin, S. Svenningsen, H.O. Coxson, D.G. McCormack, G. Parraga. Conventional non-contrast MRI of Ventilation Abnormalities in Bronchiectasis: New Tools and Measurements for an old Disease. *Imaging Network Ontario Symposium 2014*, Toronto, Ontario, Canada, March 24, 2014 (traditional poster)

31. **D.P.I. Capaldi***, K. Sheikh, G. Paulin, S. Svenningsen, H.O. Coxson, D.G. McCormack, G. Parraga. Conventional non-contrast MRI of Ventilation Abnormalities in Bronchiectasis: New Tools and Measurements for an old Disease. *London Health Research Day 2014*, London, Ontario, Canada, March 18, 2014 (traditional poster)

32. **D.P.I. Capaldi***. Automizing the Analysis of a High Precision Image Quality Phantom Manufactured for CT Imaging. *University of Windsor Undergraduate Student Coop Poster Presentation*, Windsor, Ontario, Canada, January 29, 2013 (traditional poster)

Oral Presentations (25 total; 11 first-author) **presenter*

1. **D.P.I. Capaldi***, J.S.H. Baxter, A.J. McLeod, R.L. Eddy, S. Svenningsen, F. Guo, D.G. McCormack, G. Parraga. Measuring Specific Ventilation using Four-dimensional Magnetic Resonance Ventilation Imaging: A Novel Physiological Biomarker of Asthma. *Radiological Society of North America Annual Meeting 2017*, Chicago, Illinois, USA, December 1, 2017 (Trainee Prize Winner)

2. D.A. Hoover*, T. Yamamoto, K. Sheikh, **D.P.I. Capaldi**, G. Parraga, D.A. Palma, M. Daly, A. Warner, S. Kabus, M. Bal, B.P. Yaremko. Comparison of Hyperpolarized ^{3}He MRI and CT Ventilation From a Cohort of Patients On the FLAIR Double-Blind, Randomized Trial. *American Association of Physicist in Medicine Proceedings 2017*, Denver, Colorado, USA, July 30, 2017 (Snap Presentation)

3. **D.P.I. Capaldi***, K. Sheikh, R.L. Eddy, S. Svenningsen, M. Kirby, D.G. McCormack, G. Parraga, Canadian Respiratory Research Network. Asthma Ventilation Abnormalities Measured using Fourier-Decomposition Free-breathing Pulmonary ^{1}H MRI. *International Workshop for Pulmonary Functional Imaging 2017*, Seoul, South Korea, March 25, 2017 (3-minute power pitch - Best Scientific Exhibition Award)

4. **D.P.I. Capaldi***, K. Sheikh, R.L. Eddy, S. Svenningsen, M. Kirby, D.G. McCormack, G. Parraga, Canadian Respiratory Research Network. Asthma Ventilation Abnormalities Measured using Fourier-Decomposition Free-breathing Pulmonary ^{1}H MRI. *Imaging Network Ontario Symposium 2017*, London, Ontario, Canada, March 15, 2017 (1st Place - Best Oral Presentation Award)

5. R.L. Eddy, **D.P.I. Capaldi**, K. Sheikh, S. Svenningsen, D.G. McCormack, G. Parraga*. Pulmonary MRI Ventilation Defects in Asthma: Stochastic or Deterministic? *International Society for Magnetic Resonance in Medicine Meeting Proceedings 2017*, Honolulu, Hawaii, USA, April 27, 2017

6. F. Guo, **D.P.I. Capaldi**, R. Di Cesare, A. Fenster, G. Parraga*. Registration Pipeline for Pulmonary Free-Breathing ^{1}H MRI Ventilation Measurements. *Proceedings of the Society for Photo-optical Instrumentation Engineers (SPIE) 2017*, Orlando, Florida, USA, February 16, 2017

7. **D.P.I. Capaldi***, K. Sheikh, R.L. Eddy, S. Svenningsen, M. Kirby, D.G. McCormack, G. Parraga, Canadian Respiratory Research Network. Asthma Ventilation Abnormalities Measured using Fourier-Decomposition Free-breathing Pulmonary ^{1}H MRI. *Canadian Respiratory Research Network Annual General Meeting 2017*, Ottawa, Ontario, Canada, January 11, 2017

8. A. Dasgupta, M. Kjarsgaard, **D.P.I. Capaldi**, K. Radford, F. Aleman, G. Parraga, P.M. O'Byrne, P. Nair*. Mepolizumab in COPD with eosinophilic bronchitis: A Randomized Clinical Trial. *European Respiratory Society 2016*, London, United Kingdom, September 4, 2016

9. **D.P.I. Capaldi***, K. Sheikh, D.A. Hoover, B.P. Yaremko, D.A. Palma, G. Parraga. Free-Breathing Proton MRI Functional Lung Avoidance Maps to Guide Radiation Therapy. *American Association of Physicist in Medicine Proceedings 2016,* Washington, District of Columbia, USA, August 4, 2016

10. K. Sheikh, **D.P.I. Capaldi***, D.A. Hoover, B.P. Yaremko, D.A. Palma, G. Parraga. Pulmonary Functional Imaging Biomarkers of NSCLC to Guide and Optimize Functional Lung Avoidance Radiotherapy. *American Association of Physicist in Medicine Proceedings 2016,* Washington, District of Columbia, USA, August 3, 2016

11. K. Sheikh*, F. Guo, A. Ouriadov, **D.P.I. Capaldi**, S. Svenningsen, M. Kirby, D.G. McCormack, H.O. Coxson, G. Parraga. Ventilation Estimates in Severe Uncontrolled Asthma using 3D Single breath-hold Ultra-short Echo Time MRI. *International Society for Magnetic Resonance in Medicine Meeting Proceedings 2016,* Singapore, Singapore, Friday, May 13, 2016

12. **D.P.I. Capaldi***, K. Sheikh, S. Svenningsen, M. Kirby, H.O. Coxson, D.G. McCormack, G. Parraga. Measurement of Asthma Treatment Response using Free-breathing ^{1}H Ventilation MRI. *International Conference of the American Thoracic Society Meeting Proceedings 2016*, San Francisco, California, USA, May 15, 2016

13. E. Lessard, A. Ouriadov, D. Pike*, **D.P.I. Capaldi**, D.G. McCormack, G. Parraga. Novel Biomarkers of Lung Parenchyma Destruction and Emphysema Progression in COPD Using Inhaled Gas MRI Morphometry. *International Conference of the American Thoracic Society Meeting Proceedings 2016,* San Francisco, California, USA, May 18, 2016

14. K. Sheikh*, F. Guo, S. Svenningsen, A. Ouriadov, **D.P.I. Capaldi**, R.L. Eddy, D.G. McCormack, G. Parraga. What does Magnetic Resonance Imaging Signal-Intensity mean in Asthma? *International Conference of the American Thoracic Society Meeting Proceedings 2016,* San Francisco, California, USA, May 15, 2016

15. A. Dasgupta, M. Kjarsgaard, **D.P.I. Capaldi**, K. Radford, F. Aleman, G. Parraga, P.M. O'Byrne, P. Nair*. Mepolizumab in COPD with eosinophilic bronchitis: A Randomized Clinical Trial. *American Academy of Allergy, Asthma & Immunology 2016,* Los Angeles, California, USA, March 4, 2016

16. S. Svenningsen, **D.P.I. Capaldi**, P. Nair, D.G. McCormack, G. Parraga*. Linking Ventilation Heterogeneity and Asthma Control: Out with the Old and in with the New? *International Workshop for Pulmonary Functional Imaging 2015*, Edinburgh, Scotland, September 29, 2015

17. B.P. Yaremko*, D.A. Palma, G. Parraga, K. Sheikh, **D.P.I. Capaldi**, G.B. Rodrigues, R. Dar, E. Yu, B. Dingle, M. Landis, W. Kocha, M. Sanatani, M. Vincent, J. Younus, S. Gaede, D.A. Hoover. Functional Lung Avoidance Radiotherapy for Stage III Non-

Small Cell Lung Cancer: A double-blind randomized phase II trial. *American Society for Radiation Oncology 2015*, San Antonio, Texas, USA, October 18-21, 2015

18. **D.P.I. Capaldi***, N. Zha, D. Pike, K. Sheikh, D.G. McCormack, G. Parraga. ^{3}He MRI and CT Parametric Response Mapping of Small Airways Disease: The Battle-Ground for Ground Truth. *International Society for Magnetic Resonance in Medicine Meeting Proceedings 2015,* Toronto, Ontario, Canada, June 5, 2015 (Magna Cum Laude Award)

19. **D.P.I. Capaldi***, K. Sheikh, S. Svenningsen, D. Pike, D.G. McCormack, G. Parraga. Ventilation Defect Clusters: MRI Measurements of Regional Ventilation Heterogeneity. *Imaging Network Ontario Symposium 2015*, London, Ontario, Canada, March 30, 2015

20. N. Zha*, **D.P.I. Capaldi**, D. Pike, D.G. McCormack, I.A. Cunningham, G. Parraga. Principal component analysis of the CT density histogram to generate parametric response maps of COPD. *Imaging Network Ontario Symposium 2015*, London, Ontario, Canada, March 30, 2015

21. **D.P.I. Capaldi***, S. Svenningsen, I.A. Cunningham, G. Parraga. Fourier-Based Linear Systems Description of Free-Breathing Pulmonary Magnetic Resonance Imaging. *Proceedings of the Society for Photo-optical Instrumentation Engineers (SPIE)*, Orlando, Florida, USA, February 26, 2015

22. N. Zha*, **D.P.I. Capaldi**, D. Pike, D.G. McCormack, I.A. Cunningham, G. Parraga. Principal component analysis of the CT density histogram to generate parametric response maps of COPD. *Proceedings of the Society for Photo-optical Instrumentation Engineers (SPIE)*, Orlando, Florida, USA, February 26, 2015

23. **D.P.I. Capaldi***, K. Sheikh, F. Guo, S. Svenningsen, D.G. McCormack, G. Parraga. Fourier-decomposition Pulmonary Magnetic Resonance Imaging Ventilation Defects in Ex-smokers: Relationship to Emphysema and ^{3}He ventilation defects. *Radiological Society of North America Annual Meeting 2014*, Chicago, Illinois, USA, December 3, 2014 (Trainee Prize Finalist)

24. P.S. Basran*, **D.P.I. Capaldi**. On Quantitative Assessment of Deformable CT-CT Registration. Dosimetry and Treatment Planning. *Canadian association of Radiation Oncology and the Canadian Organization of Medical Physicists 2013 Joint Scientific Meeting Proceedings 2013,* Montreal, Quebec, September 19, 2013

25. **D.P.I. Capaldi***, M.A. Pantea, R.G. Maev. Finite Element Analysis of Percussion Models: Modeling Different Complex Structures to Determine Acoustical Properties. *University of Windsor Undergraduate Thesis Presentation*, Windsor, Ontario, July 27, 2012

Academic Reports (1 total; 1 first-author)

1. **D.P.I. Capaldi**, M.A. Pantea, R.G. Maev. Finite Element Analysis of Percussion Models: Modeling Different Complex Structures to Determine Acoustical Properties. *University of Windsor Undergraduate Thesis*, Windsor, Ontario, 2012

COMMITTEES AND PROFESSIONAL ACTIVITIES

2010-2013 **University of Windsor**
Undergraduate Representative
Department of Physics

PROFESSIONAL MEMBERSHIPS

2017- Radiological Society of North America (RSNA)
Student Member
2015- American Association of Physicist in Medicine (AAPM)
Student Member
2013- International Society for Magnetic Resonance in Medicine (ISMRM)
Student Member
2013-2018 American Thoracic Society (ATS)
Student Member
2013-2014 Canadian Organization of Medical Physicists (COMP)
Student Member
2012-2013 Canadian Association of Physicists (CAP)
Student Member

COMMUNITY ACTIVITIES

2013 **Miracle League of Amherstburg,** *Buddy*
2012-2013 **Students Orienting Students,** *Volunteer***,** University of Windsor
2010-2013 **Science Rendezvous**, *Volunteer*, University of Windsor
2011-2013 **Physics Club**, *Vice President*, University of Windsor
2009-2013 **Physics Club**, *Member*, University of Windsor